



**Spatial Simulation Based Riverbank Slope
Instability and Susceptibility Assessment in the
Lower River Murray**

By

CHEN LIANG

B.E., M.Sc.

Thesis submitted in fulfilment of the requirements for the degree
of Doctor of Philosophy

The University of Adelaide
Faculty of Engineering, Computer and Mathematical Sciences
School of Civil, Environmental and Mining Engineering

Copyright © February 2015

To my beloved parents

Xu-Dong Liang and Xiao-Feng Niu

And my beloved grandparents

Tin Jiao and Zhen-xiang Luo

Shu-ren Niu and Yu-Lan Feng

Spatial Simulation Based Riverbank Slope Instability and
Susceptibility Assessment in the Lower River Murray

By:

Chen Liang, B.E.,M.Sc.

Supervised by:

Professor Mark B. Jaksa, *B.E.(Hons), Ph.D.*

and

Associate Professor Bertram Ostendorf, *B.S., Ph.D*

Thesis submitted in fulfilment of the requirements for the degree
of

Doctor of Philosophy

School of Civil, Environmental & Mining Engineering

Faculty of Engineering, Computer and Mathematical Sciences

The University of Adelaide

North Terrace, Adelaide, SA 5005, Australia

Phone: +61 8 8313 1575

Fax : +61 8 8303 4359

Email: cliang@civeng.adelaide.edu.au, mjlc7777@gmail.com

Copyright © Chen Liang, February, 2015



Abstract

Riverbank collapse is a natural and expected phenomenon associated with the evolution of rivers worldwide and has been studied extensively over the last two decades and remains an active research topic. The evolution of riverbank stability analysis has followed closely the developments in analytical methods, investigation tools, stabilisation methods and data acquisition technology. Furthermore, the stability of riverbanks is a multifaceted issue which involves the study of geology, topography, stratigraphy, hydrology, climate, spatial variation and geotechnical engineering.

The River Murray is one of the only river systems in the world that can fall below sea level due to the barrages preventing the inflow of sea water during periods of low river flows. Over the last few years, an unprecedented period of dry conditions and low flows between 2005 – 2010 led to more than 162 reported riverbank collapse-related incidents along the Lower River Murray, in South Australia (downstream of Lock 1 at Blanchetown to Wellington). Those collapse-related incidents threatened public infrastructure, private property and the safety of river users, and also provide significant challenges for environmental and river management. From the inventory of the South Australian Department of Environment, Water and Natural Resources (DEWNR), riverbank collapse, erosion, cracking, tree leaning and collapse and levee problems are the main forms of the recorded incidents.

Geographical information systems (GIS) is well known for its efficient and cost-effective spatial data processing capabilities, which include spatial data collection, manipulation and analysis, and has been widely used in riverbank instability research. As a significant feature of this thesis, GIS, incorporating high-resolution spatial data, such as aerial photographs and LIDAR (light detecting and ranging) images, facilitates the assessment of riverbank instability in several ways. Firstly, the actual location of the historical collapse can be determined and verified by the use of high-resolution aerial image comparison and interpretation to facilitate accurate back-analyses. Secondly,

the 2D and 3D geometry of the riverbank is able to be readily extracted from the LIDAR digital elevation models (DEMs). Thirdly, the dimensions of the predicted collapsed regions can be validated against high-resolution aerial images, and finally, the influencing factors are able to be manipulated and mapped with GIS to predict regions susceptible to riverbank collapse.

This thesis aims to: (1) examine the failure mechanisms affecting riverbank collapse along the Lower River Murray and identify the most relevant mechanism; (2) identify potential triggers for riverbank collapse events that should be monitored and managed in the future; (3) develop a framework, incorporating spatial information, GIS and geotechnical data, to facilitate the prediction of riverbank collapse along the Lower River Murray (between Blanchetown and Wellington, South Australia); and (4) develop a framework, based on GIS and geotechnical data, to identify regions susceptible to high risk of riverbank collapse along the Lower River Murray.

In order to realise these aims, numerical analyses have been performed using two commercially available software programs, ArcGIS and SVOOffice, which integrate the limit equilibrium method, back-analysis of collapse incidents, transient unsaturated flow modelling, steady state modelling, and DEMs and high-resolution aerial images within a GIS framework. The modelling has been informed by a series of geotechnical investigations undertaken at various sites along the River Murray.

Statement of Originality

I, **Chen Liang**, hereby certify that this work has not been previously accepted for any other degree or diploma at any other University or Institution. To the best of my knowledge and belief, no material in this thesis is from the work of other people, except where due reference are made in the text.

In addition, I certify that no part of this work will, in the future, be used in a submission for any other degree or diploma in any university or other tertiary institution without the prior approval of the University of Adelaide and where applicable, any partner institution responsible for the joint-award of this degree.

I give consent to this copy of my thesis, when deposited in the University Library, being made available for loan and photocopying, subject to the provisions of the Copyright Act 1968.

I acknowledge that copyright of published works contained within this thesis resides with the copyright holder(s) of those works.

I give permission for the digital version of this work being made available on the web, via the University's digital research repository, the Library catalogue, the Australian Digital Thesis Program (ADTP) and also through web search engines, unless permission has been granted by the University to restrict access for a period of time.

Signed..... Date:.....

Acknowledgements

I would like to give my sincerest thanks to my parents and grandparents, who have been giving their unconditional support to my life and work from the beginning to the end. Without their love, all the work I have done would hardly be possible. To revere and learn my parents' and grandparents' love, goodness, integrity and selflessness has inspired me to keep moving on.

I would like to take this opportunity to sincerely acknowledge my Principal Supervisor Professor Mark Jaksa and Co-supervisor Associate Professor Bertram Ostendorf for their guidance, invaluable support and encouragement throughout my Ph.D. studies but without requiring anything in return. Without their valuable advice and comments, I would not have been able to complete my project, nor would I have produced four journal papers. Special thanks to Professor Mark Jaksa who provided me with casual work opportunities in the School and provided me a top-up scholarship to cover my daily life expenses.

I would also like to show my appreciation to Drs. Yien Lik Kuo and An Deng who have provided me great suggestions for my research. Special thanks to the ladies in our School Office, Dr. Stephen Carr from the IT section and Gary Bowman, Dale Hodson and the other technical staff from the laboratories of the School of Civil, Environmental & Mining Engineering. They have provided me great assistance in my daily work and site investigations.

I would like to sincerely acknowledge the assistance of Jai O'Toole, Geoff Eaton and Richard Brown from DEWNR who provided me with the high resolution aerial images of the Lower River Murray, opportunities for site visits and valuable advice throughout my research. I'd also like to thank the Goyder Institute for Water Research who funded this project (*Project E1.8 Riverbank Stability*).

Finally, I would like to thank the University of Adelaide and the China Scholarship Council for awarding me the scholarship to support my Ph.D.

program. Without the CSC tuition-fee-wavier scholarship and stipend, my research and thesis would not have been possible.

Table of Contents

Abstract	V
Statement of Originality	VII
Acknowledgements	VIII
Table of Contents	X
List of Figures	XIII
List of Tables	XVII
1 Introduction	1
1.1 Background	1
1.2 Research Aims	6
1.3 Layout of Thesis	7
2 Literature Review	11
2.1 Methods for slope susceptibility assessment	11
2.2 Methods for calculating the factor of safety	12
2.2.1 Introduction	12
2.2.2 Conventional calculation	12
2.2.3 Infinite slope stability calculation	17
2.2.4 Finite slope stability calculation	18
2.2.5 Slope stability classification	20
2.2.6 Groundwater and subsurface flow	22
2.3 Failure processes	25
2.3.1 Introduction	25
2.3.2 Erosion processes	26
2.3.3 Failure mechanisms	27
2.3.4 Weakening factors	29
2.4 Effects of vegetation on slope stability	32
2.4.1 Background	32
2.4.2 Hydrological effects	33
2.4.3 Mechanical effects	35

2.4.4	Reinforcement calculation	37
2.5	GIS approaches to landslide hazard mapping	41
2.6	Summary	43
	References for Chapters 1 and 2	45
3	GIS-based Back Analysis of Riverbank Instability in the Lower River Murray	59
3.1	Introduction	62
3.2	Riverbank stability model and back-analysis	63
3.3	Analysis and discussion	69
3.4	Conclusion	74
	Acknowledgements	75
	References for Chapter 3	76
4	Influence of River Level Fluctuations and Climate on Riverbank Stability	79
4.1	Introduction	82
4.2	Study area	86
4.3	Methodology and model development	87
4.3.1	Topography	89
4.3.2	Geotechnical properties	92
4.3.3	Hydrological and climatic variables	99
4.3.4	Boundary conditions	101
4.4	Riverbank collapse back-analyses	101
4.4.1	Pore water pressure variation	103
4.4.2	Factor of safety	107
4.5	Influence of rainfall and river level drawdown	110
4.6	Conclusion	115
	Acknowledgements	116
	Notation	117
	References for Chapter 4	119
5	Back Analysis of Lower River Murray Riverbank Collapses Using Transient Water Model	127
5.1	Introduction	130

5.2	Study area and regions of collapse	132
5.3	Methodology	133
5.3.1	Topography and soil properties	138
5.3.2	River level and climatic data	140
5.4	Back-analysis and validation	141
5.5	Summary	149
	Acknowledgements	151
	References for Chapter 5	152
6	Identifying Areas Susceptible to High Risk of Riverbank Collapse along the Lower River Murray	163
6.1	Introduction	166
6.2	Study area and historical collapses	169
6.3	Methodology	171
6.3.1	Topography	172
6.3.2	Geotechnical properties and back-analysis	175
6.3.3	Cross-sectional modeling	176
6.4	Hazard prediction and validation	177
6.5	Summary	187
	Acknowledgements	188
	References for Chapter 6	189
7	Summary and Conclusions	201
7.1	Summary	201
7.2	Research contributions	203
7.3	Limitations and Recommendations for Future Research	205
8	Appendix: Copies of Papers (as published)	207

List of Figures

Figure 1.1 Overview of the River Murray and the study area.....	2
Figure 1.2 Overview of Lower River Murray (Source: SKM, 2010).....	5
Figure 1.3 Slope failure on riverbanks (a) rotational slip on over-steepened riverbanks, (b) slab failure on over-heightened riverbanks (Source: Thorne, 1999).....	6
Figure 2.1 Proposed classification of slope failure susceptibility assessment methods (Source: Aleotti and Chowdhury, 1999).	13
Figure 2.2 Method of slices: (a) division of slip mass; (b) forces on a slice (Source: Whitlow, 1990).	15
Figure 2.3 Infinite slope failure in $c-\phi$ soil with parallel seepage (Source: Abramson et al., 2002).	17
Figure 2.4 Definitions of terms used for finite element method (FEM) (Source: Abramson et al., 2002).	19
Figure 2.5 Limitation of FS compared with probability of failure.....	22
Figure 2.6 Bank failure modes (Source: Hey et al., 1991).....	31
Figure 2.7 Effect of root reinforcement on shear strength of soil (Source: Coppin and Richards, 1990).	33
Figure 2.8 Reduction in soil moisture content near a Poplar tree growing in boulder clay (Source: Biddle, 1983).....	34
Figure 2.9 Illustration of the root matrix system of vegetation on riverbank (Source: Schwarz et al., 2010).....	36
Figure 2.10 Influence of vegetation on riverbank (Source: Coppin and Richards, 1990).	36
Figure 2.11 Angle of angle of shear distortion in the shear zone.	38
Figure 2.12 Average shear stress versus displacement plots for the four tree species and the soil-only tests (Source: Docker and Hubble, 2008).	39
Figure 3.1 Location of the study area.....	63
Figure 3.2 Examples of visual interpretation on 2008 and 2010 aerial images under ArcGIS in (a) Murray Bridge and; (b) Tailem Bend.	64

Figure 3.3 Long Island Marina study site: (a) locations of 5 significant failures; (b) location plan of in situ testing and recorded collapses; (c) distribution of bank cross sections in 3-D view.....	67
Figure 3.4 River Murray water at Murray Bridge 1/12/1986 to 11/07/2011 (DFW 2010).....	68
Figure 3.5 Schematic of the locations and the deadweight of the external loads on the riverbank.....	68
Figure 3.6 Minimum FOS and potential slip surface of deep-seated rotational failure at No. 21 model when water level was 0 m AHD.....	70
Figure 3.7 Back-analyses using three geotechnical models.....	70
Figure 3.8 Factors of Safety of neighbouring cross sections (0 and 0.5 m AHD).....	72
Figure 3.9 Predictions of riverbank susceptibility with river levels at (a) 0 m AHD and (b) 0.5 m AHD.....	73
Figure 4.1 Details of the Long Island Marina site.....	88
Figure 4.2. Riverbank geometry definition.....	91
Figure 4.3. Example of adopted visual interpretation process on high resolution, aerial images within the ArcGIS framework.....	92
Figure 4.4 Geotechnical profiles based on soil samples taken from SR-BH1 and SR-CPTu6s at Long Island Marina.....	94
Figure 4.5 Particle size distributions based on the soil samples from four different depths in borehole SR-BH1.....	95
Figure 4.6 Estimated SWCCs for the three soil layers at Long Island Marina using the Fredlund and Xing fit estimation method.....	95
Figure 4.7 Typical CPTu profile and dissipation test results.....	96
Figure 4.8 Daily river levels, daily rainfall and daily mean temperature from 1 May 2008 to 28 February 2009 at Long Island Marina.....	100
Figure 4.9 Results of 2D and 3D riverbank stability analyses of Long Island Marina site at Day 282 (6 February 2008).....	102
Figure 4.10 Evolution of pore water pressure at 6 selected nodes through the entire research period accounting for, and without, evaporation.....	104
Figure 4.11 PWP distributions as a result of (a) the highest (Day 138) and (b) lowest (Day 302) river levels.....	106
Figure 4.12 Factors of safety from the 2D, 3D and CRLM models.....	108

Figure 4.13 Factors of safety for historical model (HM) and constant river stage model (CRLM) in two scenarios.....	112
Figure 4.14 Magnified rainfall model (MRM) under different river level scenarios.	114
Figure 5.1 Details of the study area.....	134
Figure 5.2: Adopted visual interpretation method of high-resolution aerial images: (a), (c), (e) and (g) are aerial photographs acquired in March 2008 at EFR, WR, MB and WS, respectively; (b), (d), (f), and (h) are aerial photographs acquired in May 2010 at EFR, WR, MB and WS, respectively.	136
Figure 5.3: Example of adopted elevation comparison method on DEMs at Woodlane Reserve (a) 1 m resolution DEM acquired in 2008; (b) 0.2 m resolution DEM acquired in 2010).....	137
Figure 5.4: Daily river levels and daily rainfall recorded at (a) East Front Road, Mannum (EFR) site in April 2009; (b) Woodlane Reserve (WR) site in February 2009; (c) River Front Road, Murray Bridge (RFR) site in February 2009; and (d) White Sands (WS) site in April 2009.....	143
Figure 5.5: Riverbank stability analysis of the East Front Road, Mannum (EFR) site on 23 April 2009.	145
Figure 5.6: Riverbank stability analysis of the Woodlane Reserve (WR) site on 26 February 2009.....	146
Figure 5.7: Riverbank stability analysis of the River Front Road, Murray Bridge (RFR) site on 6 February 2009.....	147
Figure 5.8: Riverbank stability analysis of the White Sands (WS) site on 23 April 2009.....	148
Figure 5.9: Riverbank collapse factor of safety time series for: (a) EFR in April 2009; (b) WR in February 2009; (c) RFR in February 2009; and (d) WS in April 2009.....	150
Figure 6.1 Diagram of study area, locations of historical collapses, cross-sectional models and geotechnical investigations.	173
Figure 6.2 Example of high-resolution aerial image based visual interpretation and validation.	174
Figure 6.3 Riverbank stability analyses at three historical sites under SVSlope framework.	180

Figure 6.4 Grid size based surface slope calculation.....	182
Figure 6.5 Relationships between average elevation (H), inclination (α) and factor of safety of the cross-sectional models with a 0 m AHD river level..	183
Figure 6.6 Example of riverbank collapse prediction.....	186

List of Tables

Table 2.1 Slope stability classes (modified from Ray and de Smedt, 2009). ..	23
Table 4.1 Soil parameters for stability assessment.....	97
Table 4.2 Equations used to calculate Fredlund and Xing SWCC fitting parameters based on the soil grain size distribution.....	98
Table 5.1 Historical riverbank collapse related incidents associated with the four examined sites.....	132
Table 5.2 Soil properties for saturated and unsaturated flow modelling.....	139
Table 5.3 Geotechnical models of the clay layer obtained from back-analyses.	144
Table 5.4 Model validation.....	144
Table 6.1 Riverbank collapse related incidents with associated slope inclinations.	171
Table 6.2 Soil properties for saturated and unsaturated flow modelling.....	181
Table 6.3 Acceptable H and α combination for each research region when river levels equal to 0 and -1 m AHD.....	185

Chapter 1

1 Introduction

1.1 Background

Slope instability is one of the major problems in geotechnical engineering where loss of life and property can and do occur (Vanmarcke, 1977). Slope instability can arise both in human-made or natural slopes (e.g. mountainous regions, embankments, road cuts, open-pit mining, excavations, riverbanks and landfills) throughout the world. Consequently, not only are considerable financial costs incurred, but also major ecological and environmental problems over large geographical areas (Li, 1994; Larsen and Torres-Sanchez, 1998), as well as threats to safety. Mapping or delineating areas susceptible to slope failure is essential for land-use planning in mountainous, hill-slope or riverbank areas.

Slope stability failures that have occurred along the Lower River Murray downstream of Lock 1 and riverbank instability are the focus of the current study. The River Murray is the longest river in Australia being 2,375 kilometres in length. It begins in the Australian Alps and terminates at Goolwa, South Australia at the Murray mouth in the Southern Ocean, with an annual average discharge of 767 m³/s and a history spanning more than 60 million years (Figure 1.1). The River Murray is one part of the Murray-Darling Basin catchment area which covers around one million square kilometres. This is about one-seventh of Australia's land mass, and extends across parts of South Australia, Victoria, New South Wales and Queensland.

The Lower River Murray (which is roughly a 210 km stretch from Lock 1 at Blanchetown to Wellington, as shown in Figure 1.2) was adversely affected

by unprecedented low water levels during the millennium drought, which resulted in several bank-slope failures. The instability of the riverbank caused by the low water level in the river during the drought now poses a number of economic and ecological problems for the residents and the environment adjacent to the failure location (approximately 40 metres from the centre of the river bed) in the form of land loss, tension cracks, riparian tree collapse, destabilized structures, impairment of water quality and downstream aggradations with excessive sediment delivery. As recorded in state government inventories, there were several major and 50 smaller riverbank collapses between Blanchetown and Wellington in 2009. Some of the collapses occurred catastrophically (i.e. soil mass, vegetation and infrastructure rapidly collapsing into the river without warning); while at other locations, collapse occurred less rapidly (Miller and Sias, 1998).

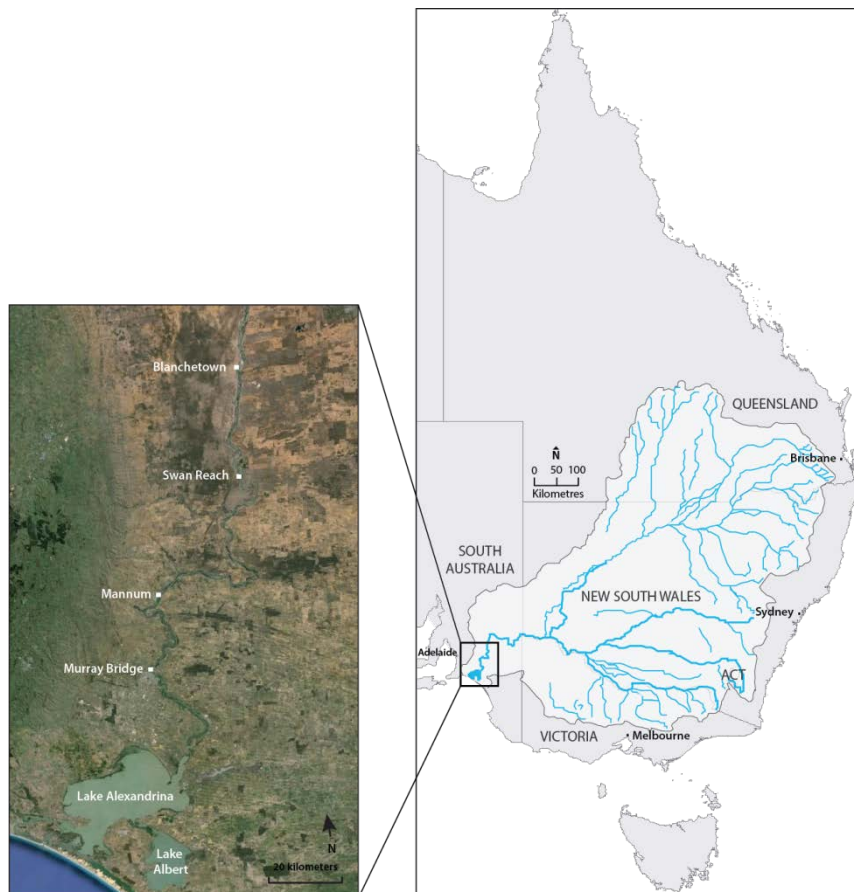


Figure 1.1 Overview of the River Murray and the study area.

Riverbank slope failures, as shown in Figure 1.3, are influenced by several factors:

- climatic, such as precipitation and evaporation;
- river level fluctuation;
- geological factors, including soil and rock properties;
- topographical factors, including slope gradient, aspect and angle;
- riparian vegetation (grasses/woody species); and
- land use/cover factors, including infrastructure.

In practice, probabilistic, deterministic, statistical, empirical and monitoring are five major approaches that are often used for slope instability assessment (Hartle'n and Viberg, 1988). The stability of a slope is usually assessed using conventional limit equilibrium methods (LEM) and finite element methods (FEM) in a deterministic or probabilistic framework, accompanied by site exploration to acquire the geotechnical data to support calculations.

However, when the areas of research expand to a regional scale, hazard assessment and mapping become complex and difficult due to the time and effort required for the manual handling and processing of the data (Dhakal et al., 1999). Furthermore, the results become inaccurate because the subsoil profiles and the land-use distributions and topographies often vary significantly due to the increasing scale.

To account for these spatial variabilities and to facilitate the analysis and mapping of slope instability, a geographical information system (GIS) based model can be adopted which provides:

- spatial data pre-treatment;
- spatial visual interpretation;
- spatial item vectorisation; and
- database construction incorporating both probabilistic and deterministic methods.

The GIS can assist researchers obtain better information in two and three-dimensional space, which leads to improved decision making. In a GIS, data

about real-world objects are linked to a map. Geographical features are accessed and displayed quickly and can be presented using different information in the database.

Recently, GIS technology has greatly facilitated the handling, processing, analysing and reporting of data (Burrough, 1986; Aronoff, 1989; Marble, 1990). In addition, with the development of remote sensor (RS) technology, more and more data have become available in a high resolution digitised format (such as LiDAR based topographical maps; soil maps; digital elevation models; and land use/cover maps). These high resolution data provide high-precision, more reliable, comprehensive and multifunctional treatment options for spatial and temporal analysis in GIS.

Recently, GIS technology has greatly facilitated the handling, processing, analysing and reporting of data (Burrough, 1986; Aronoff, 1989; Marble, 1990). In addition, with the development of remote sensor (RS) technology, more and more data have become available in a high resolution digitised format (such as LiDAR based topographical maps; soil maps; digital elevation models; and land use/cover maps). These high resolution data provide high-precision, more reliable, comprehensive and multifunctional treatment options for spatial and temporal analysis in GIS.

This report on the current study provides a brief review of the research into slope stability and the riverbank failure process, including the influence of vegetation root effect. It introduces the GIS approach to landslide hazard mapping and then identifies the key research areas and knowledge gaps related to the project.

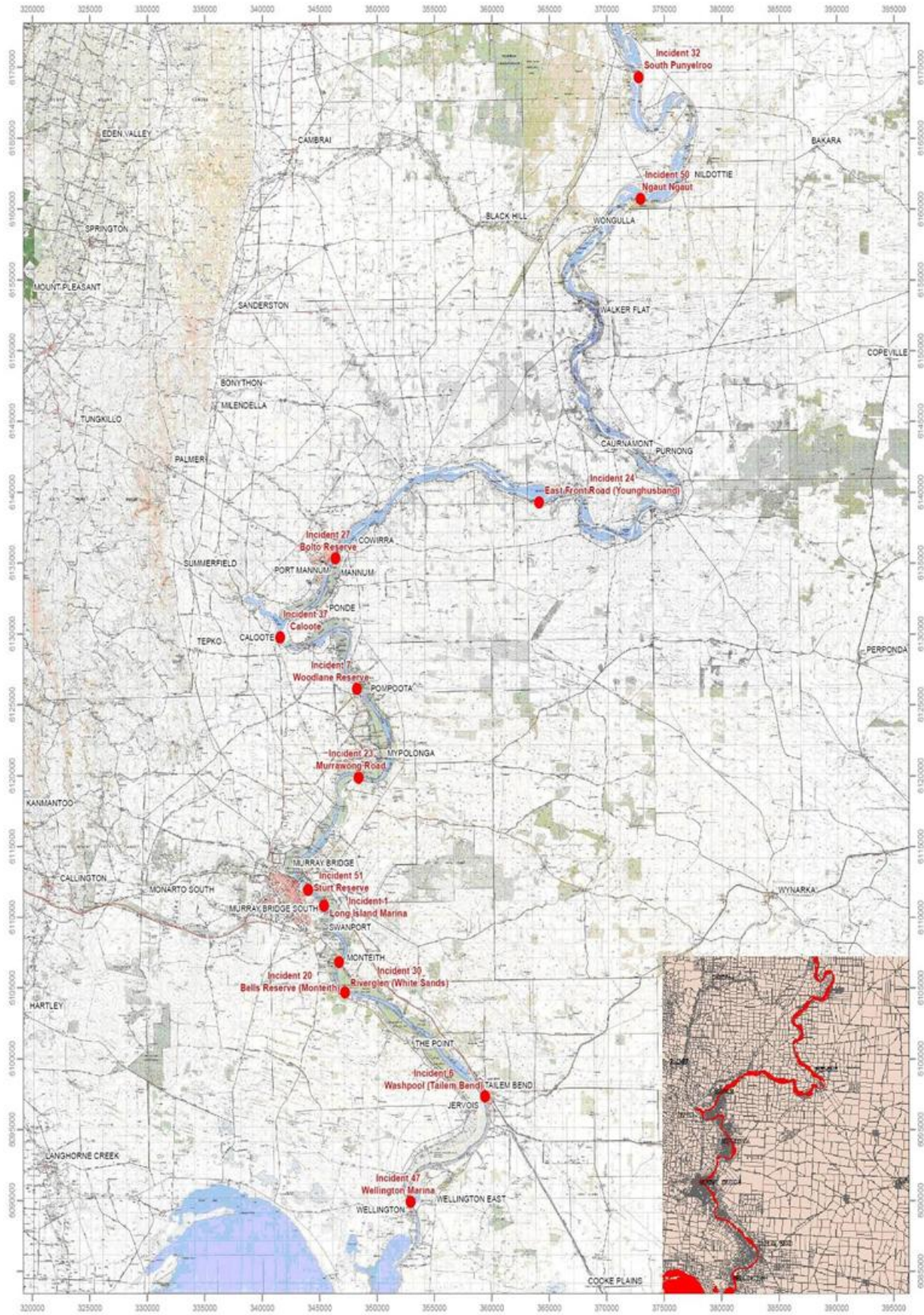


Figure 1.2 Overview of Lower River Murray (Source: SKM, 2010).

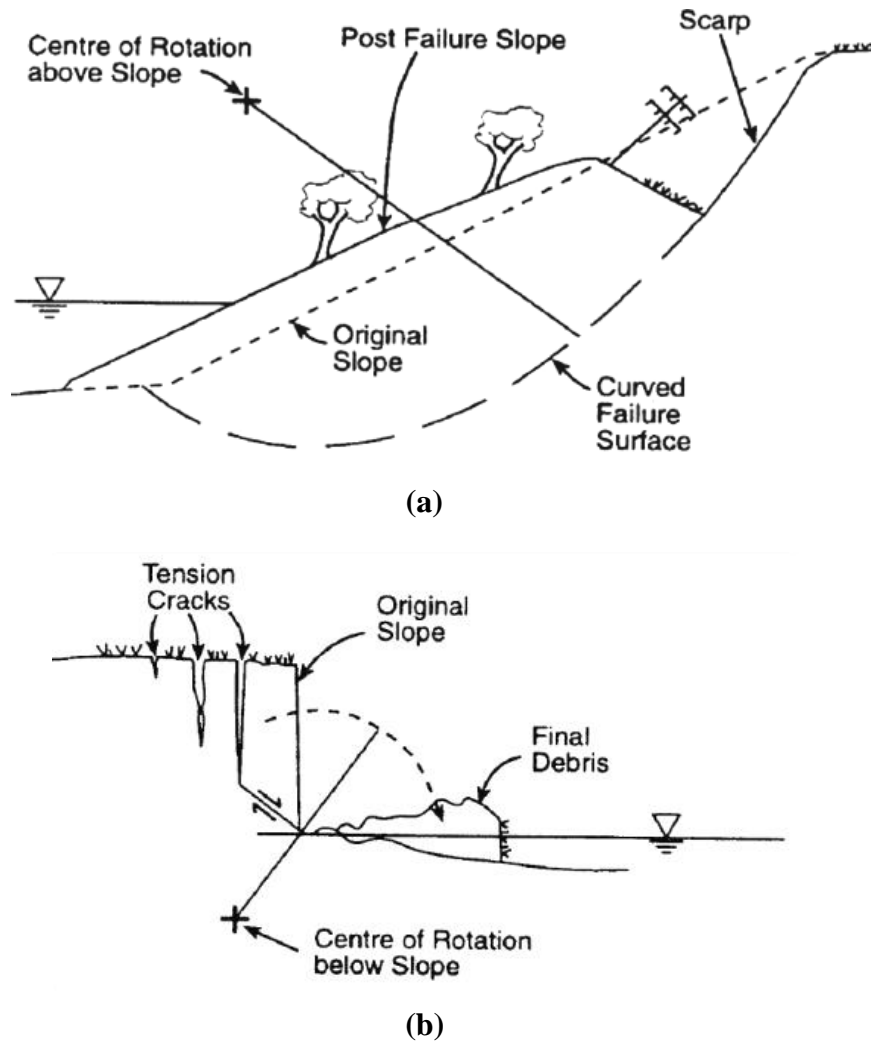


Figure 1.3 Slope failure on riverbanks (a) rotational slip on over-steepened riverbanks, (b) slab failure on over-heightened riverbanks (Source: Thorne, 1999).

1.2 Research Aims

This research study aims to address the following:

1. Examine the failure mechanisms affecting riverbank collapse along the Lower River Murray and identify the most relevant mechanism;
2. Identify potential triggers for riverbank collapse events that should be monitored and managed in the future;

3. Develop a framework, incorporating spatial information, GIS and geotechnical data, to facilitate the prediction of riverbank collapse along the 210 kilometres of the Lower River Murray (between Blanchetown and Wellington, South Australia); and
4. Develop a framework, based on GIS and geotechnical data, to identify regions susceptible to high risk of riverbank collapse along the Lower River Murray.

1.3 Layout of Thesis

This thesis consists of seven chapters and is in the format of a thesis by publication. As is evident, Chapter 1 provides a brief introduction to this research. In Chapter 2, a review of the literature that is related to this research is presented including: methods of slope stability analysis; failure processes; effects of vegetation root reinforcement; and the GIS approach to landslide hazard mapping. Chapters 3, 4, 5 and 6 include four published and/or submitted journal papers, which contain the kernel of the research undertaken in this study.

Chapter 3 includes a journal paper published in *Australian Geomechanics* and presents sensitivity study which is based on the proposed framework, as mentioned above. The sensitivity analysis was conducted adjacent to Long Island Marina with two different river levels: 0 and 0.5 m AHD and 21 cross-sectional models using the results of back-analyses. The results of this work have demonstrated that a section of the riverbank has marginal stability, whereas a number of cross sections adjacent to the study site are susceptible to riverbank collapse and require further investigation. In addition, it was observed that increased river levels generally stabilise the riverbanks but to a limited extent.

Chapter 4 includes a journal paper published in *Computers and Geotechnics* and presents sophisticated, transient and unsaturated slope stability analyses in 2D and 3D, which is also based on the proposed framework as mentioned

above. The study modelled the most significant riverbank collapse incident, which occurred at Long Island Marina, Murray Bridge, South Australia, on 4 Feb. 2009. These analyses yielded excellent predictions of the collapse when compared with the recorded date of collapse and dimensions of the failed region. A parametric study was undertaken to examine the influence and sensitivity of river level fluctuations and climatic factors on riverbank stability. The results indicated that river fluctuations, rather than climatic factors, dominate the likelihood of riverbank collapse along the Lower River Murray. However, extreme rainfall events, coinciding with medium to high river levels, are also likely to trigger riverbank collapse. Moreover, sudden or rapid drawdown scenarios were also examined. The results showed that sudden or rapid drawdown can also precipitate riverbank collapse.

Chapter 5 includes a journal paper submitted to *Australian Geomechanics* and presents transient and unsaturated slope stability analyses performed on four sites where major riverbank collapses were recorded (East Front Road; Woodlane Reserve; River Front Road and White Sands) along the Lower River Murray. The study outlined the framework implementation and demonstrated the efficacy of this framework and the accuracy of the predictions. The results of back-analysed soil shear strengths at the four sites show excellent consistency with those obtained from the results of the geotechnical site investigations adjacent to the collapse sites, and can be readily used in further simulations. The model validation demonstrated that the adopted framework provides reliable riverbank stability predictions and is recommended to be adopted in other similar studies.

Chapter 6 includes a journal paper submitted to *Computers and Geotechnics* and presents a topographically-based framework that can be used to identify the areas at high risk of riverbank collapse over large regions prior to undertaking detailed cross-sectional modeling or site investigation. Two topographical parameters (the effective height of the riverbank, H , and the bank inclination, α) are adopted and been shown to be appropriate indicators in predicting the riverbank instability along the Lower River Murray. A total of 69 cross-sectional models were developed and analysed within the study

area which greatly improve the understanding of topographical factors that influence riverbank stability. Moreover, a detailed susceptibility map of the Lower River Murray is presented.

Finally, in Chapter 7, the outcomes and contributions of this thesis are summarised. In addition, limitations of this research study, as well as recommendations for future related research, are discussed.

Chapter 2

2 Literature Review

This chapter presents a review of the literature relevant to the geotechnical modelling and assessment of riverbank stability. The chapter examines the methods used for slope susceptibility assessment and the calculation of factors of safety, riverbank failure processes, the influence of vegetation on slope stability and geographical information systems (GIS) approaches to landslide hazard mapping.

2.1 Methods for slope susceptibility assessment

Generally speaking, the methods adopted for slope susceptibility assessment can be either direct or indirect, and can be divided into two main classifications: qualitative and quantitative. There are many approaches that can be employed to assess slope stability and landslide hazards with different requirements to be emphasised in different situations (Sidle et al., 1985; Dietrich et al., 1986; Montgomery and Dietrich, 1988; Montgomery and Dietrich, 1989; Carrera et al., 1991; Dietrich et al., 1992; Sidle, 1992; Dietrich et al., 1993; Montgomery and Dietrich, 1994; Wu and Sidle, 1995; Pack, 1995).

There are four widely used methods by which slope stability is usually assessed. The choice of method depends on various characteristics of the slope, including situations where the stability is probably controlled by surface topography through shallow subsurface flow convergence; or partly controlled by soil saturation index fluctuations; sometimes by porewater pressure fluctuations; or by soil shear strength changes (Montgomery and Dietrich, 1994). Currently, there are 4 main categories of assessment methodologies by which to assess slope stability, namely: (1) field inspection

with empirical experiences to help identify sites susceptible to landslides, accompanied by the predictions made from analysis of landslide inventories; (2) multivariate analysis of physical influencing factors; (3) stability ranking with statistical analysis based on criteria such as slope, lithology, land use form, or geology structure and (4) probability analysis of slope failure based on slope stability models with hydrologic simulations. The more detailed categories of assessment methodologies are shown in Figure 2.1.

2.2 Methods for calculating the factor of safety

2.2.1 Introduction

Once the geometry and the subsoil conditions, including the groundwater level beneath a slope, have been determined, the stability can be assessed using either published chart solutions or numerical modelling (Abramson et al., 2002). The methods include the use of the limit equilibrium method (LEM) to analyse two-, and sometimes three-dimensional slope models; some complex numerical methods that employ finite element methods or boundary element methods, especially, the probabilistic slope stability analysis models such as: the first order second moment (FOSM); Rosenblueth's (1975) point estimate method; Monte Carlo simulation; and considerations for incorporating spatial variability into the finite element method (Abramson et al., 2002).

2.2.2 Conventional calculation

Conventionally, in slope stability analysis, the failure surface along which sliding occurs is speculated and an analysis is then performed to determine the shear forces acting on the failure surface and the shear resistance that the soil can mobilise against sliding (Craig, 2004). A factor of safety, FS , against failure is then calculated as the ratio of forces opposing motion to the forces causing motion, that is:

$$FS = \frac{\text{Forces opposing motion}}{\text{Forces causing motion}} = \frac{\text{Shear resistance against sliding}}{\text{Shear force acting on the failure surface}} \quad (2.1)$$

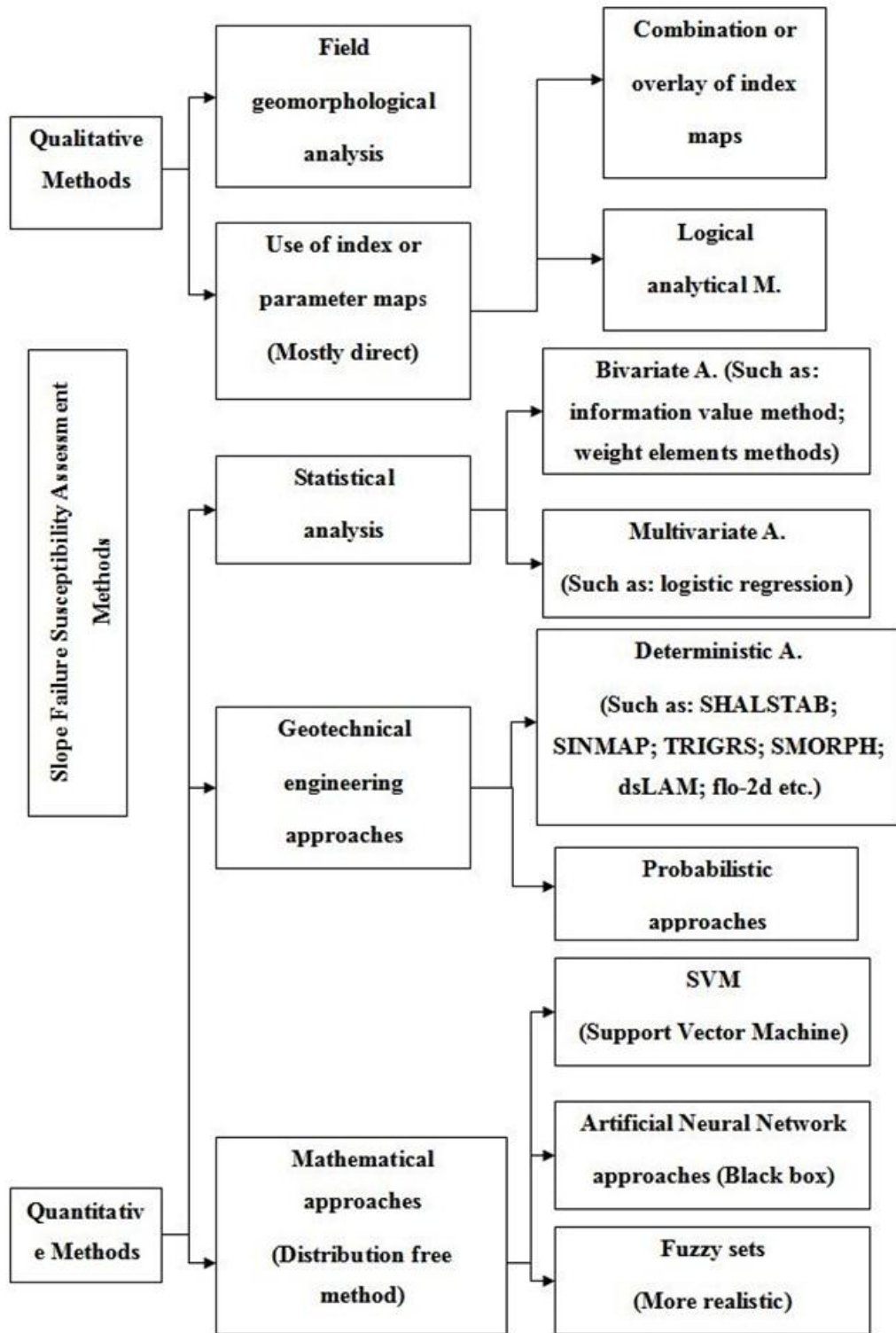


Figure 2.1 Proposed classification of slope failure susceptibility assessment methods

(Source: Aleotti and Chowdhury, 1999).

FS is calculated for a number of speculated or known potential sliding surfaces, and the minimum value is taken as the factor of safety against slope failure. A $FS < 1$ is indicative of instability. When $FS = 1$, these forces are exactly balanced, and any slight increase to the forces causing motion, or slight reduction to the forces opposing the motion can result in instability (DFW, 2010). As FS increases beyond unity, the slope becomes more stable.

In practice, to suit different conditions and the requirements of the research, the FS criteria can be modified because the various methods differ in their assumptions and the manner in which equilibrium conditions are satisfied. Based on Equation (2.1), a wide variety of methods have been developed for slope stability analysis with different kinematics associated with each (e.g. Sowers, 1979; Whitlow, 1990; Fang, 1991; Montgomery and Dietrich, 1994; van Westen and Terlien, 1996; Centre for Geotechnical Research, 1998; Burton and Bathurst, 1998; Pack et al., 1998, 2001; Borga et al., 2002; Saha et al., 2002; Dhakal and Sidle, 2004; Craig, 2004).

In most common use in geotechnical engineering is the limit equilibrium method (LEM) and several commercial software packages are available which utilise this approach. The majority of stability analyses are carried out in terms of effective stresses in problems where changes in porewater pressures take place. Because of the variations in these stresses along a trial slip surface, the slip mass is considered as a series of slices, as shown in Figure 2.2, where W = the body weight of the slice; N' = the effective normal reacting force at the base of the slice; T = the shearing force induced along the base = $W \sin \alpha$; R_1 and R_2 = forces imposed on the sides from adjacent slices, which may be resolved into: E_1 and E_2 = normal interslice forces; and X_1 and X_2 = tangential interslice forces (Whitlow, 1990). A trial slip circle is selected having a centre, O , and a radius, R , and the horizontal distance between the two ends A and B divided into slices of equal breadth, b (Whitlow, 1990).

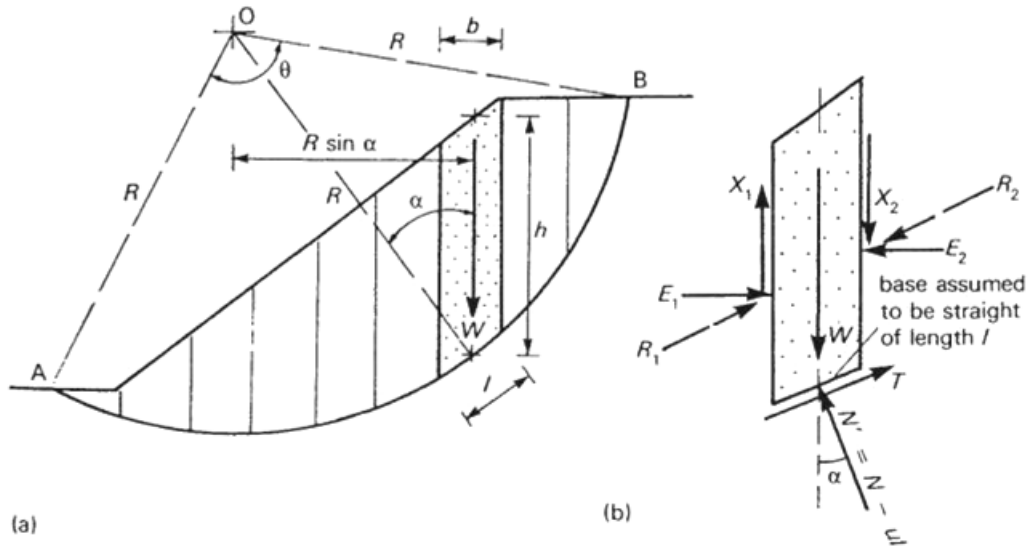


Figure 2.2 Method of slices: (a) division of slip mass; (b) forces on a slice
(Source: Whitlow, 1990).

The simplified LEM is based on two assumptions:

1. The soil mass is discretised into several vertical slices in the direction normal to the plane of the section. The forces at the ends of each slice are negligible; that is, a purely two-dimensional approach is adopted.
2. The Coulomb failure criterion applies. The factor of safety, FS , is defined such that, when c' and $\tan \phi'$ are replaced by c'/FS and $\tan \phi'/FS$, the conditions become those of limiting equilibrium. It is also assumed that all slices have the same FS .

The effects of any surcharge loading on the surface must be included in the computation of the body weight and other forces. If a number of K slices is assumed, then:

$$\text{Total disturbing force} = \sum_{i=1}^k w_i \sin \alpha_i \quad (2.2)$$

$$\text{Total resisting shear force} = \sum_{i=1}^k \tau_i l \quad (2.3)$$

In terms of effective stresses:

$$\tau = c' + \sigma'_n \tan \phi' \quad (2.4)$$

and

$$\bar{d} = c'l + N' \tan \phi' \quad (2.5)$$

Therefore:

$$FS = \frac{\sum_{i=1}^k c'_i l + \sum_{i=1}^k N' \tan \phi'}{\sum_{i=1}^k w_i \sin \alpha_i} \quad (2.6)$$

Note that the *FS* being calculated by Equation (2.6) depends on the manner in which the values of *N'* are obtained. From Equation (2.6), it is apparent that long-term (drained) shear parameters, *c'* and ϕ' , are used to determine the *FS*. However, the analysis of the riverbank failures, undertaken by several external consultants, has shown that collapses along the Lower Murray can be explained by short term (undrained) instability resulting from lowered water levels. The basis of this is an assumption that, even though the time scale involved is 2 to 3 years, the low permeability of the clayey soils suggests that undrained conditions are likely to be relevant. This research will examine this possibility in greater detail in Phases 3 and 4.

The role of effective stress on riverbank stability can be explained by Equation (2.6). A rise in groundwater level, and hence the porewater pressure, will reduce the effective normal stress, *N'*, which in turn reduces the shear resistance against sliding and the factor of safety. On the other hand, a drop in groundwater level, and hence the porewater pressure, will increase the effective normal stress, *N'*, and hence increase the shear resistance against sliding and the factor of safety. Fluctuations in river level directly affect groundwater levels.

The shear strength of soils increases with consolidation under load. The soils below the water level are generally normal-consolidated. However, the clays at levels well above the water level are usually over-consolidated as a result of desiccation. As the clay dries out, the capillary tension in the porewater rises (matric suction) and can become quite large and cause the soil to shrink. Desiccation is a common factor in over-consolidation and tension cracking.

2.2.3 Infinite slope stability calculation

The infinite slope method is used to calculate the slope stability factor (Skempton and DeLory, 1957), which relates to a slope that extends for a relatively long distance with a consistent soil and groundwater profile. The method assumes an infinite slope and a failure plane parallel to the slope surface.

For cohesive-frictional ($c-\phi$) soil in a fully saturated condition, the same limit equilibrium concept can also be applied to determine FS , as shown in Figure 2.3. As depicted in Figure 2.3, U represents the porewater force; and S is the effective normal force, determined as follows:

$$S = c'b \sec \beta + (N - U) \tan \phi' \quad (2.7)$$

and $W = \gamma_{sat}bh$. Therefore, FS can be obtained as follows:

$$FS = \frac{c' + h(\gamma_{sat} - \gamma_w) \cos^2(\beta) \tan \phi'}{\gamma_{sat} h \sin \beta \cos \beta} \quad (2.8)$$

where $\gamma' = \gamma_{sat} - \gamma_w$. For $c' = 0$ soil, the above expression may be simplified to:

$$F = \frac{\gamma'}{\gamma_{sat}} \cdot \frac{\tan \phi'}{\tan \beta} \quad (2.9)$$

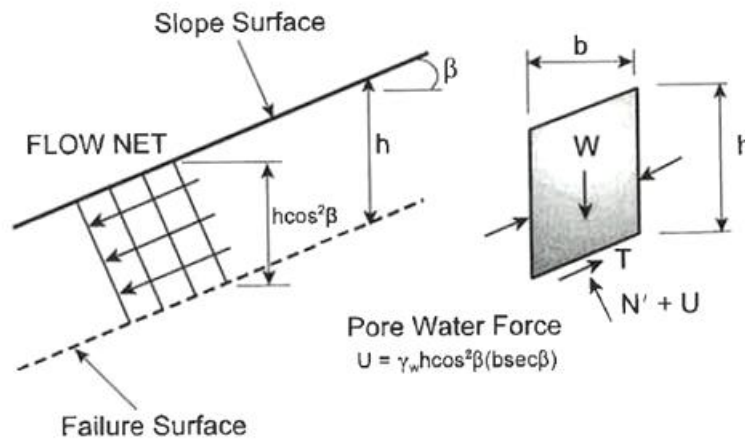


Figure 2.3 Infinite slope failure in $c-\phi$ soil with parallel seepage (Source: Abramson et al., 2002).

From Equation (2.9), it is clear that FS is independent of the slope height and depth, h , but is reduced by the parameter $\frac{\gamma'}{\gamma_{sat}}$. For typical soils, this reduction will be 50% for fully saturated conditions when compared to dry conditions (Abramson et al., 2002).

2.2.4 Finite slope stability calculation

The finite element method (FEM) is a relatively new and more powerful method for slope stability calculation, which was first introduced to geotechnical engineering by Clough and Woodward (1967). Compared with the conventional simple LEM, the FEM cannot only resolve problems, such as newly constructed embankments, recent excavations or an existing natural slope like the conventional method, but can also account for K_0 (the ratio of lateral to vertical normal effective stresses), which is ignored in conventional limit equilibrium procedures (Chowdhury, 1981).

Compared with the conventional method, the use of the FEM has been limited to the analysis of complex earth structures, such as large earth dams (Duncan, 1996). This is because the quality of the FEM is directly dependent on the ability of the selected constitutive model to simulate realistically the nonlinear behaviour of the soil within the slope (Abramson et al., 2002). The FEM therefore refers to more sophisticated concepts and typically requires more work in determining model parameters, performing the computer analyses and evaluating the results (Duncan, 1996).

As shown in Figure 2.4, the FEM essentially divides the slope surface into discrete units called elements. Each node and predefined boundaries of the continuum, as shown in Figure 2.4, connects the neighbouring elements. The displacement method formulation of the FEM is typically used for geotechnical applications and presents results in the form of displacement, stresses and strains at node points (Abramson et al., 2002). In the FEM, the soil on the failure surface is modelled as numerous discrete elements, and the failure mechanism of these discrete elements is considered as a progressive

phenomenon because not all elements fail simultaneously. The failure range can therefore extend from the point where yield first occurs to the final failure state where all elements have totally failed (Wong, 1984).

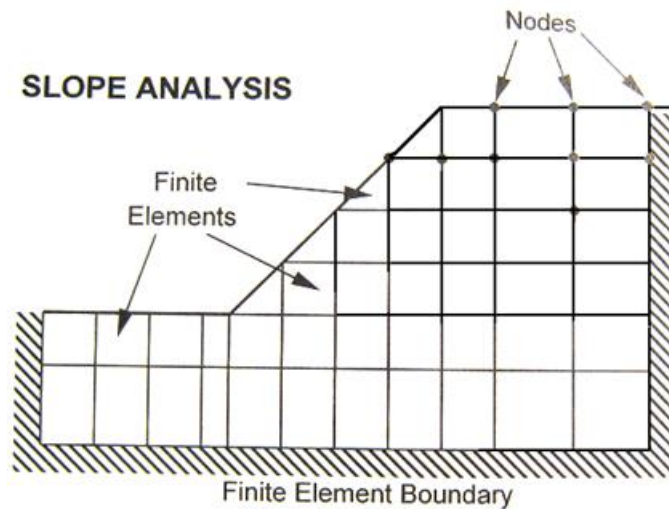


Figure 2.4 Definitions of terms used for finite element method (FEM)
(Source: Abramson et al., 2002).

The FEM was first applied to slope stability analysis by Duncan and Dunlop (1969), who referred to it as the *limit shear failure criterion*. These researchers directly used the computed FEM stresses along a potential failure surface in order to estimate the *FS* value which would correspond to the ratio of available strength along the failure plane compared to imposed stresses (Duncan and Dunlop, 1969). Zienkiewicz (1971) later defined another failure criterion for the FEM referred to as non-convergence of the solution, as the shear strength parameters are reduced until non-convergence or a wide range of failures occur; and the *FS* can be reported as the ratio of the actual available strength to the lowest strength value. Zienkiewicz's (1971) approach has been used in more recent research by Dawson et al. (1999) and Griffiths and Lane (1999).

Based on the elasto-plastic soil model, Smith and Hobbs (1974) used the FEM for slope stability analysis on $\phi_u = 0$ slopes. After that, Zienkiewicz et al. (1975) and Griffiths (1980) introduced the FEM into $c' - \phi'$ slope stability

analysis, and proved that the method was in good agreement with the results calculated by the conventional LEM. Snitbhan and Chen (1976) specified a maximum tolerable limit for the horizontal displacements of the surface of the slope, and named this new criterion *bulging of the slope line*. Since then, an increasing number of slope stability studies have focussed on the use of the FEM (e.g. Potts et al., 1990; Matsui and Sun, 1992; Jeremic, 2000; Lane and Griffiths, 2000; Lechman and Griffiths, 2000; Sainak, 2004; Zheng et al., 2006; Griffiths and Marquez, 2007; Li, 2007).

More recently, dynamic large deformation finite element (LDFE) approaches, which are based on mesh regeneration have been developed to deal with large deformations and changing geometries within the soil domain (Song et al., 2008, Wang et al., 2010a, Wang et al., 2011, Wang et al., 2013a, Wang et al., 2013b). The LDFE methods use an updated Lagrangian formulation to remesh the soil domain and map the nodal velocities and acceleration, as well as the stresses and material properties at integration points, from the old mesh to the new one. The LDFE approaches combined with extensions (such as RITSS), enhance existing geomechanical analyses, and include simple elastic-perfectly plastic model and the modified Cam-Clay model for coupled analysis (Wang et al., 2008), and a strain-softening rate-dependent Tresca model for total stress analysis (Wang et al., 2010b).

2.2.5 Slope stability classification

As discussed above, the value of the *FS* is that it is used to determine whether a slope is stable or not, and identify the stability class. Previous research has indicated that several considerations influence the selection of *FS* with respect to the slope stability class, such as the:

- uncertainties associated with and the nature of the loading;
- uncertainties associated with and variability of thickness and orientation of the soil layers;
- uncertainties in the measurement and the nature of soil strength in short term and long term loading situations;

- adoption of a reasonable lower quartile strength envelope for data;
- uncertainties in the failure mode;
- climatic influences which may affect soil strength;
- redundancy in the failure mode; and
- consequence of slope failure and the cost of over estimating the *FS*.

The selection of an appropriate *FS* depends on the levels of these uncertainties. For example, if the problem is well understood and the ground exhibits limited variability, a *FS* as low as 1.05 may be acceptable. Usually, in geotechnical engineering, however, only a small volume of the ground is tested and the problem is complex, so higher factors of safety are often adopted. On the other hand, it is because of the uncertainties described above, that the *FS* has limited value. For example, Figure 2.5(a) shows a situation where the applied load and the strength (resistance) of the soil exhibit large variability, as evidenced by the wide probability distribution functions. The overlapping area represents where the load exceeds the resistance and, hence, is the *probability of failure*. In contrast, Figure 2.5(b) shows the situation where the applied load and the strength exhibit less variability, perhaps due to a more detailed site investigation or a more homogeneous soil, and the resulting probability of failure is smaller. The *FS* in both cases, however, is identical and is not affected by uncertainties (Lee et al. 1983).

The literature recommends a long term *FS* equal to 1.5 as a minimum for slopes. Based on the work of Ray and de Smedt (2009) suggested stability classes are given in Table 2.1. Slopes are denoted as unstable for cases in which *FS* is less than 1, quasi stable if *FS* is between 1 and 1.25, moderately stable if *FS* is between 1.25 and 1.5, and stable if *FS* is larger than 1.5. This study will examine the geotechnical data gathered from site investigation and the analyses, and recommend factors of safety to be adopted for classification of riverbank stability. Where possible, the probability of failure will also be evaluated.

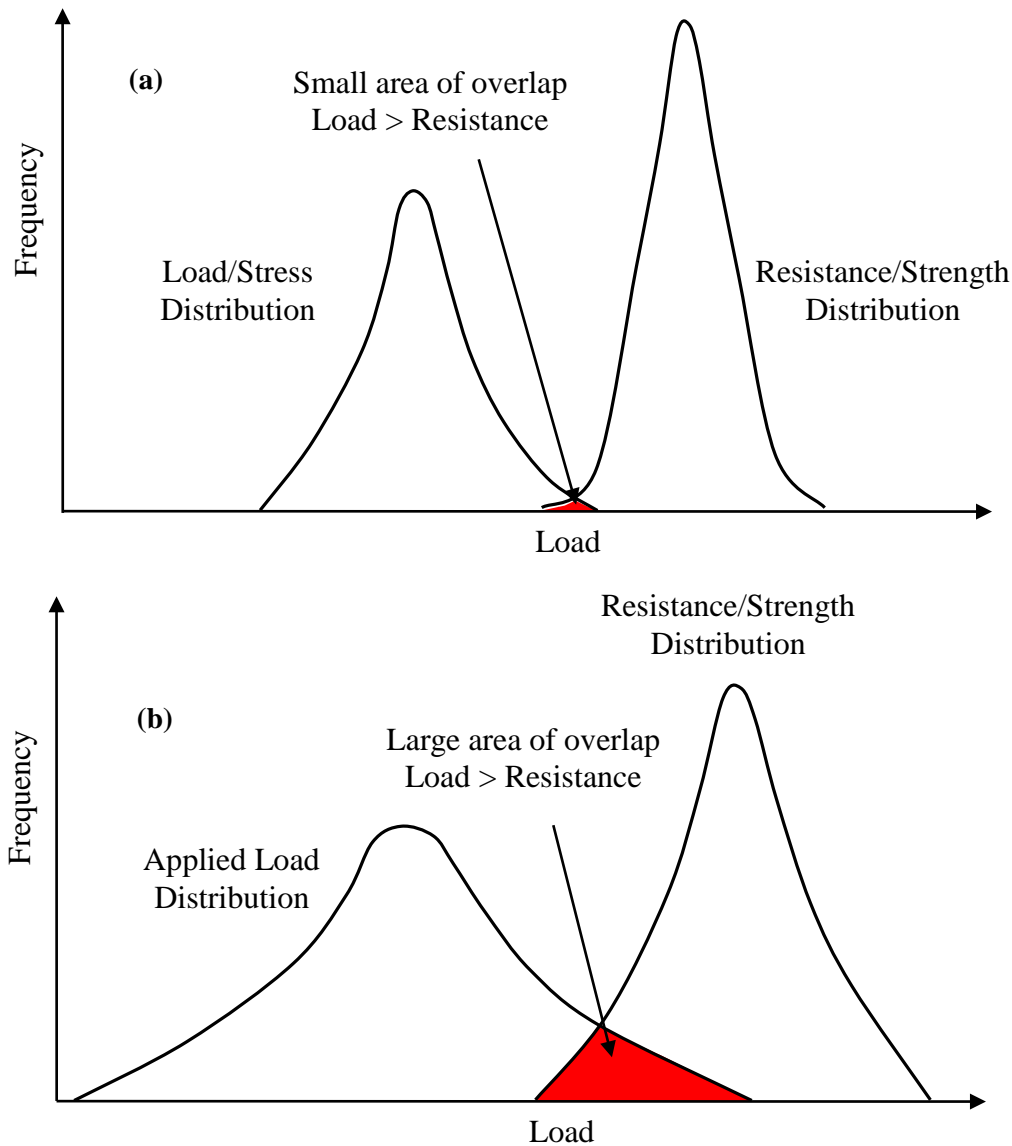


Figure 2.5 Limitation of *FS* compared with probability of failure.

2.2.6 Groundwater and subsurface flow

A rise in the groundwater table is generally considered to be a trigger mechanism for slope instability, because it raises soil saturation levels and increases porewater pressure, leading to the reduction of normal effective stresses and also the shear strength along potential failure surfaces (Ray and de Smedt, 2009). On the other hand, lowering of the river level in the Lower Murray has been found to cause slope instability; one of the reasons being the lower river level increases seepage flow pressure towards the river due to an increase in head difference.

Table 2.1 Slope stability classes (modified from Ray and de Smedt, 2009).

Safety factor	Slope class	stability	Remarks
$FS > 1.5$	Theoretically stable		Only major destabilizing factors cause instability
$1.25 < FS < 1.5$	Moderately stable		Moderate destabilizing factors cause instability
$1 < FS < 1.25$	Quasi stable		Minor destabilizing factors can cause instability
$FS < 1$	Unstable		Stabilizing factors are needed for stability

Various slope stability models, which incorporate water seepage, have been proposed by a number of researchers. An example has been discussed earlier in §2.2.3. However this method, which is based on the assumption of an infinite slope and is used widely in hill- and mountain-slope stability analysis, may not be suitable for riverbank stability analysis. Hubble et al. (2010) highlighted two ways in which they are different. Firstly, the scale of a riverbank slide feature is generally less than, but similar to, the size of the entire slope – riverbank slump commonly occupies more than 60% of the slope length (Abernethy and Rutherford, 2000). Secondly the hydrological conditions which contribute to failure are usually different, with overbank flooding saturating the soil mass and sometimes followed by rapid drawdown (e.g. Hubble and Hull, 1996, 2004), rather than direct infiltration of rainfall followed by groundwater flow. The typical riverbank failure mechanisms observed in the SKM (2009) report are deep rotational failure followed by slab failures. These types of failures also suggest that the infinite slope method is inadequate for the analysis of riverbank stability. For these reasons, it is recommended that the modelling of groundwater flow in the riverbank stability analysis in Phases 3 and 4 of this study will be undertaken using more sophisticated techniques, such as the finite element (FE) method.

There are a number of commercial FE packages available which model seepage in soil and groundwater flow. For example, SVFlux is a versatile 1D, 2D, axisymmetric and 3D FE program for modelling saturated and unsaturated groundwater flow with climatic coupling. The historical rainfall and river level data can be employed to study the change soil moisture, groundwater level, seepage flow due to seasonal fluctuations, as well as the suction (negative porewater pressure) change due to changes in soil moisture. The seepage porewater pressures obtained from SVFlux can subsequently be incorporated into SVSlope – a 2D/3D slope stability program based on limit equilibrium analysis and the FE method. Data from boreholes, CPTs and piezometers may also be used to build a sophisticated groundwater models.

As mentioned above, lowering of the river level in the Lower Murray increases seepage flow pressures towards the river due to an increase in head difference, particularly where there are lagoons adjacent to the sites. The amount of increased seepage flow also depends on the soil's permeability. Field investigation data obtained by SKM (2010) showed the riverbanks along the Lower Murray are comprised of Silty Clays, Silty/Clayey Sands, Silty/Clayey Gravels and Fills. Typical soil profiles (at sites such as Riverfont Road, Murray Bridge, Caloote and Woodlane Reserve) are comprised of a layer of Silty Clay that is underlain by a layer of Silty/Clayey Sands or Clayey Sand/Sandy Clay. A layer of engineering fill (comprising mainly Silty/Clayey Sands) can be found at the ground surface of reclaimed sites. The Silty Clay layer was typically encountered at depths of 1 m to 2.5 m below ground level, and is described as very soft and wet with a moisture content close to the liquid limit. This normally consolidated Silty Clay layer is highly impermeable but does contain some permeable sand lenses and is highly expansive.

Fluctuations in groundwater level can have significant effects on expansive clays. A highly expansive, or reactive, soil means that shrinkage cracks can develop at the surface and extend to the depth of the water table due to drying as the result of increased surface temperatures and evaporation at depth. The seasonal moisture zone in the River Murray area is approximately 4 m in

depth, so when the groundwater table drops, shrinkage cracks follow. These shrinkage cracks can subsequently fill with surface water which can initiate failure from the crest as a result of rainfall. Tree roots also exacerbate shrinkage in reactive soils. The FE method can be used to model the variation of saturated and unsaturated groundwater flow due to rainfall, groundwater, river level fluctuation, vegetation, suction and other factors. Furthermore, the role of progressive failure and possible effects due to changes in geochemistry (pH, salinity) of porewater, which can be significant in clayey soils, can also be examined using this method.

2.3 Failure processes

2.3.1 Introduction

There are different types of slope failure processes, which are controlled and influenced by a variety of factors. For instance, shallow landslides of soil slopes and deep landslides of rock slopes are controlled by different physical subsurface materials, just as planar failure and rotational failure are controlled by different slide mechanisms. For this reason, categorising failure processes is essential prior to landslide susceptibility assessment and hazard mapping. Among numerous criteria for categorising failure processes suggested by various researchers, the categories proposed by Varnes et al. (1984), Hutchinson (1988) and the Working Party commissioned by the International Consortium on Landslides (ICL) for World Landslide Inventory (Sassa, 2004) are the most relevant and internationally recognised.

Bank erosion problems are rarely the result of a single process or mechanism, but rather are usually the result of complex interactions between a number of processes and mechanisms that may operate on the bank either simultaneously or sequentially (Thorne et al. 1996). These can be grouped into three broad categories:

- 1) **Erosion processes** which detach, entrain and transport individual particles or assemblages of particles away from the toe of the face of the retreating bank;
- 2) **Failure mechanisms** which lead to collapse of all or part of the bank; and
- 3) **Weakening processes** which operate on and within the bank to increase its erodability and, hence, to reduce its geotechnical stability.

The following sections deal in turn with erosion processes, failure mechanisms and processes of weakening, and consider the role that each play in accounting for the problems of bank erosion along the Lower River Murray (SKM, 2009).

2.3.2 Erosion processes

Seven categories of bank erosion are recognised in the literature (Thorne et al. 1996):

- 1) **Parallel flow (fluvial entrainment)** – Sediment is detached and carried away by flow parallel to the bank;
- 2) **Impinging flow (fluvial entrainment)** – Sediment is carried by flow striking the bank at an angle to the long-stream direction;
- 3) **Boatwash** – Sediment is carried away by waves and currents generated by passing boats;
- 4) **Wind-waves** – Sediment is carried away by waves and currents generated by the wind;
- 5) **Rills and gullies** – Banks are eroded by concentrated surface runoff draining across the bank line;
- 6) **Piping** – Subsurface erosion occurs by water draining through the bank; and
- 7) **Freeze/thaw** – Particles and aggregates are loosened by freezing and fall off the bank face during flow or boat wash.

SKM (2009) suggested that effects of flow on the erosion of the bankline (fluvial entrainment) is low as a result of the regulated nature of the Lower Murray. The channel is generally characterised by a low energy flow regime with low shear stresses and cohesive clay banks. Under these circumstances, the potential for fluvial entrainment is limited. SKM (2009) also concluded that there was no field evidence for scouring and undercutting. However, SKM (2009) identified the fluctuations in water level as a result of weir operations, boat wash and wind-waves do appear to be effective in washing away imported sand material from the channel margins. The removal of sand material at artificial beaches and exposure of the underlying clays was noted at a number of locations. SKM (2009) concluded that bankline retreat at sites inspected along the Lower Murray is due mainly to bank slumping into the river. Nevertheless, the possibility of slopes destabilised due to slope undercutting caused by wind-waves and boat wash during low water level periods, as well as the erodibility of silt clays and clayey sands, will be examined in this project.

2.3.3 Failure mechanisms

Seven categories of mechanism responsible for bank collapse can be identified (Thorne et al. 1996):

- 1) **Shallow slide** – Shallow seated failure along a shear plane parallel to and just below the bank surface, typically occurs in weakly cohesive soils, as depicted in Figure 2.6(a) is a shallow failure and (b) a planar failure;
- 2) **Slab failure** – Blocks or columns of soil topple forward into the channel, often with deep tension cracks separating the failure blocks from the intact bank. This represents a severe type of failure involving the movement of large volumes of material and serious bank line retreat, as shown in Figure 2.6(c);
- 3) **Rotational slip** – This is a deep-seated movement of all or part of the bank profile in which a block of soil slips along a curved surface. Similar to slab failures, this is a severe type of failure that involves the

movement of a large volume of material and generates serious bank line retreat. Depicted in Figure 2.6(d) is a rotational failure in homogenous material, (e) a rotational failure with a weak zone, and (f) a massive rotational failure/landslide;

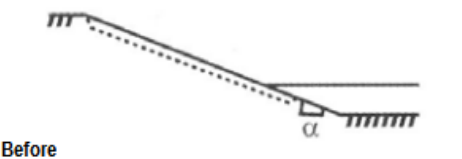
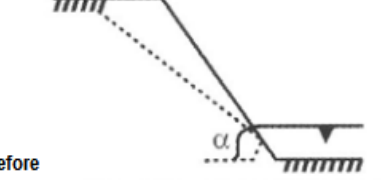

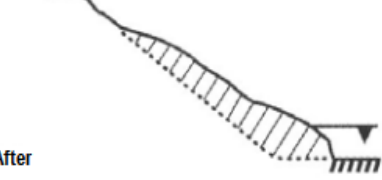
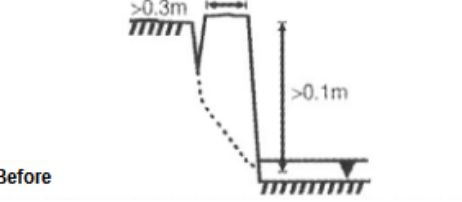
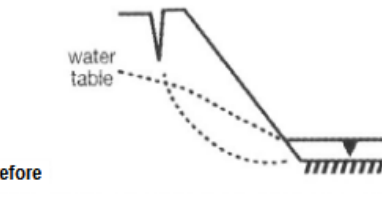
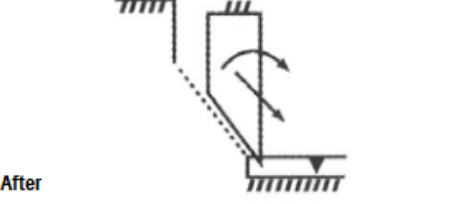

- 4) **Cantilever failure** – Overhanging blocks of soil collapse into the channel by shear, beam or tensile failure. Overhangs are found in layered banks where a resistant, cohesive or root bound layer overlies an erodible, non-cohesive layer. Shown in Figure 2.6(g) is a failure of a composite bank (in tension) and (h) failure of a composite bank (as beam);
- 5) **Soil fall** – Soil falls directly into the channel from a near-vertical or undermined, cohesive bank face. This frequently follows weakening by desiccation, saturation or frost action on a non-vegetated surface;
- 6) **Dry granular flow** – Avalanching of dry, granular bank material down the upper part of a non-cohesive bank. When it occurs in a lower bank, this can cause instability of the upper bank resulting in bank line retreat; and
- 7) **Wet earth flow** – Liquefaction and flow of a section of bank due to saturation and high pore water pressures. This can result in rapid bank line retreat in zones of strong seepage and poor drainage.

Of these bank failure modes, deep rotational slips and slab failures appeared to be the main mechanisms causing the large failures and retreat of bank lines at sites inspected along the Lower Murray. These two modes of failure can also occur together and sequentially, with a large rotational slip forming a steep face which then continues to retreat through slab failures. These types of bank failure modes appear to have occurred at Long Island Marina and Woodlane Reserve, and they represent the most severe form of bank failure. They represent a serious form of instability, which is deep and below the riparian vegetation root zone. Significant engineering intervention through re-profiling and improved drainage to increase bank stability will be necessary to mitigate bank line retreat (SKM, 2009).

2.3.4 Weakening factors

Six categories of factors responsible for decreasing the erosion resistance and mechanical stability of a riverbank have been broadly identified in the literature (Thorne et al. 1996):

- 1) **Leaching** – Leads to a weakening of the bank through a reduction in cohesion that occurs when minerals are removed by groundwater percolating through the bank. The removal of minerals and change in pH level may induce progressive failure at the micro-level in clayey platelets, forming ‘face to face’ bonds rather than ‘edge to face’. This slow and long process changes the geochemistry (pH, salinity) of the porewater, which can be significant in clayey soils, will be explored in this project.
- 2) **Trampling** – Destruction of soil fabric by crushing under the weight of pedestrians or grazing animals.
- 3) **Destruction of riparian vegetation** – Damage or destruction of riparian vegetation by a variety of natural processes and human actions.
- 4) **Mechanical damage** – Damage of banks by boat mooring, stock access or angling.
- 5) **Positive porewater pressures** – Occurs when drainage of water through the bank is restricted resulting in a build-up of porewater pressures. This reduces the effective strength of the bank material, weakens the bank and increases the probability of block failure or, in extreme cases, leads to liquefaction and wet earth flow.
- 6) **Desiccation** – Cracking and crumbling of soil due to intense drying that breaks electrochemical bonds and loosens soil peds on the exposed bank surface during hot and dry summers.

 <p>Before</p>	 <p>Before</p>
 <p>After</p>	 <p>After</p>
<p>(a) Shallow failure</p> <ul style="list-style-type: none"> • shallow bank angle • usually in non-cohesive banks • failure nearly parallel to slope at $\alpha = \phi$ • water seepage from bank can substantially reduce stable α • vegetation will normally help stabilise against failure 	<p>(b) Planar failure</p> <ul style="list-style-type: none"> • steep or vertical bank angle • frequently (but not always) in non-cohesive banks • water table/channel water level usually low relative to bank height
 <p>Before</p>	 <p>Before</p>
 <p>After</p>	 <p>After</p>
<p>(c) Planar/slab failure</p> <ul style="list-style-type: none"> • steep or near vertical banks • deep tension cracks • failure occurs by sliding and/or topping • failure more likely if crack fills with water • little affected by groundwater table 	<p>(d) Rotational failure in homogeneous materials</p> <ul style="list-style-type: none"> • usually in moderately high or steep banks • usually in cohesive material • tension crack reduce stability particularly when water filled • significantly affected by position of water tables • failure may extend beyond toe, see also type (e)

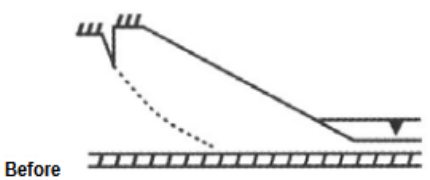
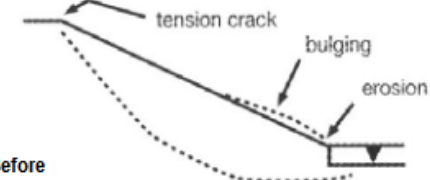
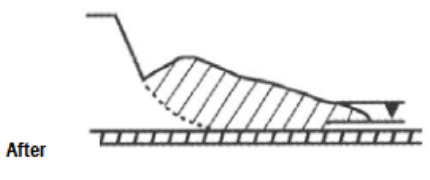
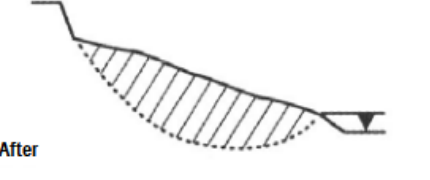
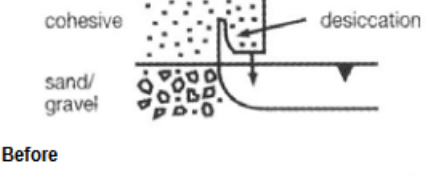
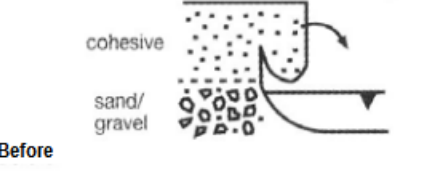
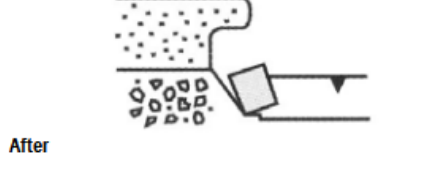
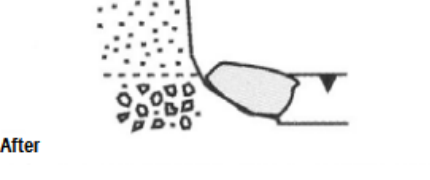
 <p>Before</p>	 <p>Before</p>
 <p>After</p>	 <p>After</p>
<p>(e) Rotational failure with weak zone</p> <ul style="list-style-type: none"> • failure surface dictated by position of weak zone • see all comments for (d) 	<p>(f) Massive rotational failure/landslide</p> <ul style="list-style-type: none"> • erosion of riverbank threatens stability of whole valley side • very large volume of slipped material • tension crack up valley side, bulging above toe, or noticeable movement are signs of potential failure
 <p>Before</p>	 <p>Before</p>
 <p>After</p>	 <p>After</p>
<p>(g) Failure of composite bank (in tension)</p> <ul style="list-style-type: none"> • occurs only where upper cohesive layer overlies erodible sand/gravel • failure by tension of lower part of overhanging rock 	<p>(h) Failure of composite bank (as beam)</p> <ul style="list-style-type: none"> • occurs as type (g) • failure with upper soil in tension, followed by rotation • after failure, block usually remains intact with vegetation towards river • failure can be by shear

Figure 2.6 Bank failure modes (Source: Hey et al., 1991).

In the case of the Lower River Murray, a number of additional factors are noted which are considered significant in decreasing the erosion resistance and mechanical stability of the riverbanks:

- 1) **Construction adjacent to banks** – Construction of infrastructure adjacent to the riverbank, such as jetties, roads and dwellings, increases the imposed load, which increases the likelihood of bank collapse and settlement.
- 2) **Fluctuation of water levels** – Changes in moisture status associated with fluctuating water levels can cause expansion and shrinking of clays and affects the porewater pressures within the banks.

This discussion has been limited by the available information and visual site inspection of a number of sites. Further geotechnical investigations are needed to quantify the role of relevant weakening factors, material properties and bank parameters. These additional investigations and testing will be undertaken as part of Task 3 of this Goyder Institute project.

2.4 Effects of vegetation on slope stability

2.4.1 Background

Riparian vegetation significantly affects the hydrological and mechanical properties of riverbanks (Schwarz et al., 2010), and its presence has both beneficial and detrimental effects on bank stability. Traditionally, however, vegetation has been assumed to have only a minor effect on slope stability. For this reason, it is sometimes ignored by scholars and engineers in conventional *FS* analysis.

Incorporating the effects of vegetation in slope stability analysis was first attempted in the 1960s, although grass, shrubs and trees have been used to stabilise slopes for many years. Terzaghi (1950) treated deforestation as a highly plausible cause of a landslide that occurred in 1915 at Hudson, New York. Following his lead, a few researchers focussed on the effects of

vegetation removal on stream bank stability using quantitative analysis, noting that after deforestation there was a significant increase in the frequency of landslides (Bethlahmy, 1962, Bishop and Stevens, 1964). These pioneering studies, among others, raised awareness of the importance of riparian vegetation on riverbanks, demonstrating that it not only provides ecological benefits, but also offers stabilisation of the riverbank slope, as shown in Figure 2.7 (Abernethy and Rutherford, 1998; Simon and Collison, 2002).

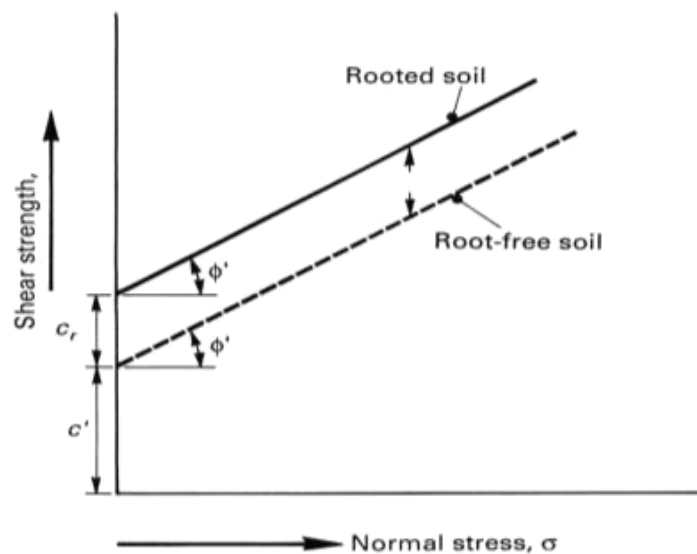


Figure 2.7 Effect of root reinforcement on shear strength of soil
(Source: Coppin and Richards, 1990).

2.4.2 Hydrological effects

The hydrological effects provided by vegetation refer to the change or modification of soil moisture content and porewater pressure caused by the hydrological cycle when woody or grassy species are present. The hydrological effects are beneficial. Firstly, the vegetation canopy intercepts precipitation thereby reducing the amount of rainfall, which infiltrates the slope. Secondly, the plant roots extract moisture from the soil, as shown in Figure 2.8, by means of transpiration. Both processes enhance soil shear strength due to a decrease in porewater pressure in saturated and semi-saturated soils or an increase in matric suction in unsaturated soils (Selby,

1993). Both the decrease of porewater pressure and increase of the matric suction raise the factor of safety (FS).

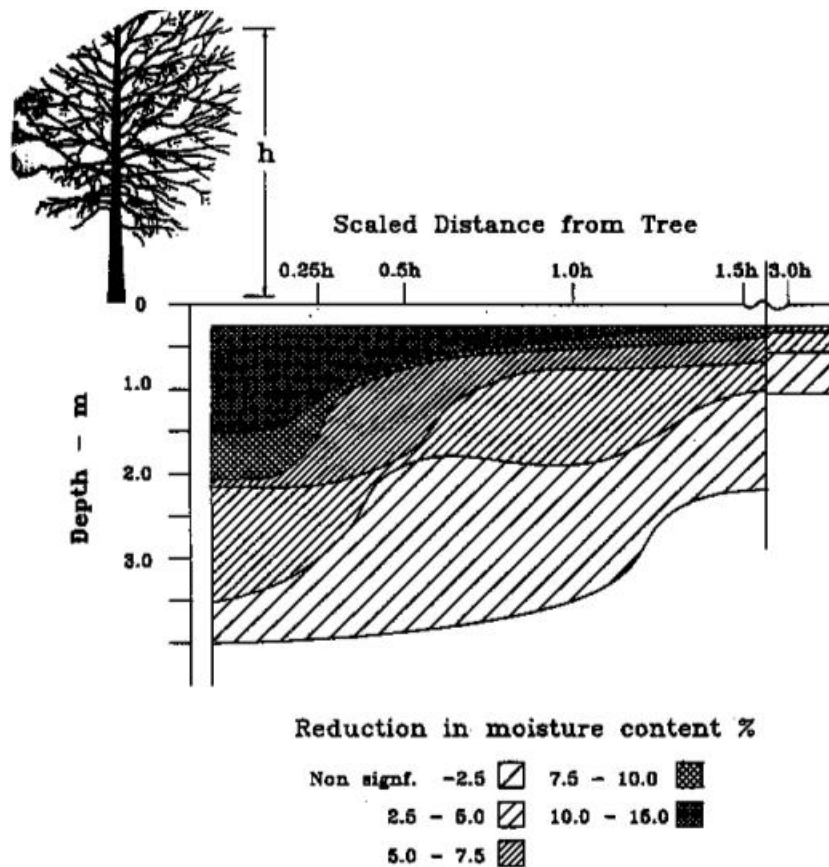


Figure 2.8 Reduction in soil moisture content near a Poplar tree growing in boulder clay (Source: Biddle, 1983).

On the other hand, vegetation can be detrimental to slope stability, due to certain soil infiltration characteristics and biological activities, which act not only on the soil surface, but also at depth. Canopy interception and stem flow tends to concentrate infiltration locally around the stem of the plants, causing higher local porewater pressures at the surface (Durocher, 1990). In addition, the increase of the infiltration rate capacity caused by deep-rooted systems and associated biological activity can accelerate the delivery of water at depth by creating preferential flow paths (Simon and Collison, 2002).

Recent research has shown that the impact of hydrological effects on riverbank stability depends on the types of vegetation and characteristics of the local rainfall. Compared to grassy species, woody species are more efficient in removing soil moisture and preventing rainfall from infiltrating into the soil (Simon and Collison, 2002). The hydrological effects are more significant in wet periods or areas.

2.4.3 Mechanical effects

The mechanical effects are caused by the physical interaction between the vegetation and the soil mass on or under the slope surface. Closely spaced root matrix systems, as shown in Figure 2.9, are able to increase the confining stress in the soil mass and provide reinforcement by transferring the shear stress in the soil to tensile resistance in the root system, as shown in Figure 2.10. Typically, mechanical effects are mostly beneficial because roots anchor themselves into the soil. As a result, the soil mass is bound together by the plant roots and the soil shear strength is increased because of the additional apparent cohesion (Coppin and Richards, 1990).

The detrimental impact of vegetation on bank slope stability is caused by the weight of the vegetation. The weight of large trees applies an additional surcharge to the slope, increasing both the down-slope forces and the confining stress of the soil at the potential slip surface. The locations of trees on the slope surface can have either adverse or beneficial effects on slope stability (Coppin and Richards, 1990). Generally speaking, trees which are located at the toe of a slope benefit slope stability by adding resistance and increasing the frictional component of soil shear strength. On the other hand, if trees are located at the top of slope, the additional load will increase the down-slope forces, thus destabilising the slope.

Furthermore, wind loads imposed on large trees can cause an increase in the driving force acting on the slope. The wind load is transmitted to the soil, becoming a driving force that ultimately reduces the factor of safety (Hsi and Nath, 1970; Brown and Sheu, 1975).

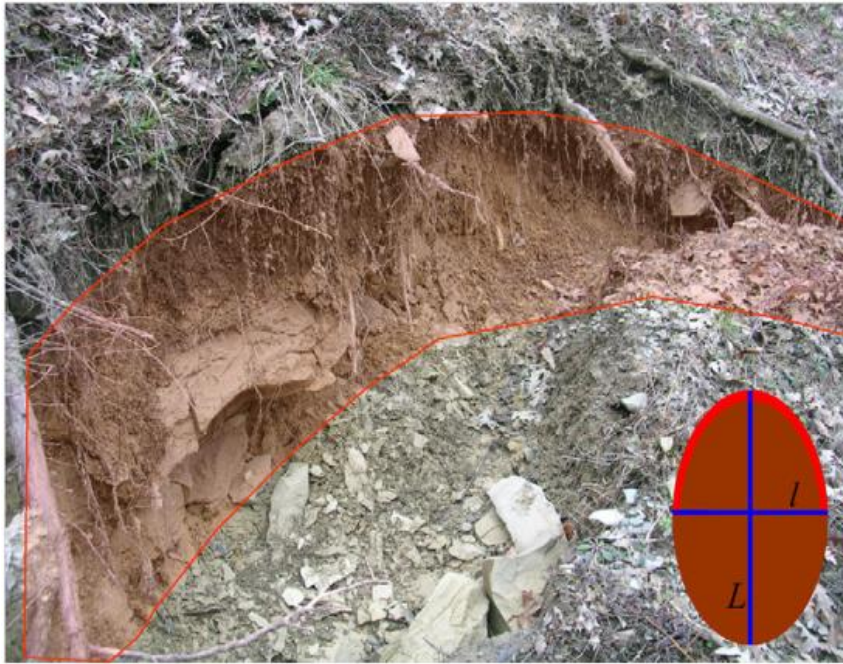


Figure 2.9 Illustration of the root matrix system of vegetation on riverbank
 (Source: Schwarz et al., 2010).

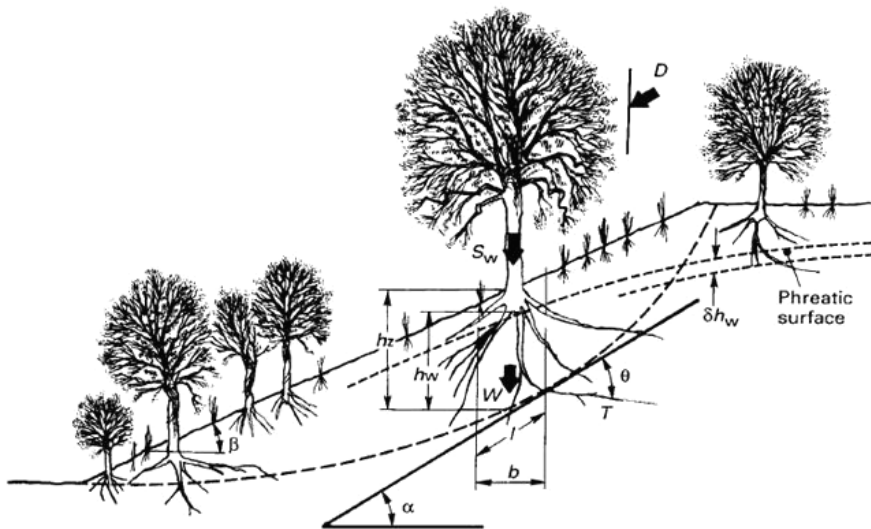


Figure 2.10 Influence of vegetation on riverbank (Source: Coppin and Richards, 1990).

Hubble et al. (2010) conducted an integrated review of field and experimental studies in eastern Australia to examine the role of native vegetation in the

mass failure of riverbanks. They found that the presence of riparian forests on riverbanks of the upper Nepean River significantly reduces the likelihood of erosion by mass failure due to root reinforcement. It was also found that a number of Australian tree species have apparently evolved roots that seek the permanent, summer water table for survival in prolonged periods of drought, and these root systems are particularly effective in mass mitigation due to rooting depths that are greater than 5 m and are sometimes well in excess of 20 m. For the Lower Murray, however, the permanent water level is much shallower. The root system might not extend deep enough beyond the slip surface to mitigate riverbank failures, but act as an additional surcharge to the slope, thus destabilising the riverbank. Furthermore, wind loads imposed on large trees increase the likelihood of riverbank collapse, as explained earlier.

2.4.4 Reinforcement calculation

Several researchers have introduced and applied root reinforcement in their *FS* estimations. A growing number of models have therefore been developed for quantifying root reinforcement. The models often include the effects of root system density and the root branching, Young's modulus and tensile strength of the roots (Greenway, 1987).

Simple perpendicular root models were proposed to calculate the root reinforcement, mostly based on the Mohr-Coulomb equation (Endo and Tsuruta, 1969; Waldron, 1977; Wu et al., 1979). In the following equation, soil shear strength is calculated from both the cohesive and frictional stresses:

$$s = c + \Delta s + (\sigma_n - u) \tan \phi \quad (2.10)$$

where s represents the shear strength of the soil (kPa); c represents soil cohesion (kPa); σ_n represents normal stress (kPa); u represents porewater pressure (kPa); and ϕ represents the soil's internal angle of friction ($^\circ$). Equation (2.10) was established based on the assumption that all roots extend vertically across a horizontal shearing zone, and act like laterally loaded piles; so tension is transferred to them as the soil is sheared.

In this model, a tangential component resisting shear and a normal component increasing the confining pressure on the shear plane was proposed by Waldron (1977). The change in shear strength, Δs , is expressed as:

$$\Delta s = T_r (\sin \theta + \cos \theta \tan \Phi)(A_R / A) \quad (2.11)$$

where T_r is average tensile strength of roots per unit area of soil (kPa); A_R / A is the root area ratio or the cross sectional area of roots crossing a plane within soil. The parameter θ represents the angle of shear distortion in the shear zone ($^\circ$), as shown in Figure 2.11.

Previous field- and laboratory-based research has shown that the angle of shear distortion, θ , is generally within the range from 40° to 70° (Gray and Leiser, 1982). Sensitivity analyses undertaken by Wu et al. (1979) showed that the term in Equation (2.11), $\sin \theta + \cos \theta \tan \Phi$, is somewhat insensitive to normal fluctuations in θ and ϕ , as it varies from 40° to 90° and 25° to 40° , respectively. The values for the first term varies from 1.0 to 1.3, therefore, Wu et al. (1979) proposed a coefficient of 1.2 as a replacement for $\sin \theta + \cos \theta \tan \Phi$ term, and the equation is then simplified as:

$$\Delta s = 1.2 T_r (A_R / A) \quad (2.12)$$

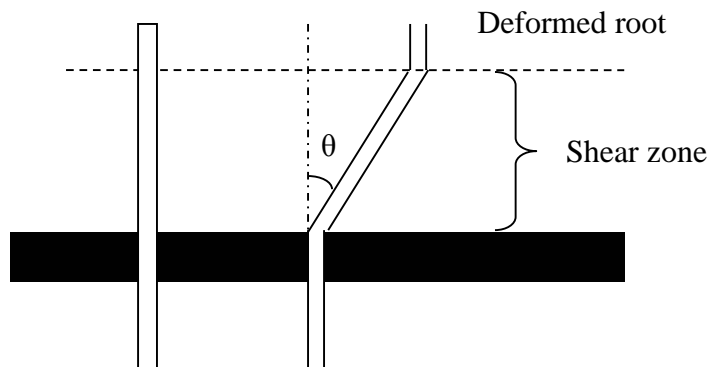


Figure 2.11 Angle of angle of shear distortion in the shear zone.

Recent research (e.g., Thomas and Bankhead, 2010) suggested that Wu et al.'s (1979) coefficient of 1.2 is inaccurate because, if root orientation is allowed to vary between 0° and 180° and both θ and ϕ remain in the same ranges, the results of $\sin \theta + \cos \theta \tan \Phi$ vary from 0.69 to 1.22, and 0.97 to 1.39,

respectively (Robert and Natasha, 2010). The field testing carried out by Docker and Hubble (2008) to study the increased shear resistance of soil due to root-reinforcement by four common Australian riparian trees, *Casuarina glauca*, *Eucalyptus amplifolia*, *Eucalyptus elata* and *Acacia floribunda* with a large-scale shear box, suggested that the tree root failed progressively rather than simultaneously, which is proposed by Wu et al. (1979). Docker and Hubble (2008) also showed that the calculated shear strength of the root-reinforced soil, assuming simultaneous root failure, yielded values 50% and 215% higher than directly measured shear strengths. The shear stress versus displacement plots for the four aforementioned tree species and soil only tests by Docker and Hubble (2008) is presented in Figure 2.12.

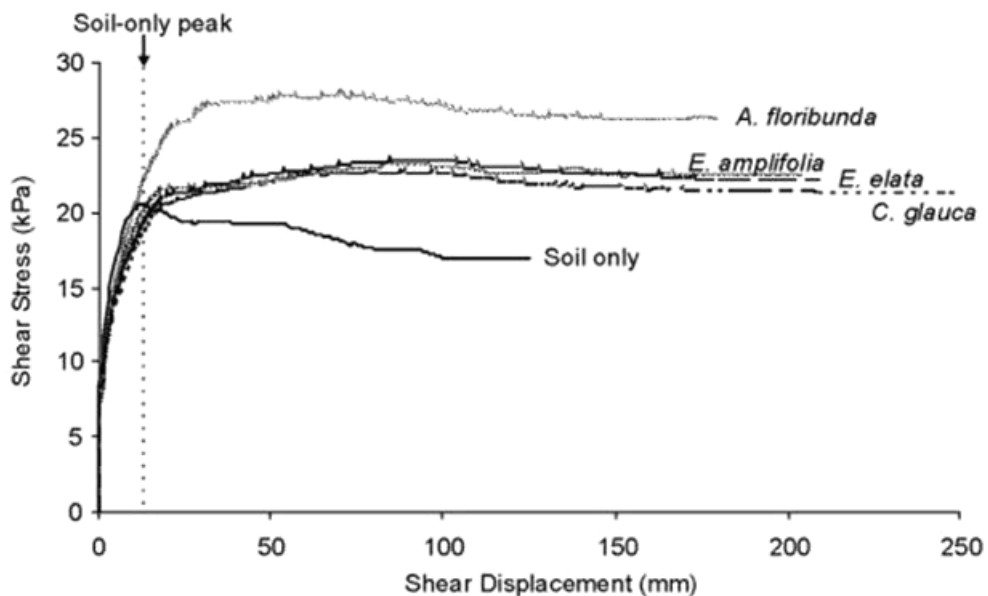


Figure 2.12 Average shear stress versus displacement plots for the four tree species and the soil-only tests (Source: Docker and Hubble, 2008).

To estimate better the increase of shear resistance of soil due to root-reinforcement, a method known as fibre-bundle models (FBMs) were introduced to overcome the overestimation introduced by Wu et al.'s (1979) equation. FBMs aid in the understanding of composite materials (Daniels, 1945). The models use a dynamic approach to remove the assumption made in the Wu et al. (1979) model that all of the roots in the soil matrix rupture simultaneously. When a load is applied to the bundle of fibres it is apportioned equally between all intact fibres (Daniels, 1945). The maximum

load that can be supported by the bundle corresponds not to the weakest or strongest fibre, but to one of the fibres in the centre of the bundle (Robert and Natasha, 2010). FBMs conform to the following rules:

- An initial load is added to the bundle which contains a number, n , of fibres and the fibres are assumed to be parallel to one another).
- Although at first the load is distributed equally among the n fibres, and hence divided into n parts, once the load is increased sufficiently for a fibre to break (conceptual research assumes one, but there may be more in practice), the load that was previously carried by the broken fibre is redistributed to the remaining $(n-1)$ intact roots.
- Each of the remaining fibres then bears a larger share of the load than before and is hence more likely to rupture.
- If this redistribution of load causes further roots to rupture, further redistribution of the load occurs (this is known as an avalanche effect in this type of model) until no further breakages occur (if no bundle of fibres is left, the analysis terminates).
- The load on the system is then increased, and the process is repeated until either all of the fibres have been broken, or the maximum driving force acting on the matrix is supported by the fibres contained within it (Robert and Natasha, 2010).

FBMs provide a means by which to identify the root reinforcement characteristics and quantify the restraining shear strength. Recent research also indicates that both of the different mechanisms of load redistribution – global load sharing (GLS) and local load sharing (LLS) (Hidalgo et al., 2002) – as well as different species of roots, different root diameters and soil saturation indices, can also affect the root reinforcement process

2.5 GIS approaches to landslide hazard mapping

Landslide hazard mapping is an essential part of landslide susceptibility evaluation. The landslide hazard map includes the predicted landslide locations, dimensions and failure types, and depicts the levels of potential slope failures with its spatial distribution. In its early stages of development, landslide hazard mapping was typically based on topographic relief maps. However, with the advent of remote sensing (RS) and global positioning systems (GPS), and combined with geographical information systems (GIS), such approaches have become mainstream in landslide hazard mapping (Varnes and The International Association of Engineering Geology Commission on Landslides and other Mass Movements, 1984; Hansen, 1984; van Westen, 1994; Bonham-Carter, 1994; Carrara et al., 1995; Hutchinson, 1995; Soeters and van Westen, 1996; van Westen et al., 1997; Aleotti and Chowdhury, 1999; Guzzetti et al., 1999; Gorsevski et al., 2003). However, such approaches are restricted by a number of limitations, such as the different types of failure, limited input data resolution and different methods of GIS interpretation.

Generally, GIS-based landslide susceptibility evaluation and hazard mapping can be classified into two major categories: qualitative and quantitative. Qualitative evaluation is typically based on the evaluation scores or ranks given by geologists and geomorphologists. This method was popular and widely used in 1970s. It uses several maps representing the spatial distribution of those physical parameters which may influence the occurrence of landslides. The spatial distribution of the factors indentified to be important in assessing slope instability are combined into a hazard map using subjective decision-making rules based on the experience of geoscientists (Anbalagan, 1992; Pachauri and Pant, 1992; Sarkar et al., 1995; Anbalagan and Singh, 1996).

More recently, with the development of GIS technology and improved computing performance, quantitative methods have become more widely

used. Generally, deterministic, statistical and mathematical methods, which are also called distribution free methods, are the three main types of the quantitative methods.

A GIS-based statistical model can account for landslide susceptibility evaluation on a wide range of scales (i.e. from the small scale [$<1:200,000$]; medium scale [$1:25,000 - 1:200,000$]; to the large scale [$>1:25,000$]). Those methods can be divided into bivariate methods, such as the information value method and weight elements method, and multivariate methods, such as logistic regression (Carrara et al., 1991; Mark and Ellen, 1995; Rowbotham and Dudycha, 1998). These techniques involve the statistical determination of the combinations of physical parameters that have led to past landslides.

Quantitative or semi-quantitative estimates were made for areas along the river currently with no recorded landslides, but conditions exist similar to those with recorded land movement. Both multiple regression and discriminant analyses have been undertaken to explore relationships between landslide occurrence and terrain variables (e.g. Yin and Yan, 1988; Carrara et al., 1991, 1995; Brunori et al., 1996). Statistically-based research has also been carried out, notably by Skirikar et al. (1998), Dhakal et al. (1999) and Pathak and Nilsen (2004). The disadvantage is the statistical results are quite sensitive to the quality of the input data.

More recently GIS-based deterministic models have been developed and have become increasingly popular. These new models concentrate mainly on the development of software routines within GIS applications that are able to perform slope stability analysis. Among these computer programs, the combination of physical slope stability models and hydrological distribution models are the most popular and widely used. The most common are:

- *SHALSTAB* (Montgomery and Dietrich, 1994);
- *TRIGRS* provided by United States Geological Survey, USGS (Baum et al. 2008);
- *SINMAP* (Pack et al., 2005);

- *SMORPH* [an acronym for a semi-empirical method: Slope MORPHology from Shaw and Vaugeois (1999)]
- *dSLAM* [an acronym for distributed Shallow Landslide Analysis Model from Sidle and Wu (1999)]
- *FLO-2D* [an acronym for 2-dimensional Flood Routing Model (FLO-2D Software Inc., 2009)].

Mathematical methods consist of GIS-based artificial intelligence methods, such as artificial neural networks (ANNs); support vector machines (SVMs) and fuzzy sets. These methods require numerous data transformations and calculations and develop predictions based on the learning of patterns from data sets (Thapa and Dhital, 2000; Dhital, 2000; Saha et al., 2002; Sarkar and Kanungo, 2004). These methods are realistic and objective but care must be exercised when using these methods, as it is difficult for the user to appreciate the nature of the internal representations generated by these methods when the number of variables is large.

2.6 Summary

In summary, the above review of the relevant literature has identified the following points and areas for potential focus:

- Idealised bank profile geometries are typically used in conventional, quantitative, 2D bank stability studies. In general, more accurate geometries are needed, which will lead to more reliable results.
- Compared with the classical 2D slope stability research, hazard mapping is undertaken on a regional scale and incorporates detailed examination of specific sites.
- Riverbank slope stability is a multifaceted issue. Compared with the slopes in mountainous regions, riverbanks are greatly influenced by river water level fluctuation, climatic factors, river flow and surface waves. In particular, more focused research is needed at a regional scale examining

riverbank instability triggered by water level fluctuation and climatic influences.

- It has been demonstrated by recent research that riparian vegetation and human infrastructure can increase soil strength and vertical loads, respectively. The interaction between these factors and those listed above requires further investigation, both at a local and a global level.
- The lack of site specific data, such as river geometry, soil properties and their variability, land use, geology and the groundwater regime, are the challenges in this research that will require attention.

References for Chapters 1 and 2

Abernethy, B. and Rutherford, I. D. (1998). Where along a river's length will vegetation most effectively stabilise stream banks? *Geomorphology*, 23(1): 55–75.

Abramson, L. W., Lee, T. S., Sharma, S. and Boyce, G. M. (2002). *Slope Stability and Stabilization Methods*, 2nd edition, New York, USA, John Wiley & Sons.

Aleotti, P. and Chowdhury, R. (1999). Landslide hazard assessment: summary review and new perspectives.' *Bulletin of Engineering Geology and the Environment*, 58(1): 21–44.

Anbalagan, D. (1992). Landslide hazard evaluation and zonation mapping in mountainous terrain. *Engineering Geology*, 32: 269–277.

Anbalagan, R. and Singh, B. (1996). Landslide hazard and risk assessment mapping of mountainous terrains: a case study from Kumaun Himalaya, India. *Engineering Geology*, 43(4): 237–246.

Aronoff, S. (1989). *Geographic Information System: A management perspective*. WDL Publications, Ottawa.

Baum, R. L., Savage, W. Z., and Godt, J. W. (2008). TRIGRS—A Fortran program for transient rainfall infiltration and grid-based regional slope-stability analysis, version 2.0. *U.S. Geological Survey Open-File Report*, No. 2008-1159.

Bethlahmy, N. (1962). First year effects of timber removal on soil moisture. *International Association of Scientific Hydrology Bulletin*, 7(2): 34–38.

Biddle, P. G. (1983). Patterns of soil drying and moisture deficit in the vicinity of trees on clay soils. *Geotechnique*, 33: 107–126.

Bishop, D. M. and Steven, M. E. (1964). *Landslides on logged areas in Southeast Alaska*. Research paper NOR-1, Northern Forest Experiment Station, Juneau, USA.

Bonham-Carter, G.F. (1994). Geographic information systems for geoscientists: Modelling with GIS. *Computer methods in the geosciences*, Vol. 13, Pergamon, 2nd edition. Ontario, Canada.

Borga, M., Dalla Fontana, G. and Cazorzi, F. (2002). Analysis of topographic and climatologic control on rainfall-triggered shallow landsliding using a quasi-dynamic wetness index. *Journal of Hydrology*, 268: 56–71.

Brown, C. B. and Sheu, M. S. (1975). Effects of deforestation on slopes. *Journal of Geotechnical Engineering Division, ASCE*, 101: 147–165.

Brunori, F., Casagli N., Fisci S., Garzonio C. A. and Moretti S. (1996). Landslide hazard mapping in Tuscany, Italy: an example of automatic evaluation. In: Slaymaker, O. (ed.) *Geomorphologic Hazards*. Wiley, Chichester, 55–67.

Burrough, P. A. (1986). *Principles of Geographical Information Systems for Land Resources Assessment*. Clarendon Press, Oxford.

Burton, A. and Bathurst, J. C. (1998). Physically based modelling of shallow landslide sediment yield at a catchment scale. *Environmental Geology*, 35(2–3): 89–99.

Carrara, A., Cardinali, M., Detti, R., Guzzetti, F., Pasqui, V. and Reichenbach, P. (1991). GIS techniques and statistical models in evaluating landslide hazard. *Earth Surface Processes and Landforms*, 16: 427–445.

Carrara, A., Cardinali, M., Guzzetti, F. and Reichenbach, P. (1995). GIS-based techniques for mapping landslide hazard. In: Carrara, A. and Guzzetti, F. (eds.) *Geographical Information Systems in Assessing Natural Hazards*, Kluwer Academic Publishing, The Netherlands, 135–176.

Centre for Geotechnical Research (1998). *Soil Mechanics Data Sheets*. Department of Civil Engineering, University of Sydney.

Clough, R. W. and Woodward, R. J. (1967). Analysis of embankment stress and deformations, *Journal of Soil Mechanics And Foundation Division*, ASCE, 93(4): 529–549.

Chowhury, R.N. (1981). Discussion of Stability Analysis of Embankment and Slope. *Journal of the Geotechnical Engineering Division*, ASCE, 107(GT-5): 691–693.

Coppin, N. J. and Richards, I. G. (1990). *Use of vegetation in civil engineering*. Butterworths, London.

Craig, R.F. (2004). *Soil Mechanics*, 7th ed. Spon Ltd.

Daniels, H. E. (1945). The statistical theory of the strength of bundles of threads – I. In: *Proc. Royal Society London*, Series A., 183, 405-435.

Dawson, E. M., Roth, W. H. and Drescher, A. (1999). ‘Slope Stability Analysis by Strength Reduction.’ *Geotechnique*, 49(6): 835–840.

De Smedt, F. (2006). Two- and three-dimensional flow of groundwater. In: Delleur, J. W. (ed.) *The Handbook of Groundwater Engineering*, Second edition, CRC Press, pp. 4.1–4.36.

DFW (2010). Riverbank Collapse Hazard Expert Panel, Submission: site reports & investigation. Department for Water, Government of South Australia.

Dhakal, A. S. and Sidle, R. C. (2004). Distributed simulation of landslides for different rainfall conditions. *Hydrological Processes*, 18: 757–775.

Dhakal, A.S., Amada T. and Aniya, M. (1999). Landslide hazard mapping and the application of GIS in the Kulekhani watershed, Nepal. *Mountain Research and Development*, 19: 3–16.

Dhital, M. R. (2000). An overview of landslide hazard mapping and rating systems in Nepal. *Journal of Nepal Geological Society*, 22: 533–538.

Dietrich, W. E., Wilson, C. J. and Reneau, S. L. (1986). Hollows, colluvium, and landslides in soil-mantled landscapes, Chapter 17 in *Hillslope Processes*, In: Abrahams, A. D. (ed.), Allen & Unwin, Boston, 361–388.

Dietrich, W. E., Wilson, C. J., Montgomery, D. R., McKean, J. and Bauer, R. (1993). Analysis of erosion thresholds, channel networks, and landscape morphology using a digital terrain model, *Journal of Geology*, 101: 259–278.

Dietrich, W. E., Wilson, C. J., Montgomery, D. R., McKean, J. and Bauer, R. (1992). Erosion Thresholds and Land Surface Morphology, *Geology*, 20: 675–679.

Docker, B. and Hubble, T. (2009). Modelling the distribution of enhanced soil shear strength beneath riparian trees of southeastern Australia. *Ecological Engineering*, 35(5): 921–934.

Duncan, J. M. (1996). State of the art: Limit equilibrium and finite-element analysis of slopes. *Journal of Geotechnical Engineering*, ASCE, 122(7): 577–596.

Duncan, J. M. and Dunlop, P. (1969). Slope in stiff-fissured clays and shales. *Journal of the Soil Mechanics and Foundations Division*, ASCE, 95(SM5): 467–492.

Durocher, M. G. (1990). Monitoring spatial variability in forest interception. *Hydrological Processes*, 4: 215–229.

Endo, T. and Tsuruta, T. (1969). Effects of tree root upon the shearing strengths of soils. *Annual Report of the Hokkaido Branch*, Tokyo Forest Experiment Station, 167–179.

Fang, H. Y. (1991). *Foundation Engineering Handbook*, Second Edition, Chapman and Hall.

FLO-2D Software Inc. (2009). FLO-2D Reference Manual. Nutrioso, AZ.

Gorsevski, P. V., Gessler, P. E. and Jankowski, P. (2003). Integrating a fuzzy k-means classification and a Bayesian approach for spatial prediction of landslide hazard. *Journal of Geographical Systems*, 5(3): 223–251.

Gray D. H. and Leiser A. T. (1982). *Biotechnical slope protection and erosion control*. Van Nostrand Reinhold Co., New York, N.Y.

Greenway, D. R. (1987). Vegetation and Slope Stability. In: Anderson. M.G. and Richards, K.S. (eds.) *Slope Stability*, John Wiley and Sons Ltd, New York, 187–230.

Griffiths, D. V. and Lane, P. A. (1999). Slope stability analysis by finite elements. *Geotechnique*, 49(3): 387–403.

Griffiths, D. V. and Marquez, R. M. (2007). Three-dimensional slope stability analysis by finite elements. *Geotechnique*, 57(6): 537–546.

Griffiths, D.V. (1980). *Finite element analysis of walls, footings and slopes*. PhD Thesis, Department of Engineering, University of Manchester.

Guzzetti, F., Carrara, A., Cardinali, M. and Reichenbach, P. (1999). Landslide hazard evaluation: a review of current techniques and their application in a multi-scale study, Central Italy. *Geomorphology*, 31(1–4): 181–216.

Hansen, A. (1984). Landslide hazard analysis. In: Brunsden, D. and Prior, D.B. (eds.) *Slope Instability*. Wiley and Sons, New York, 523–602.

Hartle'n, J. and Viberg, L. (1988). General report: Evaluation of landslide hazard. *Proceedings of the 5th International Symposium on Landslides, Lausanne, Switzerland*, Vol. 2, 1037–1057.

Hey, R.D., Heritage, G. L., Tovey, N. K., Boar, R. R., Grant, A. and Turner, R. K. (1991). *Streambank Protection in England and Wales*. R&D Note 22, National Rivers Authority, London.

Hidalgo, R. C., Kun, F. and Herrmann, H. J. (2002). Bursts in a fiber bundle model with continuous damage. *Physical Review E: Statistical, Nonlinear, and Soft Matter Physics*, 64: 66–122.

Hsi, G. and Nath, J. H. (1970). Wind drag within a simulated forest. *Journal of Applied Meteorology*, 9: 592–602.

Hubble, T., Docker, B., and Rutherford, I. (2010). The role of riparian trees in maintaining riverbank stability: A review of Australian experience and practice. *Ecological Engineering*, 36(3): 292–304.

Hutchinson, J. N. (1988). General Report: Morphological and geotechnical parameter of landslides in relation to geology and hydrogeology. In: Bonnard, C. (ed.) *Landslides: Proceedings of Fifth International Symposium on Landslides*, Lausanne, Switzerland, Vol. 1, 3–35.

Hutchinson, J. N. (1995). Keynote paper: landslide hazard assessment. In: Bell, D.H. (ed.) *Landslides, Proceeding of VI International Symposium on Landslides*, Christchurch, New Zealand, 1805–1841.

Jeremic, B. (2000). Finite element methods for three-dimensional slope stability analysis. *Slope Stability 2000, Proc. GeoDenver Symposium, Geotechnical Special Publication No. 101*, ASCE, 224–238.

Lane, P.A. and Griffiths, D.V. (2000). Assessment of stability of slopes under drawdown conditions. *Journal of Geotechnical and Geoenvironmental Engineering*, 126(5): 443–450.

Larsen, M. C. and Torres-Sanchez, A. J. (1998). The frequency and distribution of recent landslides in three montane tropical regions in Puerto Rico. *Geomorphology*, 24: 309–331.

Lechman, J. B. and Griffiths, D. V. (2000). Analysis of the progression of failure in earth slopes by finite elements. *Slope Stability 2000, Proc. GeoDenver Symposium*, Geotechnical Special Publication No. 101, ASCE, 250–265.

Lee, I. K., White, W. and Ingles, O. G. (1983). *Geotechnical Engineering*, Pitman, Boston.

Li, T. C. (1994). Landslide disasters and human responses in China. *Mountain Research and Development*, 14: 341–346.

Li, X. (2007). Finite element analysis of slope stability using a nonlinear failure criterion. *Computers and Geotechnics*, 34: 188–195.

Marble, D. F. (1990). Geographic Information Systems: An Overview, In: Peuquet, D. J and Marble, D. F, (eds.) *Introductory Readings in Geographic Information Systems*, Taylor and Francis Ltd., New York, 9–17.

Matsui, T. and Sun, K.C. (1992). Finite element slope stability analysis by shear strength reduction technique. *Soils and Foundations*, 32(1): 59–70.

Miller, D. J. and Sias, J. (1998). Deciphering large landslides: linking hydrological, groundwater and slope stability models through GIS. *Hydrological Processes*, 12(6): 923–941.

Montgomery, D. R. and Dietrich W. E. (1994). A physically based model for the topographic control on shallow landsliding. *Water Resources Research*, 30(4): 1153–1171.

Montgomery, D. R. and Dietrich, W. E. (1988). Where do channels begin? *Nature*, 336: 232–234.

Montgomery, D. R. and Dietrich, W. E. (1989). Source areas, drainage density and channel initiation, *Water Resources Research*, 25(8): 1907–1918.

Montgomery, D. R. and Dietrich, W. E. (1994). A physically based model for the topographic control on shallow landsliding, *Water Resources Research*, 30(4): 1153–1171.

Natasha, P. (2007). Temporal and spatial variability in root reinforcement of streambanks: Accounting for soil shear strength and moisture. *Catena*, 69(3): 197–205.

Pachauri, A.K. and Pant, M. (1992). Landslide hazard mapping based on geological attributes. *Engineering Geology*, 32: 81–100.

Pack, R. T., Tarboton, D .G., Goodwin, C. N. and Prasad A. (2005). *SINMAP 2. A Stability Index Approach to Terrain Stability Hazard Mapping, technical description and users guide for version 2.0*. Utah State University.

Pack, R. T., Tarboton, D. G. and Goodwin C. N. (1998). The SINMAP approach to terrain stability mapping. In: Moore, D. P. and Hungr, O. (eds.) *Proceedings of International Congress of the International Association for Engineering Geology and the Environment*, Vol. 8, No. 2, A.A. Balkema, Rotterdam, Netherlands, 1157–1165.

Pack, R. T., Tarboton, D. G. and Goodwin, C. N. (2001). Assessing terrain stability in a GIS using SINMAP. *Proceeding of 15th annual GIS conference*, GIS 2001, Vancouver, British Columbia, 19–22 February.

Pack, R.T. (1995). Statistically-based terrain stability mapping methodology for the Kamloops Forest Region, British Columbia, *Proceedings of the 48th Canadian Geotechnical Conference*, Canadian Geotechnical Society, Vancouver, BC.

Pathak, S. and Nilsen, B. (2004). Probabilistic rock slope stability analysis for Himalayan condition. *Bulletin of Engineering Geology and the Environment*, 63(1): 25–32.

Pollen, N. (2007). Temporal and spatial variability in rootreinforcement of streambanks: Accounting for soil shear strength and moisture. *Catena*, 69: 197–205.

Pollen, N. and Simon, A., (2005). Estimating the mechanical effects of riparian vegetation on streambank stability using a fiber bundle model. *Water Resources Research*, 41.

Potts, D. M., Dounias, G. T. and Vaughan, P. R. (1990). Finite element analysis of progressive failure of Carsington embankment. *Geotechnique*, 40(1): 79–102.

Ray, R. L. and De Smedt, F. (2009). Slope stability analysis on a regional scale using GIS: a case study from Dhading, Nepal. *Environmental Geology*, 57(7): 1603–1611.

Robert, E. T. and Natasha, P. B. (2010). Modeling root-reinforcement with a fiber-bundle model and Monte Carlo simulation. *Ecological Engineering*, 36(1): 47–61.

Rosenblueth, E. (1975). Point estimates for probability moments. *In Proceedings of the National Academy of Sciences*, 72(10): 3812–3814.

Saha, A. K., Gupta R. P. and Arora M. K. (2002). GIS-based landslide hazard zonation in the Bhagirathi (Ganga) Valley, Himalayas. *International Journal of Remote Sensing*, 23(2): 357–369.

Sainak, A. N. (2004). Application of three-dimensional finite-element method in parametric and geometric studies of slope stability. *Advances in geotechnical Engineering – The Skempton Conference*, Thomas Telford, London, Vol. 2, 933–942.

Sarkar, S. and Kanungo, D. P. (2004). An integrated approach for landslide susceptibility mapping using remote sensing and GIS. *Photogramm. Eng. Remote Sens.*, 70(5): 617–625.

Sarkar, S. and Kanungo, D. P. and Mehrotra, G. S. (1995). Landslide hazard zonation: a case study in Garhwal Himalaya, India. *Mountain Research and Development*, 15: 301–309.

Sassa, K. (2004). The international consortium on landslides. *Landslides: Journal of the International Consortium on Landslides*, 1(1): 91–94

Schwarz, M., Preti, F., Giadrossich, F., Lehmann, P. and Or, D. (2010). Quantifying the role of vegetation in slope stability: A case study in Tuscany, Italy. *Ecological Engineering*, 36(3): 285–291.

Selby, M. J. (1993). *Hillslope Materials and Processes*. Oxford University Press, Oxford.

Sharma, S., Raghuvanshi, T. K. and Anbalagan, R. (1995). Plane failure analysis of rock slopes. *Geotechnical and Geological Engineering*, 13(2): 105–111.

Shaw, S. C. and Vaugeois, L. M. (1999). *Comparison of GIS-based models of shallow landsliding for application to watershed management*. Olympia: Washington Department of Natural Resources Report TFW-118.

Sidle, R. C., Pearce, A. J., and O’Loughlin, C. L. (1985). *Hillslope stability and land use*. American Geophysical Union, Water Resources Monograph, No. 11.

Sidle, R. (1992). A theoretical model of the effects of timber harvesting on slope stability, *Water Resources Research*, 28(7): 1897–1910.

Sidle, R. C. and Wu, W. (1999). Simulating effects of timber harvesting on the temporal and spatial distribution of shallow landslides. *Zeitschrift für Geomorphologie N.F.* 43, 185–201.

Simon, A. and Collison, A. J. C. (2002). Quantifying the mechanical and hydrologic effects of riparian vegetation on stream-bank stability. *Earth Surface Processes and Landforms*, 27(5): 527–546.

Skempton, A. W. and DeLory, F. A. (1957). Stability of natural slopes in London clay. *Proceedings 4th International Conference on Soil Mechanics and Foundation Engineering*, Vol. 2, 378–381.

Skirikar, S. M., Rimal, L. N. and Jager, S. (1998). Landslide hazard mapping of Phewa Lake catchment area, Pokhara, Central West Nepal. *Journal of Nepal Geological Society*, 18: 335–345.

SKM (2009). *Study into river bank collapsing – Lower River Murray*. Inspection Report. Report to Department of Water, Land and Biodiversity Conservation (DWLBC).

SKM (2010). *Study into riverbank collapsing for Lower Murray River*. Geotechnical Investigation Report, Report to Department of Water, Land and Biodiversity Conservation (DWLBC).

Smith, I. M. and Hobbs, R. (1974). Finite element analysis of centrifuged and built-up slopes. *Geotechnique*, 24(4): 531–559.

Snitbhan, N. and Chen, W. F. (1976). Elastic-plastic deformation analysis of soil slopes. *Computers and Structures*, 9: 567–577.

Soeters, R. and van Westen C. J. (1996). Slope instability recognition, analysis and zonation. In: Turner, K. T. and Schuster, R. L. (eds.) *Landslide:*

investigation and mitigation. Special Report-47. Transportation Research Board, National Research Council, Washington DC, 129–177.

Sowers, G. F. (1979). *Introductory Soil Mechanics and Foundations*. Collier MacMillan.

Terzaghi, K., (1950). Mechanism of landslides, In: *Application of Geology to Engineering Practice, Berkeley Vol.*, Geological Society of America, 83–123.

Thapa, P. B. and Dhital, M. R. (2000). Landslide and debris flows of 19–21 July 1993 in the Agra Khola Watershed of Central Nepal. *Journal of Nepal Geological Society*, 21: 5–20.

Thomas, R. E. and Bankhead, N.L. (2010). Modeling root-reinforcement with a fiber-bundle model and Monte Carlo simulation. *Ecological Engineering*, 36(1): 47–61.

Thorne, C. R., Reed, S. and Doornkamp, J. C. (1996). *A Procedure for Assessing River Bank Erosion Problems and Solutions*. National Rivers Authority, Bristol, R&D Report 28.

Van Westen, C. J. (1994). GIS in landslide hazard zonation: a review, with examples from the Andes of Colombia. In: Price M. F. and Heywood D. I. (eds.) *Mountain environments and geographic information systems*, Taylor and Francis Publishers, London, 135–165.

Van Westen, C. J. and Terlien, T. J. (1996). An approach towards deterministic landslide hazard analysis in GIS: a case study from Manizales, Colombia. *Earth Surface Processes and Landforms*, 21(9): 853–868.

Van Westen, C. J., Rengers, N., Terlien, M. T. J. and Soeters, R. (1997). Prediction of the occurrence of slope instability phenomena through GIS-based hazard zonation. *Geologische Rundschau*, 86(2): 404–414.

Vanmarcke, E. H. (1977). Reliability of Earth Slope. *Journal of Geotechnical Engineering Division, ASCE*, 103(11): 1247–1265.

Varnes, D. J. and the International Association of Engineering Geology Commission on Landslides and other Mass Movements (1984). Landslide Hazard Zonation: A review of principles and practice. *Natural Hazards*, vol. 3, Paris, France, UNESCO.

Waldron, L. J. (1977). The shear resistance of root-permeated homogeneous and stratified soil. *Soil Science Society of America Journal*, 41: 843–849.

Whitlow, R. (1990). *Basic Soil Mechanics*, Second ed., Longman.

Wong, F. S. (1984). Uncertainties in FE modeling of slope stability. *Computers & Structures*, 19(5/6): 777–791.

Wu, T. H., McKinnell, W. P. and Swanston, D. N. (1979). Strength of tree roots and landslides on Prince of Wales Island, Alaska. *Canadian Geotechnical Journal*, 16: 19–33.

Wu, W. and Sidle, R. C. (1995). A distributed slope stability model for steep forested basins. *Water Resources Research*, 31: 2097–2110.

Yin, K. L. and Yan, T. Z. (1988). Statistical prediction models for slope instability of metamorphosed rocks. In: Bonnard, C. (ed.) *Proceedings 5th International Symposium on Landslides, Lausanne, Switzerland*. Balkema, Rotterdam, 1269–1272.

Zheng, H., Tham, L. G. and Liu, D. (2006). On two definitions of the factor of safety commonly used in the finite element slope stability analysis. *Computers and Geotechnics*, 33(3): 188–195.

Zienkiewicz, O. C. (1971). *The Finite Element Method in Engineering Science*. New York: McGraw-Hill.

Zienkiewicz, O. C., Humpheson, C. and Lewis, R. W. (1975). Associated and nonassociated viscoplasticity and plasticity in soil mechanics. *Geotechnique*, 25(4): 671–689.

Chapter 3

3 GIS-based Back Analysis of Riverbank Instability in the Lower River Murray

(Paper 1, published)

C. Liang¹, M. B. Jaksa¹ and B. Ostendorf²

¹School of Civil; Environmental and Mining Engineering, University of Adelaide, 5005;

²School of Earth and Environmental Sciences, University of Adelaide, 5005;

Publication:

LIANG, C., JAKSA, M. B. & OSTENDORF, B. (2012). GIS-based Back Analysis of Riverbank Instability in the Lower River Murray. *Australian Geomechanics*, 47, 59-65.

Statement of Authorship

Title of Paper	GIS-based Back Analysis of Riverbank Instability in the Lower River Murray
Publication Status	<input checked="" type="radio"/> Published, <input type="radio"/> Accepted for Publication, <input type="radio"/> Submitted for Publication, <input type="radio"/> Publication style
Publication Details	LIANG, C., JAKSA, M. B. & OSTENDORF, B. (2012). GIS-based Back Analysis of Riverbank Instability in the Lower River Murray. Australian Geomechanics, 47, 59-65.

Author Contributions

By signing the Statement of Authorship, each author certifies that their stated contribution to the publication is accurate and that permission is granted for the publication to be included in the candidate's thesis.

Name of Principal Author (Candidate)	Chen Liang		
Contribution to the Paper	Undertook Literature review, performed parametric analysis and modeling, interpreted data and acted as corresponding author.		
Signature		Date	11/Jan/2015

Name of Co-Author	Mark B. Jaksa		
Contribution to the Paper	Supervised development of work and helped with paper editing.		
Signature		Date	4/2/15

Name of Co-Author	Bertram Ostendorf		
Contribution to the Paper	Supervised development of work.		
Signature		Date	3-2-2015

Name of Co-Author			
Contribution to the Paper			
Signature		Date	

Abstract

Over the last 4 years or so, unprecedented low river levels, combined with current loading conditions, have adversely contributed to more than 137 riverbank collapse-related incidents and a long term metastable condition along the Lower River Murray, which have recently been considered as the dominating factors inducing bank collapse. With high resolution aerial photographs and digital elevation models (DEMs), this study has established the riverbank geometry prior to collapse of 26 2-dimensional cross sectional models. In order to obtain appropriate soil parameters for the Lower River Murray study area, a series of back-analyses have been conducted at 5 locations where failures were documented adjacent to Long Island Marina, Murray Bridge, South Australia. The slope stability analysis software SVSlope was employed in the back-analysis with soil data obtained from two nearby site investigations. Factors of safety were calculated to examine the potential for riverbank collapse with respect to varying river levels. The results indicate that, when the river levels return to 0 to 0.5 m AHD, a portion of the riverbank is close to collapse, whereas a large proportion of the banks remain quasi stable. A raised and maintained high river level will improve the stability but to a limited extent. Several remedial works may need to be conducted when the river level is about to decrease.

Keywords: GIS, back-analysis, slope stability, riverbank stability, River Murray

3.1 Introduction

Bank collapse along the Lower River Murray (210 km stretching from Lock 1 at Blanchetown to Wellington, South Australia) has been declared a state hazard (Ramitin et al. 2010). According to the Department for Water's inventory, during 2008 to 2011, more than 137 riverbank collapse-related incidents occurred which included ground cracking, riparian tree movement and collapse, bank collapse and erosion and destabilisation of infrastructure.

In general, bank retreat is the combined result of various influencing factors, such as bank geometry (i.e. topography, slip surface and material boundary locations), bank material, external loads acting on the bank (i.e. vegetation and infrastructure) and pore water pressure (Filz et al. 1992). Back-analysis is an analytical process and model to assess the status of inherent influencing factors on a failed or failing slope (Filz et al. 1992). For the slope stability analyses, at the time of failure, the details of influencing factors and the ways they interacted are often ambiguous (Abramson et al. 2002). On the assumption that the factor of safety (FOS) was equal to 1 at the time of failure, a back-analysis calculation could be conducted and a series of relevant parameters can be obtained for a specific location (Abramson et al. 2002).

Geographic information system (GIS) technology has greatly facilitated landslide research by providing various functions for spatial data management. Specifically as data capturing, handling, processing, analysing, integrating, simulating, visualising and modelling (Carrara et al. 1991a 1995b, Guzetti et al. 1999, Wang et al. 2005). GIS-based geotechnical models simplify the process of quantifying the spatially distributed parameters influencing collapse (Xie et al. 2004). By processing and integrating high resolution remotely-sensed data (i.e. satellite imagery, aerial photos and digital elevation models [DEMs]), GIS-based geotechnical models have been used to assess bank stability at relatively large scales (Hong et al. 2007).

The aim of this paper is to assess the susceptibility of riverbank collapses at different river levels at Long Island Marina, Murray Bridge, South Australia based on back-analysis of several failed sites.

3.2 Riverbank stability model and back-analysis

The study area outlined in this paper is located along the Lower River Murray near the Long Island Marina, Murray Bridge, South Australia, as shown in Figure 3.1. The inventory of Department for Water (DFW), South Australian, incidents that 9 riverbank collapsed related incidents occurred during 2008 to 2011. Of these, 4 were relatively minor (i.e. bank cracking, tree leaning and collapse), but the remaining 5 were significant and are located adjacent to Long Island Marina, as shown in Figure 3.3a.



Figure 3.1 Location of the study area.

For the purpose of back analysis, the collapsed sections of riverbank need to be identified with a relatively high accuracy. With reference to a series of imprecise geographical coordinates of the collapsed bank sections from DFW inventories, under ArcGIS framework, visual interpretation method was adapted on high resolution aerial images of different periods to identify

collapse region. Based on the visual comparison of aerial images of 2008 with 5m resolution and 2010 with 0.5m resolution, the collapsed region were vectorized as dotted area as shown in Figure 3.2.

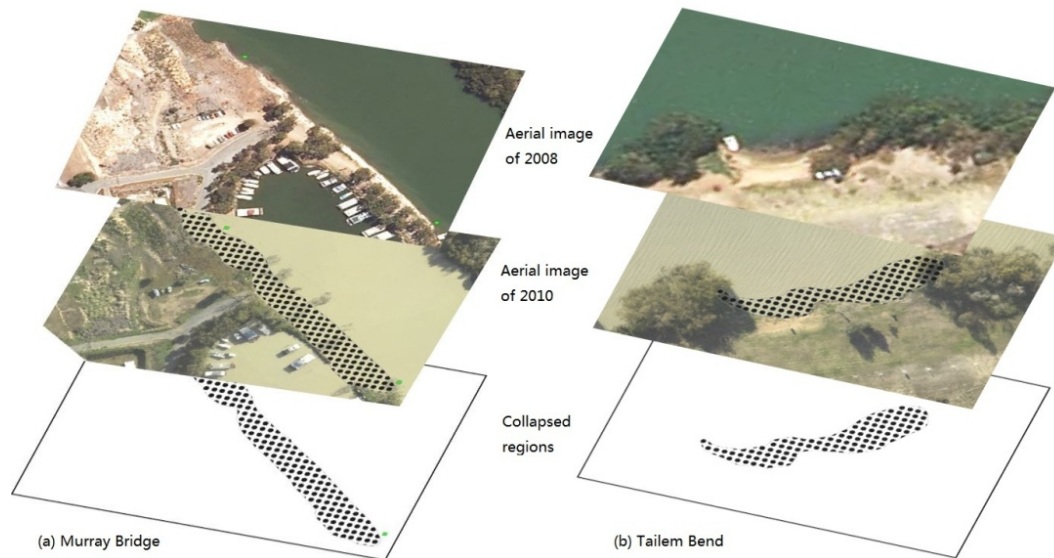


Figure 3.2 Examples of visual interpretation on 2008 and 2010 aerial images under ArcGIS in (a) Murray Bridge and; (b) Tailem Bend.

The limitations of visual interpretation based collapsed region identification method is mainly caused by the difficulties in judgment of collapsed regions. In details, it is impossible to verify by naked eyes whether a section of riverbank collapsed or submerged when the water overlapped. In order to solve this issue, a Digital Elevation Model (DEM) of 2008 was used to verify the elevation of the section before the collapse occurs. By comparison of the elevation from DEM and the elevation of the river levels in the date of airborne photo captured (data of river levels were provided by the observation point in Murray Bridge), collapsed regions were identified accurately. Furthermore, the loss of large riparian plants and the new construction of riparian infrastructures (e.g. jetty) read from later aerial image are also helpful with the collapsed region identifications.

Riverbanks similar in material, ground water and stratigraphic condition may behave significantly different depending on their particular topographies (Abramson et al., 2002a). Throughout this study, the geometries of the riverbanks were extracted from two DEMs (0.5m and 5m resolution) provided by DFW under ArcGIS. As shown in Figure 3.3b, 26 2-D riverbank cross section models were established and represented by 26 slices of polylines. Each polyline was comprised of 401 points in a line with 10 meters interval of neighbouring points. In order to conduct the back-analyses, 5 cross section models were intentionally chosen to coincide with collapsed regions which were vectorized previously. Based on the bilinear interpretation method, the elevation values were extracted from DEMs and assigned to 401 points with singular points avoided.

Stratigraphic and geotechnical data for this research were collected from a series of site investigations (Boreholes, Cone Penetration Tests, Dilatometer tests, in-situ tests including Vane Shear, Pocket Penetrometer and Standard Penetration Tests and Laboratory tests), performed by Sinclair Knight Merz (SKM) during 2009. Generally speaking, the soil profile comprises 0.8 – 1.2 m thickness of silty sand (SM/SC) overlaying silty clay, with a unit weight as $18 \pm 1 \text{ kN/m}^3$, internal friction angle of $28 \pm 2^\circ$, cohesion of $2 \pm 2 \text{ kPa}$; 11 – 20 m thickness of dark grey very soft silty clay (CH), with unit weight of $16 \pm 1 \text{ kN/m}^3$, cohesion of $10 \pm 5 \text{ kPa}$ (10 kPa at the top, maximum of 25 kPa increasing by 1.25 kPa/m); and a medium dense sandy clay (SC/CL) with unit weight of $17 \pm 1 \text{ kN/m}^3$, internal friction angle of $30 \pm 2^\circ$ and $2 \pm 2 \text{ kPa}$ cohesion.

Pore water pressure affects the river bank stability by altering the shear strength of bank material (reduce the effective stress) and the deadweight of the soil mass (Sharma et al. 2002). It is well established that positive pore water pressure, which plays a significant role in drawdown failures, reduces soil effective shear strength (Budhu and Gobin 1995). In contrast, negative pore pressure, or soil suction, offers apparent cohesion which stabilises the bank and manifests steeper banks. Casagli et al. (1997) stated that when the

bank materials become saturated, collapses are more likely to occur. However, due to seasonal influences, negative pore water pressure cannot contribute to long term stability (Sterrett and Edil 1982).

Fluctuations in river level directly affect the flow of water in and out of the bank and the pore water pressures within the bank (Green 1999). Generally, over the last 2 decades or so, the river levels at Murray Bridge have fluctuated between 1.5 – 1.7 m AHD (Australia Height Datum), as shown in Figure 3.4. In general, the river level has remained relatively constant until the end of 2006, where it fell dramatically until October 2009, after which it has returned to its pre-2006 levels.

External loads on the riverbank acting on the stability in two major ways: riparian vegetation and manmade loads. Considering the potential slip modes and the horizontal and lateral scopes of the collapse, the impacts of collapse were mainly determined by the dead weights and the distributions of the external loads (distances to the bank line).

The stabilising effects of riparian vegetation are well known as a result of root suction and root matrix reinforcement but far from clear (Stark and Eid, 1997). It is well agreed that the bank hydrology, flow hydraulics and soil properties neighbouring to the roots would be altered by the plants which are controlled by the seasons and its life cycle and, hence difficult to predict and integrate into bank stability analysis (e.g. Stark and Eid, 1995, Thiel et al., 1997). Meanwhile, the dead weights and the effects of wind load enhancement caused by the large plants destabilising the bank to a certain extent. Furthermore, consider the stabilising and destabilising factors, the surcharge of riparian plants typically exerts a marginal influence on the bank stability (Stark et al., 1996).

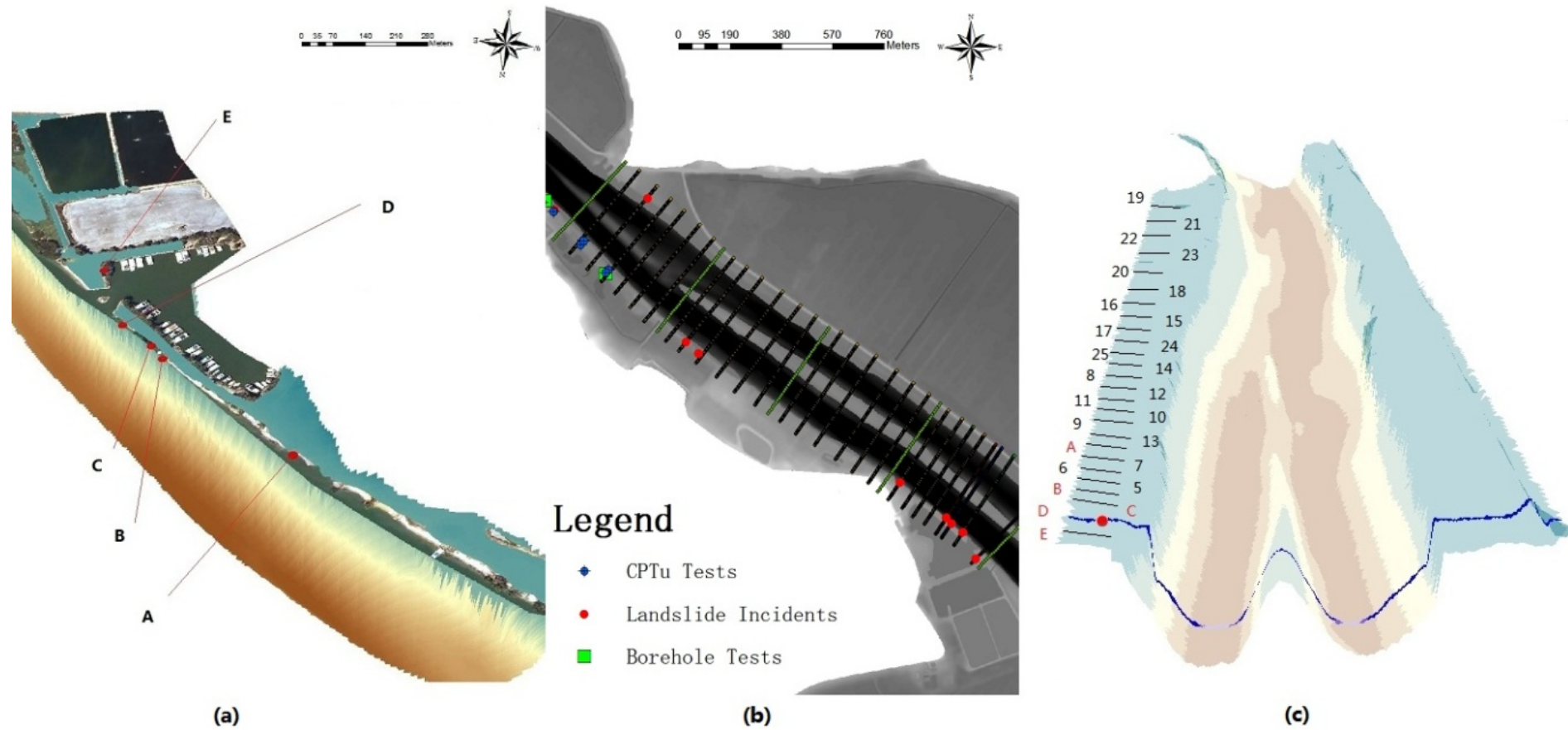


Figure 3.3 Long Island Marina study site: (a) locations of 5 significant failures; (b) location plan of in situ testing and recorded collapses; (c) distribution of bank cross sections in 3-D view.

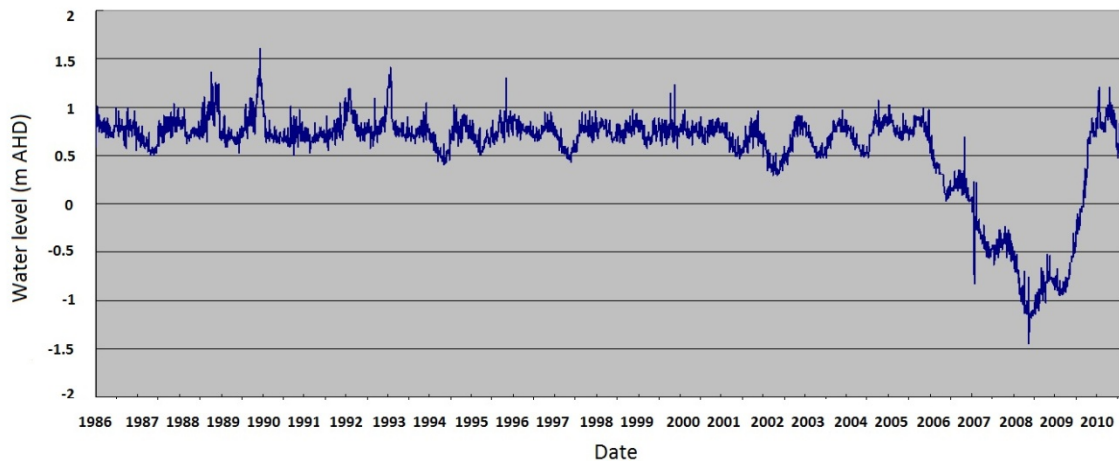


Figure 3.4 River Murray water at Murray Bridge 1/12/1986 to 11/07/2011
(DFW 2010).

As shown in Figure 3.5, based on the aerial images of 2008 and 2010, the locations of riparian residential regions were identified using visual interpretation under ArcMap. Under SVSlope (SVOoffice, 2012), the load exerted by a house to the foundation is roughly 20 kPa, which comprise the weight of the roof, walls, floor and the live loads.

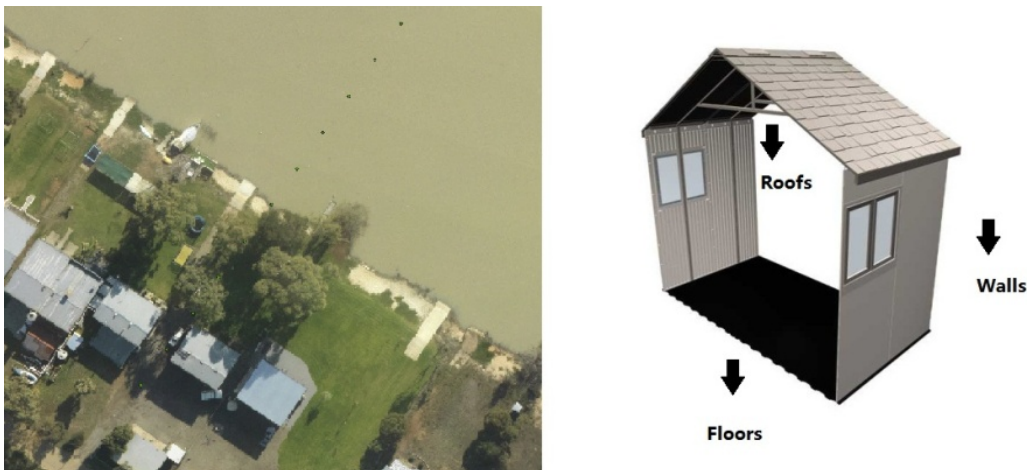


Figure 3.5 Schematic of the locations and the deadweight of the external loads
on the riverbank.

3.3 Analysis and discussion

According to the site investigations, deep-seated rotational slips and slab failure were indicated as two dominant riverbank retreat modes along Lower River Murray (Tajeddin et al. 2000). Slightly differentiate with the locations of failure; the deep-seated rotational failure typically occurred in the layer of silty clay (between -5 to -20 m AHD). The method selected for assess the stability of a slope is mainly determined by the geometry and relative locations of different soil types within soil mass and the shapes of slip surfaces (Abramson et al., 2002a). Therefore, with the consideration of dominating failure modes (Figure 3.6), study adapted Bishop Simplified method as Limit Equilibrium method of slices into calculation assuming that a FOS of unity represents incipient failure.

Under SVSlope framework, study integrated all the parameters mentioned above into 2-D cross section models. Based on the Consolidated Undrained (CU) Triaxial Tests (AS: 1289.6.4.2) on soil samples obtained from boreholes, values of effective cohesion (c') and effective internal friction angle (ϕ') were collected for corresponding representative elevations and applied as initial values in back-analyses. Hence, refer to the values of undrained shear strength collected from CPTs and the cohesion (c) and internal friction angle (ϕ) in terms of total stresses collected from Unconsolidated Undrained (UU) Triaxial Tests (AS: 1289.6.4.1), the general ranges of c' and ϕ' were estimated for the whole layers of soft or silty clay.

The results of back-analyses are summarised in Figure 3.7: two geotechnical models were adopted for the silty clay layer – Model 1: Unit weight = 16 kN/m^3 ; $c_{\text{top}} = 6.4 \text{ kPa}$; $c_{\text{max}} = 25 \text{ kPa}$; $c_{\text{ratio}} = 1.25 \text{ kPa/m}$; Model 2: Unit weight = 16 kN/m^3 ; $c_{\text{top}} = 10 \text{ kPa}$; $c_{\text{max}} = 25 \text{ kPa}$; $c_{\text{ratio}} = 0.87 \text{ kPa/m}$. The geotechnical model associated with the results of the site investigation is indicated in Figure 3.7 by “Site Investigation Model.”

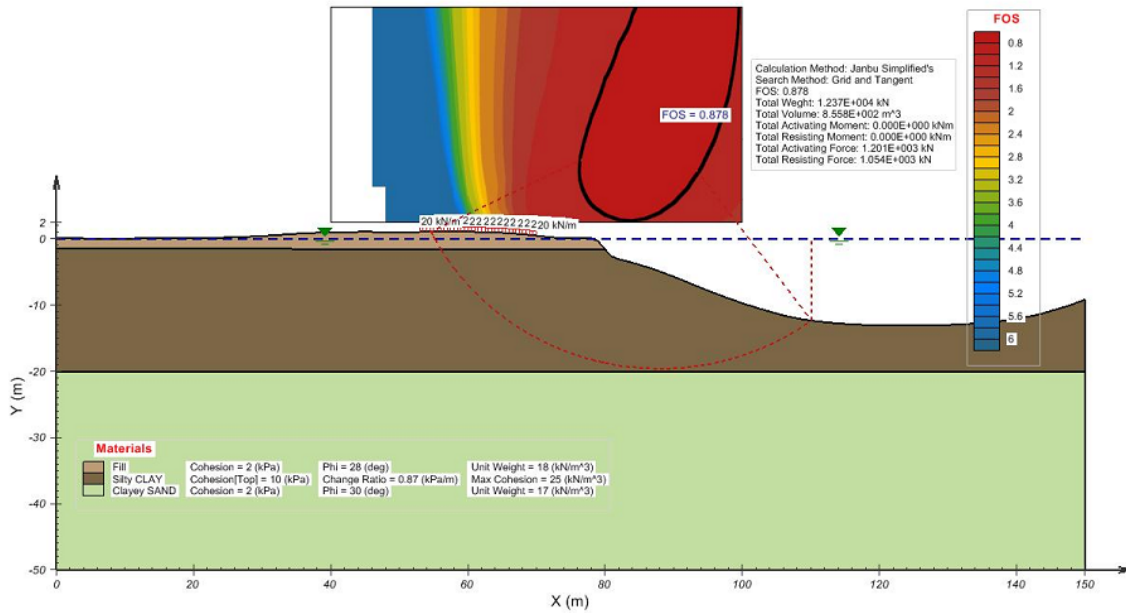


Figure 3.6 Minimum FOS and potential slip surface of deep-seated rotational failure at No. 21 model when water level was 0 m AHD.

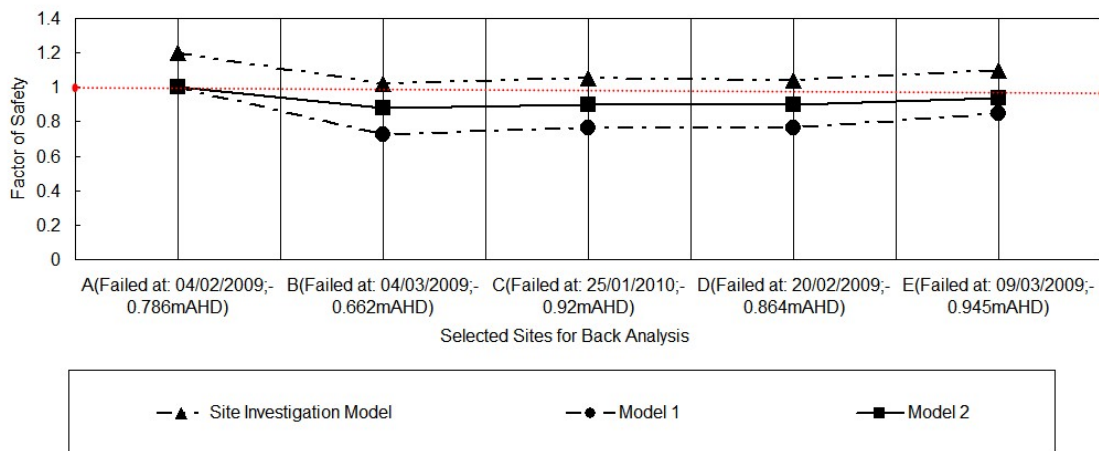


Figure 3.7 Back-analyses using three geotechnical models.

As mentioned previously, there is widespread agreement that river drawdown adversely affects riverbank stability (e.g. Spinger 1981, Mayo 1982, Thorne 1982, Springer et al. 1985, Dahm et al. 1988, Arontt 1994, and Budhu and Gobin 1995). In general, there are two types of drawdown: short term and long term, both of which remove the lateral support from the channel and destabilises the bank. The difference is the water table within the back does

not have time to equilibrate with the drawdown river level in the short term, which slightly reduces the magnitude of collapse (Budhu and Gobin 1995). The circumstances at Long Island Marina suggest that long term drawdown is more relevant, which leads to permanent changes in the properties and behaviour of bank assets and soils (SKM 2010).

With reference to the river level records at Murray Bridge during 2011, the river fluctuated between 0.5 and 1.2 m AHD, and rarely drew down below 0.5 m AHD. Based on this, a reasonable low river level boundary is expected to fall in between 0 and 0.5 m AHD in foreseeable future. In order to examine the susceptibility of the riverbank to collapse, simulations were performed at two river levels (0 and 0.5 m AHD) with two geotechnical models (Figure 3.8).

With reference to the River Murray, a long term FOS of 1.5 has been adopted as the minimum acceptable accounting for human safety and protection of assets (DFW 2010). In addition, $FOS \leq 1$ is adopted as “Unstable”, which indicates additional stabilisation is needed for stability; $1 < FOS \leq 1.25$ was assumed to be “Quasi stable”, indicating that minor destabilising factors can cause instability, such as additional surface loading, severe boat wash, river drawdown and high winds affecting trees; $1.25 < FOS \leq 1.5$ was adopted as “Moderately stable”, implying that moderate destabilising factors can cause instability, such as construction and extensive river drawdown; and $FOS > 1.5$ was adopted as “Stable”, denoting that only major destabilising factors will cause instability.

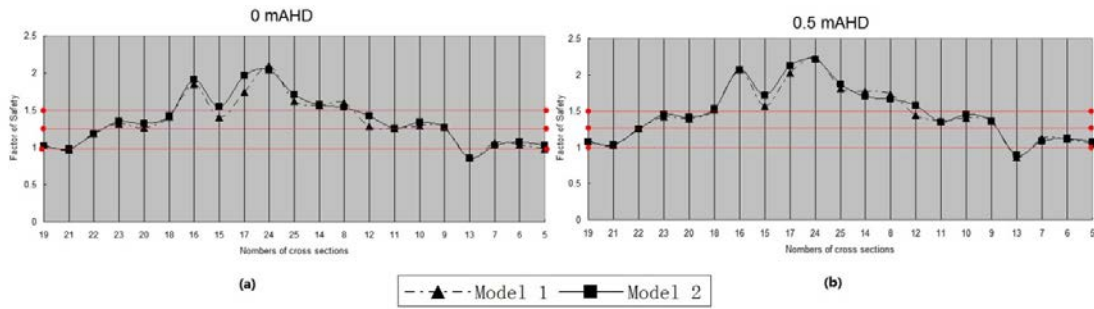


Figure 3.8 Factors of Safety of neighbouring cross sections (0 and 0.5 m AHD).

The results of the back-analysis at 0 m AHD river level is shown in Figure 3.9(a). It can be seen that Cross sections 5, 13 and 21 are about to collapse; 6, 7, 19 and 22 are at the limit of failure; 9, 10, 11, 12, 15, 18, 20 and 23 are moderately stable; and 8, 14, 16, 17, 24 and 25 are stable.

When the river levels are maintained at 0.5 m AHD, as indicated in Figure 3.9(b) it is observed that Cross section 13 is about to collapse; Cross sections 5, 6, 7, 19, 21 and 22 are at the limit of failure; 9, 10, 11, 12, 20 and 23 are moderately stable; and 8, 14, 15, 16, 17, 18, 24 and 25 are stable.

As shown in Figure 3.9, risk of riverbank instability is, in general, reduced by increasing river levels. Hence, when the river level is restore to 0.5 m AHD, a relatively large proportion of the banks examined present as quasi stable rather than moderately stable.

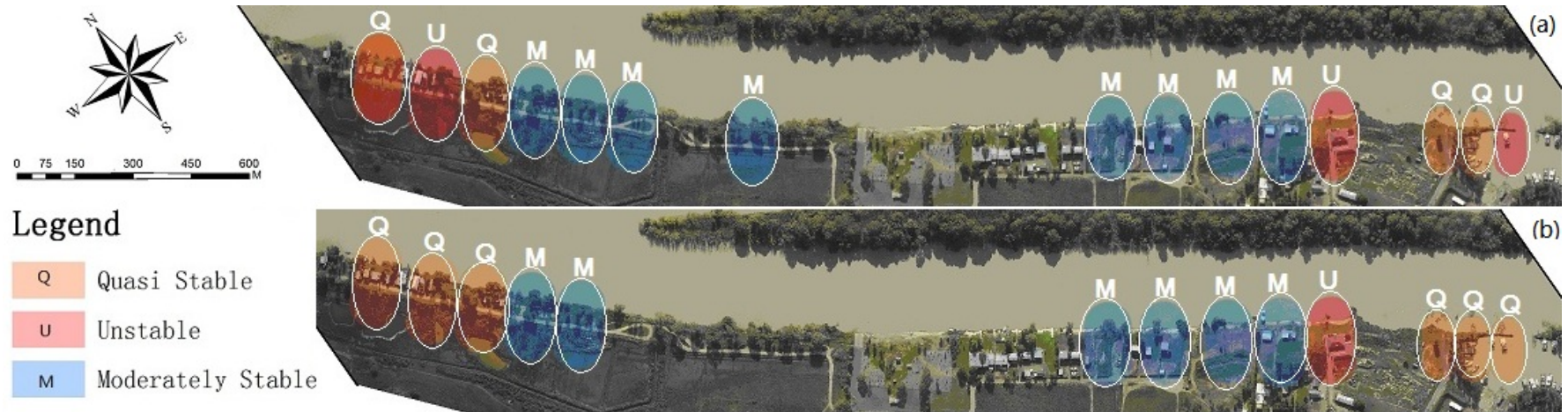


Figure 3.9 Predictions of riverbank susceptibility with river levels at (a) 0 m AHD and (b) 0.5 m AHD.

3.4 Conclusion

The recent low river levels in the Lower River Murray have caused the banks to remain in a long term metastable condition since 2007. The study site was adjacent to Long Island Marina at Murray Bridge in South Australia where a series of riverbank collapses have recently occurred. With high resolution LIDAR data and aerophotos, this research has vectorized the collapsed riverbank sections by visual interpretation and performed 2D back-analyses on 5 cross sections in the collapsed region using GIS, site investigation data and SVSlope. Hence, a series of sensitivity analyses has conducted with two different water levels: 0 and 0.5 m AHD on 21 cross section models using the results of back-analyses.

The results of this work have shown that a section of the riverbank is close to collapse, whereas a number of cross sections adjacent to the study site are susceptible to riverbank collapse and require further investigation. In addition, it has been observed that increased river levels generally stabilise the riverbanks but to a limited extent. Several remedial works may need to be conducted when the river level is predicted to fall for an extended period. Future work will incorporate climatic factors into the riverbank stability assessment at this and several other sites in the Lower River Murray.

Acknowledgements

This research was carried out with the assistance of the South Australian Department for Water (DFW). Without their data, resources and guidance this research cannot have been realised. The authors are grateful to Richard Brown, Jai O'Toole and Yani Grbich for their considerable assistance.

References for Chapter 3

Arnott, C. (1994). "Rates of stage fluctuation on the murray river between hume reservoir and albury." Honours research thesis, University of Melbourne.

Aronoff, S. (1989). "Geographic Information System: A Management Perspective." WDL Publications, Ottawa 279 pp.

Budhu, M., and R. Gogin (1995). "Seepage-induced slope failure on sandbars in grand canyon." *Journal of Geotechnical Engineering* 121(8), 601-609.

Burrough, P. A. (1986) "Principles of geographical information systems for land resources assessment." Clarendon Press, Oxford 194 pp.

Carrara, A., Cardinali, M., Detti, R., Guzzetti, F. Pasqui, V., and Reichenbach P. (1991). "GIS techniques and statistical models in evaluating landslide hazard." *Earth Surface Processes and Landforms*, 16, 427-445.

Carrara, A., Cardinali, M., Guzzetti, F. and Reichenbach, P. (1995) "GIS-based techniques for mapping landslide hazard." <<http://deis158.deis.unibo.it>>.

Dahm, J., and M. Edwards et al. (1988). "Preliminary investigation of the influence of Matahina Power Station on River bank stability along the Rangitaiki River." Hamilton, Electricity Corporation of New Zealand Ltd.

DFW (2010) "Riverbank collapse hazard expert panel, submission: site reports & investigation." Department for Water, Government of South Australia.

Filz, G. M., Brandon, T. L., and Duncan, J. M. (1992). "Back analysis of the Olmstead Landslide using anisotropic strengths." Transportation Research Board, 71st Annual Meeting, Washington, DC, January, 12-16.

Green, S.J. (1999) "Drawdown and river bank stability." Masters research thesis, Dept. of Civil and Environmental Engineering, University of Melbourne.

Hong, Y, Adler, R., and Huffman, G. (2007a). "Use of satellite remote sensing data in the mapping of global landslide susceptibility." *Natural Hazards*, 43(2).

Lee, W. Abramson, Thomas, S. Lee, Sunil, Sharma and Glenn, M. Boyce. (2002), "Slope stability and stabilization methods." 2nd ed. John Wiley & Sons, Inc., New York.

Marble, D. F. (1990). "Geographic information systems: an overview", in Peuquet, D. J., and Marble, D. F eds. *Introductory Readings in Geographic Information Systems*. Taylor and Francis Ltd., New York, pp 9-17.

Mayo, D. (1982). "Permissible rates of river rise and fall below Dartmouth Regulating Dam." State Electricity Commission of Victoria.

Okagbue, C., and T. Abam (1985). "An Analysis of Stratigraphic Control on the River Bank Failure." *Engineering Geology* 22(3): 231-245.

SKM. (2010) "Study into Riverbank Collapsing - Lower Murray River." Geotechnical Investigation Report, Report to Department of Water, Land and Biodiversity Conservation (DWLBC).

SoilVision (2012) "SVSlope." <<http://www.svslope.com/index.shtml>> (Jan. 13, 2012).

Springer, F. M. Jr., Ullrich, C. R., and Hagerty, D. J. (1985). "Streambank stability." *J. Geotech. Div., ASCE*, 111(5), 624-640.

Spinger, F. M. (1981) "Influence of the rapid drawdown events on river bank stability." Masters research thesis, University of Louisville.

Sterrett, R., and T. Edil (1982). "Ground-water flow system and stability of a slope." *Ground Water* 20(1), 5-11.

Thorne, C. R. (1982). "Processes and mechanisms of river bank erosion", in *Gravel-Bed Rivers*", Hey R. D., Bathurst, J. C., Thorne, C. R. eds., John Wiley & Sons, Chichester.

Wang, H., Liu, G., Xu, W., and Wang, G. (2005). "GIS-based landslide hazard assessment: an overview." *Progress in Physical Geography*, 29(4), 548–567.

Xie, M., Esaki, T., and Zhou, G. (2004). "GIS-based probabilistic mapping of landslide hazard using a three-dimensional deterministic model." *Natural Hazards*, 33(2), 265-282.

Chapter 4

4 Influence of River Level Fluctuations and Climate on Riverbank Stability

(Paper 2, published)

C. Liang¹, M. B. Jaksa¹, B. Ostendorf² and Y.L. Kuo¹

¹School of Civil; Environmental and Mining Engineering, University of Adelaide, 5005;

³School of Earth and Environmental Sciences, University of Adelaide, 5005;

Publication:

LIANG, C., JAKSA, M. B., OSTENDORF, B. & KUO, Y. L. (2015).
Influence of river level fluctuations and climate on riverbank stability.
Computers and Geotechnics, 63, 83-98.

Statement of Authorship

Title of Paper	Influence of River Level Fluctuations and Climate on Riverbank Stability
Publication Status	<input checked="" type="radio"/> Published, <input type="radio"/> Accepted for Publication, <input type="radio"/> Submitted for Publication, <input type="radio"/> Publication style
Publication Details	LIANG, C., JAKSA, M. B., OSTENDORF, B. & YIEN, K. L. (2015). Influence of river level fluctuations and climate on riverbank stability. Computers and Geotechnics, 63, 83-98.

Author Contributions

By signing the Statement of Authorship, each author certifies that their stated contribution to the publication is accurate and that permission is granted for the publication to be included in the candidate's thesis.

Name of Principal Author (Candidate)	Chen Liang
Contribution to the Paper	Undertook Literature review, performed parametric analysis and modeling, interpreted data and acted as corresponding author.
Signature	Date 11/Jan/2015

Name of Co-Author	Mark B. Jaksa
Contribution to the Paper	Supervised development of work and helped with paper editing.
Signature	Date 4/2/15

Name of Co-Author	Bertram Ostendorf
Contribution to the Paper	Supervised development of work.
Signature	Date 3-2-2015

Name of Co-Author	Yien Lik Kuo
Contribution to the Paper	Helped with in-situ and laboratory tests.
Signature	Date 3-2-2015

Abstract

Riverbank collapse is a natural part of the evolution of rivers. An unprecedented period of dry conditions and low flows between 2005 – 2010 led to more than 162 reported riverbank collapse-related incidents along the Lower River Murray, in South Australia (downstream of Lock 1 at Blanchetown to Wellington). On 4 February, 2009 a 60 x 20 m (70,000 m³) section of riverbank, near Long Island Marina, Murray Bridge, collapsed into the river, taking with it three unoccupied vehicles and several trees. This paper aims to: (i) model the Long Island Marina riverbank collapse incident in both 2D and 3D; (ii) examine the influence and sensitivity of river level fluctuations and climatic factors on riverbank stability; and (iii) determine the dominant triggers affecting collapse. The analysis has been undertaken using an integration of the limit equilibrium method, transient unsaturated flow modeling and digital elevation model and high resolution aerial images from a geographic information system. The paper demonstrates the efficacy of this framework and the accuracy of the predictions. It also reveals that river fluctuation, rather than climatic influences, dominates riverbank collapse in the Lower River Murray.

Keywords: GIS, riverbank stability, limit equilibrium method, drawdown, river level fluctuation, evaporation, rainfall, soil suction, River Murray

4.1 Introduction

Bank collapse is a natural and expected phenomenon associated with the evolution of rivers worldwide. Over the last 5 years or so, climatic factors such as rainfall, evaporation and river level fluctuations have combined with geographical and geotechnical factors, such as topography, stratigraphy and soil characteristics, to induce more than 162 reported riverbank collapse-related incidents along the lower River Murray, in South Australia (downstream of Lock 1 at Blanchetown to Wellington). Among these, 114 occurred during a period of extremely low river levels (lower than -0.5m AHD^1) due to an unprecedented period of dry conditions and low flows between 2005 – 2010. The most significant collapse occurred at Long Island Marina on 4 February 2009, where a $60 \times 20\text{ m}$ section of bank collapsed into the river (SKM, 2010b, Tajeddin et al., 2010, DFW, 2011, SKM, 2011, Liang et al., 2012). Based on site inspections, a large number of deep-seated circular failures in the soft and very soft clays of Holocene age were recognized as the dominant bank collapse mechanism along the lower River Murray (Coffey, 2012a).

The effects of climate and river level fluctuation on the stability of riverbanks have been extensively explored and discussed by several researchers (Hooke, 1979, Springer, 1981, Thorne, 1982, Osman and Thorne, 1988, Thorne and Osman, 1988, Casagli et al., 1999, Green, 1999, Pauls et al., 1999, Rinaldi and Casagli, 1999, Lane and Griffiths, 2000, Zhang et al., 2005, Jia et al., 2009, Yongquan et al., 2011). Compared with the assessment of landslides in mountainous regions, changes in pore water pressure, in particular soil suction (negative pore water pressure), plays a more fundamental role in the stability of riverbanks (Hooke, 1979, Thorne, 1982, Casagli et al., 1999, Rinaldi and Casagli, 1999, Abramson et al., 2002b). The pore water pressure significantly affects riverbank stability by changing the soil shear strength (Liang et al., 2012). As stated by Fredlund (Fredlund, 2006), soil suction can vary from zero to approximately 1,000 MPa in the unsaturated (or vadose) zone

¹ Australian Height Datum

(Bouwer, 1978) and is highly dependent on the properties of the soil, hydrological conditions and soil–atmospheric interactions (Lane and Griffiths, 2000).

Rainfall has long been recognized as one of the most significant factors responsible for initiating slope failures in many tropical or subtropical regions (Zhang et al., 2011). Generally, rainfall-induced slope failures are observed as shallow failures, however deep-seated rotational failures are also reported (Zhang et al., 2011). According to Rahardjo et al. (Rahardjo et al., 2007), the initial FoS of the slope is determined by the slope geometry and initial water table while the actual rainfall-induced failure conditions are greatly influenced by rainfall characteristics and soil properties. The nature of the rainfall, such as intensity, duration, spatial distribution and antecedent characteristics, significantly influences the occurrence of rainfall-induced landslides by affecting the pore water pressure distribution and increases the self weight of the slope material (Abramson et al., 2002b, Rahardjo et al., 2008, Rahimi et al., 2011, Zhang et al., 2011, Mukhlisin and Taha, 2012). Based on several studies performed in Hong Kong, Lumb (Lumb, 1975) and Brand (Brand, 1984) indicated that antecedent rainfall has a negligible effect on local rainfall-induced landslides. They concluded that rainfall intensity and duration had the most profound influence on the slope failure due to localized high conductivity soils (Lumb, 1975, Brand, 1984). Later, Rahimi and Rahardjo (Rahardjo et al., 2001, Rahardjo et al., 2008, Rahimi et al., 2011) implemented a series of more detailed studies along the Sieve River in Italy in relation to rainfall associated with soils of different conductivities. Their work showed that the rate of decrease in FoS, the time corresponding to the minimum FoS and the value of the minimum FoS are all controlled by the rainfall distribution. In comparison, rainfall can induce up to a 45% reduction in the FoS of soil slopes with lower fines content and higher saturated permeability ($K_{\text{sat}} \geq 10^{-5}$ m/s) than those with a high fines content and low permeability ($K_{\text{sat}} \leq 10^{-6}$ m/s) (Rahimi et al., 2011). These geotechnical properties greatly influence the behavior of rainfall-triggered slope failures because they affect rainwater seepage and infiltration. Rahardjo et al. (Rahardjo et al., 2007) examined the relationship between K_{sat} , soil suction,

FoS and the magnitude of rainfall. Their work found that, under modest rainfall intensity (10 mm/h), soils with $K_{\text{sat}} = 10^{-6}$ m/s were associated with the lowest FoS, followed by soil with $K_{\text{sat}} = 10^{-5}$ m/s. In contrast, under relatively intense rainfall (greater than 200 mm/h), soils with $K_{\text{sat}} = 10^{-5}$ m/s were associated with the lowest FoS.

River level fluctuation has been shown to influence riverbank stability in two important ways: (i) its effect on reducing negative pore water pressure and, hence, its consequent reduction in soil strength, and (ii) the hydrostatic pressure it applies to stabilizing the riverbank (Casagli et al., 1999, Green, 1999, Rinaldi and Casagli, 1999). Due to the limited models available at the time, studies in the 1980s typically proposed simple hypotheses on pore water pressure conditions of the riverbank (dry or total saturated) and adopted relatively simple solutions for slab failures (Hooke, 1979, Higgins, 1980, Springer, 1981, Thorne, 1982, Thorne and Osman, 1988). Later in the 1990s and 2000s, with developments in unsaturated soil mechanics theory, the effect of pore water pressure on unsaturated riverbanks and confining pressure became more widely accepted and included into drawdown analysis and research of riverbank stability (Casagli et al., 1999, Green, 1999, Pauls et al., 1999, Rinaldi and Casagli, 1999, Lane and Griffiths, 2000, Rinaldi et al., 2004, Zhang et al., 2005, Berilgen, 2007, Jia et al., 2009, Yan et al., 2010, Yongquan et al., 2011). It is generally accepted that when rivers experience an initial high-flow period, the riverbanks are stable due to the supportive effect of the hydrostatic pressure of the water. However, the processes of erosion and soil saturation during high flow events weaken many parts of the bank by undermining it and reducing the effective strength, respectively (Twidale, 1964, Hooke, 1979, Springer, 1981, Thorne, 1982, Thorne et al., 1997). Berilgen (2007) indicated that the stability of a submerged slope during drawdown greatly depends on the rate of pore water drainage. While during initial low-flow periods, the matric suction (the suction due to capillary action and water surface tension) occasionally allows the riverbank remain stable at steep angles (Casagli et al., 1999). However, subsequent rainfall increases the dead weight of the bank material and reduces the matric suction which might be sufficient trigger a mass failure (Rinaldi et al., 2004).

A very limited number of studies modeled the coupling of climatic factors and river level fluctuations. Casagli and Rinaldi (Casagli et al., 1999) used tensionmeters, piezometers and a rain gauge on the Sieve River to monitor the matric suction evolution and riverbank stability in a semi-arid climate with daily river flow changes over a 16-month period. Later, based on these monitoring works they performed transient modeling on a drawdown failure which occurred on 14 December 1996 (Rinaldi et al., 2004). In their transient model they divided the research period (13 – 18 December 1996) into 24 time steps to examine the behavior of the riverbank under different rainfall and flow events. Their work indicated that the minimum FoS always occurred after the peak level of the Sieve River, and no later than 5.5 hours after. The result suggests that riverbank collapse on Sieve River is dominated by river level fluctuations, primarily due to the reduction in the stabilizing influence of hydrostatic pressures due to river level drawdown, and marginally due to rainfall. This is further supported by the work of Twidale [38], Thorne [17, 18, 37], Springer [16] and others.

Geographic Information Systems (GISs), which are well known for their efficient and effective processing of spatial data, have greatly facilitated the research of natural hazards, especially with respect to slope instability studies (Xie et al., 2003, Zaitchik and Es, 2003, Lee et al., 2004, Xie et al., 2004, Wang et al., 2005, Acharya et al., 2006, Xie et al., 2006, Merwade, 2007, Zolfaghari and Heath, 2008, Ozdemir, 2009, Liang et al., 2012). With the integration of high-resolution, remotely-sensed (RS) data, such as LIDAR (light detecting and ranging) images and aerial photographs, the GIS framework is adopted in the present paper to facilitate riverbank stability analyses in the following three ways: (a) the topographic information of the site is obtained from data extracted from the Digital Elevation Model (DEM); (b) the collapsed regions are examined by visual interpretation of high resolution aerial images; and (c) the dimensions of the simulated collapsed regions are validated against high resolution aerial images.

The aims of the paper are to: (i) model the riverbank collapse incident, in both 2D and 3D, which occurred at Long Island Marina, Murray Bridge, South Australia, on 4 February 2009; (ii) examine the influence and sensitivity of river level fluctuations and climatic factors on riverbank stability; and (iii) determine the dominant triggers affecting collapse. Specifically, the study implements a transient water model in both two and three dimensions to evaluate the FoS of the riverbank by determining the temporal distribution of pore water pressure in the riverbank and simulating its dynamic response to river level fluctuations and rainfall. Due to the relatively low width-to-height ratio of the riverbank collapsed region, as indicated by bathymetric surveys, a three dimensional analysis is also performed to complement and validate the date and extent of the collapse and to compare this with the results derived from the 2D model. Details of the Long Island Marina site are presented in the following section.

4.2 Study area

The study area is located along the lower River Murray adjacent to the Long Island Marina, Murray Bridge, South Australia, as shown in Figure 4.1(a). The River Murray is the largest river in Australia and is one of the only river systems in the world that can fall below sea level due to the barrages preventing the inflow of sea water during periods of low river flows (SKM, 2010a). From the inventory of the South Australian Department of Environment, Water and Natural Resources (DEWNR), formerly the Department for Water (DFW), several incidents were recorded at Long Island Marina between 2008 and 2010. These included 5 major riverbank collapses, an identified significant tension crack, two riparian trees leaning into the river, and one levee bank related incident (Liang et al., 2012).

On 4 February 2009, a significant riverbank collapse incident occurred which involved a 60 meter stretch of riverbank [Region (i) in Figure 4.1(b)], which failed without warning. Several large trees, 3 unoccupied vehicles and an estimated 70,000 cubic meters of bank material collapsed into the river (SKM,

2011). The bathymetry, as shown in Figure 4.1(b), illustrates the scale of a series of collapses which occurred in the vicinity of Long Island Marina. According to the inventory, the rest two collapses occurred on 3 March 2009 (ii) and 25 January 2010 (iii), respectively.

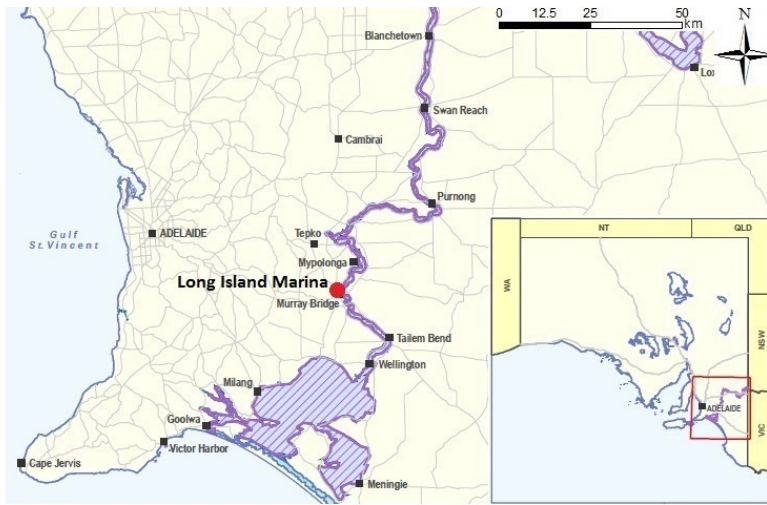
A site investigation was performed in October and November, 2009 at the Long Island Marina site by SKM (SKM, 2011) in order to obtain geotechnical information related to the collapse. Details of the investigation and geotechnical characteristics are presented later.

4.3 Methodology and model development

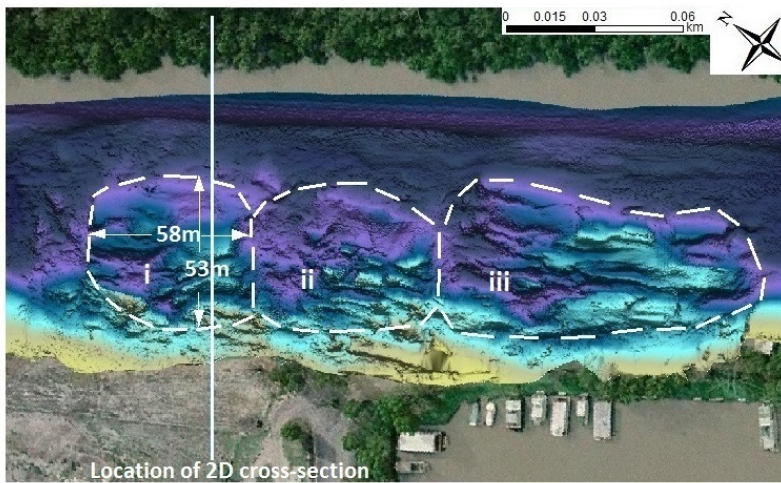
In order to investigate the factors influencing the Long Island Marina riverbank collapse, a transient slope stability model was developed in both 2D and 3D. The model incorporates riverbank geometry, geotechnical properties, river level variation, and rainfall and evaporation. The implementation of each of these into the transient model is outlined in the sub-sections that follow.

The Windows-based program SVFlux (SoilVision, 2009a) was used to undertake finite element analyses of saturated and unsaturated groundwater flows, in conjunction with SVSlope (SoilVision, 2009b), which performs limit equilibrium slope stability calculations, in this case, in both two and three dimensions. Specifically, SVFlux was employed to model the distribution of pore water pressure against time subject to different circumstances of rainfall, evaporation and river level fluctuations. These were subsequently imported into SVSlope to examine the stability of the riverbank at each time-step. The limit equilibrium method (Bishop's method of slices) was employed to perform the limit equilibrium slope stability calculations. The sliding surfaces were determined using the "grid and tangent" and "slope limit" methods, and for the 3D model, reference was made to the actual dimensions and location of the collapsed region. In order to determine the most appropriate soil properties for the high plasticity, Silty Clay layer, as explained later, and to accommodate variability of soil properties, back-analyses were performed to

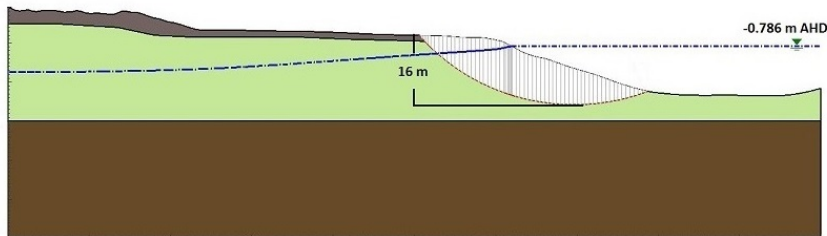
obtain the closest match between the predicted and actual date of failure (in the 2D analysis) and the dimensions of the collapsed region (3D analysis).



(a) Location of study area.



(b) Aerial bathymetry image at Long Island Marina, Murray Bridge showing the contours of the riverbed and the collapse of 70,000 m³ of material into the River Murray (Beal et al., 2010).



(c) 2D cross-section showing river level on the date of collapse.

Figure 4.1 Details of the Long Island Marina site.

4.3.1 Topography

As mentioned above, in order to determine the riverbank geometries associated with the Long Island Marina collapse, the GIS framework is adopted using topographic information obtained from the DEM; the collapsed regions are examined by visual interpretation of high resolution aerial images; and the dimensions of the simulated collapsed regions are validated against these high resolution aerial images.

It is well understood that the topography of the ground significantly influences the likelihood or otherwise of instability (Schuster and Krizek, 1978, Abramson et al., 2002b). More specifically, the landform controls the physical characteristics of the slope, which affects the potential failure modes, whereas the inclination and regional topography influences drainage and hence the distribution of pore water pressure, which in turn, influences riverbank stability.

As mentioned above, the Long Island Marina riverbank failure is examined in both two and three dimensions. It is commonplace in the assessment of slope stability for 2D cross-sections to be adopted (Rahardjo et al., 2001, Rahardjo et al., 2008, Rahimi et al., 2011). Stark (2003) undertook a study where he compared several 2D and 3D analyses and concluded that, if the width-to-height ratio of the collapsed region is larger than 6, the difference in the factors of safety obtained from the 2D and 3D analyses is marginal. In the Long Island Marina riverbank collapse, as shown by Region (i) in Figure 4.1(b) from the bathymetric data and Figure 4.1(c) from the cross-sectional model, the width-to-height ratio is found to be equal to 3.75 (60 m in width and 16 m in height). Hence, 3D modeling is beneficial in this study by affording an additional analytical technique to validate the volume of the collapsed region and to compare the FoS time history with that obtained from the 2D model.

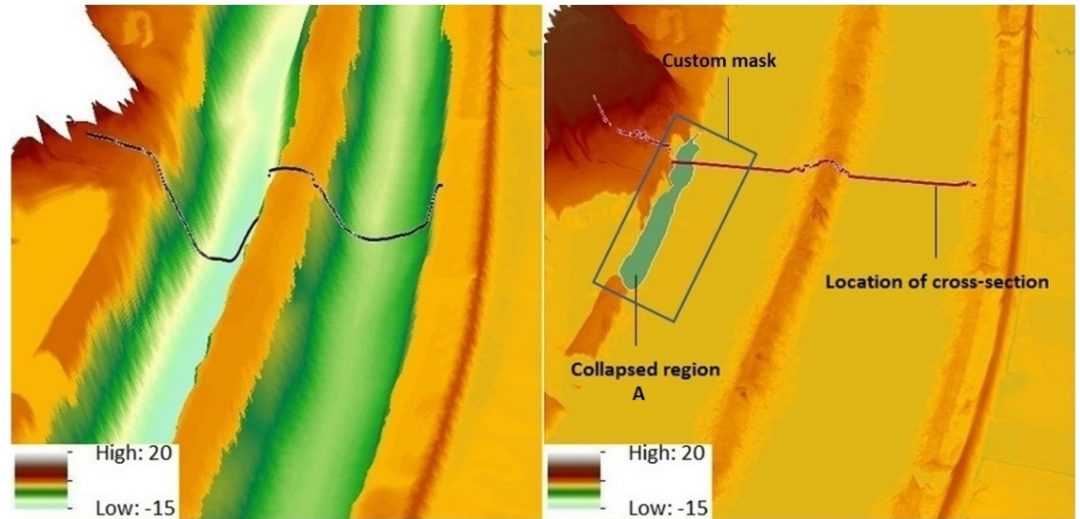
In order to establish accurate riverbank geometries, the ArcGIS software is used, incorporating the bilinear interpolation method based on elevation

extraction. As shown in Figure 4.2(a) and (b), the 2D cross-sectional model is initially obtained as a polyline comprised of 401 points with a 10 m interval between neighboring points. The location of the cross-section used in the 2D analysis was selected to coincide with the first recorded collapse, as indicated in the DEWNR riverbank collapse inventory and the bathymetric data [Region (i)], as shown in Figure 4.1(b) and Figure 4.2(b). Based on the bilinear interpolation method, the elevation values were extracted from two DEMs (a 1 m resolution model acquired in 2008 and b 0.2 m resolution model acquired in 2010) and assigned to 401 points, with singular points avoided. This approach yielded accurate and high resolution cross-sections, suitable for subsequent importing into SVFlux and SVSlope.

By utilizing the high resolution DEMs, the topography of the riverbank region of interest was extracted using custom masks within ArcGIS [Figure 4.2(b)] for the purpose of reproducing the riverbank model in three dimensions. Because of the nature of DEM data, the elevation values that were extracted were irregularly distributed. To resolve this issue, the inverse distance weighting method (IDW) was used to interpolate a new raster based on the former irregularly distributed elevation values. As shown in Figure 4.2(c), the geometry of the riverbank was established in three dimensions in SVFlux 3D from the updated elevation values extracted from the new raster.

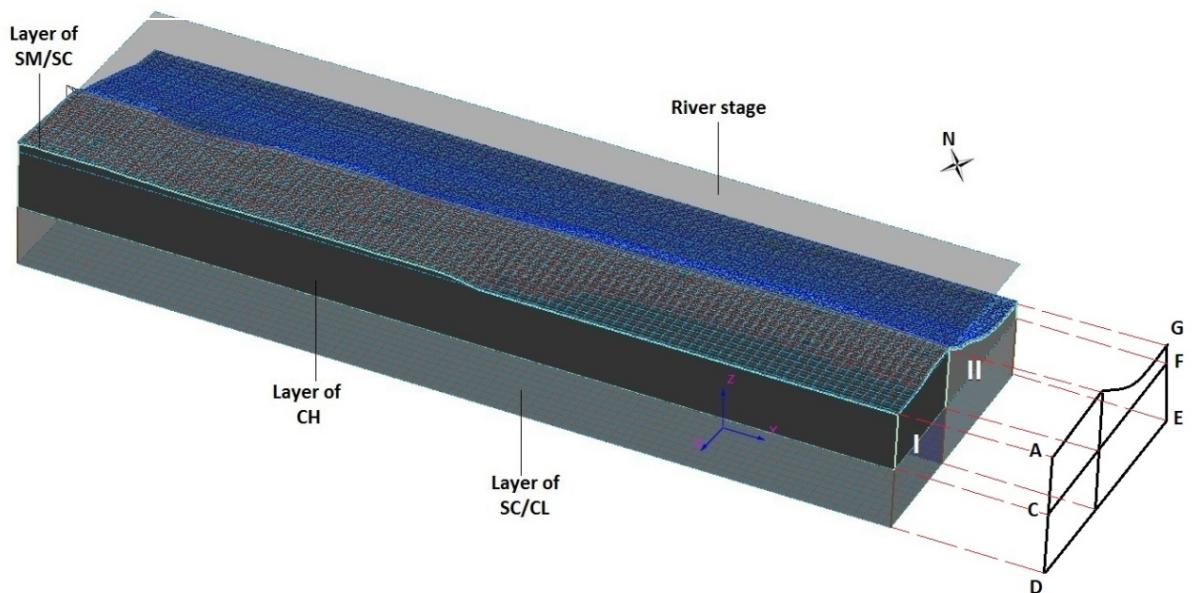
The dimensions of the collapsed regions of the riverbank need to be identified with a relatively high level of accuracy in order to facilitate the proposed modeling. In this study, this was achieved by undertaking a visual interpretation of the high resolution aerial images taken on different dates (Liang et al., 2012). By comparing the 0.5 meter resolution aerial photos acquired in March 2008 [Figure 4.3(a)] with the 0.2 meter resolution photos acquired in May 2010 [Figure 4.3(c)], the collapsed Region A was accurately identified and vectorized. Compared with the collapsed regions (i), (ii) and (iii) shown in Figure 4.1(b), Region A [shown by the dotted region in Figure 4.3(c)] is the section above the river level. To assist with the visual interpretation of the collapsed region, LIDAR DEMs obtained in 2008 [Figure 4.3(b)] and 2010 [Figure 4.3(d)] were employed, especially to verify the

elevation of the riverbank prior to the collapse with river levels at the same location subsequent to the collapse. For example, location A', where the riverbank was at 1.25 m AHD prior to the collapse, is compared with the river level at location B', which is at -0.57 m AHD subsequent to the failure. By adopting this comparative process, the identified region A is confirmed as having collapsed rather than simply having been submerged.



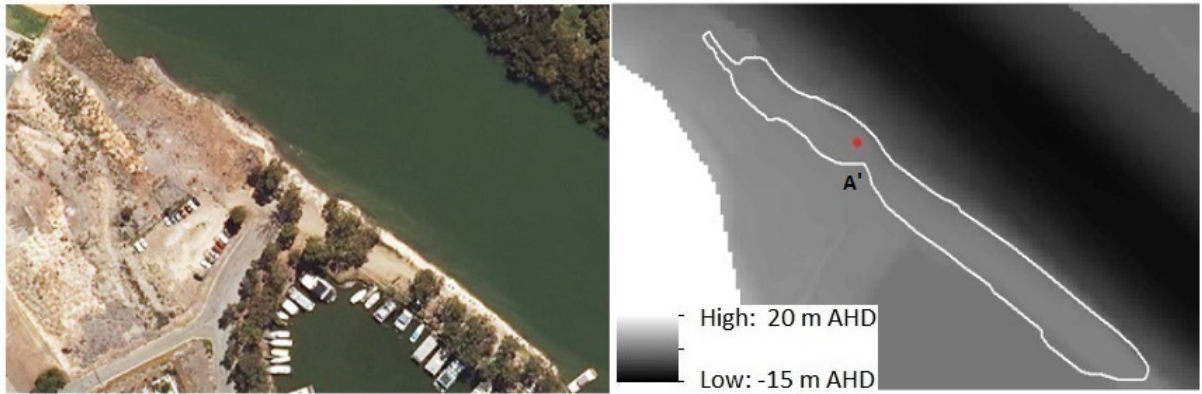
(a) Elevation extraction from the 2008 LIDAR DEM.

(b) Elevation extraction from the 2010 LIDAR DEM, with river level



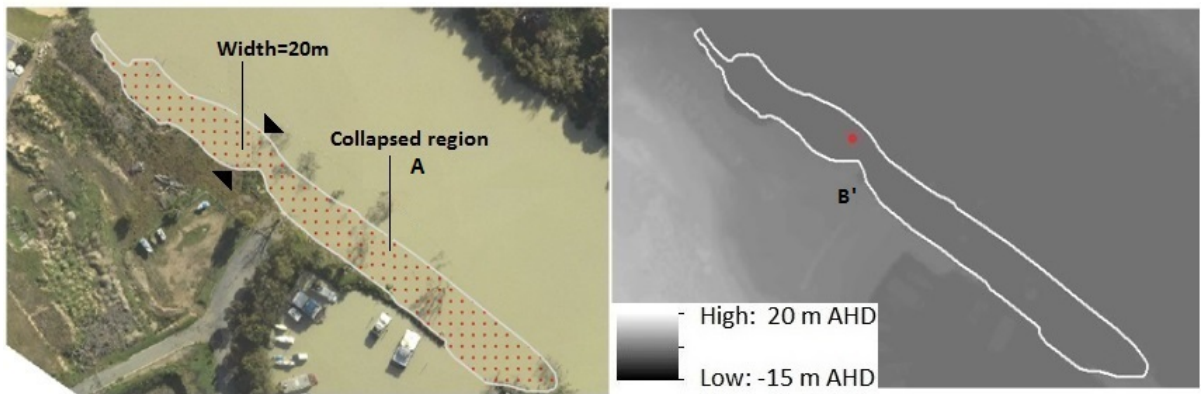
(c) 3D topographical model.

Figure 4.2. Riverbank geometry definition.



(a) Aerial photo in 2008.

(b) LIDAR DEM before collapse.



(c) Aerial photo in 2010 with collapsed region highlighted.

(d) LIDAR DEM after collapse.

Figure 4.3. Example of adopted visual interpretation process on high resolution, aerial images within the ArcGIS framework.

4.3.2 Geotechnical properties

The geotechnical model is developed from the results of a geotechnical investigation performed at Long Island Marina by SKM [4], which included the drilling of two boreholes to a depth of 20 m, 12 piezocone tests (CPTUs) with pore water pressure (u) measurements, and a series of vane shear and laboratory tests (Figure 4.4 to Figure 4.8).

In accordance with the borehole logs from SR-BH1 and SR-BH2 [4], the bank profile at Long Island Marina has previously been modeled by SKM (2010a) and Coffey (2012a) using three separate soil layers. Specifically, in the SKM and Coffey models, as summarised in Table 4.1, an effective stress analysis was performed in the Fill and SC layer using the Mohr-Coulomb failure criterion, while a total stress analysis was adopted in CH layer using a depth-dependent, undrained soil model. The adopted depth-dependent, undrained soil model incorporates linearly-increasing cohesion with depth, with c_{top} quantifying the cohesion (kPa) at the upper layer boundary, c_{ratio} representing the gradient of increasing cohesion with depth and capped at a maximum value of c_{max} (SKM, 2010a). However, in order to accommodate the effects of positive and negative pore water pressures in unsaturated river-banks, an unsaturated stress analysis is performed in the Fill and CH layer for this paper, which will be discussed later. As summarised in Table 4.1, the values recommended by SKM (2010a) and Coffey (2012) were inferred from laboratory and in situ test results obtained from their respective geotechnical investigations.

In order to determine accurately the variation of total soil suction with time and moisture, a soil water characteristic curve (SWCC) is adopted in the finite element method analyses for unsaturated soils within SVFlux. The Zapata method (Zapata et al., 2000) is used to estimate the SWCC in each of the soil layers from the particle size distributions (PSDs) shown in Figure 4.5. The weighted Plasticity Index (wPI) is used within the Zapata method and is defined as an indicator for water adsorption and retention in soil particles with different surface areas (Zapata et al., 2000). As stated by Zapata, a proportional relationship exists between the equilibrium soil suction at a given degree of saturation and the specific surface area of the soil. Compared with the plasticity index (PI), wPI is considered as a better indicator, especially for the soils which have a high PI but are associated with relatively small surface areas (Zapata et al., 2000). As shown in Table 4.1, for soil with a high plasticity ($wPI > 0$), such as the Silty Clay (CH), the Fredlund and Xing (Fredlund et. al., 1995) parameters a_f , b_f , c_f and h_f are calculated based on the relationships shown in Table 4.2 to estimate the SWCC for each of the three

layers (Figure 4.6). In contrast, for granular soils with $wPI = 0$ (i.e. non-plastic soils), the parameter D_{60} , which represents the grain diameter corresponding to 60% passing by weight from the PSD, is employed.

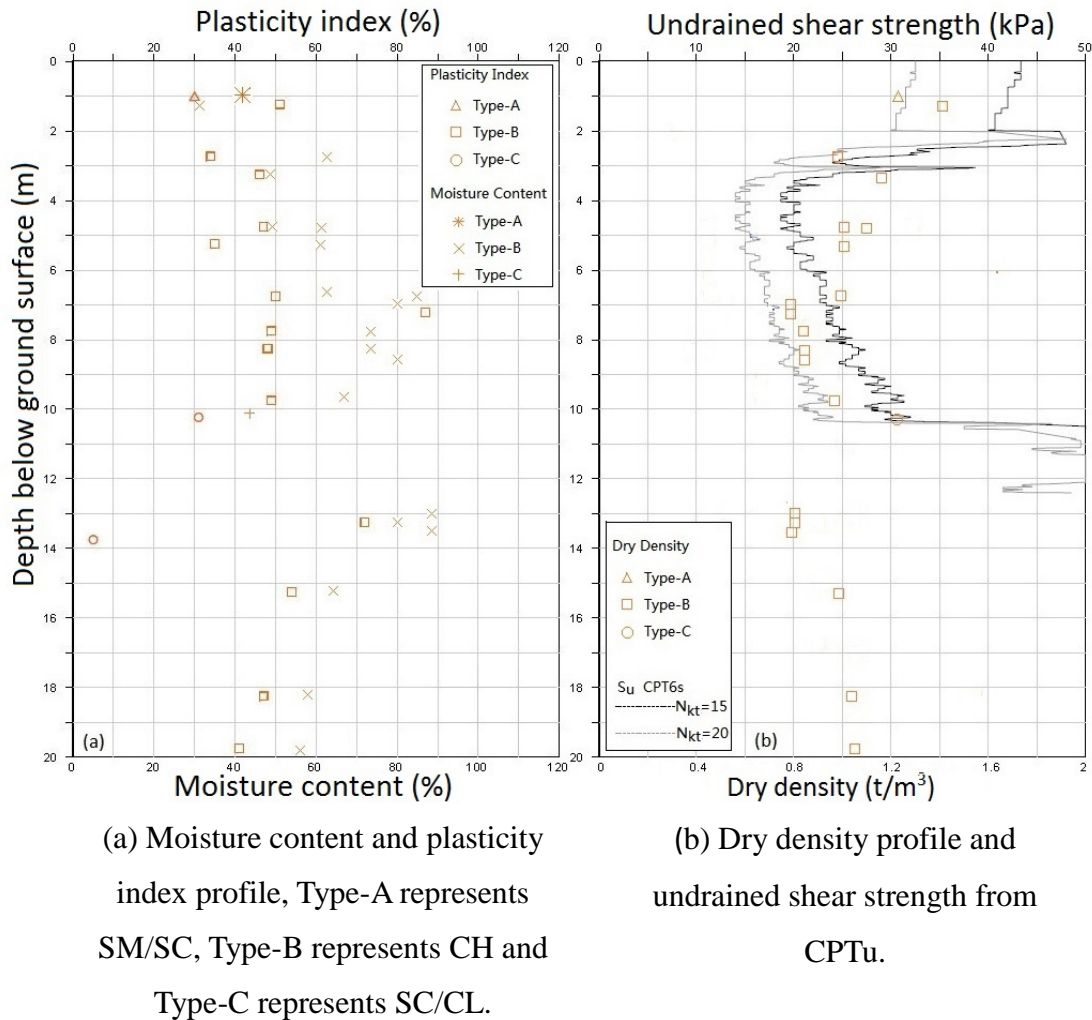


Figure 4.4 Geotechnical profiles based on soil samples taken from SR-BH1 and SR-CPTu6s at Long Island Marina.

The saturated hydraulic conductivity, K_{sat} , is derived from a CPTu pore pressure dissipation test performed in the CH layer at 5 m depth at the Murray Bridge site (Figure 4.7). Based on relationships between measured excess pore pressures and the saturated hydraulic conductivity (Voyiadjis and Song, 2003) for the clay layer, K_{sat} is found to equal approximately 9.86×10^{-5} m/day, as shown in Table 4.1. The values of K_{sat} for the Fill and SC layers are derived from empirical values (Table 4.1) as no measurements were available. In unsaturated soil, the unsaturated hydraulic conductivity, K , varies with

respect to matric suction, and is calculated indirectly from the Fredlund and Xing estimation associated with K_{sat} (Fredlund et al., 1995). Adopting Equation (4.1), the saturated volumetric water content, θ_{sat} , is determined based on tests from borehole soil samples (Table 4.1).

$$\theta_{sat} = 1 - \frac{\rho}{G_s \rho_w (1 + w)} \quad (4.1)$$

Where ρ is the dry density; ρ_w is the density of water at 4°C and w is the moisture content.

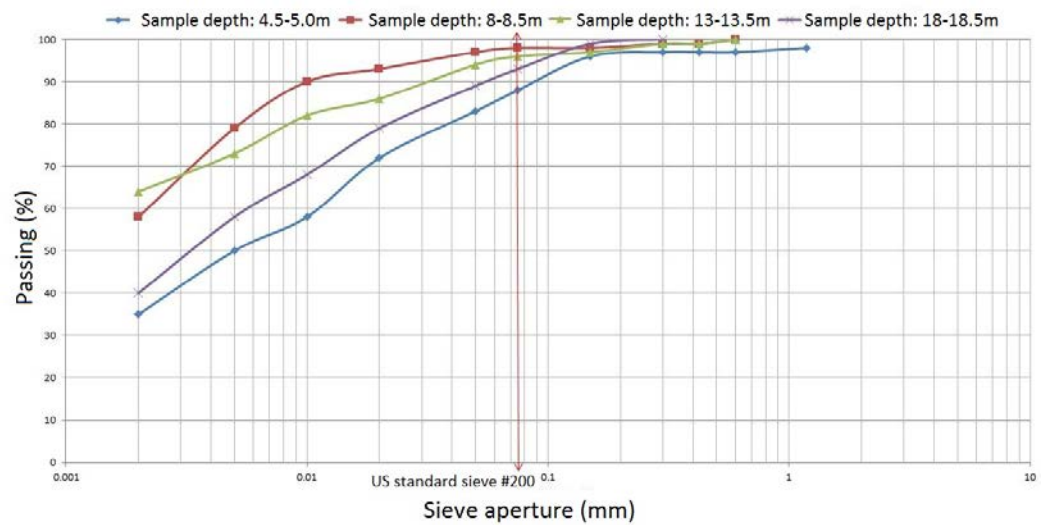


Figure 4.5 Particle size distributions based on the soil samples from four different depths in borehole SR-BH1.

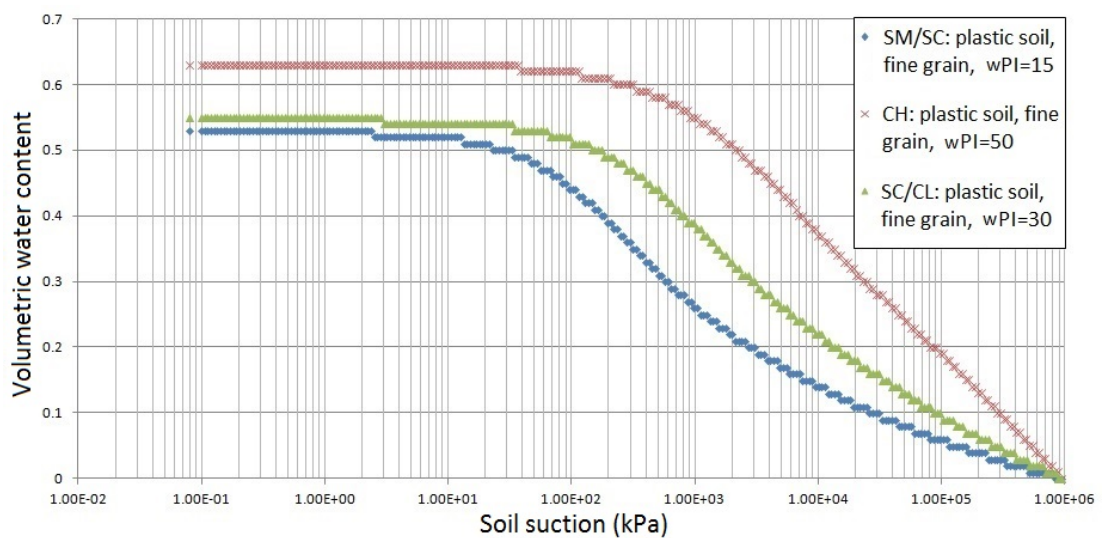
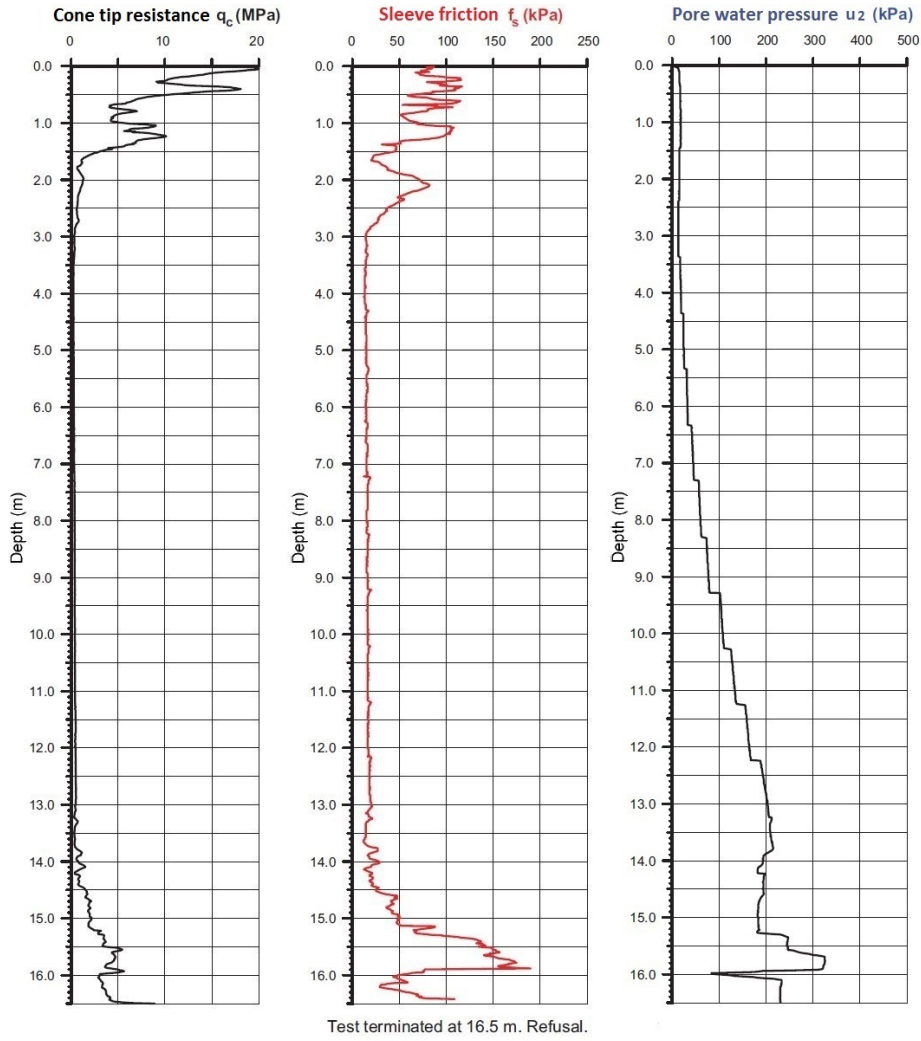
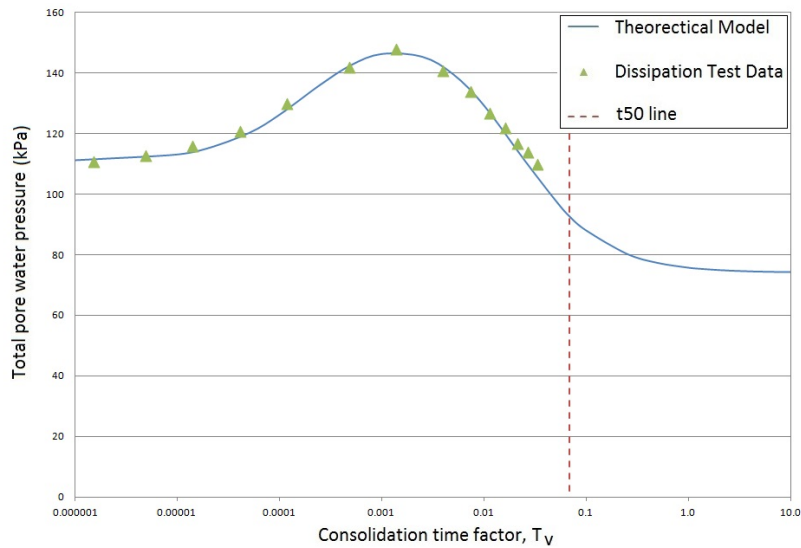


Figure 4.6 Estimated SWCCs for the three soil layers at Long Island Marina using the Fredlund and Xing fit estimation method.



(a) CPTu profile at Murray Bridge.



(b) Dissipation test data.

Figure 4.7 Typical CPTu profile and dissipation test results.

Table 4.1 Soil parameters for stability assessment.

Layer	Elevation (m AHD)	c' (kPa)	ϕ'	γ (kN/m ³)	Undrained parameters for CH layer from SKM (kPa)	Undrained parameters for CH layer from Coffey (kPa)	K_{sat} (m/day)	θ_{sat}
Silty/Clayey Sand (SM/SC)	1 to 0	$c'=2 \pm 2$	$28^\circ \pm 2^\circ$	18 ± 1	–	–	13.51	52.7%
Silty Clay (CH)	0 to –20	0	27°	16 ± 1	$c_{u-top} = 10 \pm 5$ $c_{u-ratio} = 1.25$ $c_{u-max} = 25 \pm 5$	$c_{u-top} = 5.5$ $c_{u-ratio} = 1.25$ $c_{u-max} = 25 \pm 5$	9.9×10^{-5}	63.2%
Clayey Sand/ Sandy Clay (SC/CL)	> –20	$c'=2 \pm 2$	$30^\circ \pm 2^\circ$	17 ± 1	–	–	0.187	54.6%

Table 4.2 Equations used to calculate Fredlund and Xing SWCC fitting parameters based on the soil grain size distribution.

Soil with high plasticity	Non-plastic soil
$wPI > 0$	$wPI = 0$
$a_f = 32.825 \ln(wPI) + 32.438$	$a_f = 1.14a - 0.5$
	$a = -2.79 - 14.1 \log(D_{20}) - 1.9 * 10^{-6} P_{200}^{4.34} + 7 \log(D_{30}) + 0.055 D_{100}$
$b_f = 1.42(wPI)^{-0.3185}$	$b_f = 0.936b - 3.8$
	$b = (5.39 - 0.29 \ln(P_{200}^{D_{90}/D_{10}}) + 3D_0^{0.57} + 0.0021P_{200}^{1.19})(30/\log(D_{90}) - \log(D_{60}))^{0.1}$
$c_f = -0.2154 \ln(wPI) + 0.7145$	$c_f = 0.26e^{0.758c} + 1.4D_{10}$
	$c = \log(20/\log(D_{30}) - \log(D_{10}))^{1.15} - 1 + 1/b_f$
$h_r = 500$	$h_r = 100$
$wPI = PI * P_{200}/100$	$D_{100} = 10^{4(\log(D_{90}) - \log(D_{60}))/3 + \log(D_{60})}$
	$D_0 = 10^{-3(\log(D_{30}) - \log(D_{90}))/2 + \log(D_{30})}$

Where P_{200} is the percentage of soil passing US standard sieve #200. PI is the plasticity index as shown in Figure 4.4(a); and $D_{\%}$ is the grain diameter related to the percentage of passing in mm.

4.3.3 Hydrological and climatic variables

In order to model the influence of rainfall on riverbank stability it is necessary to estimate the runoff coefficient so that infiltration of rainfall into the riverbank can be evaluated. It is well understood that the runoff coefficient is a function of hydraulic conductivity and thickness of the near-surface soil layers, the type of surface vegetation and land use. Due to the high rate of evapotranspiration, temporal and spatial variability in rainfall intensity and frequency, and the generally flat topography across most of South Australia (National Water Commission, 2005) the runoff coefficient is relatively small. Hence, based on the *Australian Rainfall and Runoff* (Institution of Engineers, 1987) a runoff coefficient of 6 is established for Murray Bridge for an average recurrence interval of 10 years.

As indicated above, extremely low river flows between 2005 and 2010 combined with evaporation of the lower lakes led to a significantly lower river level than has ever been experienced in the Lower River Murray (Tajeddin et al., 2010). The River Murray level data used in the analyses were obtained from Murray Darling Basin Authority for Murray Bridge at observation station (A4261162) incorporating data from No. 1 Pump Station (A4260522) and (A4261003) (MDBA, 2014). From these data, the river levels at Murray Bridge had remained relatively constant between 0.5 to 1 m AHD until the end of 2006, where it started to fall continuously and significantly to -1.5 m AHD until September 2009. It then gradually returned to the pre-2006 river levels. As shown in Figure 4.8, the study period from 1 May 2008 to 28 February 2009 (304 days) was selected during this period of low river levels to model the Long Island Marina riverbank collapse with the combined influence of river level fluctuation, rainfall and evaporation.

As summarized in Figure 4.8, mean daily rainfall, as well as mean daily temperature, at the Long Island Marina site were collected from the Australian Bureau of Meteorology (Meteorology, 2014), in addition to evaporation and humidity, in order to provide climatic data for the riverbank stability modeling.

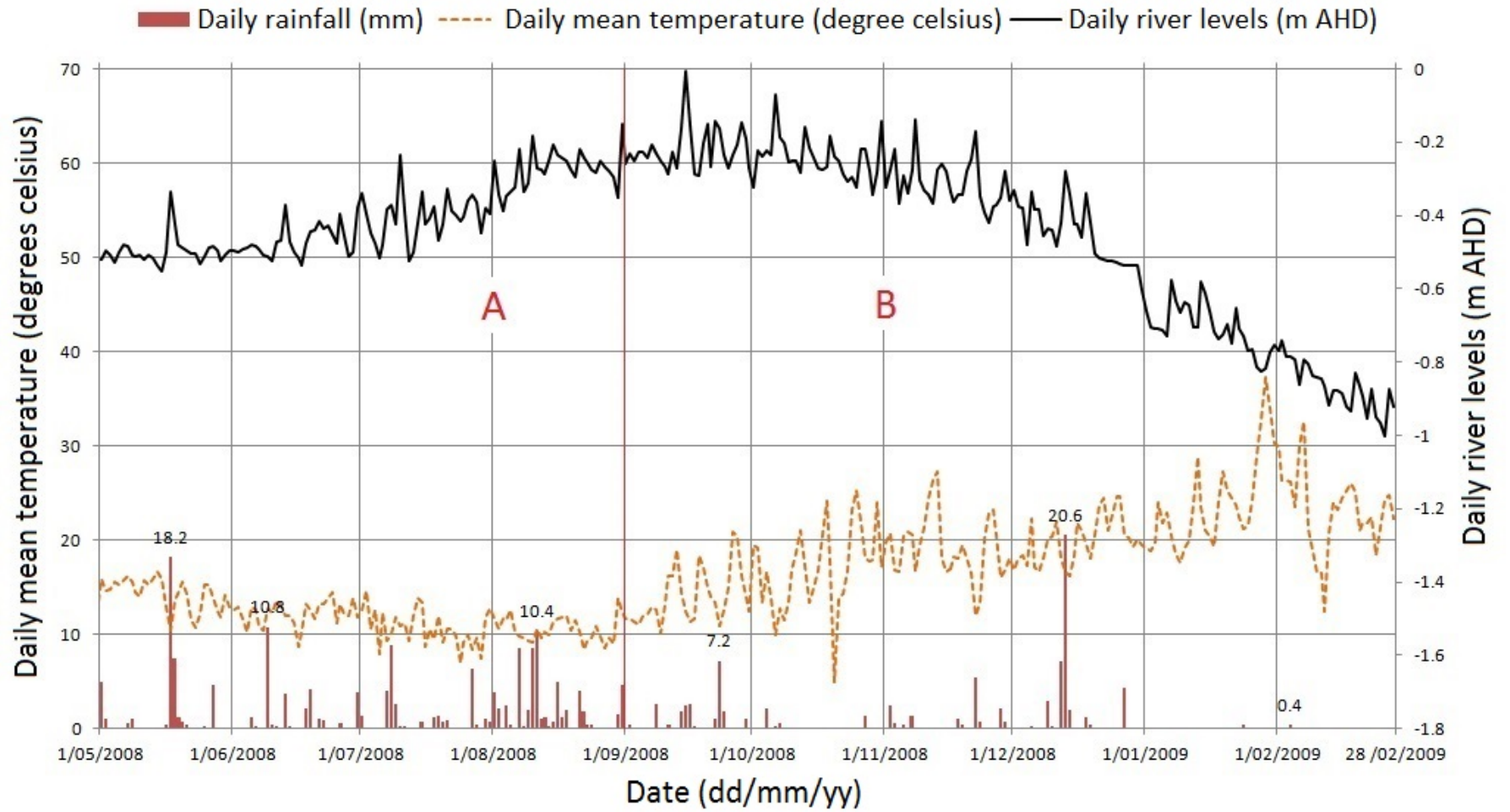


Figure 4.8 Daily river levels, daily rainfall and daily mean temperature from 1 May 2008 to 28 February 2009 at Long Island Marina.

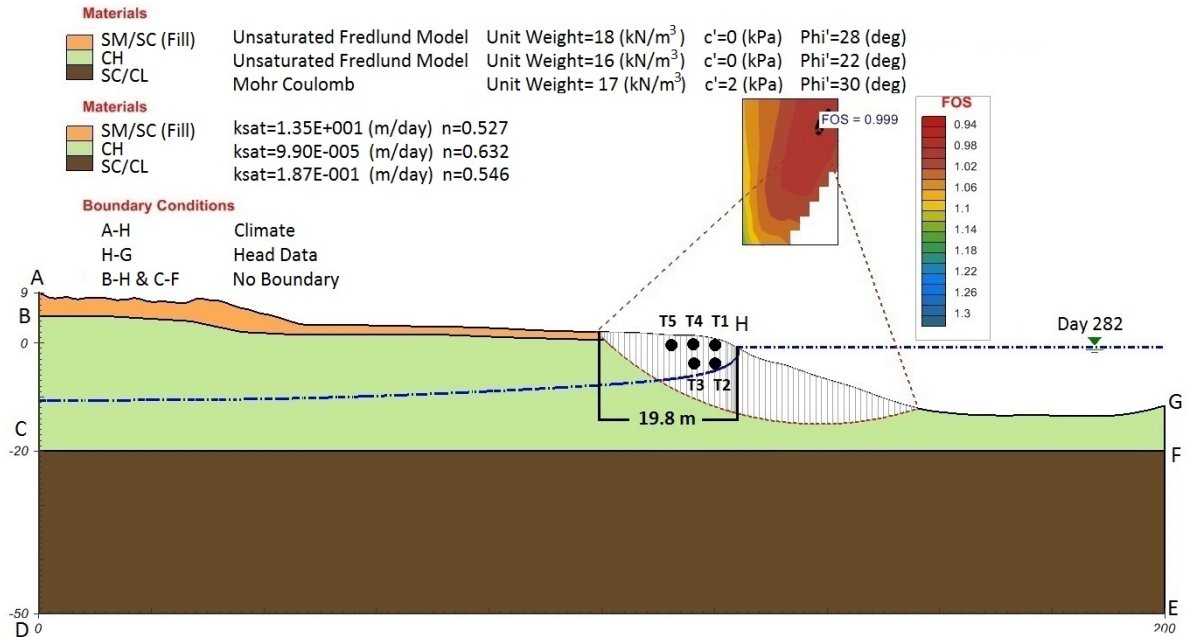
4.3.4 Boundary conditions

Within the SVFlux 2D framework, the riverbank geometry was established from the DEM and ArcGIS, as mentioned above and shown in Figure 4.9. The boundary conditions were established to represent the actual site circumstances as: boundary AH was set to '*climate*' which represents the combined effects of precipitation and evaporation over the 304 day study period; boundary HG was set as '*head data review*' to account for the effects of river level variation over this period; and boundaries BH and CF were set to the '*no boundary*' condition, which indicates a barrier free condition for water flux; and the remainder were set to '*zero flux*' to simulate no water flux through these boundaries.

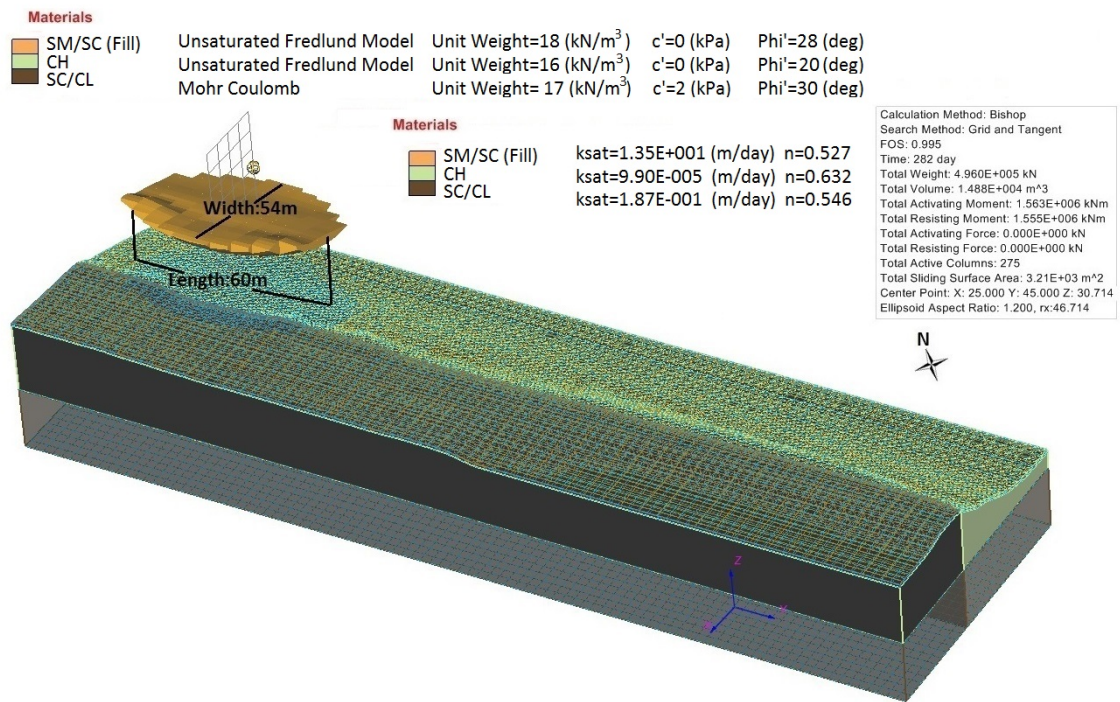
In the SVFlux 3D model, in order to facilitate modeling pore water pressure variations due to river level fluctuation and climatic influences, the riverbank was divided into two zones, as shown in Figure 4.2(c). The climatic data of rainfall, evaporation, air temperature and humidity were assigned the '*climate*' boundary condition to the ground surface of Zone I, while the river level fluctuation was applied as a ground surface boundary condition in Zone II as '*head data review*'; the sidewall boundary between Zones I and II was assigned the '*no boundary condition*' to permit flux; while the remaining three sidewalls associated with both zones were assigned '*zero flux*' to simulate no water flux.

4.4 Riverbank collapse back-analyses

This section presents the results of the 2D back-analyses, using SVFlux 2D and SVSlope 2D, and those in 3D, using SVFlux 3D and SVSlope 3D. The resulting pore water pressure and FoS time histories are examined with reference to river level fluctuation and climatic influences.



(a) 2D cross-sectional model.



(b) 3D stability model.

Figure 4.9 Results of 2D and 3D riverbank stability analyses of Long Island Marina site at Day 282 (6 February 2008).

4.4.1 Pore water pressure variation

As mentioned above, SVFlux was used to model the variation in pore water pressure (PWP) as a consequence of rainfall, evaporation and river level fluctuations based on the transient seepage model. As shown in Figure 4.9, five nodes were selected to monitor the PWP variation above the slip surface at locations T1, T2, T3, T4 and T5 with x - and y -coordinates of (120, -0.5), (120, -3), (115, -3), (115, -0.5) and (110, -0.5), respectively.

Figure 4.10 shows the evolution of PWP as obtained from SVFlux 2D at locations T1 – T5, with (solid lines) and without (dashed and dotted lines) the effects of evaporation. As indicated, the entire study period of 304 days is divided into two parts: Part A includes late autumn and winter (the rainy season in South Australia); and Part B the subsequent spring and summer seasons, which are warmer and drier.

Horizontally, the daily PWP profiles exhibit a very similar trend (e.g. T1, T4 and T5 at -0.5 m AHD; and T2 and T3 at -3 m AHD) throughout the 304 day period. Specifically, at locations T1, T4 and T5, the profiles of PWP fluctuate about 0 kPa in late autumn and winter, and then diverge in spring and summer. It is interesting to note, as a consequence of river drawdown, the reduction in PWP is not equal horizontally in the 5 nodes. Compared with the soil close to the river channel (e.g. T1 and T2), the reduction in PWP (increase in suction) is slightly greater than that associated with the soil farther from the bank and at the same elevation (e.g. T5 and T3). The reason for this is the influence of evaporation. Within the riverbank, the sensitivity to climatic factors increases as the distance from the river's edge increases (Calabresi et al., 2013).

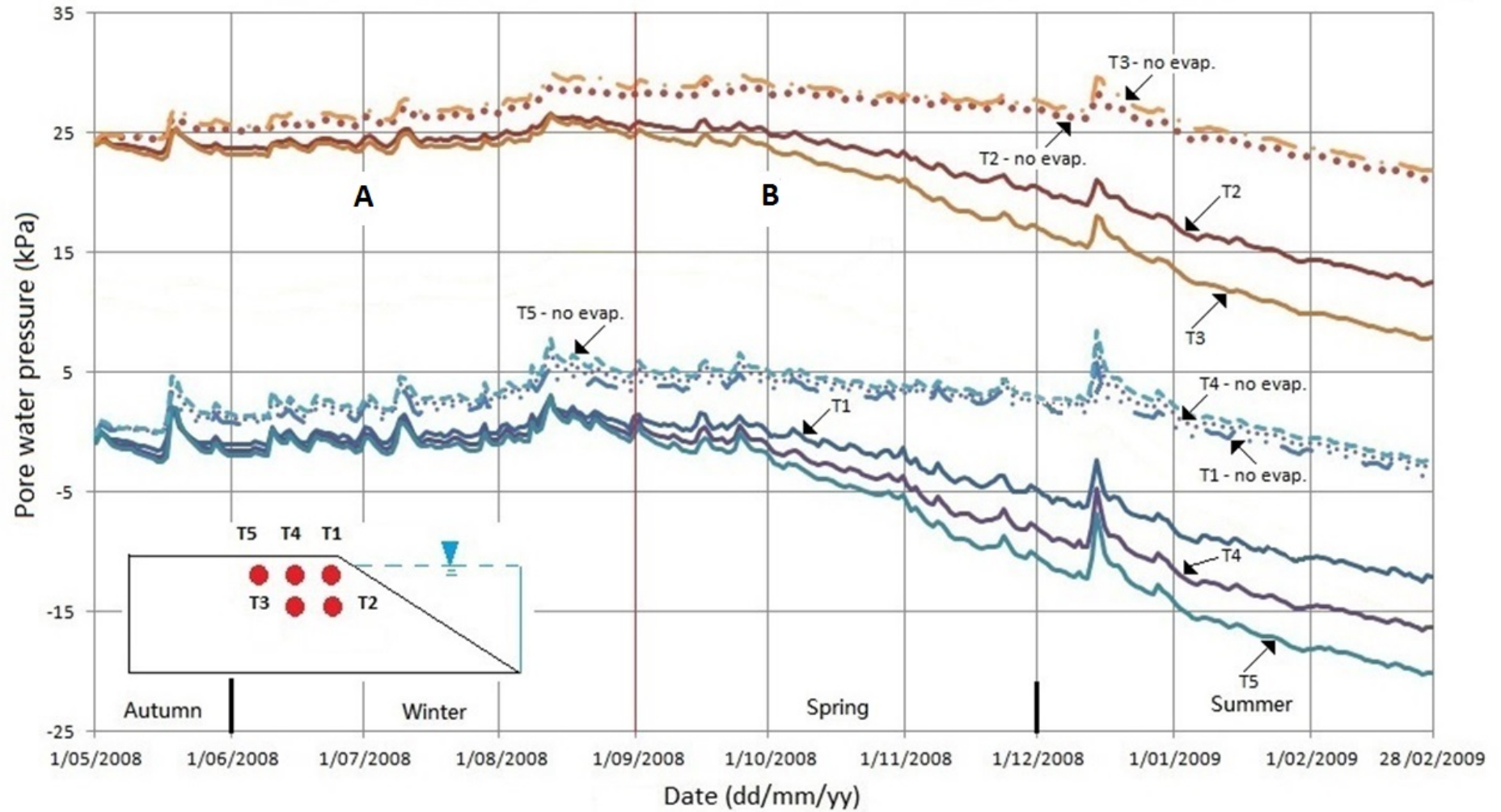
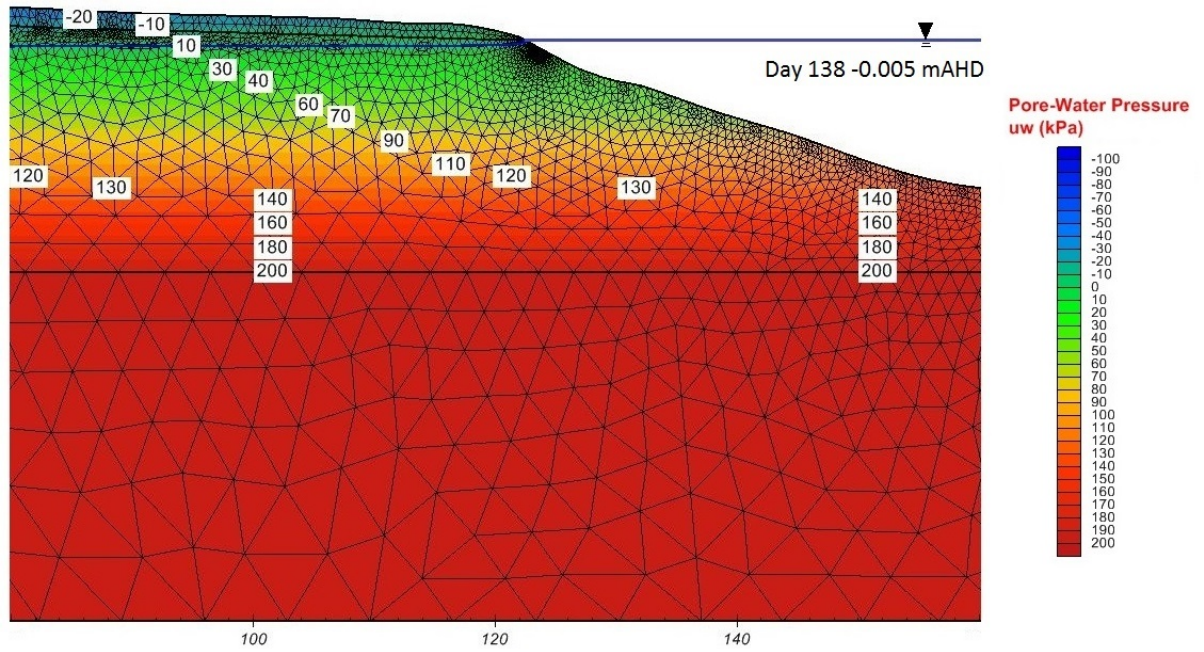


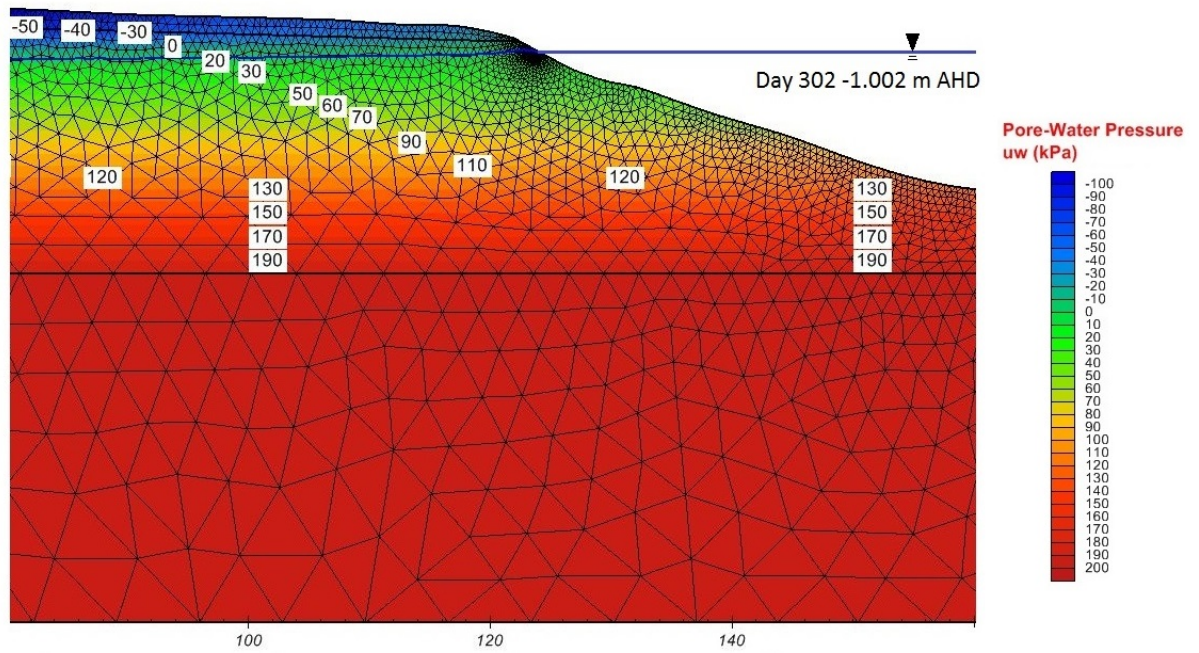
Figure 4.10 Evolution of pore water pressure at 6 selected nodes through the entire research period accounting for, and without, evaporation.

For locations at the same elevation (T1, T4 and T5; and T2 and T3) the evolution of PWP excluding the influence of evaporation, remain relatively consistent throughout the entire study period. In contrast, the PWP incorporating evaporation begin to diverge at the beginning of spring (1/09/2008). On the other hand, in the vertical direction, the variability in PWP is much more pronounced with depth (i.e. T1 and T2; and T4 and T3). Specifically, the sensitivity to the combined effects of rainfall, evaporation and lateral bank seepage, as a consequence of river level fluctuation, diminishes with increasing depth. For example, as a consequence of the 3-day storm between 12 – 14 December 2008, the change in PWP, immediately before and after the storm, is roughly 2 times greater at T1 than at T2.

During Part A, as indicated in Figure 4.10, roughly 164.7 mm rainfall was recorded (70% of that over the entire 304 day period), the river rose by approximately 0.3 m, and the lower daily temperatures resulted in modest daily evaporation, the trend in PWP in each of the 5 nodes is generally flat. In contrast, in Part B, a moderate rainfall (81.5 mm), accompanied by relatively high daily evaporations and a significant drawdown of river level (0.9 m), contributed to a significant reduction in pore water pressure. A summary of the PWP distribution is shown in Figure 4.11, with Figure 4.11(a) showing the PWP during the day with the highest river level (Day 138, 15/09/2008) and Figure 4.11(b) illustrating the PWP during the day with the lowest river level (Day 302, 26/02/2009).



(a)



(b)

Figure 4.11 PWP distributions as a result of (a) the highest (Day 138) and (b) lowest (Day 302) river levels.

4.4.2 Factor of safety

As mentioned previously, deep-seated, circular slip failures in the soft and very soft clays of Holocene age were indicated as the dominant bank collapse mechanism along the lower River Murray. Therefore, back-analyses are performed using the limit equilibrium method (Bishop's method of slices) implemented in SVSlope 2D and 3D. Given that the riverbank collapse is recorded to have occurred on 4 February 2009, the back-analyses are benchmarked against this date, as well as the dimensions and extent of failure indicated by the bathymetric survey summarized in Figure 4.1(b). The geotechnical properties of the high plasticity, Silty Clay (CH) layer were varied marginally against the results of the site investigation (Table 4.1) until a FoS of 1.00 was obtained close to the recorded date of collapse.

Figure 4.12 presents the results of the 2D and 3D back-analyses in terms of FoS as a function of date. The nearest boreholes and CPTus suggested an unsaturated Fredlund model (Fredlund et al., 1996) for the Fill and CH layers, which is able to accommodate soil suction changes in the unsaturated bank materials, as shown by Equation (4.2).

$$\tau = c' + (\sigma_n - u_a) \tan \phi' + (u_a - u_w) [\theta(u_a - u_w) / \theta_s]^b \tan \phi' \quad (4.2)$$

Where: $\theta(u_a - u_w)$ = the volumetric water content at any suction; θ_s = saturated volumetric water content; b= fitting parameters that have a value close to unity for sands and increasing with plasticity. Based on the models adopted and data obtained by SKM [4], the following models are incorporated in the analyses which follow: Fill layer: $c' = 0$ kPa; $\phi' = 28^\circ$; and CH layer: $c' = 0$ kPa; $\phi' = 22^\circ$. The latter model aligns reasonably well with the single CU triaxial test performed by SKM (SKM, 2010b) ($\phi' = 27^\circ$), noting that only one soil sample was tested and the model adopted in the analyses utilizes an average value of c' throughout the entire CH layer.

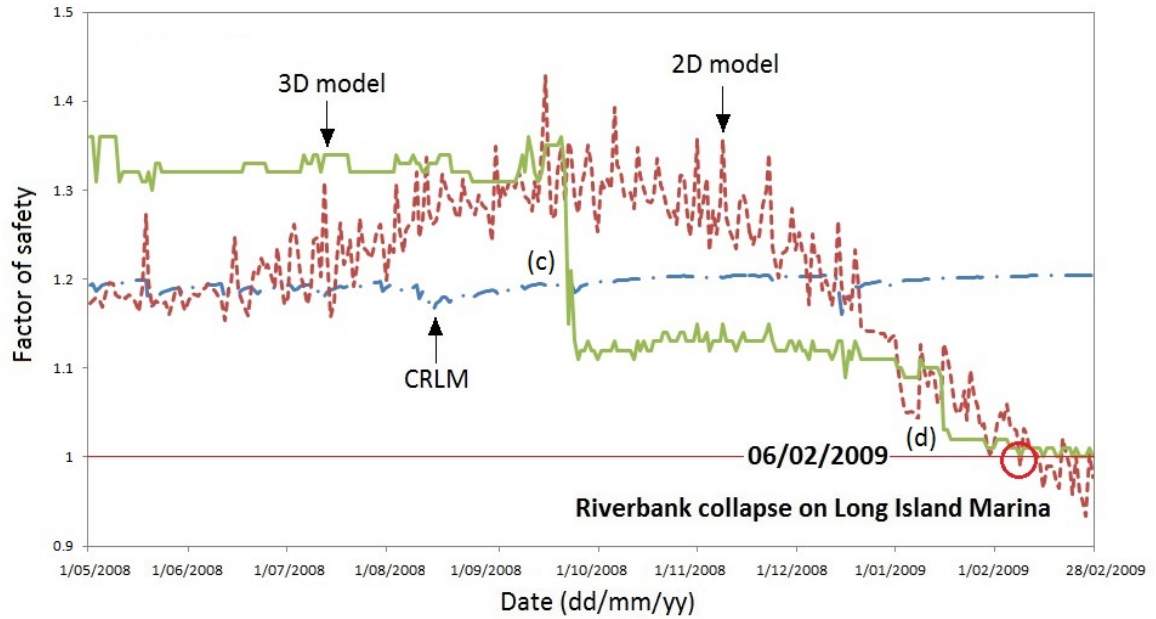


Figure 4.12 Factors of safety from the 2D, 3D and CRLM models.

The results of the 2D analyses shown by the dashed line in Figure 4.12 are extremely encouraging. Firstly, the predicted date of failure is Day 282 (6 February 2009) compares very favorably with the recorded date of failure 4 February 2009 (Day 280). Secondly, the FoS is consistently above 1.00 from the beginning of the analysis period until the predicted date of failure. Finally, the predicted slip surface is shown in Figure 4.9(a). The width of the collapsed region from the crest to the riverbank line is 19.8 m, which again compares extremely favorably with the actual width of 20 m determined from aerial photos [Figure 4.3(b)].

As mentioned above, a 3D slope stability analysis is performed to complement and enhance the 2D riverbank slope stability analyses. Generally, 2D riverbank slope stability analysis, which assumes that the failure surface is infinitely wide, is suitable for stability estimation or assessment over a relatively extensive region, such as adopting a large number of 2D cross-sections, spaced at appropriate intervals, to assess the stability of a large extent of the river. However, 3D riverbank slope stability analysis is generally more accurate for collapse back-analysis over relatively small regions where the dimensions or volume of the collapse zone are known (Stark and Eid,

1998). As shown in Figure 4.1(b), the bathymetric data clearly shows three, what appear to be, separate failures, identified as Regions (i) – (iii). From the DEWNR database of recorded riverbank collapse incidents, it is clear that Region (i) collapsed first, and hence attention is directed solely to this failure. The modeling of Regions (ii) and (iii) is beyond the scope of this paper, as the failure of Region (i) affects the pre-collapse topography associated with Regions (ii) and (iii) and, given the limited extent of available observational and survey data, presents significant challenges and uncertainties. Figure 4.12 also shows, by means of the solid line, the results of the 3D back-analysis of the riverbank. As for the 3D analysis, an unsaturated Fredlund model is again adopted with the following properties: $c' = 0$ kPa; $\phi' = 20^\circ$. As can be seen, this model again incorporates a modest reduction in soil density and cohesion when compared with the 2D model, with the only change being ϕ' reducing from 22° to 20° in the 3D model. As shown in Figure 4.12, two major reductions in FoS can be observed in the 3D model, which likely relate to: (c) the 0.3 m reduction in the daily river level (from -0.005 to -0.291 m AHD) incorporating with a 16.2 mm rainfall event; and (d) the 0.2 m reduction in daily river level (from -0.537 to -0.73 m AHD). As can be observed, river level fluctuation dominates the likelihood of FoS variation in both 2D and 3D. Compared with the 2D model, the 3D model FoS appears to be less sensitive to river level variation, however a significant drawdown may incur a significant reduction in FoS, as shown by the reductions (c) and (d) explained above. Again, the results represent extremely good correlation between the predictions and observations. Firstly, the predicted date of failure is again, as with the 2D analysis, Day 282 (6 February 2009) which aligns well with the recorded date of failure 4 February 2009 (Day 280). Secondly, the FoS is again consistently above 1.00 from the beginning of the analysis period until the predicted date of failure. Finally, the predicted volume of the slip surface is in Figure 4.9(b). The dimensions of 54 m width x 60 m length compare extremely well with the results of the bathymetric survey of 53 m width x 58 m length [Figure 4.1(b)].

4.5 Influence of rainfall and river level drawdown

In order to understand better the relationship between rainfall, river level fluctuations and riverbank stability, additional 2D analyses are performed using SVFlux 2D and SVSlope 2D. The first series of analyses examines the situation where the river level remains static while rainfall continues to vary in accordance with the historical record. The second series examines the situation of extreme rainfall events.

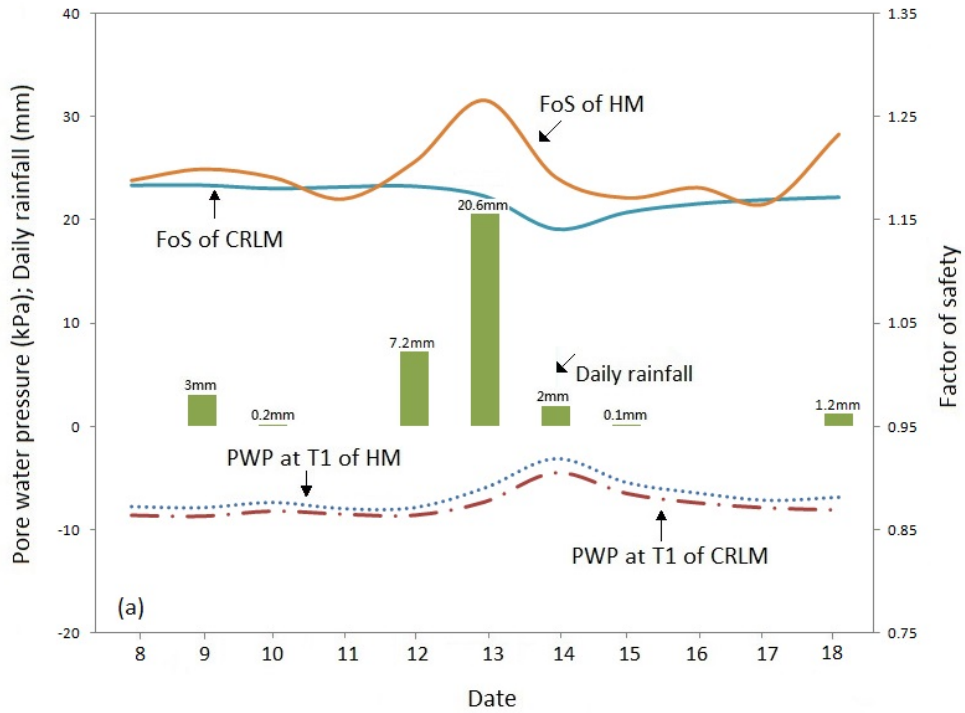
Figure 4.12 and Figure 4.13 present the results of analyses adopting a constant river level model (CRLM) with a static level at -0.521 m AHD for the entire 304 day study period. This level coincides with the initial river level associated with the actual historical model (HM) examined in the previous section. As can be seen from Figure 4.12, compared with the HM 2D and 3D factors of safety, the CRLM FoS generally remains constant and consistently greater than 1.00, with several minor reductions as a result of intensive rainfall events. Figure 4.13(a) presents the time histories of FoS and PWP in both the HM and CRLM in mid-December 2008, when the most intense storm of the 304 study day period resulted in 29.8 mm of rainfall in 3 days. It can be observed that the PWPs associated with the CRLM at location T1 (refer to Figure 4.9) are considerably lower than those derived from the HM. This is because the lower river level (-0.521 m AHD) creates a depressed groundwater table resulting in decreased PWPs. It can also be observed in Figure 4.13(a), that the riverbank is less stable in the HM than the CRLM on 11 December due to the lower river level, but more stable in the HM than in the CRLM after the storm. The river levels during these 5 days (10–14 December) were -0.439 m AHD, -0.486 m AHD, -0.421 m AHD, -0.278 m AHD and -0.344 m AHD, respectively. It can also be seen clearly that the CLRM FoS is generally constant throughout mid-December 2008, albeit with a negligible reduction after the storm. This demonstrates that daily river level fluctuation has an observable influence on the FoS, while the effect of daily rainfall is modest. In contrast, relatively minor precipitation was recorded (0.8 mm) during the intervening period leading up to the collapse on 4 February

2009. As shown in Figure 4.13(b), the HM FoS continues to decline until collapse is predicted on 6 February 2009. During this period the CRLM FoS remains constant and consistently greater than 1.00.

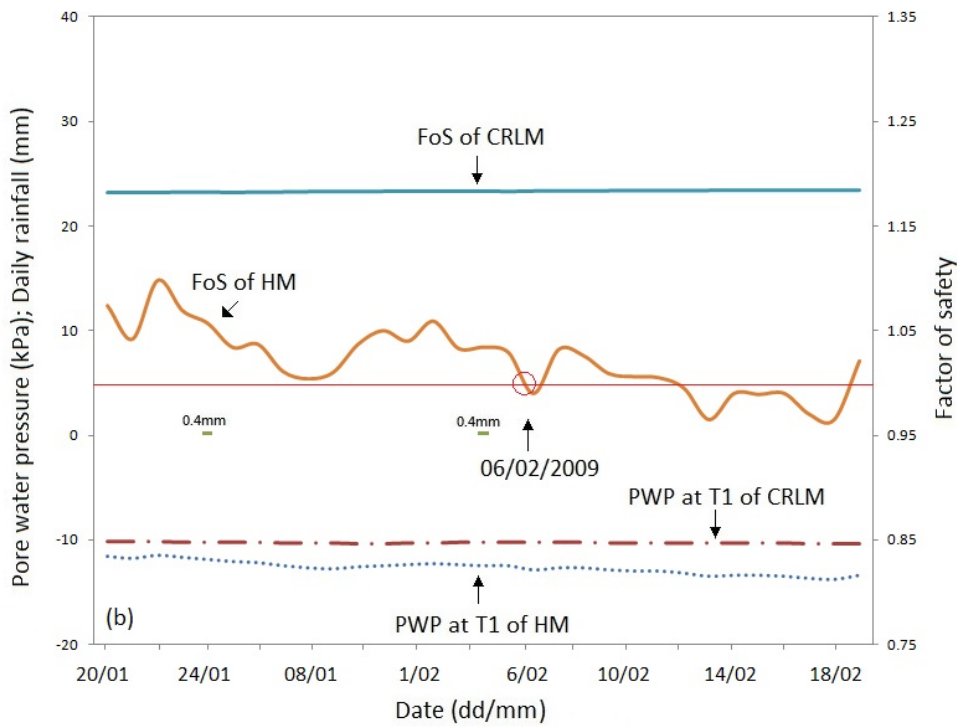
Further examining the influence of rainfall on riverbank collapse, an extreme rainfall scenario is modeled. The most significant storm on record at Murray Bridge occurred in January 1941 when 189.6 mm of rain fell over a period of 5 days. This is more than 6 times greater than the storm examined above. Figure 4.14 presents the results of the magnified rainfall model (MRM), which incorporates the January 1941 storm. Four different scenarios are presented: Figure 4.14(a) shows the results of the HM for benchmarking purposes; whereas Figures 4.14(b) – (d) present the results of the MRM with high (–0.2 m AHD in September 2008), medium (–0.5 m AHD in May 2008) and low (–0.8 m AHD January 2009) river levels, respectively.

Figure 4.14(a) shows the behavior of the HM as a result of the historical storm that occurred in December 2008. The FoS remains consistently above 1.00 with daily river levels fluctuating around –0.5 m AHD. In contrast, the FoS resulting from the MRM with high and medium daily river levels, as shown in Figures 4.14(b) and 14(c) respectively, reduces significantly with collapse predicted. The extreme storm results in an approximate increase of 30 kPa in PWP, and consequently triggers a rapid and significant decrease in FoS in both scenarios.

Figure 4.14(d) shows a similar outcome to that of the HM in Figure 14(a), where the FoS remains relatively consistent above 1.00, in the former as a result of the MRM with low daily river levels. After the extreme rainfall event, the change in PWP at T1 is 20 kPa, which is roughly 10 kPa less than that observed in the high and medium river level scenarios in Figures 14(b) and (c).



(a) Storm in mid-Dec. 2008.



(b) Scenario of the riverbank collapse at Long Island Marina on 4 Feb. 2009.

Figure 4.13 Factors of safety for historical model (HM) and constant river stage model (CRLM) in two scenarios.

In order to understand better the influence of river level fluctuations on bank stability, two drawdown scenarios are examined based on the HM. The river level is first modeled adopting a linear decrease from its highest level throughout the study period (i.e. -0.005 m AHD on Day 138) to its lowest level (-1.002 m AHD on Day 302) over a period of 2 days (i.e. a drawdown rate of 0.5 m/day) and, second, over a 5-day period (0.2 m/day). The results show that, as expected, the most rapid drawdown event (0.5 m/day) gives rise to the lowest of the two calculated factors of safety, $FoS = 0.88$, with the 5-day drawdown scenario yielding a $FoS = 0.914$. In contrast, the HM, which incorporates the actual and recorded river drawdown over a 164-day period (0.006 m/day), yields a $FoS = 0.934$. It needs to be stressed, however, that the Lower River Murray is a regulated river, as a consequence of a lock situated at Blanchetown, at the upstream end of the river, and the barrages situated at the downstream end. Hence, it is extremely unlikely that such a rapid drawdown event, similar to the two scenarios examined above, could actually occur.

These analyses demonstrate that river level fluctuations have a far greater influence on riverbank collapse than rainfall. However, if an extreme rainfall event coincides with a medium (-0.5 m AHD) to high (-0.2 m AHD) river level collapse is likely to occur. Whilst not a key objective of the present paper, a series of additional analyses has also been performed to examine the influence of evaporation on FoS . The results, however, demonstrate that evaporation has a marginal effect on FoS .

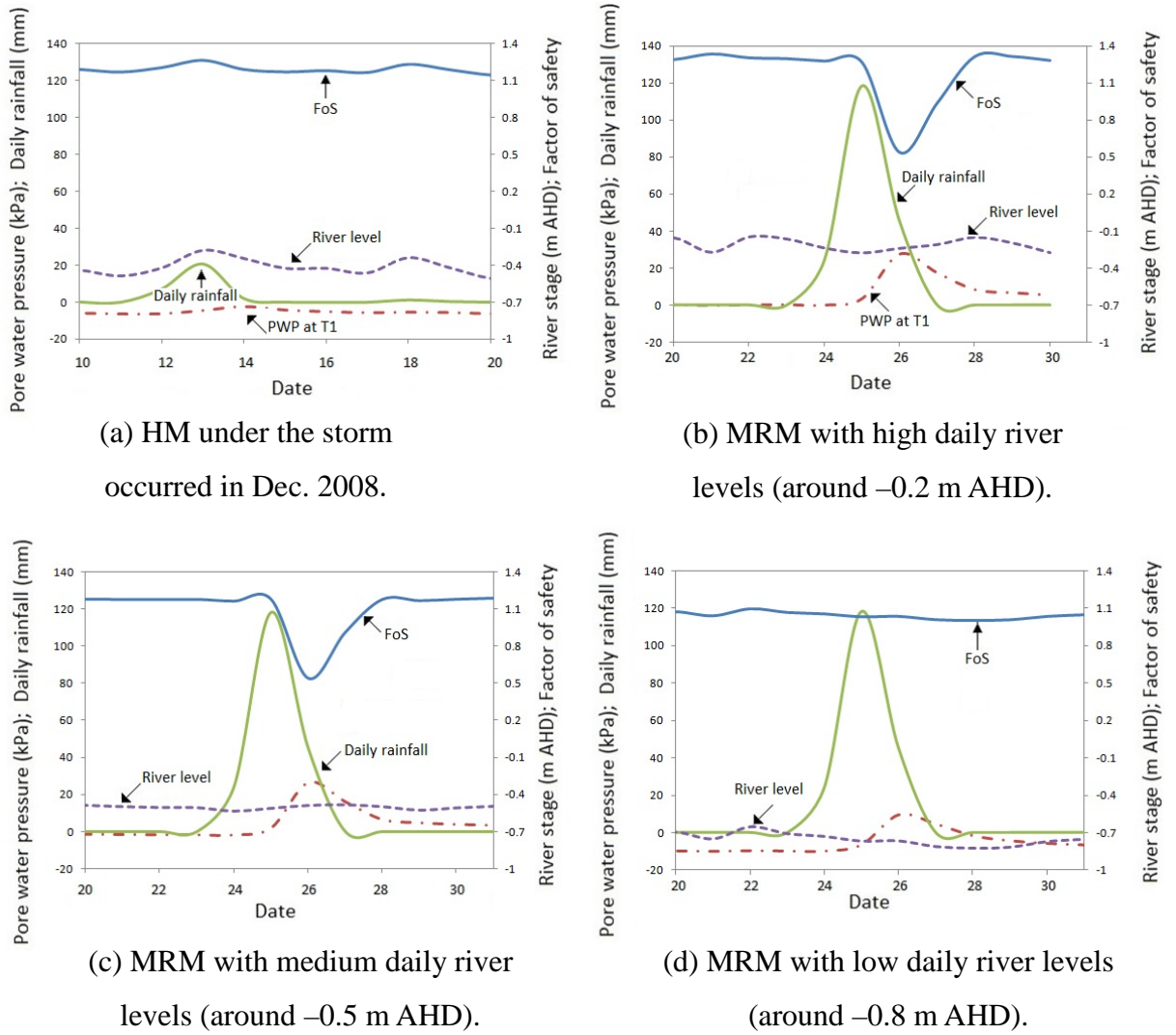


Figure 4.14 Magnified rainfall model (MRM) under different river level scenarios.

4.6 Conclusion

This paper has sought to: (i) model the riverbank collapse incident, in both 2D and 3D, which occurred at Long Island Marina, Murray Bridge, South Australia, on 4 Feb. 2009; (ii) examine the influence and sensitivity of river level fluctuations and climatic factors on riverbank stability; and (iii) determine the dominant triggers affecting collapse. The modeling has been undertaken using the limit equilibrium method in 2D and 3D using SVFlux and SVSlope. To facilitate the stability analyses, a GIS framework has been adopted, which involved: examination of the recorded collapsed regions by visual interpretation of high resolution aerial images; obtaining topographic information of the site from a digital elevation model; and calculation of the dimensions of the collapsed regions from high resolution aerial images. Back-analyses have been performed using geotechnical data obtained from a site investigation incorporating both in situ and laboratory testing and validated against data from the recorded collapse.

The study has shown that:

- (a) Both the adopted process of 2D and 3D stability modeling yielded excellent predictions of the collapse when compared against the recorded date of collapse and dimensions of the failed region. The adopted geotechnical model parameters align with those derived from the site investigation.
- (b) The integration of GIS with transient soil-moisture modeling has proved to be an effective tool for accurately predicting riverbank stability.
- (c) River fluctuations, rather than climatic factors, dominate the likelihood of riverbank collapse along the Lower River Murray.
- (d) Sudden or rapid drawdown can result in riverbank collapse.
- (e) Extreme rainfall events, coinciding with medium to high river levels, are also likely to trigger riverbank collapse.

Acknowledgements

The authors are grateful for the support and valuable advice provided by Jai O'Toole, Geoff Eaton and Richard Brown from DEWNR. This project is funded by the Goyder Institute for Water Research, under *Project E1.8 Riverbank Stability*, and the authors are grateful for their support.

Notation

AHD	Australian Height Datum
ARI	average recurrence interval
b	fitting parameters of Unsaturated Fredlund model that have a value close to unity for sands and increasing with plasticity
c'	effective cohesion
c_{top}	cohesion at the top of Silty Clay
c_{ratio}	rate of increase of undrained shear strength with depth for Silty Clay
c_{max}	maximum value of cohesion in Silty Clay
CH	Silty Clay, high plasticity
CL	Sandy Clay, low plasticity
CPT(u)	piezocone tests with pore water pressure measurements
CRLM	constant river level model
$D_{\%}$	grain diameter related to the percentage of passing in mm
DEM	Digital Elevation Model
DFW	Department for Water
DEWNR	Department of Environment, Water and Natural Resources
FEM	Finite Element Method
FoS	factor of safety
G_s	specific gravity of solids
GIS	Geographic Information Systems
HM	historical model
I_{thr}	threshold rainfall intensity
K	unsaturated hydraulic conductivity
K_{sat}	saturated hydraulic conductivity
LIDAR	light detecting and ranging
MRM	magnified rainfall model
P_{200}	percentage of soil passing US standard sieve #200
PI	plasticity index

PSD	particle size distribution
RS	remotely-sensed
SM	Silty Sand
SC	Clayey Sand
SWCC	soil water characteristic curve
w	moisture content
wPI	weighted Plasticity Index
θ_{sat}	saturated volumetric water content
ρ	dry density
ρ_w	density of water at 4°C
ϕ'	effective internal angle of friction
γ	unit weight of soil

References for Chapter 4

- Abramson, L. W., Lee, T. S., Sharma, S. & Boyce, G. M. 2002a. *Slope stability and stabilization methods*, New York, John Wiley and Sons.
- Abramson, L. W., Lee, T. S., Sharma, S. & Boyce, G. M. (eds.) 2002b. *Slope Stability and Stabilization Methods*, New York: John Wiley & Sons, Inc.
- Acharya, G., De Smedt, F. & Long, N. 2006. Assessing landslide hazard in GIS: a case study from Rasuwa, Nepal. *Bulletin of Engineering Geology and the Environment*, 65, 99-107.
- Beal, A., Brown, R. & Toole, J. O. 2010. Expert Panel Workshop - Riverbank Collapse Hazard Program.
- Berilgen, M. M. 2007. Investigation of stability of slopes under drawdown conditions. *Computers and Geotechnics*, 34, 81-91.
- Bouwer, H. 1978. *Groundwater hydrology*, New York, New York : McGraw-Hill.
- Brand, E. W. Landslides in Southeast Asia: A State-of-the-art Report. 4th International Symposium on Landslides, 1984 Toronto. 17-59.
- Calabresi, G., Colleselli, F., Danese, D., Giani, G. P., Mancuso, C., Montrasio, L., Nocilla, A., Pagano, L., Reali, E. & Sciotti, A. 2013. A research study of the hydraulic behaviour of the Po river embankments. *Canadian Geotechnical Journal*.
- Casagli, N., Rinaldi, M., Gargini, A. & Curini, A. 1999. Pore water pressure and streambank stability: results from a monitoring site on the Sieve River, Italy. *Earth Surface Processes and Landforms*, 24, 1095-1114.
- Coffey. 2012. *RE: Review of Management Options for Four Riverbank Collapse High Risk Sites*. Type to Department of Environmental, W. a. N. R.
- DFW 2011. Lower River Murray Riverbank Collapse Hazard Site Status Report (May 2011).

Fredlund, D. G. 2006. Unsaturated Soil Mechanics in Engineering Practice. *Journal of Geotechnical & Geoenvironmental Engineering*, 132, 286-321.

Fredlund, D. G., Xing, A., Fredlund, M. D. & Barbour, S. L. 1996. The relationship of the unsaturated soil shear to the soil-water characteristic curve. *Canadian Geotechnical Journal*, 33, 440-448.

Fredlund, D. G., Xing, A. & Huang, S. 1995. Predicting the permeability function for unsaturated soils using the soil-water characteristic curve. *International Journal of Rock Mechanics and Mining Sciences and Geomechanics Abstracts*, 32, 159A-159A.

Green, S. J. 1999. *Drawdown and river bank stability*, University of Melbourne, Dept. of Civil and Environmental Engineering.

Higgins, D. T. 1980. Unsteady drawdown in 2D water-table aquifer *Journal of the Irrigation and Drainage Division-Asce*, 106, 237-251.

Hooke, J. M. 1979. An analysis of the processes of river bank erosion. *Journal of Hydrology*, 42, 39-62.

Institution of Engineers, A. (ed.) 1987. *Australian Rainfall and Runoff: A Guide to Flood Estimation*

Jia, G. W., Zhan, T. L. T., Chen, Y. M. & Fredlund, D. G. 2009. Performance of a large-scale slope model subjected to rising and lowering water levels. *Engineering Geology*, 106, 92-103.

Lane, P. A. & Griffiths, D. V. 2000. Assessment of stability of slopes under drawdown conditions. *Journal of Geotechnical & Geoenvironmental Engineering*, 126, 443.

Lee, S., Choi, J. & Min, K. 2004. Probabilistic landslide hazard mapping using GIS and remote sensing data at Boun, Korea. *International Journal of Remote Sensing*, 25, 2037-2052.

Liang, C., Jaksa, M. B. & Ostendorf, B. 2012. GIS-based Back Analysis of Riverbank Instability in the Lower River Murray. *Australian Geomechanics*, 47, 59-65.

- Lumb, P. 1975. Slope failures in Hong Kong. *Quarterly Journal of Engineering Geology and Hydrogeology*, 8, 31-65.
- MDBA 2014. River Murray at Murray Bridge (Long Island) information sheet. Murray Darling Basin Authority.
- Merwade, V. M. 2007. An Automated GIS Procedure for Delineating River and Lake Boundaries. *Transactions in GIS*, 11, 213-231.
- Meteorology, B. o. 2014. Climate data Online, Commonwealth of Australia , Bureau of Meteorology Bureau of Meteorology.
- Miller, D. J. & Sias, J. 1998. Deciphering large landslides: linking hydrological, groundwater and slope stability models through GIS. *Hydrological Processes*, 12, 923-941.
- Mukhlisin, M. & Taha, M. 2012. Numerical model of antecedent rainfall effect on slope stability at a hillslope of weathered granitic soil formation. *Journal of the Geological Society of India*, 79, 525-531.
- National Water Commission, A. G. 2005. *Bureau of Rural Sciences* [Online]. http://www.water.gov.au/WaterAvailability/Whatisourtotalwaterresource/Runoff/index.aspx?Menu=Level1_3_1_5.
- Osman, A. M. & Thorne, C. R. 1988. Riverbank Stability Analysis .1. Theory. *Journal of Hydraulic Engineering-Asce*, 114, 134-150.
- Ozdemir, A. 2009. Landslide susceptibility mapping of vicinity of Yaka Landslide (Gelendost, Turkey) using conditional probability approach in GIS. *Environmental Geology*, 57, 1675-1686.
- Pauls, G. J., Sauer, E. K., Christiansen, E. A. & Widger, R. A. 1999. A transient analysis of slope stability following drawdown after flooding of a highly plastic clay. *Canadian Geotechnical Journal*, 36, 1151-1171.
- Rahardjo, H., Leong, E. C. & Rezaur, R. B. 2008. Effect of antecedent rainfall on pore-water pressure distribution characteristics in residual soil slopes under tropical rainfall. *Hydrological Processes*, 22, 506-523.

Rahardjo, H., Li, X. W., Toll, D. G. & Leong, E. C. 2001. The effect of antecedent rainfall on slope stability. *Geotechnical & Geological Engineering*, 19, 371-399.

Rahardjo, H., Ong, T. H., Rezaur, R. B. & Leong, E. C. 2007. Factors Controlling Instability of Homogeneous Soil Slopes under Rainfall. *Journal of Geotechnical & Geoenvironmental Engineering*, 133, 1532-1543.

Rahimi, A., Rahardjo, H. & Leong, E. C. 2011. Effect of Antecedent Rainfall Patterns on Rainfall-Induced Slope Failure. *Journal of Geotechnical and Geoenvironmental Engineering*, 137, 483-491.

Rinaldi, M. & Casagli, N. 1999. Stability of streambanks formed in partially saturated soils and effects of negative pore water pressures: the Sieve River (Italy). *Geomorphology*, 26, 253-277.

Rinaldi, M., Casagli, N., Dapporto, S. & Gargini, A. 2004. Monitoring and modelling of pore water pressure changes and riverbank stability during flow events. *Earth Surface Processes and Landforms*, 29, 237-254.

Schuster, R. L. & Krizek, R. J. (eds.) 1978. *LaLandslides: Analysis and Control (Special report - Transportation Research Board, National Research Council ; 176)*.

SKM 2010a. Study into River Bank Collapsing for Lower River Murray.

SKM 2010b. Study into River Bank Collapsing for Lower River Murray: Appendix A Riverfront Road - Murray Bridge In - situ and Laboratory Test Results.

SKM 2011. Research into processes, triggers and dynamics of riverbank collapse in the Lower River Murray.

SoilVision 2009a. SVFlux. 4.23 ed.

SoilVision 2009b. SVSlope. 4.23 ed.

Springer, F. M. 1981. *Influence of Rapid Drawdown Events on River Bank Stability*. Master in Engineering, University of Louisville.

Stark, T. & Eid, H. 1998. Performance of Three-Dimensional Slope Stability Methods in Practice. *Journal of Geotechnical and Geoenvironmental Engineering*, 124, 1049-1060.

Stark, T. D. 2003. Three-dimensional slope stability methods in geotechnical practice.

Stark, T. D. & Eid, H. T. 1995. Drained Residual Strength of Cohesive Soils - Closure. *Journal of Geotechnical Engineering-Asce*, 121, 672-673.

Stark, T. D. & Eid, H. T. 1997. Slope stability analyses in stiff fissured clays. *Journal of Geotechnical and Geoenvironmental Engineering*, 123, 335-343.

Stark, T. D., Williamson, T. A. & Eid, H. T. 1996. HDPE geomembrane/geotextile interface shear strength. *Journal of Geotechnical Engineering-Asce*, 122, 197-203.

Tajeddin, R., Ramsey, N., Pain, D., Mollison, D. & Sandercock, P. 2010. Influence of Water Level Risk on River Bank Collapse, Lower River Murray. Sinclair Knight Merz, Australia.

Thiel, R. S., Stark, T. D. & Eid, H. T. 1997. Shear behavior of reinforced geosynthetic clay liners - Discussion and closure. *Geosynthetics International*, 4, 539-541.

Thorne, C. R. 1982. Processes and mechanisms of River Bank Erosion. In: Hey, R. D., Bathurst, J. C. & Thorne, C. R. (eds.) *Gravel-bed rivers. Fluvial processes, engineering and management. Earth Surface Processes and Landforms*. John Wiley & Sons, Ltd.

Thorne, C. R., Hey, R. D. & Newson, M. D. (eds.) 1997. *Bank erosion and instability. In Applied fluvial geomorphology for river engineering and management / edited by Colin R. Thorne, Richard D. Hey, Malcolm D. Newson.*; 1997: New York : John Wiley.

Thorne, C. R. & Osman, A. M. 1988. Riverbank Stability Analysis .2. Applications. *Journal of Hydraulic Engineering-Asce*, 114, 151-172.

Twidale, C. R. 1964. Erosion of an alluvial bank at Birdwood, South Australia. *Zeitschrift für Geomorphologie, NF*, 8, 189-211.

Voyiadjis, G. & Song, C. 2003. Determination of Hydraulic Conductivity Using Piezocone Penetration Test. *International Journal of Geomechanics*, 3, 217-224.

Wang, H., Liu, G., Xu, W. & Wang, G. 2005. GIS-based landslide hazard assessment: an overview. *Progress in Physical Geography*, 29, 548-567.

Xie, M., Esaki, T. & Zhou, G. 2004. GIS-Based Probabilistic Mapping of Landslide Hazard Using a Three-Dimensional Deterministic Model. *Natural Hazards*, 33, 265-282.

Xie, M. W., Esaki, T. & Cai, M. F. 2006. GIS-based implementation of three-dimensional limit equilibrium approach of slope stability. *Journal of Geotechnical and Geoenvironmental Engineering*, 132, 656-660.

Xie, M. W., Zhou, G. Y. & Tetsuro, E. 2003. GIS COMPONENT BASED 3D LANDSLIDE HAZARD ASSESSMENT SYSTEM: 3DSLOPEGIS. *Chinese Geographical Science*, 13, 66-72.

Yan, Z.-L., Wang, J.-J. & Chai, H.-J. 2010. Influence of water level fluctuation on phreatic line in silty soil model slope. *Engineering Geology*, 113, 90-98.

Yongquan, L., Yong, F. & Shenghua, J. Stability analysis of soil slope during rapid drawdown of water level. *Mechanic Automation and Control Engineering (MACE)*15-17, July 2011. 3454-3457.

Zaitchik, B. F. & Es, H. M. v. 2003. Applying a GIS slope-stability model to site-specific landslide prevention in Honduras. (Research).(geographic information system). *Journal of Soil and Water Conservation*, 58, 45(9).

Zapata, C. E., Houston, W. N., Walsh, K. D. & Houston, S. L. 2000. Soil–Water Characteristic Curve Variability. *Advances in Unsaturated Geotechnics*.

Zhang, J. F., Li, Z. G. & Qi, T. 2005. Mechanism analysis of landslide of a layered slope induced by drawdown of water level. *Science in China Series E-Engineering & Materials Science*, 48, 136-145.

Zhang, L. L., Zhang, J., Zhang, L. M. & Tang, W. H. 2011. Stability analysis of rainfall-induced slope failure: a review. *Proceedings of the Institution of Civil Engineers-Geotechnical Engineering*, 164, 299-316.

Zolfaghari, A. & Heath, A. C. 2008. A GIS application for assessing landslide hazard over a large area. *Computers and Geotechnics*, 35, 278-285.

Chapter 5

5 Back Analysis of Lower River Murray Riverbank Collapses Using Transient Water Model

(Paper 3, published)

C. Liang¹, M. B. Jaksa¹ Y. L. Kuo¹ and B. Ostendorf²

¹School of Civil; Environmental and Mining Engineering, University of Adelaide, 5005;

²School of Earth and Environmental Sciences, University of Adelaide, 5005;

Publication:

LIANG, C., JAKSA, M. B., KUO, Y. L. & OSTENDORF, B. (2015). Back Analysis of Lower River Murray Riverbank Collapses. *Australian Geomechanics*. Vol 50: No.2, 29-41.

Statement of Authorship

Title of Paper	Back Analysis of Lower River Murray Riverbank Collapses
Publication Status	<input type="radio"/> Published, <input checked="" type="radio"/> Accepted for Publication, <input type="radio"/> Submitted for Publication, <input type="radio"/> Publication style
Publication Details	Liang, C., Jaksa, M. B., Kuo, Y. L. and Ostendorf, B. (2015). Back Analysis of Lower River Murray Riverbank Collapses. Australian Geomechanics. Accepted for publication: 03 May 2015.

Author Contributions

By signing the Statement of Authorship, each author certifies that their stated contribution to the publication is accurate and that permission is granted for the publication to be included in the candidate's thesis.

Name of Principal Author (Candidate)	Chen Liang	
Contribution to the Paper	Undertook Literature review, performed parametric analysis and modeling, interpreted data and acted as corresponding author.	
Signature	Date	11/Jan/2015

Name of Co-Author	Mark B. Jaksa	
Contribution to the Paper	Supervised development of work and helped with paper editing.	
Signature	Date	4/2/15

Name of Co-Author	Bertram Ostendorf	
Contribution to the Paper	Supervised development of work.	
Signature	Date	3-2-2015

Name of Co-Author	Yien Lik Kuo	
Contribution to the Paper	Helped with in-situ and laboratory test	
Signature	Date	3-2-2015

Abstract

Riverbank collapses in the Lower River Murray threaten public infrastructure, private property and the safety of river users, and also provides significant challenges for environmental and river management. According to the inventory of the South Australian Department of Environment, Water and Natural Resources (DEWNR), between 2007 and 2010, 50 riverbank collapse-related incidents were reported at four very high risk sites: East Front Road, Mannum; Woodlane Reserve; River Front Road, Murray Bridge and White Sands. The objectives of this paper are to: (i) model four known and representative riverbank collapses at these four sites; and (ii) determine the soil shear strength properties by undertaking back-analyses. Adopting a GIS framework incorporating light detecting and ranging (LIDAR) digital elevation models (DEMs) and high-resolution aerial images, four cross-sectional models have been accurately established based on the examined historical collapses. Slope geometries have been determined using topographic information obtained from the DEMs. Finite element analyses based on a transient water model have been adopted to simulate the response of pore water pressure under dynamic variations of rainfall, evaporation and river level fluctuations. The limit equilibrium method has been used to undertake the slope stability calculations. The model results, which agree closely with the findings of historical incidents, demonstrate the efficacy of the framework and the accuracy of the predictions.

Keywords: GIS, riverbank stability, back-analysis, transient water model, DEM, rainfall, river level, River Murray

5.1 Introduction

Riverbank collapse is a natural and expected characteristic of the evolution of rivers. An unprecedented period of dry conditions and low flows between 2005 and 2010 instigated more than 162 reported riverbank collapse-related incidents along the Lower River Murray, in South Australia (downstream of Lock 1 at Blanchetown to Wellington). In particular, four sites: East Front Road, Mannum; Woodlane Reserve; River Front Road, Murray Bridge and White Sands which have involved 50 reported riverbank collapse-related incidents of the total 162, were identified as very high hazard areas by geotechnical engineering consultant Sinclair Knight Merz (2010a). Damage has been identified to houses, vehicles (River Front Road), riparian trees (White Sands) and a pump station (Woodlane Reserve) (SKM, 2010a). Two geotechnical investigations have been undertaken by SKM in 2009 which indicated deep-seated, circular slip failures in the soft and very soft clays of Holocene age are the dominant bank collapse mechanism along the Lower River Murray (SKM, 2010b, SKM, 2010c, SKM, 2010d). However, to improve the understanding of each individual collapse more localised geotechnical information is required.

Back-analysis is an effective method to estimate uncertainties in slope stability research, especially to ascertain the soil shear strengths (Abramson et al., 2002b). An alternative and valid approach to back-analysis is the determination of soil shear strengths by means of direct measurement in the laboratory and/or in situ. However, laboratory testing is associated with a number of shortcomings, such as sample disturbance and that the field conditions need to be accurately replicated in the laboratory, including the following prior to failure: effective normal stress acting on the failure surface; pre-existing shear deformation; and the drainage conditions during shear (Tang et al., 1999). Back calculated soil shear strengths have advantages over laboratory determined data, because they represent a large scale of soil mass over slip surfaces and they were determined from a in situ state (Gilbert et al., 1998). Limitations of in situ testing include the uncertainty of the models used

to translate the measurements into their associated soil properties, as well as variations in the testing equipment and procedures. Based on the assumptions of: (i) the factor of safety of the slope is equal to unity at the moment of failure; and (ii) the original slope geometry, back-analysis is widely used in slope stability research and design (Okui et al., 1997, Gilbert et al., 1998, Urgeles et al., 2006, Bozzano et al., 2012, Harris et al., 2012, Wang et al., 2013c).

The Geographic Information System (GIS) has greatly facilitated the research of natural hazards with its efficient and effective spatial data processing capabilities. With the integration of high-resolution, remotely-sensed (RS) data, such as light detecting and ranging (LIDAR) images and aerial photographs, the GIS framework has been widely applied to slope instability studies (Xie et al., 2006, Cai et al., 2007, Hashimoto et al., 2008, Kamp et al., 2008, Li et al., 2008, Magliulo et al., 2008, Pantha et al., 2008, Zolfaghari and Heath, 2008, Ray and Smedt, 2009, Wen et al., 2009). As in the present paper, the GIS framework plays a fundamental role in the following three aspects: (a) slope geometries of the four aforementioned sites are determined using topographic information which is extracted from the LIDAR DEM; (b) the accurate location of the collapse regions are established by the comparison of high-resolution aerial images; and (c) the dimensions of the predicted collapsed regions are validated against high-resolution aerial images.

In this paper, an efficient framework for the back-analysis of riverbank collapses is adopted at four sites identified as being high risk (SKM, 2010a). The framework employs a finite element analysis-based transient water model to evaluate the dynamic distribution of pore water pressure under different circumstances of rainfall, evaporation and river level fluctuations. Subsequently, limit equilibrium slope stability analyses are performed to back-analyse the failure. The paper aims to: (i) simulate the four aforementioned riverbank collapses using 2D cross-sectional models; and (ii) determine the soil shear strength profiles from the back-analyses.

5.2 Study area and regions of collapse

As mentioned above, the study examines four sites along the Lower River Murray including East Front Road, Mannum (EFR), Woodlane Reserve (WR), River Front Road, Murray Bridge (RFR) and White Sands (WS). The detailed location of the sites, cross-sections, recorded historical major riverbank collapses and the site investigation boreholes are shown in Figure 5.1. According to the inventory of the South Australian Department of Environment, Water and Natural Resources (DEWNR), several incidents were recorded at these sites between 2008 and 2010, as shown in Table 5.1.

Table 5.1 Historical riverbank collapse related incidents associated with the four examined sites.

Sites	Bank collapse	Bank cracking	Tree leaning and collapse	Levee problem
EFR	6	7	7	0
WR	3	3	0	0
RFR	8	3	6	2
WS	3	0	3	1

Specifically, EFR was observed to exhibit cracking along the riverbank, suggesting impending failure zones had been developed. At WR, a 45 x 14 m riverbank collapse, which damaged pumping infrastructure, was reported and further reduction of the river level was indicated as a major threat to riverbank stability. At RFR, which has been studied and modelled a number of times (Liang et al., 2012, Liang et al., 2014), an unprecedented period of dry conditions and low flows induced a significant section of riverbank (60 x 20 m, 70,000 m³) to collapse into the river, taking with it three unoccupied vehicles and several trees. At WS, two large riverbank collapses were reported: 20 x 6 m on 14 February 2009 and 25 x 4 m on 22 April 2009 (SKM, 2010a).

5.3 Methodology

In order to determine the location of the collapses with a relatively high degree of accuracy, visual interpretation of high-resolution aerial images has been implemented in conjunction with DEWNR's inventory of historical riverbank failures (shown as green squares in Figure 5.2). For each riverbank collapse, two aerial photographs were used to identify the extent of the collapse regions. Figure 5.2(a), 2(c), 2(e) and 2(g) were acquired in March 2008 with a 0.5 metre resolution, whereas Figure 5.2(b), 2(d), 2(f) and 2(h) incorporate a 0.2 metre resolution which were acquired after the recorded collapses (May 2010). As shown in Figure 5.2, the examined regions of collapse were vectorised with dotted areas within the ArcGIS framework, and were linked to the closest DEWNR collapse record (EFR-50, WR-7, MB-1 and WS-51).

In this paper, a transient, unsaturated flow-based riverbank stability model was developed in two dimensions to facilitate back-analyses at 4 sites along the Lower River Murray as mentioned above. The model incorporates riverbank geometry, geotechnical properties, river level variation, and rainfall and evaporation. Back-analyses were performed to obtain the closest match between the predicted and actual date of failure, while comparing the predicted failure geometry with the high-resolution aerial images.

An elevation comparison method was employed at each of the sites to assist with visual interpretation. Specifically, LIDAR DEMs obtained in 2008 [Figure 5.3(a)] were used to verify the elevation of the examined collapses with the LIDAR DEMs obtained in 2010 [Figure 5.3(b)], which include the elevation of the river level. For example, point A in Figure 5.3(a), where the elevation of the bank was at 1.484 m AHD prior to the collapse, is compared with point B, where the river level was at -0.45 m AHD subsequent to the failure. By comparing the DEMs, each of the examined regions [Figure 5.2(b), (d), (f) and (h)] is confirmed as collapsed rather than simply submerged beneath a higher river level.

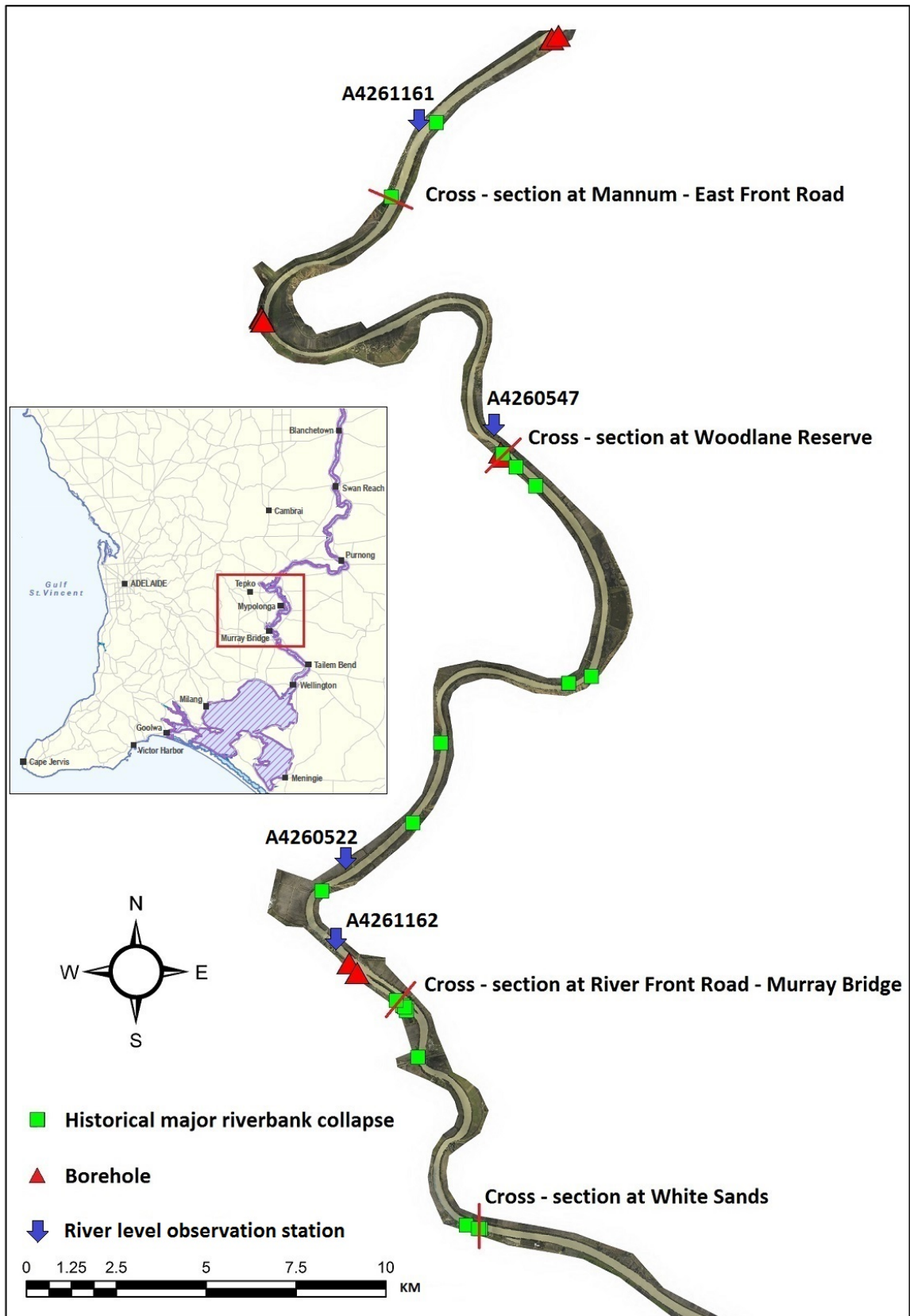
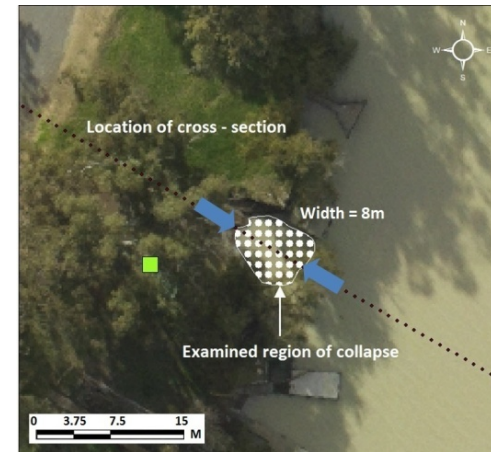


Figure 5.1 Details of the study area.



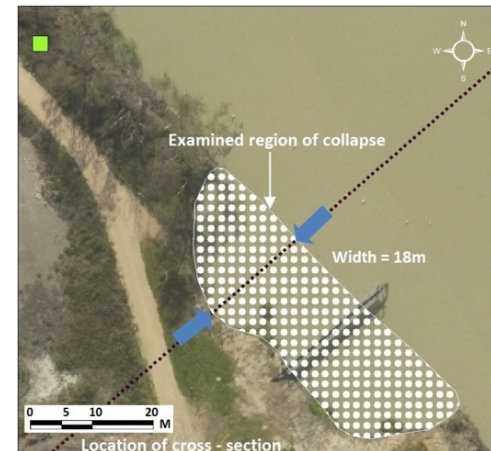
(a)



(b)



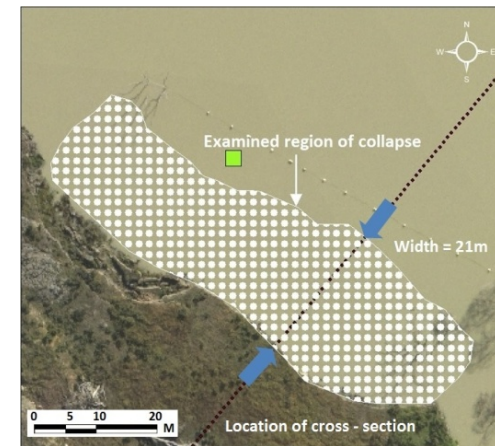
(c)



(d)



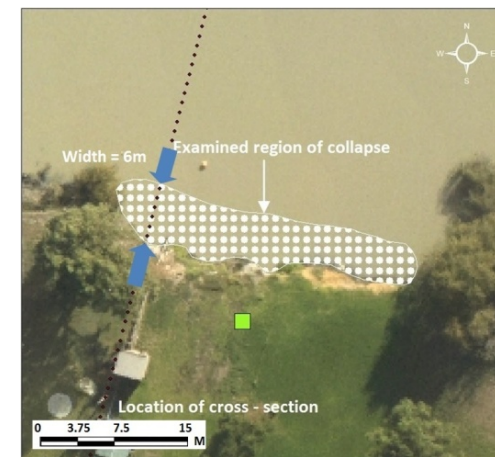
(e)



(f)



(g)



(h)

Figure 5.2: Adopted visual interpretation method of high-resolution aerial images: (a), (c), (e) and (g) are aerial photographs acquired in March 2008 at EFR, WR, MB and WS, respectively; (b), (d), (f), and (h) are aerial photographs acquired in May 2010 at EFR, WR, MB and WS, respectively.

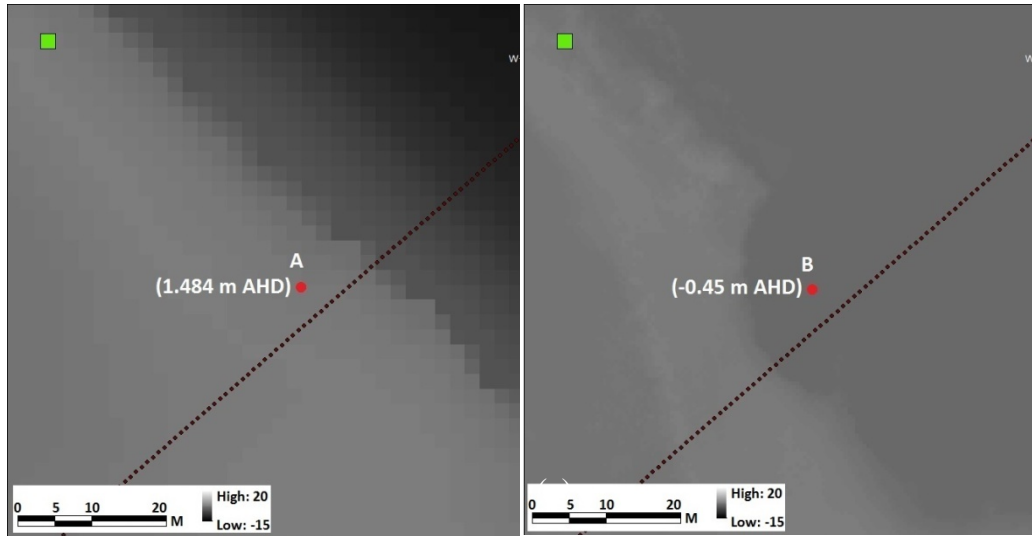


Figure 5.3: Example of adopted elevation comparison method on DEMs at Woodlane Reserve (a) 1 m resolution DEM acquired in 2008; (b) 0.2 m resolution DEM acquired in 2010).

With reference to the DEWNR riverbank collapse inventory, visual interpretation was implemented on high-resolution aerial images to examine the region of collapse within the ArcGIS framework. The 2D cross-sections that coincided with the collapse regions were used to analyse the evolution of the factor of safety (FoS) of the riverbank at the 4 sites. The saturated and unsaturated ground water flows within the riverbank were simulated using the finite element method within the PC-based program SVFlux (SoilVision, 2009a). The 2D limit equilibrium slope stability calculations were performed using SVSlope (SoilVision, 2009b). Specifically, in SVFlux, variations in rainfall, evaporation and river level fluctuations are entered to model the dynamic distribution of pore water pressure within the riverbank. These are subsequently imported into SVSlope to assess the stability of the riverbank against time. By considering the depth of the collapse, back-analyses were performed on the layer of high plasticity, Silty Clay (CH), as outlined below, using Unsaturated Fredlund soil model (Fredlund et al., 1996) informed by geotechnical investigations performed near each site.

5.3.1 Topography and soil properties

In this paper, the geometries of the riverbank associated with the 4 sites mentioned above are obtained from DEMs using the ArcGIS framework. An example of a cross-section location is shown in Figure 5.3. Each of the cross-sections initially comprised of 401 points, with a 10 m lateral interval between each neighbouring point. Based on the bilinear interpolation method, the elevation data were then extracted from the two DEMs (a 1 m resolution DEM acquired in 2008 and a 0.2 m resolution DEM acquired in 2010, as mentioned above) and assigned to those 401 points for each cross-section, with singular points avoided. As indicated in Figure 5.2, the locations of the 4 cross-sections coincide with and cross each examined region of collapse. This process generated high-resolution cross-sections which provided effective modelling of the riverbanks in both SVFlux and SVSlope.

In October and November 2009, geotechnical investigations were performed by SKM at three sites, including EFR (3 boreholes and 1 piezocone [CPTu]), WR (2 boreholes and 5 CPTus) and RFR (2 boreholes and 13 CPTus) (SKM, 2010b). Based on the data from investigations, summarised in Table 5.2, the geotechnical models have been developed at each of the 4 sites. The WS and RFR sites share a common geotechnical model, which was obtained from the RFR geotechnical investigation, whereas the models for EFR and WR were established from their respective investigations, as indicated above.

For the purpose of modelling the variation of soil suction under saturated and unsaturated conditions, soil water characteristic curves (SWCCs) are used in each of the soil layers within SVFlux. The SWCC parameters are estimated from the particle size distributions (PSDs) in each soil layer using the Zapata method (Torres Hernandez et al., 2011) which incorporates the weighted Plasticity Index (wPI). Adopting Equation (5.1), wPI is determined based on the PSDs from the borehole soil samples (Table 5.2), and PI is the plasticity index and P_{200} is the percentage of soil passing the US standard #200 sieve.

$$wPI = PI \times P_{200}/100 \quad (5.1)$$

The saturated hydraulic conductivity, K_{sat} , is derived from a CPTu pore pressure dissipation test performed at 5 m depth in Murray Bridge. Based on relationships between the penetration excess pore pressure and the saturated hydraulic conductivity (Voyiadjis and Song, 2003) for the clay layer, the K_{sat} is found to equal approximately 9.9×10^{-5} m/day, as shown in Table 5.2. In unsaturated soil, the unsaturated hydraulic conductivity, K , varies with respect to matric suction, and is calculated indirectly from the Fredlund and Xing estimation associated with K_{sat} (Fredlund et al., 1995).

Table 5.2 Soil properties for saturated and unsaturated flow modelling.

Layer	Elevation (m AHD)	K_{sat} (m/day)	θ_{sat} (%)	ρ (t/m ³)	w (%)	PI (%)	γ (kN/m ³)
East Front Road (EFR)							
Silty/Clayey Sand (SM/SC)	3.5 to 1	13.51	45.2	1.7	17.1	2	20 ± 1
Silty Clay (CH)	1 to -1	9.9×10^{-5}	59.8	1.4	26.6	16	17 ± 1
Silty Clay (CH)	-1 to -5	9.9×10^{-5}	80.7	0.95	79	42	17 ± 1
Clayey Sand (SC)	> -5	0.187	49.7	1.6	59	38	20 ± 1
Woodlane Reserve (WR)							
Sand (SP)	2.5 to 2	15.21	62	1.35	35.4	40	17 ± 1
Silty Clay (CH)	2 to -1	9.9×10^{-5}	76	1	56	41	17 ± 1

Clayey/Silty Sand (SC/SM)	-1 to -5	0.187	57	1.7	48.6	17	20 ± 1
Sandy/Silty Clay (CL)	-5 to -11	9.9 × 10 ⁻⁵	52	1.6	22	14	20 ± 1
Silty Sand/ Gravel (SM)	> -11	0.187	51	1.6	22	3	20 ± 1
River Front Road (RFR) & White Sands (WS)							
Silty/Clayey Sand (SM/SC)	1 to 0	13.51	52.7	1.25	42	30	18 ± 1
Silty Clay (CH)	0 to -20	9.9 × 10 ⁻⁵	63.2	1.01	61	50	16 ± 1
Clayey Sand/Sandy Clay (SC/CL)	> -20	0.187	54.6	1.23	44	50	17 ± 1

5.3.2 River level and climatic data

The River Murray level data used in this study are obtained from 4 observation stations: A4261161, A4260547 (WaterConnect, 2014), A4261162 and A4260522 (MDBA, 2014), as shown in Figure 5.1. The climatic data, which include mean daily rainfall, mean daily temperature, evaporation and humidity, at the 4 sites are collected from the Australian Bureau of Meteorology (2014). In order to back-analyse the known riverbank collapses under the combined influence of river level fluctuation, rainfall and evaporation, a one-month historical record was adopted prior to the recorded date of each riverbank collapse.

As shown in Figure 5.4, unexpected low inflows, combined with evaporation of the lower lakes, resulted in the daily river levels remaining between -1.1 to

–0.8 m AHD at these 4 sites. More specifically, compared with the relatively constant daily river levels at WR and RFR, significant high flow events were observed at EFR and WS in the last 7 days of the month. Approximately 30 mm and 35 mm rainfall were observed at EFR and WS, respectively, however, the rainfall at WR and RFR sites were negligible.

5.4 Back-analysis and validation

As mentioned above, back-analyses are performed on the adopted cross-sections at the 4 sites, shown previously in Figure 5.2. The dates of each riverbank collapse incident are obtained from the most relevant DEWNR record, and the back-analyses are benchmarked against these dates. The riverbank profiles at the 4 sites were modelled previously by SKM (2010a) and Coffey (2012a) using separate soil layers informed by borehole logs from (SKM, 2010 a–e). Specifically, the static SKM and Coffey analyses, as summarised in Table 5.3 and Figure 5.5 to 5.8, incorporated effective stress parameters for the Fill and SC layers using the Mohr-Coulomb failure criterion, while total stress parameters were adopted in the CH layers using the following depth-dependent, undrained model: linearly-increasing cohesion with depth, with c_{top} quantifying the cohesion (kPa) at the upper layer boundary, c_{ratio} representing the gradient of increasing cohesion with depth and capped at a maximum value of c_{max} . Each of the values recommended by SKM (2010a) and Coffey (2012) were inferred from laboratory and in situ test results obtained from their respective geotechnical investigations. However, in order to accommodate the effects of positive and negative pore water pressures in the partially-saturated riverbanks, an unsaturated, effective stress analysis, based on the Unsaturated Fredlund model (Fredlund et al., 1996) is performed on the Fill and CH layers in the present paper, as shown by Equation (5.2).

$$\tau = c' + (\sigma_n - u_a) \tan \phi' + (u_a - u_w) [\theta(u_a - u_w) / \theta_s]^b \tan \phi \quad (5.2)$$

Where: $\theta(u_a - u_w)$ = the volumetric water content at any suction; θ_s = saturated volumetric water content; b = a fitting parameter that has a value close to unity for sands and increases with plasticity. At each site, the geotechnical properties of the high plasticity, clay (CH) layers are varied marginally, with respect to the results of the corresponding site investigations, until the factors of safety (FoSs) of unity were obtained in close proximity to the recorded dates of collapse. As shown in Figures 5.5 to 5.8, values of FoS = 1.0 were obtained from the most appropriate Unsaturated Fredlund soil model as summarised in Table 3. For example, at the River Front Road (RFR) site at Murray Bridge, the soil model for the CH layer adopted $c' = 0$ kPa; $\phi' = 22^\circ$, which aligns reasonably well with the single CU triaxial test performed by SKM (2010b) ($\phi' = 27^\circ$). The variation in pore water pressure with time has been presented previously by Liang et al. (2015).

As mentioned above, the models are validated in two ways. Firstly, the predicted dates of bank collapse are compared with the historical collapse dates from DEWNR inventory. As can be seen from Table 5.4 and Figure 5.9 the predicted dates compare very favourably with the historical dates. This is not particularly unexpected, given that the values of ϕ' were varied until the predicted and historical collapse dates were in good agreement. However, Figure 5.9 is particularly encouraging in that the FoS time series, prior to collapse, consistently plot above unity, which is consistent with increasing pore water pressure prior to failure. In addition, the second independent validation measure is the volume of the collapsed region. By scrutinising the high-resolution aerial images (Figure 5.2), the dimensions of the collapsed regions can be determined, as explained earlier. Table 5.4 also shows the predicted widths of the collapsed regions from the back analyses of the 4 sites. As can be seen, the predicted widths compare extremely well with those of the actual collapse.

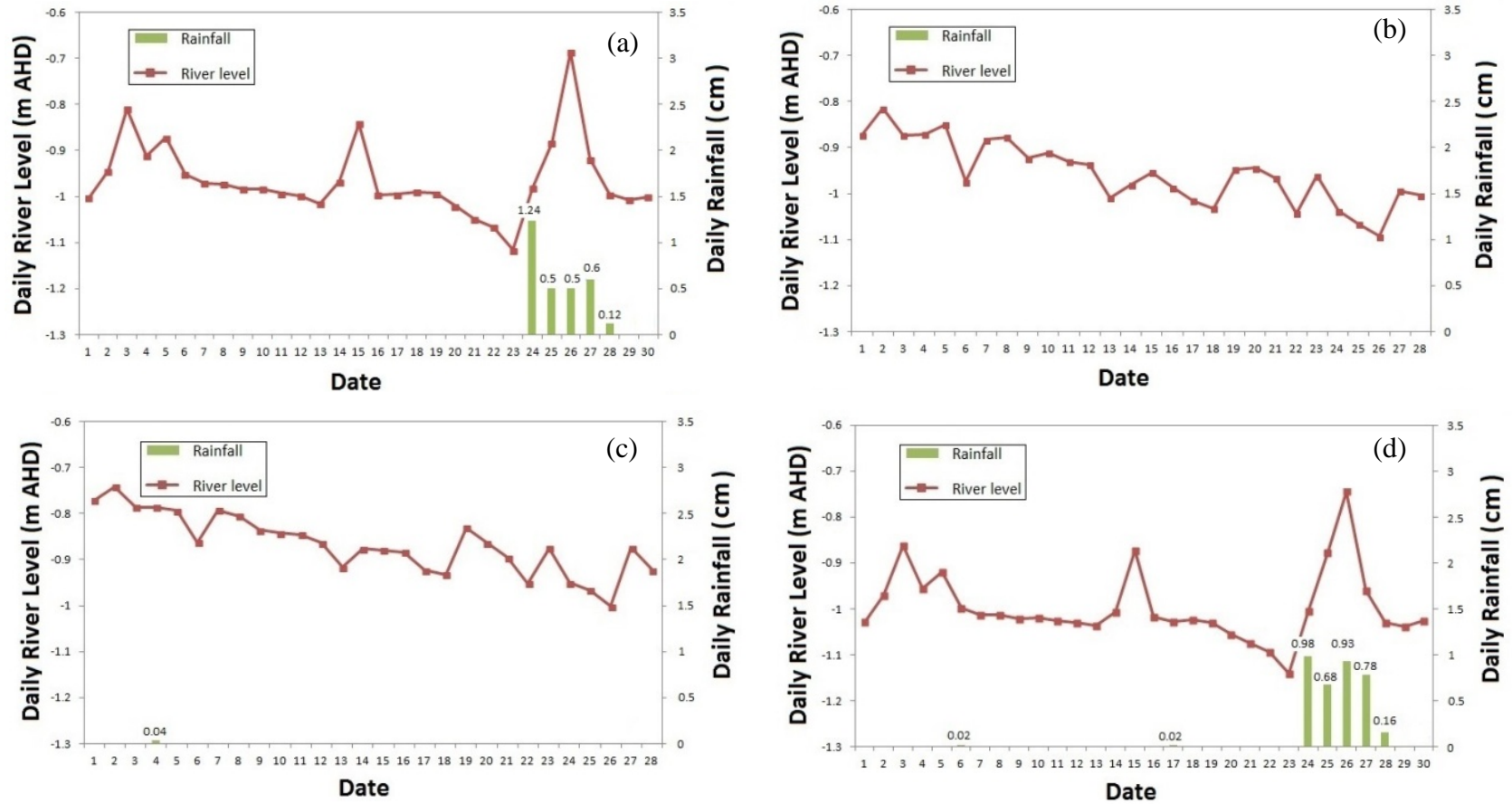


Figure 5.4: Daily river levels and daily rainfall recorded at (a) East Front Road, Mannum (EFR) site in April 2009; (b) Woodlane Reserve (WR) site in February 2009; (c) River Front Road, Murray Bridge (RFR) site in February 2009; and (d) White Sands (WS) site in April 2009.

Table 5.3 Geotechnical models of the clay layer obtained from back-analyses.

Sites	Undrained parameters for CH layer from SKM (2012)	Undrained parameters for CH layer from Coffey (2012)	Effective stress parameters from back analysis
EFR	$c_{u-B} = 50 \pm 10$ (kPa) $c_{u-B1} = 17.5 \pm 2.5$ (kPa) $c_{u-B2} = 14 \pm 2$ (kPa)	$c_{u-top} = 5.5$ (kPa) $c_{u-ratio} = 1.25$ (kPa/m) $c_{u-max} = 25 \pm 5$ (kPa)	$c' = 0, \phi' = 23^\circ$
WR	$c_u = 20 \pm 5$ (kPa)		$c' = 0, \phi' = 20^\circ$
RFR	$c_{u-top} = 10 \pm 5$ (kPa) $c_{u-ratio} = 1.25$ (kPa/m) $c_{u-max} = 25 \pm 5$ (kPa)		$c' = 0, \phi' = 19^\circ$
WS	N/A	N/A	$c' = 0, \phi' = 24^\circ$

Table 5.4 Model validation.

Sites	Recorded date of collapse	Predicted date of collapse	Width of collapsed region from aerial photos	Predicted width of collapsed region
EFR	Approx. Day 20	Day 23	8 m	8 m
WR	Approx. Day 28	Day 26	18 m	17.7 m
MB	Approx. Day 4	Day 6	20 m	19.5 m
WS	Approx. Day 22	Day 23	6 m	5 m

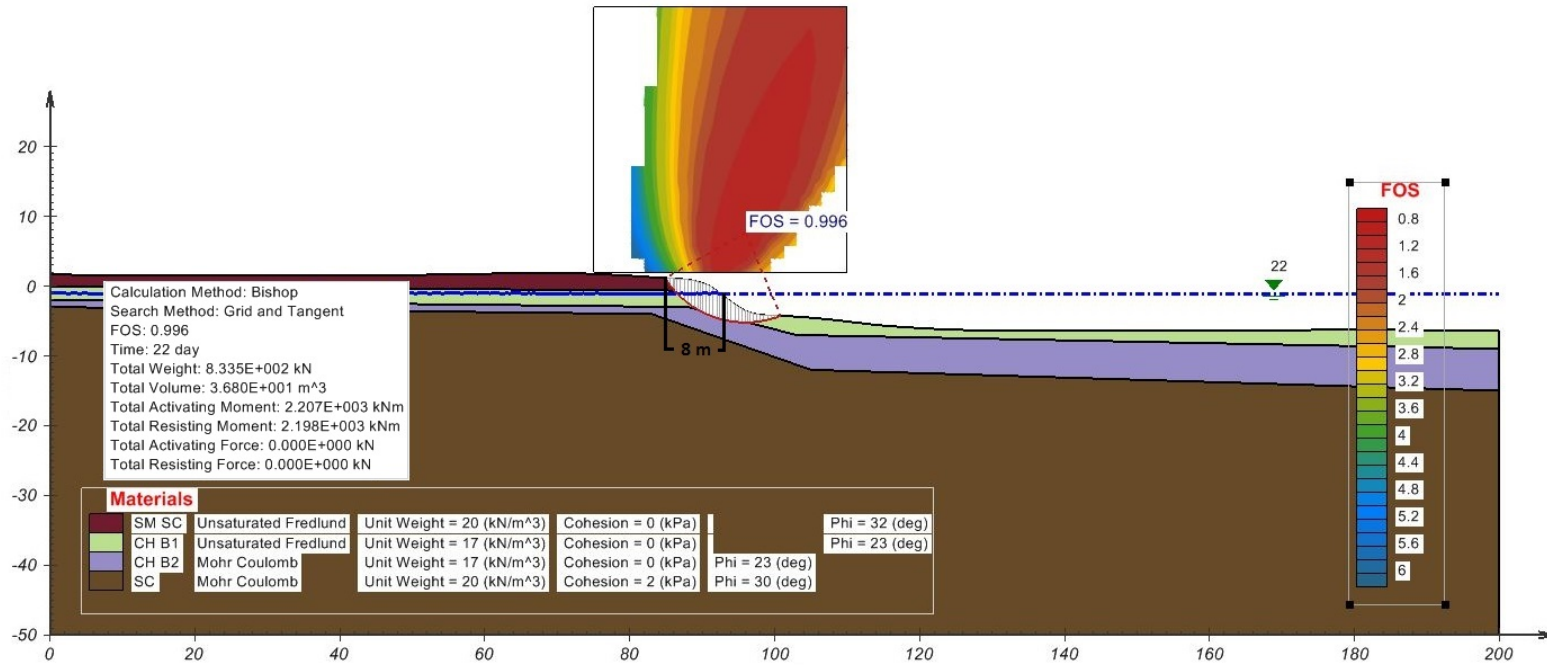


Figure 5.5: Riverbank stability analysis of the East Front Road, Mannum (EFR) site on 23 April 2009.

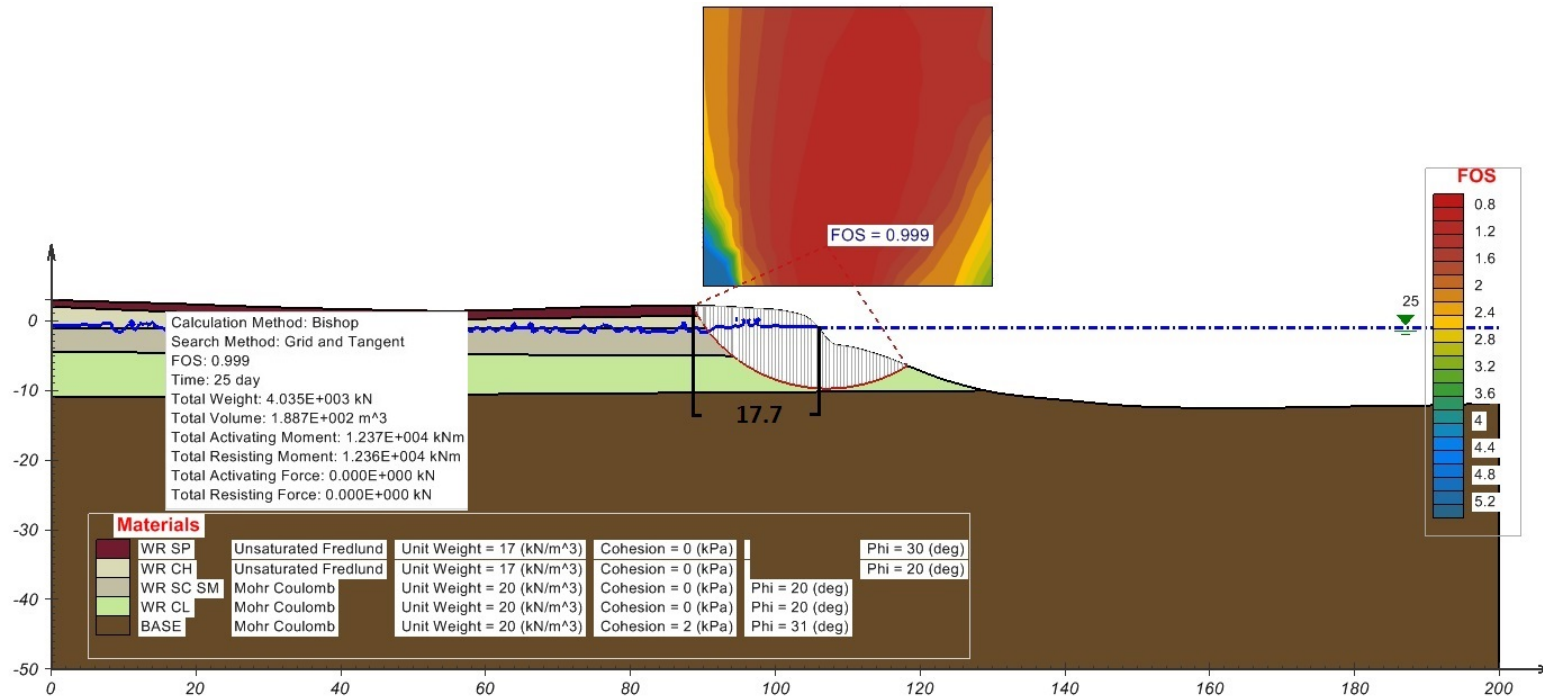


Figure 5.6: Riverbank stability analysis of the Woodlane Reserve (WR) site on 26 February 2009.

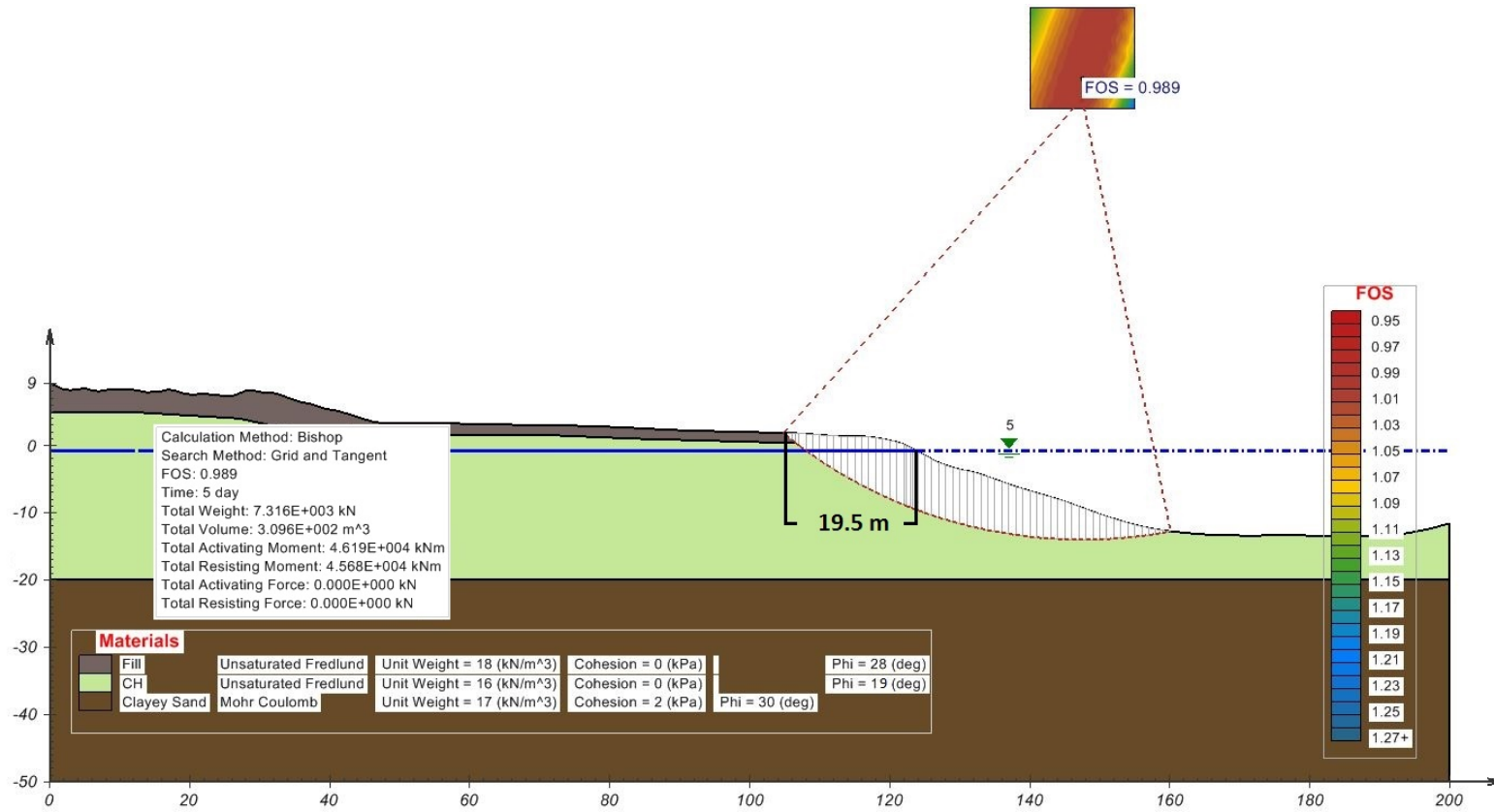


Figure 5.7: Riverbank stability analysis of the River Front Road, Murray Bridge (RFR) site on 6 February 2009.

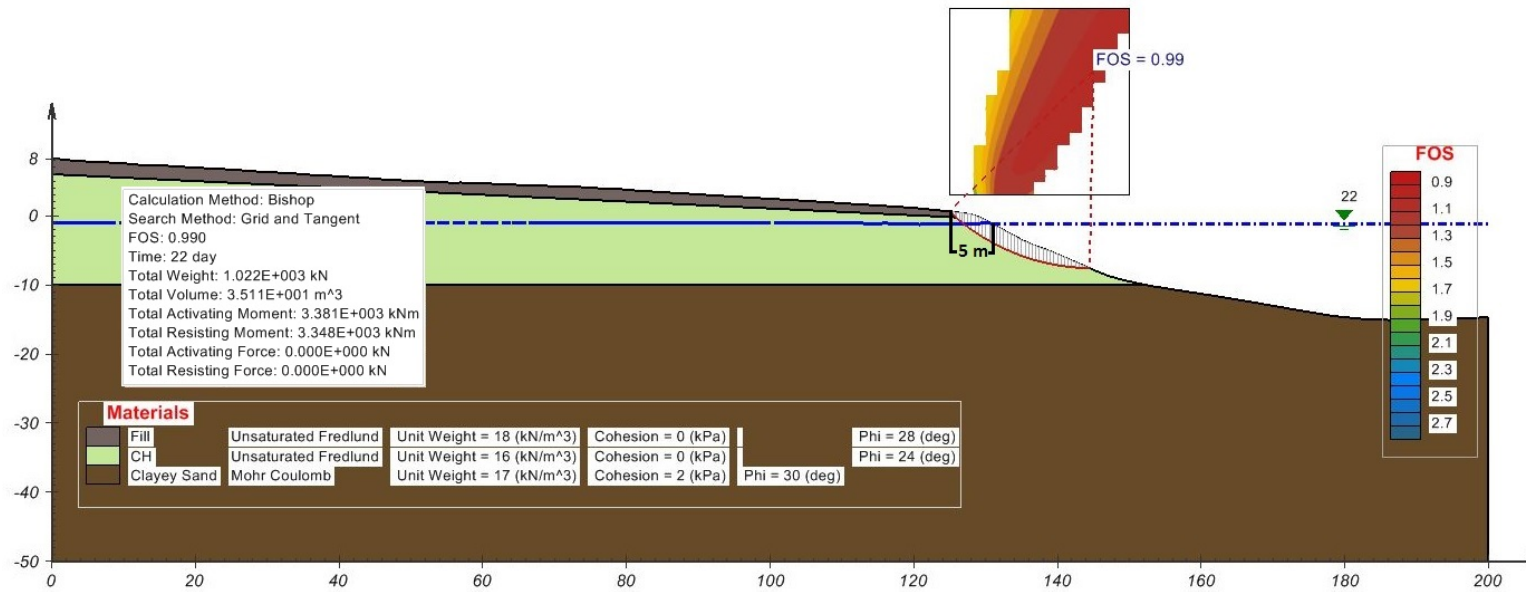


Figure 5.8: Riverbank stability analysis of the White Sands (WS) site on 23 April 2009.

5.5 Summary

In this paper, an efficient approach for back-analysis of riverbank collapse has been introduced and applied to 4 high-risk sites along the Lower River Murray. A GIS framework, incorporating LIDAR digital elevation models and high-resolution aerial images, has been used to quantify the riverbank geometries and examine the actual collapsed regions according to the inventory. Geotechnical data, which have been used in back-analyses, were obtained from the site investigations performed at the 4 sites. A transient, unsaturated flow-based riverbank stability model was implemented using SVSlope in conjunction with SVFlux.

The study has shown that:

- (a) The results of back-analysed soil shear strengths at the 4 sites have shown great consistency with those proposed by the geotechnical consultant (SKM) commissioned to undertake site investigations adjacent to the collapse sites.
- (b) Model validation demonstrates the adopted framework provides reliable riverbank stability predictions.
- (c) The integration of GIS with high-resolution spatial data facilitates the process of collapsed region identification, model geometry development and the calculation of the dimensions of the collapsed regions.

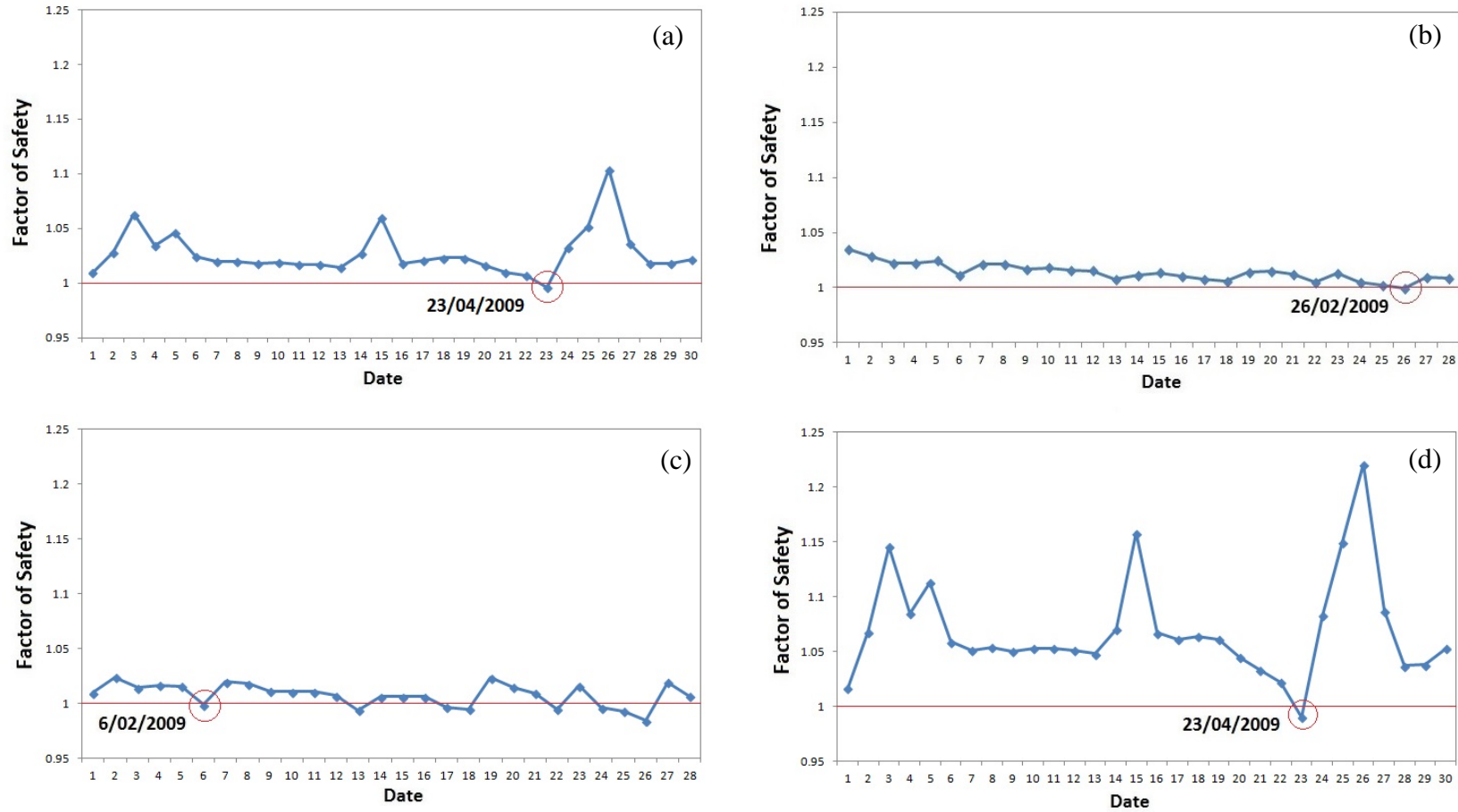


Figure 5.9: Riverbank collapse factor of safety time series for: (a) EFR in April 2009; (b) WR in February 2009; (c) RFR in February 2009; and (d) WS in April 2009.

Acknowledgements

The authors are grateful for the support and valuable advice provided by Jai O'Toole, Geoff Eaton and Richard Brown from DEWNR. This project is funded by the Goyder Institute for Water Research, under Project E.1.8 Riverbank Stability, and the authors are grateful for their support.

References for Chapter 5

Abramson, L. W., Lee, T. S., Sharma, S. & Boyce, G. M. 2002a. *Slope stability and stabilization methods*, New York, John Wiley and Sons.

Abramson, L. W., Lee, T. S., Sharma, S. & Boyce, G. M. (eds.) 2002b. *Slope Stability and Stabilization Methods*, New York: John Wiley & Sons, Inc.

Acharya, G., De Smedt, F. & Long, N. 2006. Assessing landslide hazard in GIS: a case study from Rasuwa, Nepal. *Bulletin of Engineering Geology and the Environment*, 65, 99-107.

Akgün, A. & Bulut, F. 2007. GIS-based landslide susceptibility for Arsin-Yomra (Trabzon, North Turkey) region. *Environmental Geology*, 51, 1377-1387.

Baum, R. L., Savage, W. Z. & Godt, J. W. 2008. TRIGRS—A Fortran Program for Transient Rainfall Infiltration and Grid-Based Regional Slope-Stability Analysis, Version 2.0. U.S. Department of the Interior U.S. Geological Survey.

Beal, A., Brown, R. & Toole, J. O. 2010. Expert Panel Workshop - Riverbank Collapse Hazard Program.

Berilgen, M. M. 2007. Investigation of stability of slopes under drawdown conditions. *Computers and Geotechnics*, 34, 81-91.

Bouwer, H. 1978. *Groundwater hydrology*, New York, New York : McGraw-Hill.

Bozzano, F., Martino, S., Montagna, A. & Prestininzi, A. 2012. Back analysis of a rock landslide to infer rheological parameters. *Engineering Geology*, 131-132, 45-56.

Brand, E. W. Landslides in Southeast Asia: A State-of-the-art Report. 4th International Symposium on Landslides, 1984 Toronto. 17-59.

Cai, M. F., Xie, M. W. & Li, C. L. 2007. GIS-based 3D limit equilibrium analysis for design optimization of a 600 m high slope in an open pit mine. *Journal of University of Science and Technology Beijing*, 14, 1-5.

Calabresi, G., Colleselli, F., Danese, D., Giani, G. P., Mancuso, C., Montrasio, L., Nocilla, A., Pagano, L., Reali, E. & Sciotti, A. 2013. A research study of the hydraulic behaviour of the Po river embankments. *Canadian Geotechnical Journal*.

Carrara, A., Cardinali, M., Guzzetti, F. & Reichenbach, P. 1995. Gis Technology in Mapping Landslide Hazard. *In: Carrara, A. & Guzzetti, F. (eds.) Geographical Information Systems in Assessing Natural Hazards*. Springer Netherlands.

Carrara, A., Guzzetti, F., Cardinali, M. & Reichenbach, P. 1999. Use of GIS Technology in the Prediction and Monitoring of Landslide Hazard. *Natural Hazards*, 20, 117-135.

Casagli, N., Rinaldi, M., Gargini, A. & Curini, A. 1999. Pore water pressure and streambank stability: results from a monitoring site on the Sieve River, Italy. *Earth Surface Processes and Landforms*, 24, 1095-1114.

Cha, K.-S. & Kim, T.-H. 2011. Evaluation of slope stability with topography and slope stability analysis method. *KSCCE Journal of Civil Engineering*, 15, 251-256.

Coffey. 2012a. *RE: Review of Management Options for Four Riverbank Collapse High Risk Sites*. Type to Department of Environmental, W. a. N. R.

Coffey 2012b. Review of management options for four river bank collapse high risk sites. *In: Department of Environment, W. a. N. R. (ed.)*. Depart.

Crozier, M. J. 1999. Prediction of rainfall-triggered landslides: a test of the Antecedent Water Status Model. *Earth Surface Processes and Landforms*, 24, 825-833.

De Vincenzo, A., Palma, D., Scuccimarra, V., Sdao, F. & Sole, A. 2005. GIS analysis for the study of slope instability processes in a fluvial basin. *Water Resources Management III*, 80, 321-329.

DFW 2011. Lower River Murray Riverbank Collapse Hazard Site Status Report (May 2011).

Dietrich, W. E., Reiss, R., Hsu, M.-L. & Montgomery, D. R. 1995. A process-based model for colluvial soil depth and shallow landsliding using digital elevation data. *Hydrological Processes*, 9, 383-400.

Esaki, T., Xie, M. W., Zhou, G. Y. & Mitani, Y. 2001. Monte Carlo method for locating and evaluating 3D critical slope slip based on GIS Database. *Frontiers of Rock Mechanics and Sustainable Development in the 21st Century*, 17-21.

Fredlund, D. G. 2006. Unsaturated Soil Mechanics in Engineering Practice. *Journal of Geotechnical & Geoenvironmental Engineering*, 132, 286-321.

Fredlund, D. G., Xing, A., Fredlund, M. D. & Barbour, S. L. 1996. The relationship of the unsaturated soil shear to the soil-water characteristic curve. *Canadian Geotechnical Journal*, 33, 440-448.

Fredlund, D. G., Xing, A. & Huang, S. 1995. Predicting the permeability function for unsaturated soils using the soil-water characteristic curve. *International Journal of Rock Mechanics and Mining Sciences and Geomechanics Abstracts*, 32, 159A-159A.

Giardino, M., Giordan, D. & Ambrogio, S. 2004. GIS technologies for data collection, management and visualization of large slope instabilities: two applications in the Western Italian Alps. *Natural Hazards and Earth System Sciences*, 4, 197-211.

Gilbert, R. B., Wright, S. G. & Liedtke, E. 1998. Uncertainty in Back Analysis of Slopes: Kettleman Hills Case History. *Journal of Geotechnical & Geoenvironmental Engineering*, 124, 1167-1176.

Green, S. J. 1999. *Drawdown and river bank stability*, University of Melbourne, Dept. of Civil and Environmental Engineering.

Guzzetti, F., Carrara, A., Cardinali, M. & Reichenbach, P. 1999. Landslide hazard evaluation: a review of current techniques and their application in a multi-scale study, Central Italy. *Geomorphology*, 31, 181-216.

Harris, S. J., Orense, R. P. & Itoh, K. 2012. Back analyses of rainfall-induced slope failure in Northland Allochthon formation. *Landslides*, 9, 349-356.

Hashimoto, A., Oguchi, T., Hayakawa, Y., Lin, Z., Saito, K. & Wasklewicz, T. A. 2008. GIS analysis of depositional slope change at alluvial-fan toes in Japan and the American Southwest. *Geomorphology*, 100, 120-130.

Higgins, D. T. 1980. Unsteady drawdown in 2D water-table aquifer *Journal of the Irrigation and Drainage Division-Asce*, 106, 237-251.

Hooke, J. M. 1979. An analysis of the processes of river bank erosion. *Journal of Hydrology*, 42, 39-62.

Institution of Engineers, A. (ed.) 1987. *Australian Rainfall and Runoff: A Guide to Flood Estimation*.

Jaksa, M. B., Hubble, T. C. T., Kuo, Y. L., Liang, C. & De Carli, E. V. 2013. Goyder Institute Research Project: E.1.8 Riverbank Collapse in the Lower River Murray – Literature Review and Knowledge Gap Analysis. Adelaide: Goyder Institute for Water Research.

Jia, G. W., Zhan, T. L. T., Chen, Y. M. & Fredlund, D. G. 2009. Performance of a large-scale slope model subjected to rising and lowering water levels. *Engineering Geology*, 106, 92-103.

Jiménez-Perálvarez, J., Irigaray, C., El Hamdouni, R. & Chacón, J. 2009. Building models for automatic landslide-susceptibility analysis, mapping and validation in ArcGIS. *Natural Hazards*, 50, 571-590.

Kamp, U., Growley, B. J., Khattak, G. A. & Owen, L. A. 2008. GIS-based landslide susceptibility mapping for the 2005 Kashmir earthquake region. *Geomorphology*, 101, 631-642.

Kim, K.-S., Park, H.-J., Lee, S. & Woo, I. 2004. Geographic Information System (GIS) based stability analysis of rock cut slopes. *Geosciences Journal*, 8, 391-400.

Lane, P. A. & Griffiths, D. V. 2000. Assessment of stability of slopes under drawdown conditions. *Journal of Geotechnical & Geoenvironmental Engineering*, 126, 443.

Lee, S., Choi, J. & Min, K. 2004. Probabilistic landslide hazard mapping using GIS and remote sensing data at Boun, Korea. *International Journal of Remote Sensing*, 25, 2037-2052.

Li, X. & Tang, H. 2005. Application of GIS-based grouped data Logistic model in evaluation of slope stability. *Jilin Daxue Xuebao : Diqu Kexue Ban (Journal of Jilin University :Earth Science Edition)*, 35, 361-365.

Li, X. P., Tang, H. M. & Chen, S. 2008. A GIS-supported logistic regression model applied in regional slope stability evaluation. *Landslides and Engineered Slopes: From the Past to the Future, Vols 1 and 2*, 789-794.

Liang, C., Jaksa, M. B. & Ostendorf, B. 2012. GIS-based Back Analysis of Riverbank Instability in the Lower River Murray. *Australian Geomechanics*, 47, 59-65.

Liang, C., Jaksa, M. B., Ostendorf, B. & Kuo, Y. L. 2015. Influence of river level fluctuations and climate on riverbank stability. *Computers and Geotechnics*, 63, 83-98.

Lumb, P. 1975. Slope failures in Hong Kong. *Quarterly Journal of Engineering Geology and Hydrogeology*, 8, 31-65.

Magliulo, P., Di Lisio, A., Russo, F. & Zelano, A. 2008. Geomorphology and landslide susceptibility assessment using GIS and bivariate statistics: a case study in southern Italy. *Natural Hazards*, 47, 411-435.

MDBA 2014. River Murray at Murray Bridge (Long Island) information sheet. Murray Darling Basin Authority.

Merwade, V. M. 2007. An Automated GIS Procedure for Delineating River and Lake Boundaries. *Transactions in GIS*, 11, 213-231.

Meteorology, B. o. 2014. Climate data Online, Commonwealth of Australia , Bureau of Meteorology Bureau of Meteorology.

Miller, D. J. & Sias, J. 1998. Deciphering large landslides: linking hydrological, groundwater and slope stability models through GIS. *Hydrological Processes*, 12, 923-941.

Montgomery, D. R. & Dietrich, W. E. 1994. A physically based model for the topographic control on shallow landsliding. *Water Resources Research*, 30, 1153-1171.

Moore, I. D., Gessler, P. E., Nielsen, G. A. & Peterson, G. A. 1993. Soil Attribute Prediction Using Terrain Analysis. *Soil Sci. Soc. Am. J.*, 57, 443-452.

Mukhlisin, M. & Taha, M. 2012. Numerical model of antecedent rainfall effect on slope stability at a hillslope of weathered granitic soil formation. *Journal of the Geological Society of India*, 79, 525-531.

National Water Commission, A. G. 2005. *Bureau of Rural Sciences* [Online]. http://www.water.gov.au/WaterAvailability/Whatisourtotalwaterresource/Runoff/index.aspx?Menu=Level1_3_1_5.

Okui, Y., Tokunaga, A., Shinji, M. & Mori, S. 1997. New back analysis method of slope stability by using field measurements. *International Journal of Rock Mechanics and Mining Sciences*, 34, 234.e1-234.e16.

Osman, A. M. & Thorne, C. R. 1988. Riverbank Stability Analysis .1. Theory. *Journal of Hydraulic Engineering-Asce*, 114, 134-150.

Ozdemir, A. 2009. Landslide susceptibility mapping of vicinity of Yaka Landslide (Gelendost, Turkey) using conditional probability approach in GIS. *Environmental Geology*, 57, 1675-1686.

Oztekin, B. & Topal, T. 2005. GIS-based detachment susceptibility analyses of a cut slope in limestone, Ankara-Turkey. *Environmental Geology*, 49, 124-132.

Pack, R. T., Tarboton, D. G. & Goodwin, C. N. 1998. Terrain Stability Mapping with SINMAP, technical description and users guide for version 1.00. *In: Salmon Arm, B. C. (ed.)*. Canada.

Pack, R. T., Tarboton, D. G. & Goodwin, C. N. 2001. Assessing Terrain Stability in a GIS using SINMAP. *15th annual GIS conference*. Vancouver, British Columbia.

Pantha, B. R., Yatabe, R. & Bhandary, N. P. 2008. GIS-based landslide susceptibility zonation for roadside slope repair and maintenance in the Himalayan region. *Episodes*, 31, 384-391.

Pauls, G. J., Sauer, E. K., Christiansen, E. A. & Widger, R. A. 1999. A transient analysis of slope stability following drawdown after flooding of a highly plastic clay. *Canadian Geotechnical Journal*, 36, 1151-1171.

Pike, R. 1988. The geometric signature: Quantifying landslide-terrain types from digital elevation models. *Mathematical Geology*, 20, 491-511.

Rahardjo, H., Leong, E. C. & Rezaur, R. B. 2008. Effect of antecedent rainfall on pore-water pressure distribution characteristics in residual soil slopes under tropical rainfall. *Hydrological Processes*, 22, 506-523.

Rahardjo, H., Li, X. W., Toll, D. G. & Leong, E. C. 2001. The effect of antecedent rainfall on slope stability. *Geotechnical & Geological Engineering*, 19, 371-399.

Rahardjo, H., Ong, T. H., Rezaur, R. B. & Leong, E. C. 2007. Factors Controlling Instability of Homogeneous Soil Slopes under Rainfall. *Journal of Geotechnical & Geoenvironmental Engineering*, 133, 1532-1543.

Rahimi, A., Rahardjo, H. & Leong, E. C. 2011. Effect of Antecedent Rainfall Patterns on Rainfall-Induced Slope Failure. *Journal of Geotechnical and Geoenvironmental Engineering*, 137, 483-491.

Ray, R. L. & Smedt, F. d. 2009. Slope stability analysis on a regional scale using GIS: a case study from Dhading, Nepal. *Environmental Geology*, 57, 1603-1611.

Rinaldi, M. & Casagli, N. 1999. Stability of streambanks formed in partially saturated soils and effects of negative pore water pressures: the Sieve River (Italy). *Geomorphology*, 26, 253-277.

Rinaldi, M., Casagli, N., Dapporto, S. & Gargini, A. 2004. Monitoring and modelling of pore water pressure changes and riverbank stability during flow events. *Earth Surface Processes and Landforms*, 29, 237-254.

Rowbotham, D. N. & Dudycha, D. 1998. GIS modelling of slope stability in Phewa Tal watershed, Nepal. *Geomorphology*, 26, 151-170.

Schuster, R. L. & Krizek, R. J. (eds.) 1978. *LaLandslides: Analysis and Control (Special report - Transportation Research Board, National Research Council ; 176)*.

SKM 2010a. Study into River Bank Collapsing for Lower River Murray.

SKM 2010b. Study into River Bank Collapsing for Lower River Murray: Appendix A Riverfront Road - Murray Bridge In - situ and Laboratory Test Results.

SKM 2010c. Study into River Bank Collapsing for Lower River Murray: Appendix B Caloote In - situ and Laboratory Data.

SKM 2010d. Study into River Bank Collapsing for Lower River Murray: Appendix C Woodlane Reserve In - situ and Laboratory Data.

SKM 2010e. Study into River Bank Collapsing for Lower River Murray: Appendix E East Front Road In - situ and Laboratory Data.

SKM 2011. Research into processes, triggers and dynamics of riverbank collapse in the Lower River Murray.

SoilVision 2009a. SVFlux. 4.23 ed.

SoilVision 2009b. SVSlope. 4.23 ed.

Springer, F. M. 1981. *Influence of Rapid Drawdown Events on River Bank Stability*. Master in Engineering, University of Louisville.

Stark, T. & Eid, H. 1998. Performance of Three-Dimensional Slope Stability Methods in Practice. *Journal of Geotechnical and Geoenvironmental Engineering*, 124, 1049-1060.

Stark, T. D. 2003. Three-dimensional slope stability methods in geotechnical practice.

Stark, T. D. & Eid, H. T. 1995. Drained Residual Strength of Cohesive Soils - Closure. *Journal of Geotechnical Engineering-Asce*, 121, 672-673.

Stark, T. D. & Eid, H. T. 1997. Slope stability analyses in stiff fissured clays. *Journal of Geotechnical and Geoenvironmental Engineering*, 123, 335-343.

Stark, T. D., Williamson, T. A. & Eid, H. T. 1996. HDPE geomembrane/geotextile interface shear strength. *Journal of Geotechnical Engineering-Asce*, 122, 197-203.

Tajeddin, R., Ramsey, N., Pain, D., Mollison, D. & Sandercock, P. 2010. Influence of Water Level Risk on River Bank Collapse, Lower River Murray. Sinclair Knight Merz, Australia.

Tang, W. H., Stark, T. D. & Angulo, M. 1999. RELIABILITY IN BACK ANALYSIS OF SLOPE FAILURES. *SOILS AND FOUNDATIONS*, 39, 73-80.

Thiel, R. S., Stark, T. D. & Eid, H. T. 1997. Shear behavior of reinforced geosynthetic clay liners - Discussion and closure. *Geosynthetics International*, 4, 539-541.

Thorne, C. R. 1982. Processes and mechanisms of River Bank Erosion. In: Hey, R. D., Bathurst, J. C. & Thorne, C. R. (eds.) *Gravel-bed rivers. Fluvial processes, engineering and management. Earth Surface Processes and Landforms*. John Wiley & Sons, Ltd.

Thorne, C. R., Hey, R. D. & Newson, M. D. (eds.) 1997. *Bank erosion and instability. In Applied fluvial geomorphology for river engineering and management / edited by Colin R. Thorne, Richard D. Hey, Malcolm D. Newson.*; 1997: New York : John Wiley

Thorne, C. R. & Osman, A. M. 1988. Riverbank Stability Analysis .2. Applications. *Journal of Hydraulic Engineering-Asce*, 114, 151-172.

Torres Hernandez, G., Zapata, C., Houston, S. & Witczak, M. 2011. Estimating the Soil-Water Characteristic Curve Using Grain Size Analysis and Plasticity Index. Arizona State University.

Tsai, K. J., Yu, S. H., Hsiao, C. P., Ho, M. C. & Chen, C. C. 2005. Investigations by using GPS/GIS/RS technology on the slope stability of Kaohsiung communities on slopeland in Taiwan. *Proceedings of the Fifteenth (2005) International Offshore and Polar Engineering Conference, Vol 2*, 757-763.

Twidale, C. R. 1964. Erosion of an alluvial bank at Birdwood, South Australia. *Zeitschrift für Geomorphologie, NF*, 8, 189-211.

Urgeles, R., Leynaud, D., Lastras, G., Canals, M. & Mienert, J. 2006. Back-analysis and failure mechanisms of a large submarine slide on the ebro slope, NW Mediterranean. *Marine Geology*, 226, 185-206.

Vanacker, V., Vanderschaeghe, M., Govers, G., Willems, E., Poesen, J., Deckers, J. & De Bievre, B. 2003. Linking hydrological, infinite slope stability and land-use change models through GIS for assessing the impact of deforestation on slope stability in high Andean watersheds. *Geomorphology*, 52, 299-315.

Voyiadjis, G. & Song, C. 2003. Determination of Hydraulic Conductivity Using Piezocone Penetration Test. *International Journal of Geomechanics*, 3, 217-224.

Wang, H., Liu, G., Xu, W. & Wang, G. 2005. GIS-based landslide hazard assessment: an overview. *Progress in Physical Geography*, 29, 548-567.

Wang, L., Hwang, J. H., Luo, Z., Juang, C. H. & Xiao, J. 2013. Probabilistic back analysis of slope failure – A case study in Taiwan. *Computers and Geotechnics*, 51, 12-23.

Wang, W.-D., Guo, J., Fang, L.-G. & Chang, X.-S. 2012. A subjective and objective integrated weighting method for landslides susceptibility mapping based on GIS. *Environmental Earth Sciences*, 65, 1705-1714.

WaterConnect 2014. Real Time Water Data - Latest hourly observation. WaterConnect - Government of South Australia.

Wen, H.-j., Li, X. & Zhang, J.-l. 2009. An evaluation-management information system of high slope geo-risk for mountainous city based on GIS. *2009 1st International Conference on Information Science and Engineering (ICISE 2009)*, 1975-8.

Wu, T. H. & Abdel-Latif, M. A. 2000. Prediction and mapping of landslide hazard. *Canadian Geotechnical Journal*, 37, 781-795.

Xie, M., Esaki, T. & Zhou, G. 2004. GIS-Based Probabilistic Mapping of Landslide Hazard Using a Three-Dimensional Deterministic Model. *Natural Hazards*, 33, 265-282.

Xie, M. W., Esaki, T. & Cai, M. F. 2006. GIS-based implementation of three-dimensional limit equilibrium approach of slope stability. *Journal of Geotechnical and Geoenvironmental Engineering*, 132, 656-660.

Xie, M. W., Zhou, G. Y. & Tetsuro, E. 2003. GIS Component Based 3D Landslide Hazard Assessment System: 3DSlopeGIS. *Chinese Geographical Science*, 13, 66-72.

Yan, Z.-L., Wang, J.-J. & Chai, H.-J. 2010. Influence of water level fluctuation on phreatic line in silty soil model slope. *Engineering Geology*, 113, 90-98.

Yokota, S. 1996. Multi-Purpose Digital Hazard Map for Slope Failures. *Geoinformatics*, 7, 51-59.

Yongquan, L., Yong, F. & Shenghua, J. Stability analysis of soil slope during rapid drawdown of water level. *Mechanic Automation and Control Engineering (MACE)*, 15-17 July 2011 2011. 3454-3457.

Zaitchik, B. F. & Es, H. M. v. 2003. Applying a GIS slope-stability model to site-specific landslide prevention in Honduras. (Research).(geographic information system). *Journal of Soil and Water Conservation*, 58, 45(9).

Zapata, C. E., Houston, W. N., Walsh, K. D. & Houston, S. L. 2000. Soil–Water Characteristic Curve Variability. *Advances in Unsaturated Geotechnics*.

Zhang, J. F., Li, Z. G. & Qi, T. 2005. Mechanism analysis of landslide of a layered slope induced by drawdown of water level. *Science in China Series E-Engineering & Materials Science*, 48, 136-145.

Zhang, L. L., Zhang, J., Zhang, L. M. & Tang, W. H. 2011. Stability analysis of rainfall-induced slope failure: a review. *Proceedings of the Institution of Civil Engineers-Geotechnical Engineering*, 164, 299-316.

Zolfaghari, A. & Heath, A. C. 2008. A GIS application for assessing landslide hazard over a large area. *Computers and Geotechnics*, 35, 278-285.

Chapter 6

6 Identifying Areas Susceptible to High Risk of Riverbank Collapse along the Lower River Murray

(Paper 4, published)

C. Liang¹, M. B. Jaksa¹ Y. L. Kuo¹ and B. Ostendorf²

¹School of Civil; Environmental and Mining Engineering, University of Adelaide, 5005;

²School of Earth and Environmental Sciences, University of Adelaide, 5005;

Publication:

LIANG, C., JAKSA, M. B., KUO, Y. L. & OSTENDORF, B. (2015). Identifying areas susceptible to high risk of riverbank collapse along the Lower River Murray. *Computers and Geotechnics*, 69, 236-246.

Statement of Authorship

Title of Paper	Identifying Areas Susceptible to High Risk of Riverbank Collapse along the Lower River Murray
Publication Status	<input checked="" type="radio"/> Published, <input type="radio"/> Accepted for Publication, <input type="radio"/> Submitted for Publication, <input type="radio"/> Publication style
Publication Details	LIANG, C., JAKSA, M. B., KUO, Y. L. & OSTENDORF, B. (2015). Identifying areas susceptible to high risk of riverbank collapse along the Lower River Murray. <i>Computers and Geotechnics</i> , 69, 236-246.

Author Contributions

By signing the Statement of Authorship, each author certifies that their stated contribution to the publication is accurate and that permission is granted for the publication to be included in the candidate's thesis.

Name of Principal Author (Candidate)	Chen Liang	
Contribution to the Paper	Undertook Literature review, performed parametric analysis and modeling, interpreted data and acted as corresponding author.	
Signature		Date 11/Jan/2015

Name of Co-Author	Mark B. Jaksá	
Contribution to the Paper	Supervised development of work and helped with paper editing.	
Signature		Date 4/2/15

Name of Co-Author	Yien Lik Kuo	
Contribution to the Paper	Helped with in-situ and laboratory test	
Signature		Date 3-2-2015

Name of Co-Author	Bertram Ostendorf	
Contribution to the Paper	Supervised development of work.	
Signature		Date 3-2-2015

Abstract

Riverbank collapse is a natural phenomenon in the evolution of rivers. Along the lower reaches of the River Murray, from downstream of East Front Road to the town of Wellington in South Australia, there were more than 100 riverbank collapse-related incidents reported between 2005 and 2010 in the forms of mass riverbank collapse, erosion, cracking, riparian tree leaning or collapse, as well as levee-related problems. The River Murray is the largest river in Australia. The objective of this paper is to develop a topographically-based framework that can be used, prior to undertaking detailed cross-sectional modelling or site investigation, to identify high risk areas susceptible to riverbank collapse over extensive reaches of the river. The proposed framework is based on the results of numerical analyses that have been undertaken using an integration of several approaches, which includes slope stability analysis using the limit equilibrium method with the assumption of a steady-state condition, identifying the actual locations of previously known riverbank collapse sites through the visual interpretation of historical, high-resolution aerial images, topography mapping using digital elevation models and a geographic information system, and interpretation of field and laboratory test results for model construction and geological and soil stratigraphy mapping. Back-analyses were used to estimate the likely in situ shear strength at the historical collapse sites. The results from the back-analyses were compared with those from field and laboratory testing. A total of 69 numerical analyses were undertaken at three different regions along the Lower River Murray, to identify the factors influencing the stability of the riverbank. Finally, cross-validation was used to measure the predictive performance of the proposed framework. This paper has demonstrated the efficacy of the proposed predicting framework as a useful and reliable tool for riverbank collapse hazard mapping.

Keywords: GIS, riverbank stability, hazard prediction, mapping, topography, River Murray

6.1 Introduction

The stability of the riverbanks is dependent on many factors and the failure of the riverbank can cause losses of life and substantial damages to properties and public infrastructure (Jaksa et al., 2013). Generally, the factors that may affect the stability of the riverbanks can be classified into two different groups: natural and artificial (Abramson et al., 2002b). Natural factors include site topography, bank and riverbed stratigraphy, soil and rock properties, river level fluctuation and climatic factors which include precipitation and evaporation (Cha and Kim, 2011). In the case of the Lower River Murray, more than 162 riverbank collapse-related incidents were reported between 2005 and 2010 and the collapses were identified as dominantly triggered by unprecedented low river levels (SKM, 2010a, SKM, 2011, Jaksa et al., 2013, Liang et al., 2015). In order to understand better the collapse processes, as well as the triggers for riverbank collapse along the Lower River Murray, downstream of Lock 1 at Blanchetown to Wellington, South Australia, several detailed geotechnical investigations and 2D slope stability analyses have been undertaken previously (Liang et al., 2012, Jaksa et al., 2013, Liang et al., 2014, Liang et al., 2015). However, each of these aforementioned investigations and analyses were focused solely on historical riverbank collapse sites, which accounts for only a small fraction of potential and recorded riverbank collapse sites along the Lower River Murray. The River Murray is extremely important in the Australian context as it is Australia's largest river and is the major domestic water supply for more than 1.5 million households. It is the third longest navigable river in the world and spans three states, New South Wales, Victoria and South Australia.

Slope failure susceptibility prediction and mapping have been undertaken using a variety of methods (Wu and Abdel-Latif, 2000), and which can be classified into two main categories: subjective and objective methods (Wang et al., 2012). Subjective methods consist of inventory mapping and expert evaluation, while objective methods comprise weighted linear combination (WLC) statistical models and qualitative map combination (QMC) models (Akgün and Bulut, 2007, Wang et al., 2012). More specifically, the subjective

method is based mainly on field experience; while both the WLC and QMC models of the objective method generate the composite and numeric maps by overlaying the various causal factor layers such as geology, hydrology, topography and geomorphology (Akgün and Bulut, 2007, Wang et al., 2012). As the most important parameter for evaluation of slope instabilities (Cha and Kim, 2011), topography is considered as an indicator of past failures and potential future instability (Abramson et al., 2002b). Vanacker et al. (Vanacker et al., 2003) believed that the prediction of slope failure is usually based solely upon topographical attributes. According to Abramson et al. (Abramson et al., 2002b), topographic maps play a fundamental role in the identification of slope failure and areas of potential instability. However, additional detailed site reconnaissance and aerial photographic mapping are necessary to supplement the topographic information (Abramson et al., 2002b). Yokota (Yokota, 1996) developed a slope failure hazard map of the Kagoshima area based, not only on topographical data, but also used on digitized geological data. More recently, some additional and advanced slope susceptibility prediction models have been proposed, which incorporate storm characteristics with topographical and soil data (Crozier, 1999, Wu and Abdel-Latif, 2000). Indeed, a large number of the papers, have recognized topographical variables (steepness, height, length, form, aspect, etc.) and the spatial variation of soil attributes as the most relevant factors in slope failure hazard assessment (Pike, 1988, Moore et al., 1993, Montgomery and Dietrich, 1994, Carrara et al., 1995, Dietrich et al., 1995). However, most of the studies mentioned above, as well as the models which are compatible with ArcGIS such as SINMAP (Pack et al., 1998, Pack et al., 2001) and TRIGERS (Baum et al., 2008), were focused solely on the prediction of landslides in mountainous regions rather than riverbank slope instability and susceptibility predictions.

In order to facilitate slope failure susceptibility prediction at medium or large scales, Geographic Information System (GIS) modeling and mapping are usually adopted (Jiménez-Perálvarez et al., 2009). The GIS is well known for its efficient and cost-effective spatial data processing capabilities, which include spatial data collection, manipulation and analysis, and has been

widely used in slope instability research, especially to undertake slope failure susceptibility assessment (Rowbotham and Dudyca, 1998, Carrara et al., 1999, Guzzetti et al., 1999, Esaki et al., 2001, Zaitchik and Es, 2003, Giardino et al., 2004, Kim et al., 2004, Xie et al., 2004, De Vincenzo et al., 2005, Li and Tang, 2005, Oztekin and Topal, 2005, Tsai et al., 2005, Acharya et al., 2006, Akgün and Bulut, 2007, Hashimoto et al., 2008, Kamp et al., 2008, Li et al., 2008, Pantha et al., 2008, Zolfaghari and Heath, 2008, Liang et al., 2012). The major constraint in using GIS to evaluate susceptibility of slope failure is the complexity of the influencing factors. These are sometimes known or unknown but cannot be effectively incorporated and manipulated in GIS (Carrara et al., 1999). Furthermore, the latest GIS technologies have not significantly facilitated the acquisition of geotechnical data (Carrara et al., 1999). In this paper, the collection of soil data and river level data follows the traditional procedures based on field surveys, while the topographical data incorporate a DEM (digital elevation model) within the ArcGIS environment collected using LIDAR (light detecting and ranging). To simplify the process, the following assumptions have been made: (i) the geotechnical properties of the soils are homogeneous and geological profiles are relatively uniform in each region, as shown in Figure 6.1, and can be represented by the data obtained from the corresponding field investigation; and (ii) deep-seated circular failure, in the soft and very soft clays of Holocene age, is the typical collapse mechanism along the lower reaches of the River Murray (Coffey, 2012b). With these aforementioned assumptions, the GIS framework facilitates the riverbank susceptibility prediction in the following three ways: (a) the actual locations of the historical collapses are determined and verified by high resolution aerial image comparison and interpretation to facilitate accurate back-analyses; (b) the riverbank geometries and cross-sections are extracted from the LIDAR DEMs; and (c) the influencing factors are manipulated and mapped using GIS to predict the susceptible areas.

The main objective of this paper is to develop an approximate and generic topographically-based riverbank slope instability and susceptibility prediction framework. This framework can be used to predict riverbank collapses over large extents prior to undertaking detailed cross-sectional modeling or site

investigation. Specifically, this paper aims to: (i) understand better the topographical factors that affect the stability of Lower River Murray riverbanks; and (ii) identify high risk areas of riverbank collapse in the Lower River Murray and, hence, facilitate the establishment of riverbank collapse susceptibility maps. The analysis has been undertaken using an integration of the steady state model, limit equilibrium method, back-analysis, visual interpretation, LIDAR DEMs and high resolution aerial images from GIS. The soil data used in this paper were obtained from site investigations incorporating both in situ and laboratory testing.

6.2 Study area and historical collapses

The study area is located along the Lower River Murray, which stretches from East Front Road (near Mannum) to the town of Wellington in South Australia, as shown in Figure 6.1. According to the Department of Environment Water and Natural Resources (DEWNR) inventory (SKM, 2010a, DFW, 2011), more than 100 riverbank collapse-related incidents with given GPS coordinates have been reported within this region. The main forms of the recorded incidents in the DEWNR inventory include riverbank collapse, erosion, cracking, tree leaning and collapse and levee problems (SKM, 2010a).

A general statistical analysis has been performed on the historical dataset and the results are summarized in Table 6.1, which classifies the occurrence of the incidents in the forms of riverbank collapse, cracking and riparian tree problems, subject to the inclination of riverbank slope. The occurrence of riverbank collapse appears to increase with an increase in riverbank slope inclination. For example, for steeper riverbanks, which have slope inclinations greater than 40° , the probabilities of occurrence of riverbank collapse, ground surface cracking and tree leaning or collapse are 62%, 59% and 48%, respectively.

In order to identify the locations of the historical riverbank collapses and the extents of these collapses, visual interpretation was undertaken using high-

resolution aerial images (Figure 6.2). With reference to the DEWNR inventory, the visual interpretation is implemented in following manner. Firstly, high-resolution aerial images with a 0.5 meter resolution, which were acquired in March 2008, an example of which is shown in Figure 6.2(a), were compared with 0.2 meter resolution aerial images, which were acquired after the collapse (May 2010), as shown in Figure 6.2(b) . The difference is then vectorized and identified as a region of collapse [Figure 6.2(b)]. As shown in Figure 6.2, there is a large discrepancy between the recorded location of the riverbank collapse in the inventory database and that determined location using the method outlined above. This is perhaps due to limitations with the GPS equipment used or records entered when the incident was reported.

The river level downstream of Lock 1 (at Blanchetown, South Australia) fluctuated significantly between 2008 to 2010, due mainly to unprecedented low river flows during this period. Accurate determination of the riverbank collapse location through visual interpretation of aerial photographs can sometime be misinformed by the river level fluctuation. For example, a riverbank could be misidentified as collapsed due to a high river level. In order to overcome this, elevations were compared to assist with the visual interpretation. The LIDAR DEMs obtained in 2008 [Figure 6.2(c)] were used to verify the elevation of the examined collapses with the LIDAR DEMs obtained in 2010 [Figure 6.2(d)], which include the elevation of the river level. For example, Point A in Figure 6.2(c), where the elevation of the bank was at 1.48 m AHD (Australian Height Datum) prior to the collapse, is compared with Point B, where the river level was at -0.47 m AHD subsequent to the failure. By comparing the LIDAR DEMs, the examined region is confirmed as having collapsed rather than simply having been submerged beneath a higher river level. This process yielded accurate locations of the historical collapse sites, which facilitated subsequent back-analyses.

Table 6.1 Riverbank collapse related incidents with associated slope inclinations.

Slope inclination	Bank collapse	Cracking	Tree leaning and collapse
< 20°	N/A	1	1
20° to 25°	N/A	2	4
25° to 30°	2	2	2
30° to 35°	4	6	2
35° to 40°	4	3	3
40° to 45°	4	9	5
45° to 50°	6	3	1
> 50°	6	8	5

6.3 Methodology

In order to identify areas susceptible to high risk of riverbank collapse with sufficient accuracy over large extents of the river, the study area is subdivided into three separate regions: Regions i, ii and iii (Figure 6.1), with each region having distinctive geotechnical and geological characteristics. A total of 69, 2D back-analyses are undertaken to determine the relationships between riverbank stability, in terms of the conventional factor of safety (FoS), and the topographical factors in each region. These relationships are then used to predict other areas at high risk of riverbank collapse in corresponding regions.

The proposed framework is based on the results of the 2D numerical analyses that have been undertaken. The analyses require an integration of several different methods, which includes: slope stability analysis using the limit equilibrium method, with the assumption of steady-state conditions; identification of the actual locations and extents of previously known riverbank collapse sites through visual interpretation of historical high-resolution aerial images, topography mapping using DEMs and GIS, and interpretation of field and laboratory testing results for model construction and geological and soil stratigraphy mapping.

The analyses were undertaken using two, commercially available software tools *ArcGIS* and *SVSlope*. Specifically, the 2D cross-sectional numerical modelling was carried out using the PC Windows-based program *SVSlope* (SoilVision, 2009b). The FoS was determined using Bishop's method of slices, which is based on the limit equilibrium method, while the sliding surfaces were determined using the grid and tangent method. As mentioned previously, the actual locations and extents of the historical collapse sites were identified by visual interpretation of high-resolution aerial images with reference to the DEWNR inventory (Figure 6.2). Riverbank geometries were extracted from two sets of LIDAR DEMs, a 1 m resolution model acquired in 2008 and a 0.2 m resolution model acquired in 2010, using *ArcGIS*. Back-analyses were performed on three historical collapses in each region to obtain representative in situ soil shear strengths and these were compared with results from field tests, as well as laboratory testing on soil samples collected from the nearest boreholes (Figure 6.1). The detailed description of each process is outlined in the sub-sections that follow.

6.3.1 Topography

As mentioned above, the riverbank geometries are extracted from two LIDAR DEMs, which were acquired on different dates: 2008 [Figure 6.2(c)] and 2010 [Figure 6.2(d)]. By implementing the *ArcGIS* framework, each of the riverbank cross-sections initially comprised 401 points, with a 10 m lateral spacing between each neighboring point. Based on the bilinear interpolation method, the elevation data were then extracted from the two DEMs and assigned to the 401 points for each cross-section, with singular points avoided (Liang et al., 2014, Liang et al., 2015). This process facilitated the creation of accurate and high-resolution riverbank cross-sections.

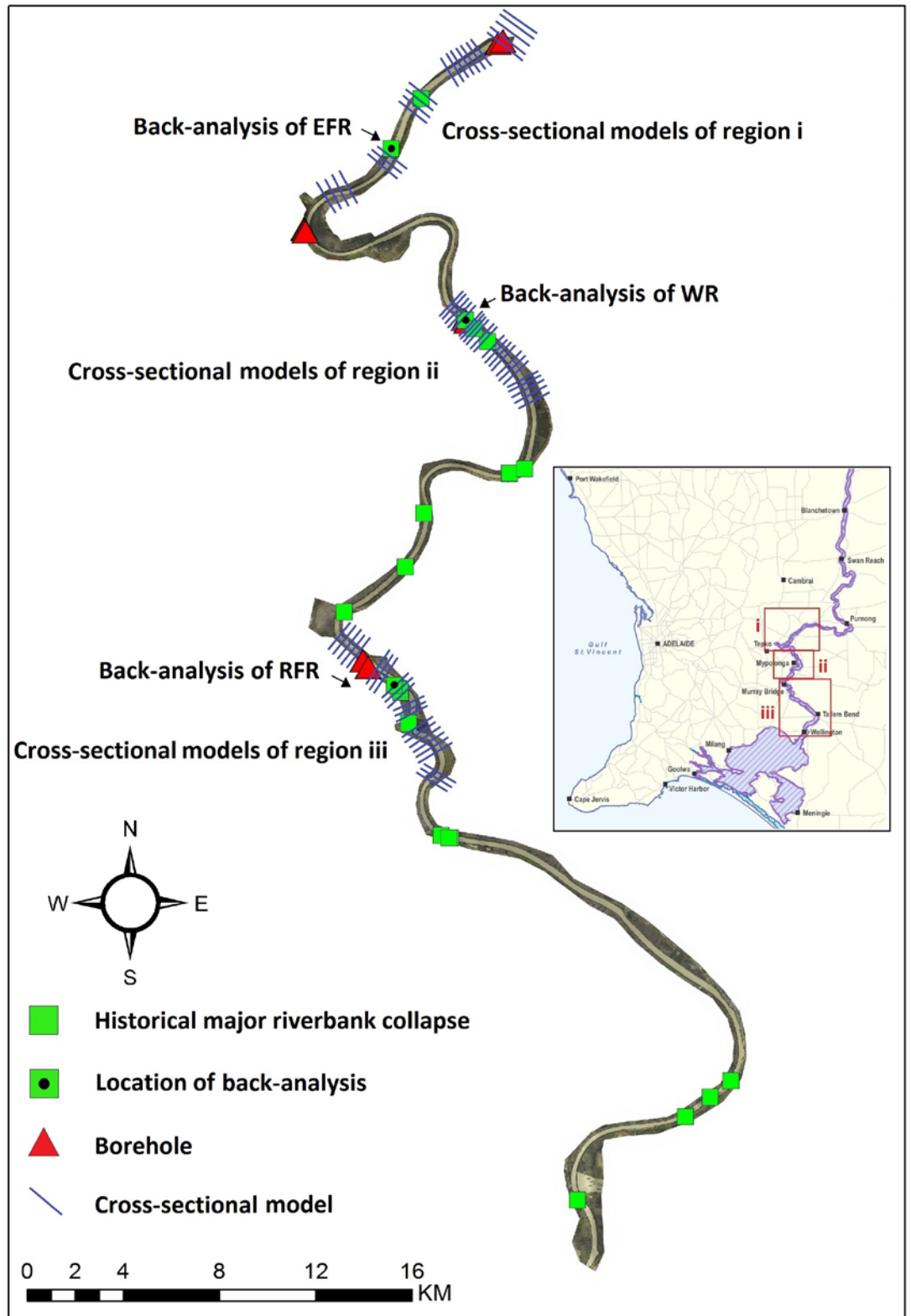
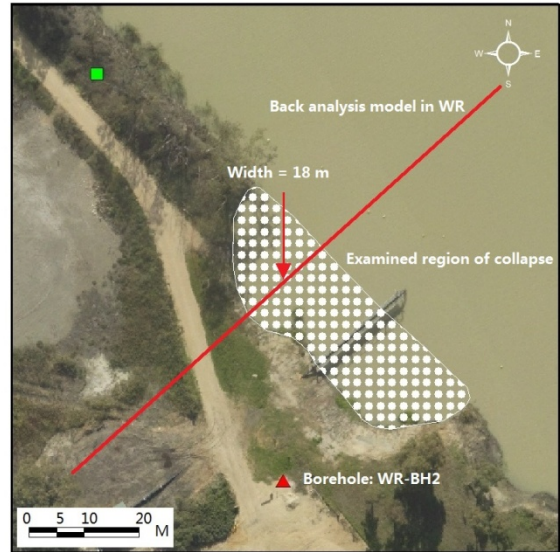


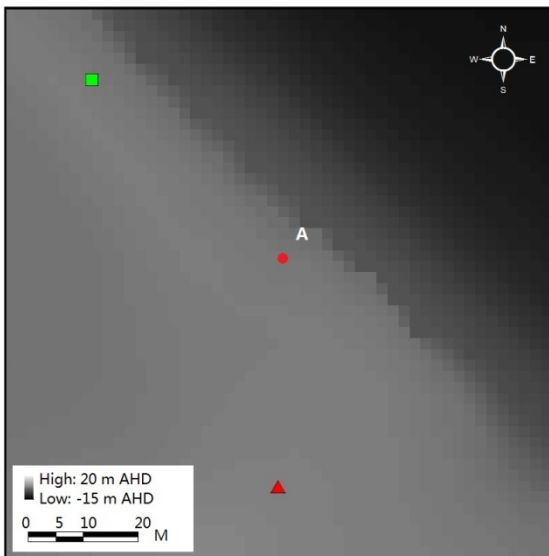
Figure 6.1 Diagram of study area, locations of historical collapses, cross-sectional models and geotechnical investigations.



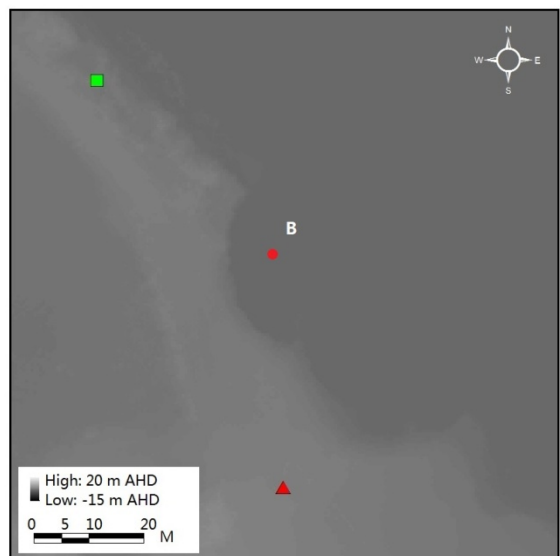
(a) Aerial image with 0.5 metre resolution acquired in March 2008



(b) Aerial image with 0.2 metre resolution acquired after collapse



(c) 1 metre resolution DEM obtained in 2008



(d) 0.2 metre resolution DEM obtained in 2010

Figure 6.2 Example of high-resolution aerial image based visual interpretation and validation.

6.3.2 Geotechnical properties and back-analysis

The geotechnical model used in this research is developed based on the geotechnical investigations performed by SKM at three sites in 2009, including East Front Road (EFR) (3 boreholes and 1 piezocone sounding [CPTu]), Woodlane Reserve (WR) (2 boreholes and 5 CPTus) and Riverfront Road (RFR) (2 boreholes and 13 CPTus) (SKM, 2010a–e). As stated in the external consultants' reports (SKM, 2011, Coffey, 2012a), deep-seated circular failures on soft and very soft clay layers (CH) of Holocene age are the most familiar collapse mechanism along the Lower River Murray. As summarized in Table 6.2, the riverbank profiles in this paper are modelled using separate soil layers according to the borehole logs at the above three sites. Consistent with the geotechnical models adopted by SKM (SKM, 2010a) and Coffey (Coffey, 2012a), a depth-dependent, undrained soil model which accommodates total stress analysis is used in the CH layers (soft high plasticity clay), while a Mohr-Coulomb soil model which accommodate effective stress analysis is performed in the Fill and SC/CL (clayey sand or sandy clay) layers. More specifically, the depth-dependent undrained soil model incorporates linearly-increasing cohesion with depth, with c_{top} quantifying the cohesion (kPa) at the upper layer boundary, c_{ratio} representing the gradient of increasing cohesion with depth, which is capped at a maximum value of c_{max} (SKM, 2010a). The geotechnical values, which are summarized in Table 6.2, are derived from the laboratory and in situ test results.

As mentioned previously, back-analyses are performed on three selected, historical collapsed sites, as shown in Figures 6.1 and 6.3, using geotechnical data locally obtained from the nearest geotechnical investigations, in order to inform the framework so that it can be adopted at untested locations. At each site, the geotechnical properties of the high plasticity clay (CH) layers are varied marginally, with respect to the results of the corresponding site investigations, until factors of safety (FoSs) equal to unity are obtained. Within SVSlope the “Slope limit” is defined in the back-analyses to obtain closest match between the predicted and actual failure dimensions. As

summarized in Figure 6.3, values of $FoS = 1.00$ were obtained from the most appropriate, depth-dependent, undrained soil models (Table 6.2). The values of c_{top} obtained from the back-analyses align extremely well with those suggested by SKM and Coffey, and represent modest variations in the strengths incorporated in their models.

Ideally, it would be preferable to employ a probabilistic approach, i.e. one based on the probability of failure, than the FoS . Probabilistic methods account for spatial variability and uncertainty in a more systematic fashion. Unfortunately, it was not possible to adopt this approach because of the paucity of geotechnical data.

The slip surfaces at three of the back-analyzed sites are shown in Figure 6.3. The predicted widths of the collapsed region from the crest to the riverbank line at EFR, ER and RFR are 7 m, 18.1 m and 22 m, respectively, and these values again compare extremely favorably with the actual widths of 8 m, 18 m and 21 m, respectively. As mentioned earlier, the actual widths of the collapse regions are determined from visual interpretation of high resolution, aerial photographs within ArcGIS.

6.3.3 Cross-sectional modeling

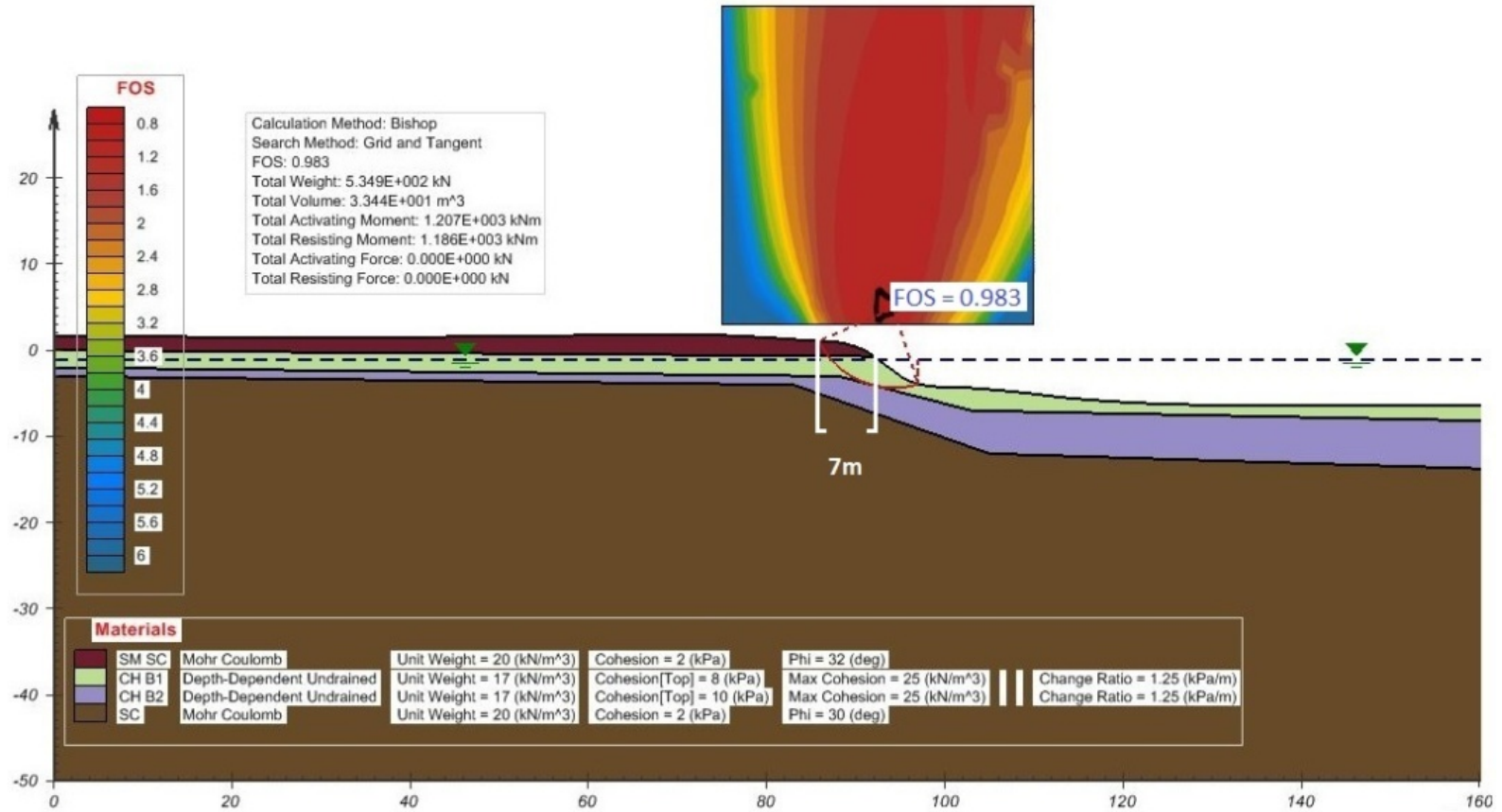
In order to investigate the relationship between riverbank stability and the topographic parameters, a total of 69 cross-sectional models are examined in the study area along the Lower River Murray, as shown in Figure 6.1. In contrast to earlier work undertaken by the authors (Liang et al., 2015), where climatic influences, such as rainfall and evapotranspiration, are ignored in this study due to the assumption of steady state conditions and to simplify the analyses and subsequent framework. The topography of the riverbank is characterized by the inclination angle of the riverbank (α), the height of the riverbank (H), which will be explained later, and the geometry and shape of the riverbank (Figure 6.4). The first two characteristics are used as the indicators to aid with high risk area identification within ArcGIS, as will be discussed later. The geometry of the riverbank, which is extracted from the

DEM, is directly imported into *SVSlope* to build the cross-sectional model. These 69 cross sectional models were derived from three different regions: Regions i, ii and iii, as shown in Figure 6.1. These cross sections were selected specifically to account for riverbanks with a wide range of slope angles (20° to 70°), as shown in Figure 6.5.

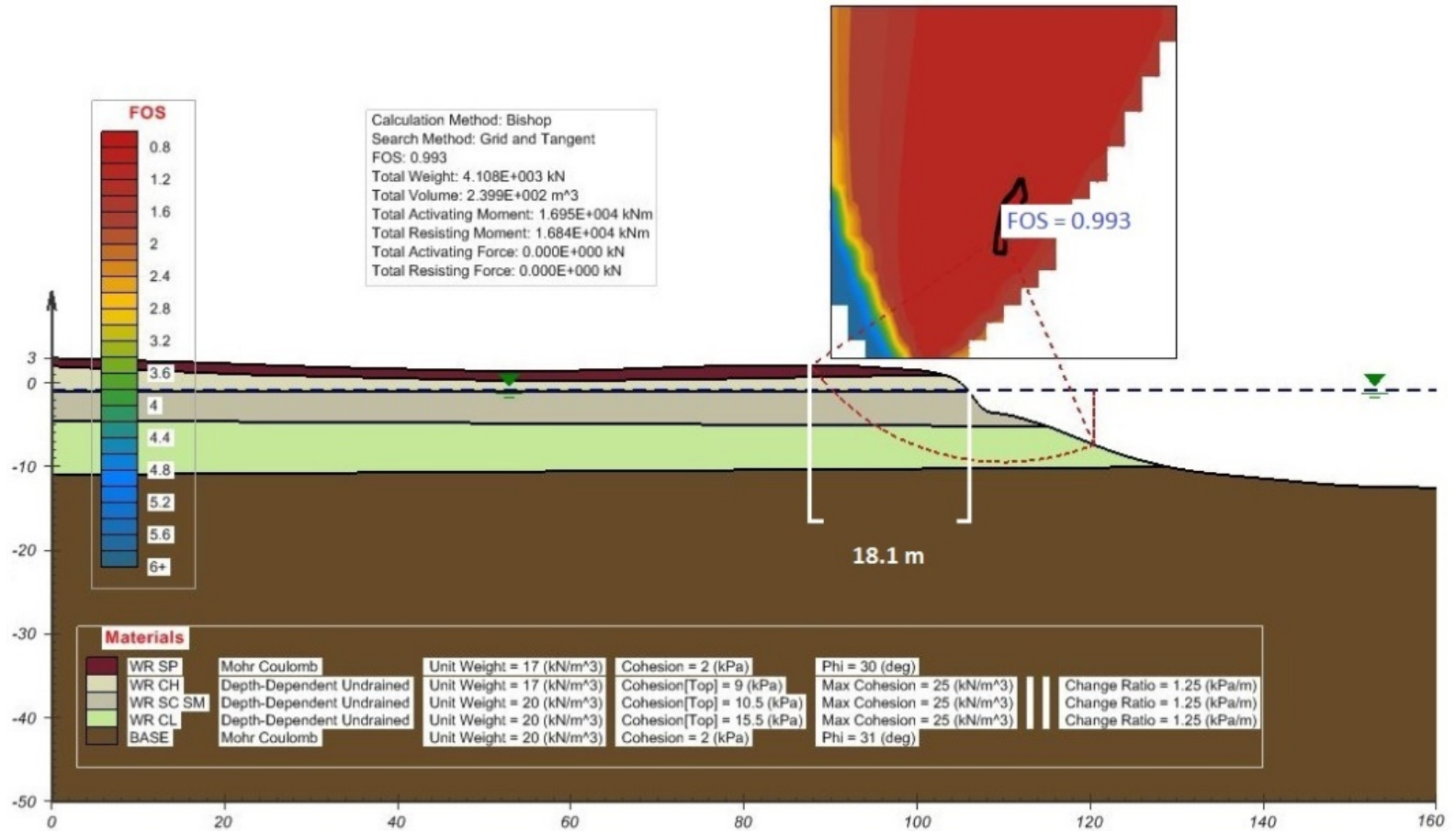
6.4 Hazard prediction and validation

The inclination of the riverbank along the Lower River Murray was calculated and mapped using the DEMs within the ArcGIS framework. Figure 6.4 shows an example of the surface slope calculation undertaken at cross section WR1 (Woodlane Reserve). In the evaluation of landslide and riverbank slope failure in wide natural slopes, it is typical to assume the slope surface is perfectly straight. However, natural slopes are generally undulating and irregular, an example of which is WR1, as shown in Figure 6.4(c). ArcGIS uses the matrix of grids from the DEM to evaluate the inclination of the riverbank slope. As shown in Figure 6.4, the size of the grid used can greatly influence the evaluation of the inclination. For example, it can be observed that a flatter and uniform (10° to 30°) inclination is obtained when a 10×10 matrix of grids is used [Figure 6.3(a)], while a more detailed and variable (from a low value of 10° up to, in some cases, 70°) inclination is obtained with a finer grid [e.g. 2×2 matrix of grids as shown Figure 6.3(b)].

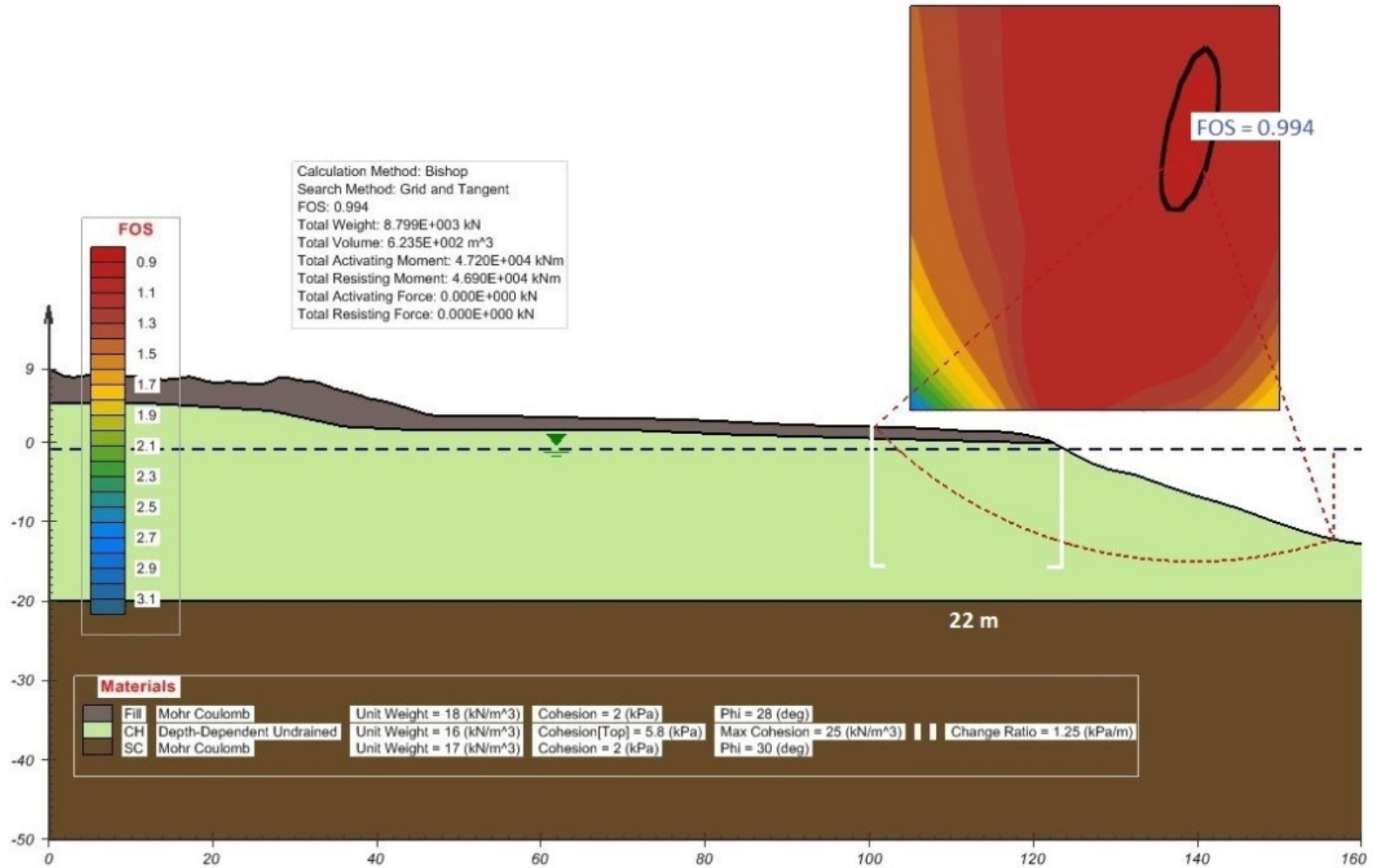
The parameter H represents the elevation of the predicted region of collapse prior to the actual failure, as shown in Figure 6.4(c). The actual slip surface varies with the riverbank's geometry, geotechnical properties and topography. To simplify the analyses, a section of riverbank, 15 m in width, measured from the crest of the riverbank to the water line (0 m AHD), is selected as shown in Figure 6.4(c), and is deemed to be the region that has greatest potential for collapse. The 15 m width of riverbank was selected as it represents the average extent of failure of the historical collapsed sites.



(a) Back-analysis of EFR site on 21 April 2009.



(b) Back-analysis of ER site on 26 February 2009.

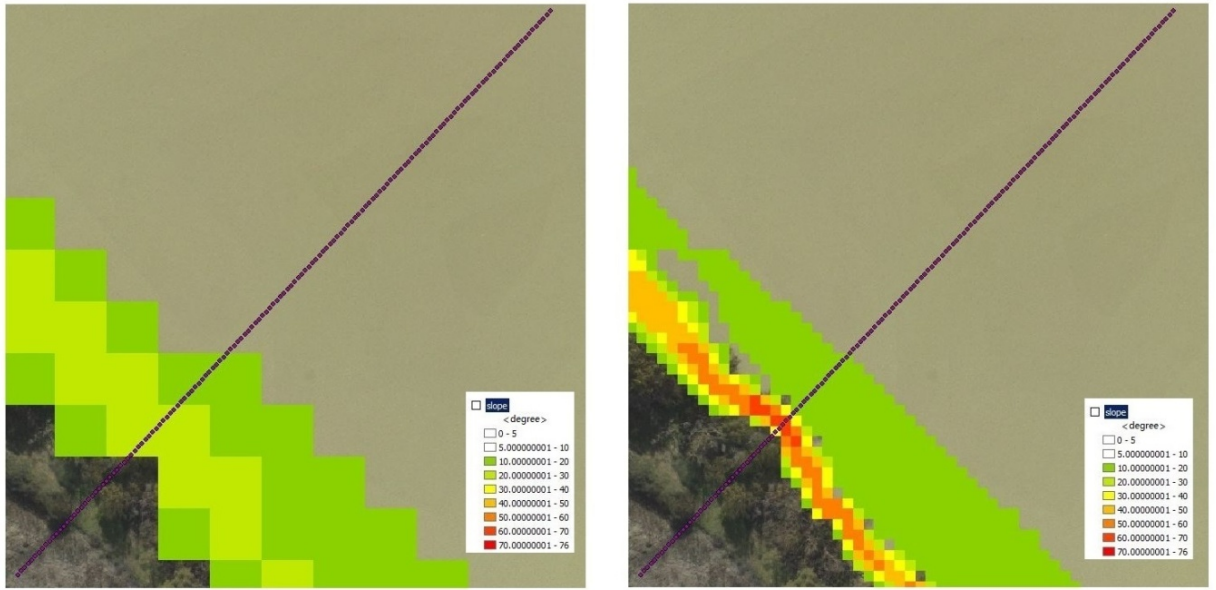


(c) Back-analysis of MB site on 6 February 2009.

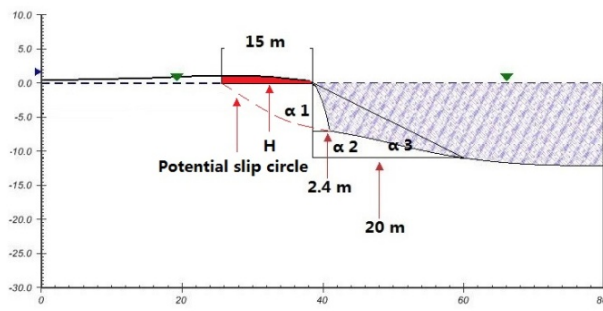
Figure 6.3 Riverbank stability analyses at three historical sites under SVSlope framework.

Table 6.2 Soil properties for saturated and unsaturated flow modelling.

Layer	Elevation (m AHD)	Parameters suggested by SKM (kPa)	Parameters suggested by Coffey (kPa)	Parameters from back-analysis (kPa)	γ (kN/m ³)
East Front Road (EFR)					
Silty/Clayey Sand (SM/SC)	3.5 to 1	$c'=2 \pm 2$ $\phi'=31^\circ \pm 2^\circ$			20 ± 1
Silty Clay (CH)	1 to -1	$c_u = 17.5$	$c_{u-top} = 5.5 \pm 5$ $c_{u-ratio} = 1.25$ $c_{u-max} = 25 \pm 5$	$c_{u-top} = 8$ $c_{u-ratio} = 1.25$ $c_{u-max} = 25$	17 ± 1
Silty Clay (CH)	-1 to -5	$c_u = 14$			17 ± 1
Clayey Sand (SC)	> -5	$c'=2 \pm 2$ $\phi'=31^\circ \pm 2^\circ$			20 ± 1
Woodlane Reserve (WR)					
Sand (SP)	2.5 to 2	$c'=2 \pm 2$ $\phi'=30^\circ \pm 2^\circ$			17 ± 1
Silty Clay (CH)	2 to -1	$c_u = 20$	$c_{u-top} = 5.5 \pm 5$ $c_{u-ratio} = 1.25$ $c_{u-max} = 25 \pm 5$	$c_{u-top} = 9$ $c_{u-ratio} = 1.25$ $c_{u-max} = 25$	17 ± 1
Clayey/Silty Sand (SC/SM)	-1 to -5	$c'=2$ $\phi'=29^\circ$			20 ± 1
Sandy/Silty Clay (CL)	-5 to -11	$c'=2$ $\phi'=30^\circ$			20 ± 1
Silty Sand/ Gravel (SM)	> -11	$c'=2 \pm 2$ $\phi'=31^\circ \pm 2^\circ$			20 ± 1
River Front Road (RFR)					
Silty/Clayey Sand (SM/SC)	1 to 0	$c'=2 \pm 2$ $\phi'=28^\circ \pm 2^\circ$			18 ± 1
Silty Clay (CH)	0 to -20	$c_{u-top} = 10 \pm 5$ $c_{u-ratio} = 1.25$ $c_{u-max} = 25 \pm 5$	$c_{u-top} = 5.5 \pm 5$ $c_{u-ratio} = 1.25$ $c_{u-max} = 25 \pm 5$	$c_{u-top} = 5.8$ $c_{u-ratio} = 1.25$ $c_{u-max} = 25$	16 ± 1
Clayey Sand/Sandy Clay (SC/CL)	> -20	$c'=2 \pm 2$ $\phi'=30^\circ \pm 2^\circ$			17 ± 1

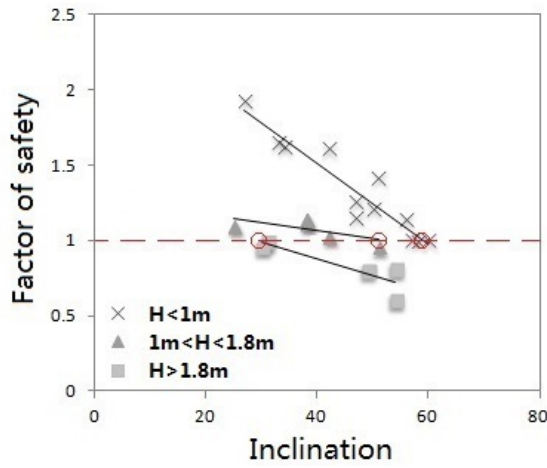


(a) Surface slope on WR1 based on 10×10 DEM. (b) Surface slope on WR1 based on 2×2 DEM.

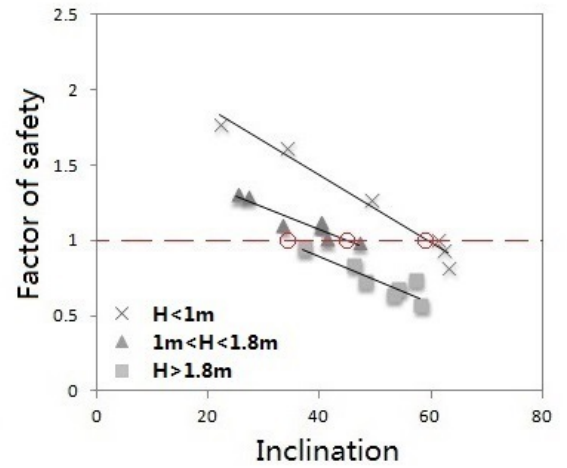


(c) Riverbank profile of WR1.

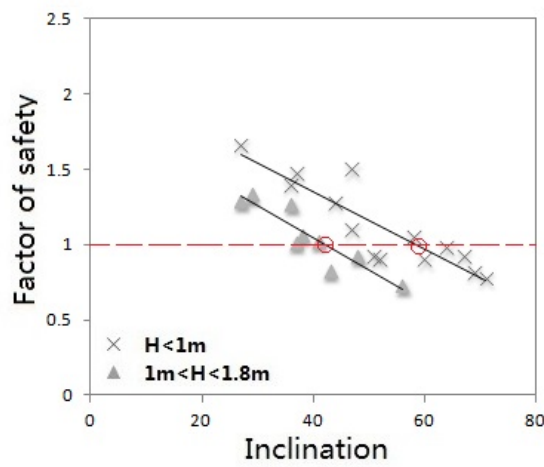
Figure 6.4 Grid size based surface slope calculation.



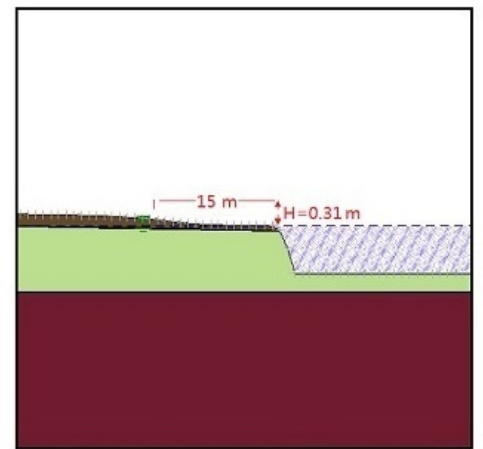
(a) Results of cross-sectional modeling in EFR.



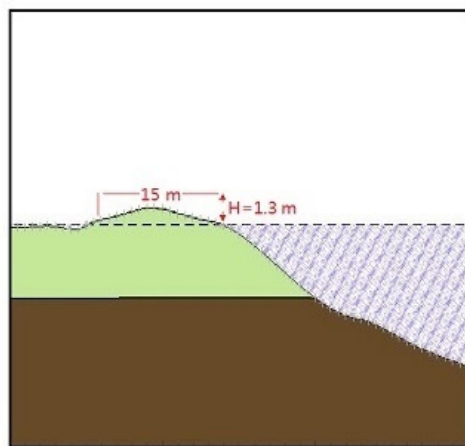
(b) Results of cross-sectional modeling in WR.



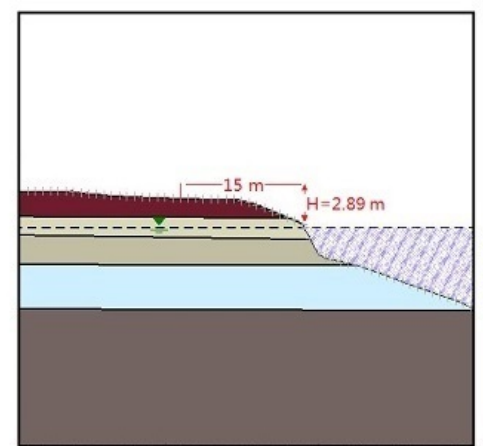
(c) Results of cross-sectional modeling in RFR.



(d) Example of riverbank (EFR20) with $H < 1\text{m}$.



(e) Example of riverbank (RFR16) with $1\text{m} < H < 1.8\text{m}$.



(f) Example of riverbank (WR1) with $H > 1.8\text{m}$.

Figure 6.5 Relationships between average elevation (H), inclination (α) and factor of safety of the cross-sectional models with a 0 m AHD river level.

By assigning the back-analysed geotechnical models, as shown in Table 6.2, to the corresponding cross sections, the FoSs of the 69 cross-sectional models, with a river level at 0 m AHD, are evaluated, as shown in Figure 6.5. In this study, the riverbanks, as well as the consequent FoSs, are classified into three groups based on the riverbank height, H : low riverbanks [Figure 6.5(d) with an average $H < 1\text{ m}$]; medium height riverbanks [Figure 6.5(e) with an average $H > 1\text{ m}$ and $< 1.8\text{ m}$]; and high riverbanks [Figure 6.5(f) with an average $H > 1.8\text{ m}$]. As shown in Figures 6.5(a) – (c), the FoS decreases with increasing riverbank inclination, as one would expect. However, the rates of change vary depending on H and the local geotechnical characteristics. As shown in Figures 6.5(a) – (c), again, as one would expect, high riverbanks typically have lower FoSs than low riverbanks, with the other characteristics, such as inclination and geotechnical properties, being similar. For example, as shown in Figure 6.5(b), riverbank WR18 ($H = 0.75\text{ m}$, $\alpha = 49^\circ$) has a larger FoS compared to riverbanks WR22 ($H = 1.42\text{ m}$, $\alpha = 46^\circ$) and WR5 ($H = 2.74\text{ m}$, $\alpha = 48^\circ$) although each of these riverbanks has almost identical inclination angles.

In order to identify high risk areas of riverbank instability, two river levels are examined (0 and -1 m AHD) in combination with the three riverbank height classifications described above (low, medium, high) and the geotechnical properties and topographies associated with the three sites (EFR, WR, RFR). For each of these scenarios, *SVSlope* is used to determine the inclination angle, α , which yields a FoS equal to unity; i.e. indicating impending slope failure. Table 6.3 summarizes the values of α obtained.

Based on these values of α , color ramps are generated using ArcGIS, which highlight the variation in riverbank inclination (α) and riverbank height (H). Two such examples are shown in Figure 6.6, with elevation contour lines and labels added to assist in determining H . For example, the riverbank adjacent to Avoca Dell, as shown in Figure 6.6(a), is predicted to have a high risk of collapse when river level is at -1 m AHD. The riverbank inclination (α) is approximately equal to 38° , while the H is 1.4 m . With reference to the prediction criteria for the EFR region, as summarized in Table 6.3, the values

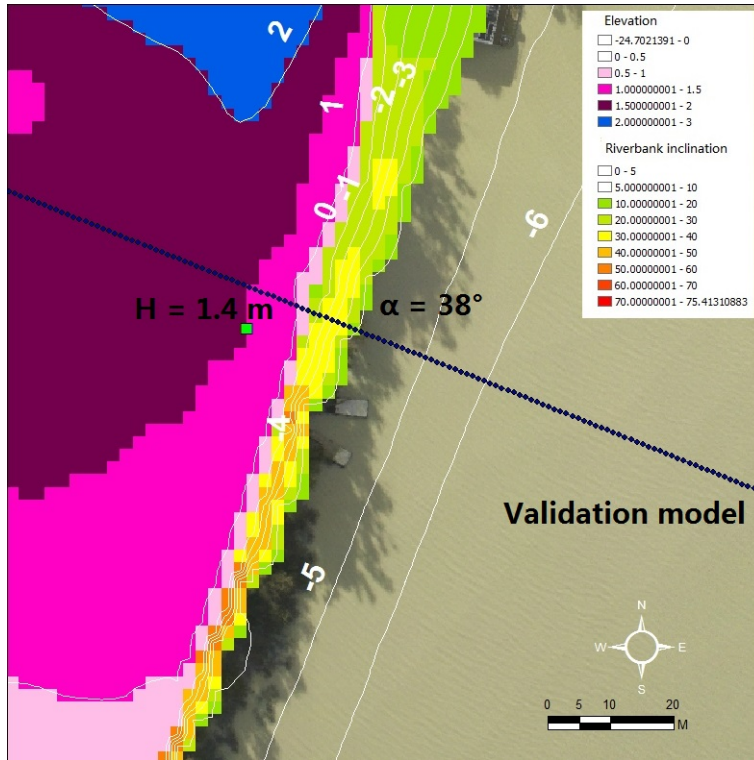
of α and H mentioned above indicate a strong possibility collapse when the river level falls to -1 m AHD. However, the riverbank is shown to be more stable when the river level rises to 0 m AHD, as indicated in Table 6.3.

Another similar example is the riverbank shown in Figure 6.6(b), which is close to Murray Bridge. As can be seen, the riverbank inclination (α) is approximately 60° with $H = 1.8$ m. With reference to the prediction criteria for the RFR region, as summarized in Table 6.3, this combination of α and H represents high risk of collapse when the river level drops to 0 m AHD.

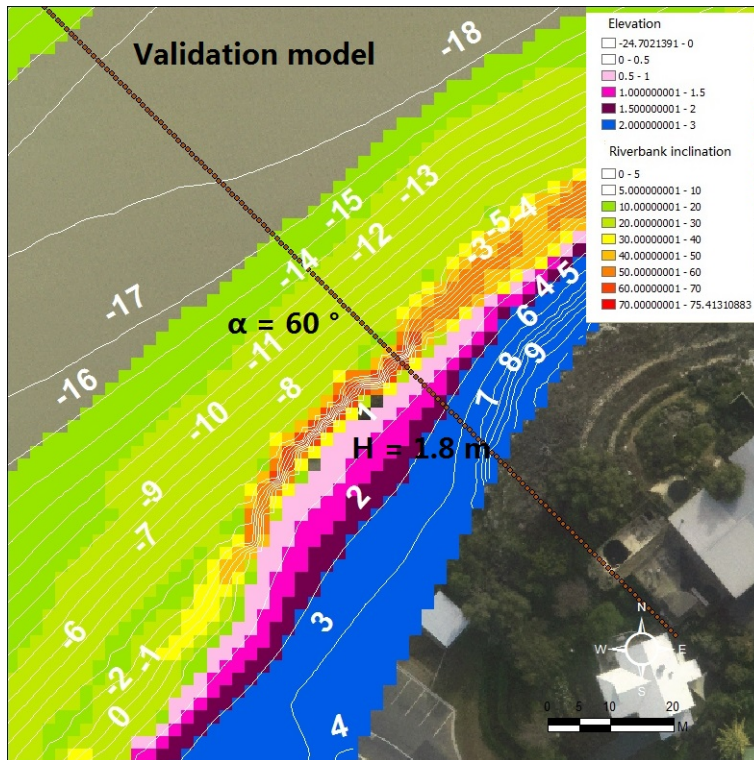
In order to validate these predictions, they were analyzed using *SVSlope*, using the cross-sectional validation models shown in Figure 6.6. The FoS thus obtained for the situation shown in Figure 6.6(a), when the river level is at -1 m AHD, is 1.01. The FoS for the situation shown in Figure 6.6(b), when the river is at 0 m AHD, is 0.83. Both of these compare extremely favorably with the predictions identified as high risk areas of collapse using the procedure outlined in this paper.

Table 6.3 Acceptable H and α combination for each research region when river levels equal to 0 and -1 m AHD.

Site	H < 1 m		1 < H < 1.8 m		H > 1.8 m	
	Level (RL) of River Water Surface (m AHD)					
	0	-1	0	-1	0	-1
EFR	$\alpha = 58^\circ$	$\alpha = 46^\circ$	$\alpha = 50^\circ$	$\alpha = 25^\circ$	$\alpha = 29^\circ$	$\alpha = 17^\circ$
WR	$\alpha = 60^\circ$	$\alpha = 50^\circ$	$\alpha = 45^\circ$	$\alpha = 35^\circ$	$\alpha = 35^\circ$	$\alpha = 27^\circ$
RFR	$\alpha = 59^\circ$	$\alpha = 44^\circ$	$\alpha = 43^\circ$	$\alpha = 30^\circ$	N/A	N/A



(a) Predicted area of riverbank instability near Mannum.



(b) Predicted area of riverbank instability near Murray Bridge.

Figure 6.6 Example of riverbank collapse prediction.

6.5 Summary

This paper has sought to: (i) improve the understanding of the topographical factors that influence the stability of the Lower River Murray riverbanks; (ii) identify regions of high risk of riverbank collapse; and (iii) present a framework that can be used to identify locations susceptible to riverbank collapse over long reaches of the river, prior to undertaking a site investigation or detailed slope stability analyses. The framework incorporates the integration of a steady state model, the limit equilibrium method, digital elevation models (DEMs), visual interpretation of high-resolution aerial images and GIS modeling. The recorded historical collapses have been examined using visual interpretation of high-resolution aerial images. Digital elevation models were used to provide accurate riverbank geometries. Using data from site investigations, incorporating both in situ and laboratory test results, back-analyses were undertaken at historical collapse sites to determine soil shear strengths at failure. A total of 69 cross-sectional models were applied to three separate regions of the river with the aim of better understanding the factors influencing riverbank stability.

The results of this study have shown that:

- (a) The proposed framework presents an efficient and effective method for identifying locations of potential riverbank instability which can be used to inform the planning of site investigation campaigns and slope stability modeling to provide a more accurate assessment;
- (b) The topographical factors H and α adopted in this paper are appropriate indicators for identifying the steady state riverbank instability along the Lower River Murray; and
- (c) Spatial analysis tools such as GIS, incorporating high-resolution spatial data, in association with limit equilibrium, slope stability modeling, facilitate the identification of bank instability over long sections of river.

Acknowledgements

The authors are grateful for the support and valuable advice provided by Jai O'Toole, Geoff Eaton and Richard Brown from DEWNR. This project is funded by the Goyder Institute for Water Research, under *Project E1.8 Riverbank Stability*, and the authors are grateful for their support.

References for Chapter 6

- Abramson, L. W., Lee, T. S., Sharma, S. & Boyce, G. M. 2002a. *Slope stability and stabilization methods*, New York, John Wiley and Sons.
- Abramson, L. W., Lee, T. S., Sharma, S. & Boyce, G. M. (eds.) 2002b. *Slope Stability and Stabilization Methods*, New York: John Wiley & Sons, Inc.
- Acharya, G., De Smedt, F. & Long, N. 2006. Assessing landslide hazard in GIS: a case study from Rasuwa, Nepal. *Bulletin of Engineering Geology and the Environment*, 65, 99-107.
- Akgün, A. & Bulut, F. 2007. GIS-based landslide susceptibility for Arsin-Yomra (Trabzon, North Turkey) region. *Environmental Geology*, 51, 1377-1387.
- Baum, R. L., Savage, W. Z. & Godt, J. W. 2008. TRIGRS—A Fortran Program for Transient Rainfall Infiltration and Grid-Based Regional Slope-Stability Analysis, Version 2.0. U.S. Department of the Interior U.S. Geological Survey.
- Beal, A., Brown, R. & Toole, J. O. 2010. Expert Panel Workshop - Riverbank Collapse Hazard Prpgram.
- Berilgen, M. M. 2007. Investigation of stability of slopes under drawdown conditions. *Computers and Geotechnics*, 34, 81-91.
- Bouwer, H. 1978. *Groundwater hydrology*, New York, New York : McGraw-Hill.
- Bozzano, F., Martino, S., Montagna, A. & Prestininzi, A. 2012. Back analysis of a rock landslide to infer rheological parameters. *Engineering Geology*, 131–132, 45-56.
- Brand, E. W. Landslides in Southeast Asia: A State-of-the-art Repor. 4th International Symposium on Landslides, 1984 Toronto. 17-59.
- Cai, M. F., Xie, M. W. & Li, C. L. 2007. GIS-based 3D limit equilibrium analysis for design optimization of a 600 m high slope in an open pit mine. *Journal of University of Science and Technology Beijing*, 14, 1-5.

Calabresi, G., Colleselli, F., Danese, D., Giani, G. P., Mancuso, C., Montrasio, L., Nocilla, A., Pagano, L., Reali, E. & Sciotti, A. 2013. A research study of the hydraulic behaviour of the Po river embankments. *Canadian Geotechnical Journal*.

Carrara, A., Cardinali, M., Guzzetti, F. & Reichenbach, P. 1995. Gis Technology in Mapping Landslide Hazard. *In: CARRARA, A. & GUZZETTI, F. (eds.) Geographical Information Systems in Assessing Natural Hazards*. Springer Netherlands.

Carrara, A., Guzzetti, F., Cardinali, M. & Reichenbach, P. 1999. Use of GIS Technology in the Prediction and Monitoring of Landslide Hazard. *Natural Hazards*, 20, 117-135.

Casagli, N., Rinaldi, M., Gargini, A. & Curini, A. 1999. Pore water pressure and streambank stability: results from a monitoring site on the Sieve River, Italy. *Earth Surface Processes and Landforms*, 24, 1095-1114.

Cha, K.-S. & Kim, T.-H. 2011. Evaluation of slope stability with topography and slope stability analysis method. *KSCCE Journal of Civil Engineering*, 15, 251-256.

Coffey. 2012a. *RE: Review of Management Options for Four Riverbank Collapse High Risk Sites*. Type to DEPARTMENT OF ENVIRONMENTAL, W. A. N. R.

Coffey 2012b. Review of management options for four river bank collapse high risk sites. *In: DEPARTMENT OF ENVIRONMENT, W. A. N. R. (ed.)*. Depart.

Crozier, M. J. 1999. Prediction of rainfall-triggered landslides: a test of the Antecedent Water Status Model. *Earth Surface Processes and Landforms*, 24, 825-833.

De Vincenzo, A., Palma, D., Scuccimarra, V., Sdao, F. & Sole, A. 2005. GIS analysis for the study of slope instability processes in a fluvial basin. *Water Resources Management III*, 80, 321-329.

DFW 2011. Lower River Murray Riverbank Collapse Hazard Site Status Report (May 2011).

Dietrich, W. E., Reiss, R., Hsu, M.-L. & Montgomery, D. R. 1995. A process-based model for colluvial soil depth and shallow landsliding using digital elevation data. *Hydrological Processes*, 9, 383-400.

Esaki, T., Xie, M. W., Zhou, G. Y. & Mitani, Y. 2001. Monte Carlo method for locating and evaluating 3D critical slope slip based on GIS Database. *Frontiers of Rock Mechanics and Sustainable Development in the 21st Century*, 17-21.

Fredlund, D. G. 2006. Unsaturated Soil Mechanics in Engineering Practice. *Journal of Geotechnical & Geoenvironmental Engineering*, 132, 286-321.

Fredlund, D. G., Xing, A., Fredlund, M. D. & Barbour, S. L. 1996. The relationship of the unsaturated soil shear to the soil-water characteristic curve. *Canadian Geotechnical Journal*, 33, 440-448.

Fredlund, D. G., Xing, A. & Huang, S. 1995. Predicting the permeability function for unsaturated soils using the soil-water characteristic curve. *International Journal of Rock Mechanics and Mining Sciences and Geomechanics Abstracts*, 32, 159A-159A.

Giardino, M., Giordan, D. & Ambrogio, S. 2004. GIS technologies for data collection, management and visualization of large slope instabilities: two applications in the Western Italian Alps. *Natural Hazards and Earth System Sciences*, 4, 197-211.

Gilbert, R. B., Wright, S. G. & Liedtke, E. 1998. Uncertainty in Back Analysis of Slopes: Kettleman Hills Case History. *Journal of Geotechnical & Geoenvironmental Engineering*, 124, 1167-1176.

Green, S. J. 1999. *Drawdown and river bank stability*, University of Melbourne, Dept. of Civil and Environmental Engineering.

Guzzetti, F., Carrara, A., Cardinali, M. & Reichenbach, P. 1999. Landslide hazard evaluation: a review of current techniques and their application in a multi-scale study, Central Italy. *Geomorphology*, 31, 181-216.

Harris, S. J., Orense, R. P. & Itoh, K. 2012. Back analyses of rainfall-induced slope failure in Northland Allochthon formation. *Landslides*, 9, 349-356.

Hashimoto, A., Oguchi, T., Hayakawa, Y., Lin, Z., Saito, K. & Wasklewicz, T. A. 2008. GIS analysis of depositional slope change at alluvial-fan toes in Japan and the American Southwest. *Geomorphology*, 100, 120-130.

- Higgins, D. T. 1980. Unsteady drawdown in 2D water-table aquifer *Journal of the Irrigation and Drainage Division-Asce*, 106, 237-251.
- Hooke, J. M. 1979. An analysis of the processes of river bank erosion. *Journal of Hydrology*, 42, 39-62.
- Institution of Engineers, A. (ed.) 1987. *Australian rainfall and runoff: a guide to flood estimation*
- Jaksa, M. B., Hubble, T. C. T., Kuo, Y. L., Liang, C. & De Carli, E. V. 2013. Goyder Institute Research Project: E.1.8 Riverbank Collapse in the Lower River Murray – Literature Review and Knowledge Gap Analysis. Adelaide: Goyder Institute for Water Research.
- Jia, G. W., Zhan, T. L. T., Chen, Y. M. & Fredlund, D. G. 2009. Performance of a large-scale slope model subjected to rising and lowering water levels. *Engineering Geology*, 106, 92-103.
- Jiménez-Perálvarez, J., Irigaray, C., El Hamdouni, R. & Chacón, J. 2009. Building models for automatic landslide-susceptibility analysis, mapping and validation in ArcGIS. *Natural Hazards*, 50, 571-590.
- Kamp, U., Growley, B. J., Khattak, G. A. & Owen, L. A. 2008. GIS-based landslide susceptibility mapping for the 2005 Kashmir earthquake region. *Geomorphology*, 101, 631-642.
- Kim, K.-S., Park, H.-J., Lee, S. & Woo, I. 2004. Geographic Information System (GIS) based stability analysis of rock cut slopes. *Geosciences Journal*, 8, 391-400.
- Lane, P. A. & Griffiths, D. V. 2000. Assessment of stability of slopes under drawdown conditions. *Journal of Geotechnical & Geoenvironmental Engineering*, 126, 443.
- Lee, S., Choi, J. & Min, K. 2004. Probabilistic landslide hazard mapping using GIS and remote sensing data at Boun, Korea. *International Journal of Remote Sensing*, 25, 2037-2052.
- Li, X. & Tang, H. 2005. Application of GIS-based grouped data Logistic model in evaluation of slope stability. *Jilin Daxue Xuebao : Diqu Kexue Ban (Journal of Jilin University :Earth Science Edition)*, 35, 361-365.

- Li, X. P., Tang, H. M. & Chen, S. 2008. A GIS-supported logistic regression model applied in regional slope stability evaluation. *Landslides and Engineered Slopes: From the Past to the Future, Vols 1 and 2*, 789-794.
- Liang, C., Jaksa, M. B. & Ostendorf, B. 2012. GIS-based Back Analysis of Riverbank Instability in the Lower River Murray. *Australian Geomechanics*, 47, 59-65.
- Liang, C., Jaksa, M. B., Ostendorf, B. & Yien, K. L. 2015. Influence of river level fluctuations and climate on riverbank stability. *Computers and Geotechnics*, 63, 83-98.
- Liang, C., Jaksa, M. B., Yien, K. L. & Ostendorf, B. 2014. Back Analysis of Lower Murray Riverbank Collapses.
- Lumb, P. 1975. Slope failures in Hong Kong. *Quarterly Journal of Engineering Geology and Hydrogeology*, 8, 31-65.
- Magliulo, P., Di Lisio, A., Russo, F. & Zelano, A. 2008. Geomorphology and landslide susceptibility assessment using GIS and bivariate statistics: a case study in southern Italy. *Natural Hazards*, 47, 411-435.
- MDBA 2014. River Murray at Murray Bridge (Long Island) information sheet. Murray Darling Basin Authority.
- Merwade, V. M. 2007. An Automated GIS Procedure for Delineating River and Lake Boundaries. *Transactions in GIS*, 11, 213-231.
- Meteorology, B. o. 2014. Climate data Online, Commonwealth of Australia , Bureau of Meteorology Bureau of Meteorology.
- Miller, D. J. & Sias, J. 1998. Deciphering large landslides: linking hydrological, groundwater and slope stability models through GIS. *Hydrological Processes*, 12, 923-941.
- Montgomery, D. R. & Dietrich, W. E. 1994. A physically based model for the topographic control on shallow landsliding. *Water Resources Research*, 30, 1153-1171.
- Moore, I. D., Gessler, P. E., Nielsen, G. A. & Peterson, G. A. 1993. Soil Attribute Prediction Using Terrain Analysis. *Soil Sci. Soc. Am. J.*, 57, 443-452.

Mukhlisin, M. & Taha, M. 2012. Numerical model of antecedent rainfall effect on slope stability at a hillslope of weathered granitic soil formation. *Journal of the Geological Society of India*, 79, 525-531.

National Water Commission, A. G. 2005. *Bureau of Rural Sciences* [Online]. Available:
http://www.water.gov.au/WaterAvailability/Whatisourtotalwaterresource/Runoff/index.aspx?Menu=Level1_3_1_5.

Okui, Y., Tokunaga, A., Shinji, M. & Mori, S. 1997. New back analysis method of slope stability by using field measurements. *International Journal of Rock Mechanics and Mining Sciences*, 34, 234.e1-234.e16.

Osman, A. M. & Thorne, C. R. 1988. Riverbank Stability Analysis .1. Theory. *Journal of Hydraulic Engineering-Asce*, 114, 134-150.

Ozdemir, A. 2009. Landslide susceptibility mapping of vicinity of Yaka Landslide (Gelendost, Turkey) using conditional probability approach in GIS. *Environmental Geology*, 57, 1675-1686.

Oztekin, B. & Topal, T. 2005. GIS-based detachment susceptibility analyses of a cut slope in limestone, Ankara-Turkey. *Environmental Geology*, 49, 124-132.

Pack, R. T., Tarboton, D. G. & Goodwin, C. N. 1998. Terrain Stability Mapping with SINMAP, technical description and users guide for version 1.00. In: SALMON ARM, B. C. (ed.). Canada.

Pack, R. T., Tarboton, D. G. & Goodwin, C. N. 2001. Assessing Terrain Stability in a GIS using SINMAP. *15th annual GIS conference*. Vancouver, British Columbia.

Pantha, B. R., Yatabe, R. & Bhandary, N. P. 2008. GIS-based landslide susceptibility zonation for roadside slope repair and maintenance in the Himalayan region. *Episodes*, 31, 384-391.

Pauls, G. J., Sauer, E. K., Christiansen, E. A. & Widger, R. A. 1999. A transient analysis of slope stability following drawdown after flooding of a highly plastic clay. *Canadian Geotechnical Journal*, 36, 1151-1171.

Pike, R. 1988. The geometric signature: Quantifying landslide-terrain types from digital elevation models. *Mathematical Geology*, 20, 491-511.

Rahardjo, H., Leong, E. C. & Rezaur, R. B. 2008. Effect of antecedent rainfall on pore-water pressure distribution characteristics in residual soil slopes under tropical rainfall. *Hydrological Processes*, 22, 506-523.

Rahardjo, H., Li, X. W., Toll, D. G. & Leong, E. C. 2001. The effect of antecedent rainfall on slope stability. *Geotechnical & Geological Engineering*, 19, 371-399.

Rahardjo, H., Ong, T. H., Rezaur, R. B. & Leong, E. C. 2007. Factors Controlling Instability of Homogeneous Soil Slopes under Rainfall. *Journal of Geotechnical & Geoenvironmental Engineering*, 133, 1532-1543.

Rahimi, A., Rahardjo, H. & Leong, E. C. 2011. Effect of Antecedent Rainfall Patterns on Rainfall-Induced Slope Failure. *Journal of Geotechnical and Geoenvironmental Engineering*, 137, 483-491.

Ray, R. L. & Smedt, F. d. 2009. Slope stability analysis on a regional scale using GIS: a case study from Dhading, Nepal. *Environmental Geology*, 57, 1603-1611.

Rinaldi, M. & Casagli, N. 1999. Stability of streambanks formed in partially saturated soils and effects of negative pore water pressures: the Sieve River (Italy). *Geomorphology*, 26, 253-277.

Rinaldi, M., Casagli, N., Dapporto, S. & Gargini, A. 2004. Monitoring and modelling of pore water pressure changes and riverbank stability during flow events. *Earth Surface Processes and Landforms*, 29, 237-254.

Rowbotham, D. N. & Dudycha, D. 1998. GIS modelling of slope stability in Phewa Tal watershed, Nepal. *Geomorphology*, 26, 151-170.

Schuster, R. L. & Krizek, R. J. (eds.) 1978. *LaLandslides: Analysis and Control (Special report - Transportation Research Board, National Research Council ; 176)*.

SKM 2010a. Study into river bank collapsing for Lower River Murray.

SKM 2010b. Study into river bank collapsing for Lower River Murray: Appendix A Riverfront Road - Murray Bridge In - situ and laboratory test results.

SKM 2010c. Study into river bank collapsing for Lower River Murray: Appendix C Woodlane Reserve In - situ and laboratory data.

SKM 2010d. Study into river bank collapsing for Lower River Murray: Appendix E East Front Road In - situ and laboratory data.

SKM 2011. Research into processes, triggers and dynamics of riverbank collapse in the Lower River Murray.

SoilVision 2009a. SVFlux. 4.23 ed.

SoilVision 2009b. SVSlope. 4.23 ed.

Song, Z., Hu, Y. & Randolph, M. 2008. Numerical Simulation of Vertical Pullout of Plate Anchors in Clay. *Journal of Geotechnical and Geoenvironmental Engineering*, 134, 866-875.

Springer, F. M. 1981. *Influence of rapid drawdown events on riverbank stability*. Master in Engineering, University of Louisville.

Stark, T. & Eid, H. 1998. Performance of Three-Dimensional Slope Stability Methods in Practice. *Journal of Geotechnical and Geoenvironmental Engineering*, 124, 1049-1060.

Stark, T. D. 2003. Three-dimensional slope stability methods in geotechnical practice.

Stark, T. D. & Eid, H. T. 1995. Drained Residual Strength of Cohesive Soils - Closure. *Journal of Geotechnical Engineering-Asce*, 121, 672-673.

Stark, T. D. & Eid, H. T. 1997. Slope stability analyses in stiff fissured clays. *Journal of Geotechnical and Geoenvironmental Engineering*, 123, 335-343.

Stark, T. D., Williamson, T. A. & Eid, H. T. 1996. HDPE geomembrane/geotextile interface shear strength. *Journal of Geotechnical Engineering-Asce*, 122, 197-203.

Tajeddin, R., Ramsey, N., Pain, D., Mollison, D. & Sandercock, P. 2010. Influence of water level risk on river bank collapse, Lower River Murray. Sinclair Knight Merz, Australia.

- Tang, W. H., Stark, T. D. & Angulo, M. 1999. Reliability in back analysis of slope failures. *SOILS AND FOUNDATIONS*, 39, 73-80.
- Thiel, R. S., Stark, T. D. & Eid, H. T. 1997. Shear behavior of reinforced geosynthetic clay liners - Discussion and closure. *Geosynthetics International*, 4, 539-541.
- Thorne, C. R. 1982. Processes and mechanisms of River Bank Erosion. In: HEY, R. D., BATHURST, J. C. & THORNE, C. R. (eds.) *Gravel-bed rivers. Fluvial processes, engineering and management. Earth Surface Processes and Landforms*. John Wiley & Sons, Ltd.
- Thorne, C. R., Hey, R. D. & Newson, M. D. (eds.) 1997. *Bank erosion and instability. In applied fluvial geomorphology for river engineering and management / edited by Colin R. Thorne, Richard D. Hey, Malcolm D. Newson.*; 1997: New York : John Wiley
- Thorne, C. R. & Osman, A. M. 1988. Riverbank stability analysis .2. Applications. *Journal of Hydraulic Engineering-Asce*, 114, 151-172.
- Torres Hernandez, G., Zapata, C., Houston, S. & Witczak, M. 2011. Estimating the Soil-Water Characteristic Curve using grain size analysis and plasticity index. Arizona State University.
- Tsai, K. J., Yu, S. H., Hsiao, C. P., Ho, M. C. & Chen, C. C. 2005. Investigations by using GPS/GIS/RS technology on the slope stability of Kaohsiung communities on slopeland in Taiwan. *Proceedings of the Fifteenth (2005) International Offshore and Polar Engineering Conference, Vol 2*, 757-763.
- Twidale, C. R. 1964. Erosion of an alluvial bank at Birdwood, South Australia. *Zeitschrift für Geomorphologie, NF*, 8, 189-211.
- Urgeles, R., Leynaud, D., Lastras, G., Canals, M. & Mienert, J. 2006. Back-analysis and failure mechanisms of a large submarine slide on the ebro slope, NW Mediterranean. *Marine Geology*, 226, 185-206.
- Vanacker, V., Vanderschaeghe, M., Govers, G., Willems, E., Poesen, J., Deckers, J. & De Bievre, B. 2003. Linking hydrological, infinite slope stability and land-use change models through GIS for assessing the impact of deforestation on slope stability in high Andean watersheds. *Geomorphology*, 52, 299-315.

Voyiadjis, G. & Song, C. 2003. Determination of hydraulic conductivity using piezocone penetration test. *International Journal of Geomechanics*, 3, 217-224.

Wang, D., Gaudin, C. & Randolph, M. F. 2013a. Large deformation finite element analysis investigating the performance of anchor keying flap. *Ocean Engineering*, 59, 107-116.

Wang, D., Hu, Y. & Randolph, M. 2010a. Three-Dimensional Large Deformation Finite-Element Analysis of Plate Anchors in Uniform Clay. *Journal of Geotechnical and Geoenvironmental Engineering*, 136, 355-365.

Wang, D., Hu, Y. & Randolph, M. 2011. Keying of Rectangular Plate Anchors in Normally Consolidated Clays. *Journal of Geotechnical and Geoenvironmental Engineering*, 137, 1244-1253.

Wang, D., Randolph, M. F. & White, D. J. 2013b. A dynamic large deformation finite element method based on mesh regeneration. *Computers and Geotechnics*, 54, 192-201.

Wang, D., White, D. J. & Randolph, M. F. 2010b. Large-deformation finite element analysis of pipe penetration and large-amplitude lateral displacement. *Canadian Geotechnical Journal*, 47, 842-856.

Wang, H., Liu, G., Xu, W. & Wang, G. 2005. GIS-based landslide hazard assessment: an overview. *Progress in Physical Geography*, 29, 548-567.

Wang, L., Hwang, J. H., Luo, Z., Juang, C. H. & Xiao, J. 2013c. Probabilistic back analysis of slope failure – A case study in Taiwan. *Computers and Geotechnics*, 51, 12-23.

Wang, W.-D., Guo, J., Fang, L.-G. & Chang, X.-S. 2012. A subjective and objective integrated weighting method for landslides susceptibility mapping based on GIS. *Environmental Earth Sciences*, 65, 1705-1714.

WaterConnect 2014. Real time water data - latest hourly observation. WaterConnect - Government of South Australia.

Wen, H.-j., Li, X. & Zhang, J.-l. 2009. An evaluation-management information system of high slope geo-risk for mountainous city based on GIS. *2009 1st International Conference on Information Science and Engineering (ICISE 2009)*, 1975-8.

Wu, T. H. & Abdel-Latif, M. A. 2000. Prediction and mapping of landslide hazard. *Canadian Geotechnical Journal*, 37, 781-795.

Xie, M., Esaki, T. & Zhou, G. 2004. GIS-based probabilistic mapping of landslide hazard using a three-dimensional deterministic model. *Natural Hazards*, 33, 265-282.

Xie, M. W., Esaki, T. & Cai, M. F. 2006. GIS-based implementation of three-dimensional limit equilibrium approach of slope stability. *Journal of Geotechnical and Geoenvironmental Engineering*, 132, 656-660.

Xie, M. W., Zhou, G. Y. & Tetsuro, E. 2003. GIS component based 3D landslide hazard assessment system: 3DSLOPEGIS. *Chinese Geographical Science*, 13, 66-72.

Yan, Z.-L., Wang, J.-J. & Chai, H.-J. 2010. Influence of water level fluctuation on phreatic line in silty soil model slope. *Engineering Geology*, 113, 90-98.

Yokota, S. 1996. Multi-purpose digital hazard map for slope failures. *Geoinformatics*, 7, 51-59.

Yongquan, L., Yong, F. & Shenghua, J. Stability analysis of soil slope during rapid drawdown of water level. *Mechanic Automation and Control Engineering (MACE)*, 15-17 July 2011. 3454-3457.

Zaitchik, B. F. & Es, H. M. v. 2003. Applying a GIS slope-stability model to site-specific landslide prevention in Honduras. (Research).(geographic information system). *Journal of Soil and Water Conservation*, 58, 45(9).

Zapata, C. E., Houston, W. N., Walsh, K. D. & Houston, S. L. 2000. Soil-Water Characteristic Curve Variability. *Advances in Unsaturated Geotechnics*.

Zhang, J. F., Li, Z. G. & Qi, T. 2005. Mechanism analysis of landslide of a layered slope induced by drawdown of water level. *Science in China Series E-Engineering & Materials Science*, 48, 136-145.

Zhang, L. L., Zhang, J., Zhang, L. M. & Tang, W. H. 2011. Stability analysis of rainfall-induced slope failure: a review. *Proceedings of the Institution of Civil Engineers-Geotechnical Engineering*, 164, 299-316.

Zolfaghari, A. & Heath, A. C. 2008. A GIS application for assessing landslide hazard over a large area. *Computers and Geotechnics*, 35, 278-285.

Chapter 7

7 Summary and Conclusions

7.1 Summary

The stability of riverbanks is a multifaceted issue. The River Murray is one of the only river systems in the world that can fall below sea level due to the barrages preventing the inflow of sea water during periods of low river flows. Other riverbank collapse events globally, typically result from lower bank scour erosion and rapid drawdown of river levels during and after flood events or periods of high flow. An understanding of geology, topography, hydrology and soil properties is critical in the research of riverbanks instability along River Murray. In order to appreciate the processes affecting riverbank collapse and to understand the mechanics driving these collapse events along River Murray, research presented in this thesis was undertaken using an integration of advanced modelling techniques, sophisticated engineering analysis and a large amount of site- or region-specific data (e.g. riverbank and channel geometry, soil properties and their variability). All the analyses have been undertaken based on two major assumptions which are: (i) the geotechnical properties of the soils are homogeneous and geological profiles are relatively straightforward, i.e. the strata are uniform over a fairly large region, and can be represented by the data obtained from the corresponding field investigation; and (ii) deep-seated circular failure in the soft and very soft clays of Holocene age is the typical collapse mechanism along the lower reaches of the River Murray (Coffey, 2012b).

Using recorded evidence of previous riverbank collapse incidents in the Lower River Murray, the study implemented back-analyses which were based on steady state modelling (Paper 1) and transient unsaturated flow modelling (Papers 2, 3 and 4) to determine the at-failure, in situ shear strength and

compare these with the field test performed at, and laboratory tests undertaken on samples from, adjacent boreholes.

High-resolution spatial data and the ArcGIS software environment were used in this research to: (a) determine and validate the actual locations of the historical collapses by high-resolution aerial image comparison and interpretation to allow accurate back-analyses to be performed; (b) specify the 2D and 3D geometries of the riverbanks extracted from LIDAR DEMs; (c) calculate the dimensions of the predicted collapsed regions validated against the high-resolution aerial images; and (d) predict and map areas susceptible to riverbank collapse using GIS and assess the factors influencing the identification of these regions.

As outlined in §1.2, this research study sought to address the following:

1. Examine the failure mechanisms affecting riverbank collapse along the Lower River Murray and identify the most relevant mechanism;
2. Identify potential triggers for riverbank collapse events that should be monitored and managed in the future;
3. Develop a framework, incorporating spatial information, GIS and geotechnical data, to facilitate the prediction of riverbank collapse along the 210 kilometres of the Lower River Murray (between Blanchetown and Wellington, South Australia); and
4. Develop a framework, based on GIS and geotechnical data, to identify regions susceptible to high risk of riverbank collapse along the Lower River Murray.

In relation to Aim 1, as outlined above, deep-seated circular failure in the soft and very soft clays of Holocene age was identified as the most relevant collapse mechanism along the Lower River Murray. Subsequent analyses were based on this mechanism, as outlined in Papers 1 – 4.

Aim 2 was examined in Papers 2 and 4, where it was found that river fluctuations, rather than climatic factors, dominate the likelihood of riverbank collapse along the Lower River Murray. However, extreme rainfall events, coinciding with medium to high river levels, are also likely to trigger riverbank collapse. In addition, sudden or rapid drawdown scenarios can also precipitate riverbank collapse. The topographical factors of H (effective height of the riverbank) and α (bank inclination) were also identified as important parameters affecting riverbank stability.

Aim 3 was presented in Papers 2 and 3 and Aim 4 in Paper 4.

7.2 Research contributions

The overall contribution of the present research is the proposed numerical analysis based framework which can be used to assess riverbank instability. The framework incorporates two commercially available software packages: ArcGIS and SVOOffice (SVSlope and SVFlux) and is implemented using an integration of the limit equilibrium method, back-analysis, transient unsaturated flow modeling or steady state modelling, and digital elevation models and high resolution aerial images from GIS. As the most significant feature of this framework, spatial analysis tools like GIS, incorporating high-resolution spatial data are used which greatly facilitate the riverbank slope instability research in several aspects as mentioned above. Details of the more important outcomes of the research presented in Chapters 2 – 5 are outlined below:

1. Chapter 3/Paper 1 presented a sensitivity study which was based on the framework outlined above. The sensitivity analysis was conducted adjacent to Long Island Marina with two different river levels (0 and 0.5 m AHD) applied to 21 cross-sectional models using the results of back-analyses. The results of this work have demonstrated that a section of the riverbank has marginal stability, whereas a number of cross sections adjacent to the study site are susceptible to riverbank collapse and require further investigation. In addition, it was observed

that increased river levels generally stabilise the riverbanks but to a limited extent.

2. Chapter 4/Paper 2 presented sophisticated, transient and unsaturated slope stability analyses in 2D and 3D, which is also based on the proposed framework as mentioned above. The study modelled the most significant riverbank collapse incident, which occurred at Long Island Marina, Murray Bridge, South Australia, on 4 Feb. 2009. These analyses yielded excellent predictions of the collapse when compared with the recorded date of collapse and dimensions of the failed region. A parametric study was undertaken to examine the influence and sensitivity of river level fluctuations and climatic factors on riverbank stability. The results indicated that river fluctuations, rather than climatic factors, dominate the likelihood of riverbank collapse along the Lower River Murray. However, extreme rainfall events, coinciding with medium to high river levels, are also likely to trigger riverbank collapse. Moreover, sudden or rapid drawdown scenarios were also examined. The results showed that sudden or rapid drawdown can also precipitate riverbank collapse.

3. Chapter 5/Paper 3 presented transient and unsaturated slope stability analyses performed on four sites where major riverbank collapses were recorded (East Front Road; Woodlane Reserve; River Front Road and White Sands) along the Lower River Murray. The study outlined the framework implementation and demonstrated the efficacy of this framework and the accuracy of the predictions. The results of back-analysed soil shear strengths at the four sites show excellent consistency with those obtained from the results of the geotechnical site investigations adjacent to the collapse sites, and can be readily used in further simulations. The model validation demonstrated that the adopted framework provides reliable riverbank stability predictions and is recommended to be adopted in other similar studies.

4. Chapter 6/Paper 4 presented a topographically-based framework that can be used to identify the areas at high risk of riverbank collapse over large regions prior to undertaking detailed cross-sectional modeling or site investigation. Two topographical parameters (the effective height of the riverbank, H , and the bank inclination, α) are adopted and been shown to be appropriate indicators in predicting the riverbank instability along the Lower River Murray. A total of 69 cross-sectional models were developed and analysed within the study area and which greatly improve the understanding of topographical factors that influence riverbank stability. Moreover, a detailed susceptibility map of the Lower River Murray is presented.

7.3 Limitations and Recommendations for Future Research

As with all research, compromises and idealisations have been necessary to progress the analyses. Limitations and opportunities for future work include the following:

1. The present research is excluded the effects of riparian vegetation. As outlined in Chapter 2, it is clear that riparian vegetation affects riverbank stability both mechanically and hydrologically. Including the influence of riparian vegetation in the numerical models and GIS analyses is likely to improve the accuracy of future riverbank stability research.
2. In order to facilitate the analyses and the lack of compelling evidence, the study has focused on the deep-seated circular failures in the soft

and very soft clays of Holocene age. The Bishop method of slices was adopted to perform the stability analyses. However, it is known that the riverbank collapses also take the form of either: (i) translational, (ii) plane or wedge surface, (iii) circular, or (iv) noncircular, or a combination of these types. Future studies may consider examining these other slip surface geometries.

3. 3D riverbank stability modelling was conducted in Paper 2, which was shown to yield excellent results. The modelling was validated using bathymetric maps [e.g. Figure 4.1(b)]. However, due to limitations with the bathymetric data and the inventory records, as well as the fact that the collapse consisted of a number of separate failures, it was difficult to correlate each of the individual collapses, from the bathymetry [e.g. Regions i, ii and iii in Figure 6.1(b)], with the official inventory records.

8 Appendix: Copies of Papers (as published)

LIANG, C., JAKSA, M. B. & OSTENDORF, B. (2012). GIS-based Back Analysis of Riverbank Instability in the Lower River Murray. *Australian Geomechanics*, 47, 59-65.

LIANG, C., JAKSA, M. B., OSTENDORF, B. & KUO, Y. L. (2015). Influence of river level fluctuations and climate on riverbank stability. *Computers and Geotechnics*, 63, 83-98.

LIANG, C., JAKSA, M. B., KUO, Y. L. & OSTENDORF, B. (2015). Identifying areas susceptible to high risk of riverbank collapse along the Lower River Murray. *Computers and Geotechnics*, 69, 236-246.

LIANG, C., JAKSA, M. B., KUO, Y. L. & OSTENDORF, B. (2015). Back Analysis of Lower River Murray Riverbank Collapses. *Australian Geomechanics*. Vol 50: No.2, 29-41.

Liang, C., Jaksa, M. B. & Ostendorf, B. (2012). GIS-based back analysis of riverbank instability in the Lower River Murray.
Australian Geomechanics, v. 47 (4), pp. 59-65

NOTE:

This publication is included on pages 208 - 214 in the print copy of the thesis held in the University of Adelaide Library.

Liang, C., Jaksa, M. B., Ostendorf, B. & Kuo, Y. L. (2015). Influence of river level fluctuations and climate on riverbank stability.
Computers and Geotechnics, v. 63, pp. 83-98

NOTE:

This publication is included on pages 215 - 230 in the print copy of the thesis held in the University of Adelaide Library.

It is also available online to authorised users at:

<http://dx.doi.org/10.1016/j.compgeo.2014.08.012>

Liang, C., Jaksa, M. B., Kuo, Y. L. & Ostendorf, B. (2015). Identifying areas susceptible to high risk of riverbank collapse along the Lower River Murray. *Computers and Geotechnics*, v. 69, pp. 236-246

NOTE:

This publication is included on pages 231 - 241 in the print copy of the thesis held in the University of Adelaide Library.

It is also available online to authorised users at:

<http://dx.doi.org/10.1016/j.compgeo.2015.05.019>

Liang, C., Jaksa, M. B., Kuo, Y. L. & Ostendorf, B. (2015). Back analysis of Lower River Murray Riverbank collapses.
Australian Geomechanics, v. 50 (2), pp. 29-41

NOTE:

This publication is included on pages 242 - 254 in the print copy of the thesis held in the University of Adelaide Library.